Fault decomposition characteristics and application feasibility assessment of C4F7N-CO2-O2 mixed insulating gas

Fanchao Ye

l'Université Wuhan]

ÉCOLE DOCTORALE Energie – Matériaux – Sciences de la Terre et de l'Univers

Laboratoire GREMI / School of Electrical Engineering

THÈSE EN COTUTELLE INTERNATIONALE présentée par :

Fanchao YE

soutenue le : 7 Décembre 2023

pour obtenir le grade de :

Docteur de Université d'Orléans
et de l'Université de Wuhan

Discipline/ Spécialité : Physique/ Génie électrique

Fault decomposition characteristics and application feasibility assessment of C_4F_7N-CO_2-O_2 mixed insulating gas

THÈSE dirigée par :

M. HONG Dunpin	Professeur, Université d'Orléans
M. ZHANG Xiaoxing	Professeur, Université de Wuhan

RAPPORTEURS :

M. ANDRE Pascal	Professeur, Université Clermont Auvergne
M. WU Tiezhou	Professor, Hubei University of Technology, China

---

JURY :

M. BRAULT Pascal	Directeur de Recherche, CNRS, Président du jury
M. ANDRE Pascal	Professeur, Université Clermont Auvergne
M. HONG Dunpin	Professeur, Université d'Orléans
Mme. TIAN Shangshang	Associate Professor, Hubei University of Technology, China
M. WU Tiezhou	Professor, Hubei University of Technology, China
M. ZHANG Xiaoxing	Professeur, Université de Wuhan

Catalogue

Abstract **7**

Chapter 1 Introduction **9**

1.1 Background and significance of the research 9

1.2 Current status of research on eco-friendly insulating medium C_4F_7N gas mixture 13

1.2.1 Insulation and arc extinguishing properties of C_4F_7N gas mixtures 13

1.2.2 Failure decomposition characteristics of C_4F_7N gas mixtures 22

1.2.3 Biosafety of C_4F_7N gas mixture 31

1.2.4 The engineering application examples of C_4F_7N gas mixture 32

1.3 Thesis research content and chapter organization 34

1.3.1 Main contents 34

1.3.2 Research ideas and technical lines 36

1.3.3 Thesis structure and chapter organization 38

Chapter 2. Characteristics of thermal decomposition of C_4F_7N-CO_2-O_2 and mechanism of product evolution **41**

2.1 Kinetic modelling of the evolutionary properties of C_4F_7N-CO_2-O_2 thermal decomposition particles 41

2.1.1 ReaxFF reaction molecular dynamics and force field methods 41

2.1.2 C_4F_7N-CO_2-O_2 thermal decomposition reaction model creation 48

2.2 Particle evolutionary properties of C_4F_7N-CO_2-O_2 thermal decomposition 51

2.2.1 Kinetic analysis of the effect of O_2 on the thermal decomposition particles of C_4F_7N-CO_2-O_2 51

2.2.2 Kinetic analysis of the effect of temperature on the thermal decomposition particles of C_4F_7N-CO_2-O_2 57

2.3 Thermal decomposition properties of C_4F_7N-CO_2-O_2 62

2.3.1 Thermal decomposition test platform and method 62

2.3.2 Characteristics of thermal decomposition of C_4F_7N-CO_2-O_2 with different O_2 contents 66

2.3.3 Thermal decomposition characteristics of C_4F_7N-CO_2-O_2 at different temperatures 74

2.4 Summary of the chapter 79

Chapter 3 C_4F_7N-CO_2-O_2 PD and its decomposition properties **81**

3.1 PD decomposition test platform and method 81
3.1.1 Test platforms 81
3.1.2 PD signal detection system 83
3.1.3 Test content and method 85
3.2 C_4F_7N-CO_2-O_2 PD characteristics 85
3.2.1 Effect of O_2 on the properties of C_4F_7N-CO_2-O_2 PD characteristics 85
3.2.2 Effect of externally applied voltage on the properties of C_4F_7N-CO_2-O_2 PD characteristics 91
3.3 C_4F_7N-CO_2-O_2 PD decomposition characteristics 93
3.3.1 Decomposition characteristics of C_4F_7N-CO_2-O_2 PD at different O_2 contents 93
3.3.2 Decomposition characteristics of C_4F_7N-CO_2-O_2 PD under different applied voltages 96
3.4 Mechanism of O_2 effect on C_4F_7N-CO_2-O_2 PD and its decomposition characteristics 99
3.4.1 Mechanism of O_2 effect on C_4F_7N-CO_2-O_2 PD characteristics 99
3.4.2 Mechanism of O_2 effect on the decomposition properties of C_4F_7N-CO_2-O_2 PDs 101
3.5 Solid precipitates under the action of C_4F_7N-CO_2-O_2 PD 102
3.6 Summary of the chapter 108
Chapter 4 C_4F_7N-CO_2 -O_2 frequency breakdown and its decomposition characteristics 111
4.1 Industrial Frequency Breakdown Test Platform and Methods 111
4.1.1 Test platforms 111
4.1.2 Test content and method 113
4.2 C_4F_7N-CO_2-O_2 frequency breakdown characteristics 113
4.2.1 Effect of O_2 on the insulation strength of C_4F_7N-CO_2-O_2 113
4.2.2 Effect of O_2 on the dispersion of C_4F_7N-CO_2-O_2 breakdown voltage 116
4.3 C_4F_7N-CO_2-O_2 Breakdown Characteristics 117
4.3.1 C_4F_7N-CO_2-O_2 breakdown product 117
4.3.2 Effect of O_2 on the breakdown properties of C_4F_7N-CO_2-O_2 breakdown 118
4.4 Mechanism of O_2 effect on C_4F_7N-CO_2-O_2 insulation strength and decomposition properties 125

4.4.1 Mechanism of the effect of O_2 on the insulation strength of C_4F_7N-CO_2-O_2 125
4.4.2 Mechanism of O_2 influence on the breakdown properties of C_4F_7N-CO_2-O_2 breakdown 126
4.5 Mechanism of C_4F_7N discharge decomposition and product generation under O_2 participation reaction 128
4.5.1 Density Functional Theory and Transition State Theory 128
4.5.2 Decomposition of C_4F_7N and generation of O-containing products under O_2 participation reaction 132
4.6 Summary of the chapter 138
Chapter 5 Feasibility assessment of C_4F_7N-CO_2-O_2 applications considering decomposition and biosafety 141
5.1 Optimal C_4F_7N-CO_2-O_2 ratio and characteristic components for equipment fault diagnosis 141
5.1.1 Optimal ratio of C_4F_7N-CO_2-O_2 for medium pressure equipment 141
5.1.2 C_4F_7N-CO_2-O_2 equipment troubleshooting characterization decomposition components 145
5.2 Biosafety of pure C_4F_7N gas 147
5.2.1 Test platforms and methods 147
5.2.2 C_4F_7N biosafety test results 148
5.3 C_4F_7N mixed gas arc decomposition product biosafety 156
5.3.1 Test platforms and methods 157
5.3.2 Arc Breakdown Characteristics of C_4F_7N Gas Mixture 159
5.3.3 C_4F_7N mixed gas arc decomposition product biosafety 162
5.4 Recommendations for the safe application of C_4F_7N-CO_2-O_2 165
5.5 Summary of the chapter 169
Chapter 6 Conclusions and outlook 171
6.1 Conclusions 171
6.2 Prospects for follow-up research 174
Extended abstract in French - Résumé long en français 177
Reference 189

Abstract

Sulfur hexafluoride (SF_6), as an ideal insulating and arc extinguishing dielectric, is widely used in various gas-insulated transmission and distribution equipment. However, the greenhouse effect potential (GWP) of SF_6 is 23500 times that of CO_2, and the atmospheric life is up to 3200 years. SF_6 is an extremely strong greenhouse gas. Looking for eco-friendly gas insulation media that can be applied to various medium and high voltage gas-insulated equipment (GIE) can fundamentally solve the dependence of the power industry on the large use of SF_6. In recent years, Perfluoroisobutyronitrile (C_4F_7N) gas mixture is considered as a potential SF_6 substitute gas because of its excellent environmental protection and insulation performance. In this paper, theoretical and experimental studies are carried out around the insulation and decomposition characteristics of eco-friendly C_4F_7N-CO_2-O_2 gas mixture under different fault conditions, and the application feasibility and safety of C_4F_7N-CO_2-O_2 gas mixture are evaluated in combination with the biological safety of C_4F_7N and its decomposition products. The main research work and achievements are as follows:

The model of C_4F_7N-CO_2-O_2 gas mixture reaction system was constructed, the thermal decomposition process of gas mixture under different O_2 content and temperature was simulated based on ReaxFF reaction molecular dynamics method. The influence of O_2, temperature and simulation time on the composition, distribution and reaction rate of C_4F_7N-CO_2-O_2 thermal decomposition particles was analyzed, and the thermal decomposition dynamic process of C_4F_7N-CO_2-O_2 and the evolution mechanism of product particles under different conditions were revealed. The thermal decomposition test platform was built to carry out the thermal decomposition test of C_4F_7N-CO_2-O_2 gas mixture, and the composition and content change rule of decomposition products under different O_2 content and overheat temperature were obtained. The thermal decomposition mechanism of C_4F_7N-CO_2-O_2 gas mixture was clarified through the combination of simulation and test results.

The power frequency breakdown and partial discharge (PD) decomposition tests of C_4F_7N-CO_2-O_2 gas mixture were carried out, and the effects of O_2 content and breakdown times on the insulation strength and breakdown voltage dispersion of the gas mixture were analyzed. The statistical characteristic parameters, such as discharge repetition rate, mean discharge magnitude and accumulation discharge magnitude were extracted, revealing the influence mechanism of O_2 and applied voltage on the PD characteristics of C_4F_7N-CO_2-O_2 gas mixture. The composition and formation rules of decomposition products under discharge fault were obtained, and the correlation characteristics between the types and contents of characteristic decomposition products and fault types and different influencing factors were

analyzed, as well as the mechanism of O_2's influence on the formation and inhibition of gas and solid by-products during the discharge decomposition of C_4F_7N-CO_2-O_2 gas mixture. Based on the density functional theory (DFT) and the transition state theory (TST), the thermodynamic parameters of the reaction process of C_4F_7N after the addition of O_2 were calculated. Combined with the experimental results, the influence of O_2 on the discharge decomposition of C_4F_7N-CO_2-O_2 gas mixture and the formation mechanism of products containing O were clarified.

Finally, the influence of O_2 content on the insulation and decomposition characteristics of C_4F_7N-CO_2-O_2 gas mixture under discharge and overheating faults is summarized and analyzed, and the optimal O_2 addition of C_4F_7N-CO_2-O_2 gas mixture for medium-voltage gas-insulated equipment is proposed to be 4%-6%. Based on the correlation characteristics of fault conditions and various influencing factors with the types and contents of decomposition products, the characteristic products that can represent the types and severity of equipment faults were extracted, which provides a reference for equipment fault diagnosis methods. The acute inhalation toxicity test on mice of C_4F_7N gas mixture and its arc decomposition products was carried out, and LC50, toxicity classification and toxic effects on mice were obtained. The feasibility and safety of the application of C_4F_7N-CO_2-O_2 gas mixture to the equipment are comprehensively evaluated based on the relevant results.

This paper systematically revealed the influence of O_2 on the insulation and decomposition characteristics of C_4F_7N-CO_2-O_2 gas mixture under different fault conditions through a lot of theoretical and experimental studies, and evaluated the bio-safety of C_4F_7N gas mixture and its arc decomposition products. The optimal ratio and fault diagnosis characteristic products of C_4F_7N-CO_2-O_2 gas mixture in actual equipment were proposed, and the safety application suggestions were given, which provide important theoretical and technical support for the engineering application of C_4F_7N-CO_2-O_2 gas mixture.

Keywords: Eco-friendly gas; C_4F_7N-CO_2-O_2; Insulation characteristics; Fault decomposition characteristics; Biosafety

Chapter 1 Introduction

1.1 Background and significance of the research

At present, sulfur hexafluoride (SF_6) gas is most widely used in all kinds of gas-insulated electrical equipment by virtue of its excellent insulating properties and arc extinguishing ability. SF_6 gas-insulated equipment mainly includes gas-insulated switchgear (GIS), gas-insulated transformer (GIT), gas-insulated transmission line (GIL), etc. Due to the small footprint of these equipment, they can operate safely and stably in the power grid, and can be used for the safe and stable operation of gas-insulated transmission pipelines (GIL), etc. Due to the small footprint of these equipment, they can be safely and stably operated in the grid and are easy to be maintained, so they are used in large quantities in the electric power industry [1-3]. With the construction and development of modern power grids, the demand for gas-insulated transmission and distribution equipment increases year by year, resulting in a rapid increase in the use of SF_6 gas. However, SF_6 gas is an extremely potent greenhouse gas with a greenhouse effect potential GWP (Global Warming Potential) of 23,500 times that of CO_2 and an atmospheric lifetime of up to 3200 years [4-6]. The trend of SF_6 in the global atmosphere is given in Figure 1.1, and it can be seen that the global atmospheric content of SF_6 has increased by 16.3% over the past five years, and the global temperature rise caused by SF^6 in the atmosphere has reached 0.004°C [6].

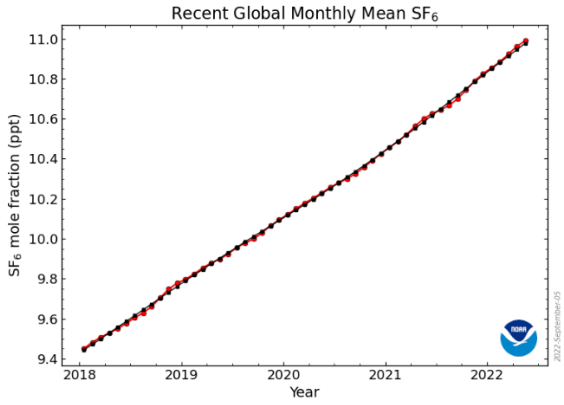

Fig 1.1 Trends in global atmospheric levels of SF_6

In today's world, the problem of global warming is becoming increasingly serious, and the international community has reached a consensus on reducing greenhouse gas emissions and controlling global warming. The report of the United Nations Governmental Panel on Climate Change points out that nearly 80% of SF_6 gas produced globally is used in the power industry, and the annual emissions are as high as 1,000 tons [7], and the parties to the United Nations Framework Convention on Climate Change (UNFCCC) listed SF_6 gas as one of the

six greenhouse gases of restricted use in the Kyoto Protocol, which was signed in 1997 [8].The Paris Agreement, which was adopted in 2015, also explicitly proposed to limit the emission of greenhouse gases with the goal of limiting the global average temperature increase to 2°C by the end of this century [9,10].

In order to solve the greenhouse effect problem brought about by the massive application of SF_6 gas, Europe, North America, Australia, and some countries in Asia have begun to levy an emission tax on the use of SF_6 gas in order to gradually limit the use of SF_6 gas [8]. However, with the economic development, the increasing demand for electricity in various industries, the demand for various types of medium- and high-voltage gas-insulated equipment is also increasing, and in 2018, the domestic use of SF_6 gas applied to GIS was as high as 7,000 tons (equivalent to 160 million tons of CO_2) [11]. The State Council's "13th Five-Year Plan" for controlling greenhouse gas emissions puts forward the need to further limit the emission of SF_6 and other greenhouse gases; the National Energy Administration issued the "Thirteenth Five-Year Plan for Electric Power Development", which points out that "clean, low-carbon and green development" is the key to the development of GIS. The "Thirteenth Five-Year Plan for Electric Power Development" issued by the National Energy Administration points out that the development of the power industry is based on the principles of "low carbon and green development"; General Secretary Xi Jinping announced to the world in his speech at the 75th General Debate of the United Nations General Assembly that "China will increase the strength of its national autonomous contribution, adopt more vigorous policies and measures, strive to peak carbon dioxide emissions by 2030, and make efforts to achieve carbon neutrality by 2060. achieve carbon neutrality by 2060". Therefore, the search for environmentally friendly gas-insulated dielectrics for all types of medium- and high-voltage gas-insulated electrical equipment can be a fundamental solution to the power industry's dependence on the use of large quantities of SF_6 gas.

Since the 1970s, researchers at home and abroad have been committed to developing and finding a gas insulation medium with excellent environmental performance to replace SF_6 [12]. At present, the SF_6 replacement gases are divided into three major categories: conventional gases (air, N_2 and CO_2), gas mixtures of SF_6 with N_2 and CO_2, and strong electronegative gases and their gas mixtures [13]. Conventional gases are relatively easy to prepare and inexpensive, but their insulation and arc extinguishing capabilities are poor, and they are usually used only as buffer gases [14-17]. SF_6 gas mixtures are able to reduce the use of SF_6 to a certain extent, but they cannot fundamentally solve the problem of its greenhouse effect [18-21]. Strong electronegative gases mainly include perfluorocarbon gases (C_2F_6, C_3F_8, c-C_4F_8), trifluoroiodomethane (CF_3I), perfluoroketone ($C_5F_{10}O$, $C_6F_{12}O$), perfluoroisobutyronitrile (C_4F_7N), and HFO-1234ze(E), etc. Table 1.1 shows the physicochemical characteristic

parameters of the above several strong electronegative gases and SF_6. Although the insulating properties of perfluorocarbon gases are close to or even better than those of SF_6, the GWP values of these gases are still high, and thus they have a low potential for application [22-25]; CF_3I has better insulating properties and a GWP value close to 1, but its application is limited by the fact that it is categorized as a type 3 mutagen and is prone to produce iodine monomers after multiple discharges [26-30]; HFO-1234ze(E) will show carbon particle deposition after flashover and has the risk of flammability [31]; $C_5F_{10}O$ and $C_6F_{12}O$ have GWP values of 1 and insulation properties more than twice those of pure SF_6 gas [32-34], which provide excellent insulation and environmental protection properties, but the liquefaction temperatures are as high as 26.9°C and 49°C [35, 36], although their combination with CO_2, N_2 or dry air can alleviate this problem, but the gas mixtures still cannot be used in high-voltage gas-insulated equipment.

Table 1.1 Characteristic parameters of SF_6 and its alternative gases

Gas	Dielectric strength (relative to SF_6)	Liquefaction temperature/°C	Atmospheric lifetime/year	GWP
SF_6	1	-64	3200	23500
C_2F_6	0.67-0.90	-78	10000	9200
C_3F_8	0.88	-37	2600	7000
c-C_4F_8	1.11-1.80	-8	3200	8700
CF_3I	1.2	-22.5	0.005	1-5
HFO-1234ze(E)	0.85	-19.4	0.05	6
$C_5F_{10}O$	2	26.5	0.04	<1
$C_6F_{12}O$	2.7	49	0.019	1
C_4F_7N	2.1-2.2	-4.7	30	2090

Perfluoroisobutyronitrile (C_4F_7N, Novec TM 4710) is a new type of environmentally friendly gas insulation medium, which was introduced by Alston and 3M in 2014 as the main gas for g3 (commercial designation, green gas for grid) [37]. The GWP of C_4F_7N is 2090, which is about 1/11 of the GWP value of SF_6. The atmospheric lifetime is only 30 years, the ozone depletion potential (ODP) is 0, which will not bring any impact on the ozone layer, and the insulation capacity of pure C_4F_7N is more than twice that of SF_6, which is excellent in terms of environmental protection and insulation strength [38]. However, due to its high liquefaction temperature (-4.7°C), it cannot be used directly as a gaseous insulating medium in equipment, and it needs to be mixed with buffer gases such as CO_2, N_2, dry air, and O_2 in order to satisfy the minimum operating temperature of the equipment in actual working conditions [37]. The GWP values of C_4F_7N-CO_2 gas mixtures containing 4% and 10% C_4F_7N are 327 and 690, respectively, which are only 2% to 3% of SF_6 [38]. In addition, C_4F_7N-CO_2 gas mixtures with C_4F_7N content of 18% to 20% have comparable insulating properties to SF_6 [39, 40]. C_4F_7N gas mixture as insulation and arc extinguishing medium equipment has been demonstrated in

various countries and regions of the world, General Electric (General Electric, GE) developed a 245 kV current transformer (Current transformer, CT) and a 145 kV GIS with C_4F_7N gas mixture as the insulating medium, and put it into trial operation [41]. The State Grid of China and the Southern Power Grid Corporation of China have developed 1000 kV GILs and 12 kV switchgears using C_4F_7N gas mixture as insulation and arc extinguishing medium, and realized demonstration applications.

Environmental protection and insulation properties are only part of the research on gas insulating medium C_4F_7N gas mixtures. To assess the feasibility of its application, it is necessary to carry out research on its insulation and decomposition properties under discharge faults, decomposition properties under overheating faults, arc extinguishing properties and biosafety, etc. Among them, the investigation of its decomposition properties under different fault conditions is an important task to be completed before its large-scale application. Among them, the investigation of the decomposition characteristics of environmentally friendly insulating gases under different fault conditions is an important task that needs to be accomplished before its large-scale popularization and application. The faults of gas-insulated equipment are mainly in the form of discharge faults and overheating faults, of which the discharge faults mainly include partial discharge (Partial Discharge, PD), spark discharge and arc discharge. PD faults are generally caused by the special concentration of the local electric field inside the insulating medium or on the insulating surface, which is characterized by a long duration and low energy release, and is one of the most common faults inside the gas-insulated equipment. It is one of the most common faults inside the equipment. Spark discharge is a gas discharge phenomenon in which the gas between high-voltage electrodes is punctured and flashes and bursts of sound appear, of which IF breakdown is a common spark discharge. The arc discharge that occurs in the switchgear is called switching arc, which is a form of gas self-sustained discharge, and the whole process is accompanied by luminescence, heat and the release of high energy, which leads to a serious decomposition of the gas insulation medium. In addition, the presence of defects such as poor contact, magnetic saturation or overloading within the equipment can lead to a Partial Overthermal Fault (POF). PD and POF, these early localized faults will damage the gas insulating medium to varying degrees, leading to a series of decomposition and compounding reactions, generating a variety of complex gaseous and solid decomposition products [42, 43], accelerating the deterioration of the insulating medium, and ultimately may lead to insulation breakdowns triggering a power grid outage. In addition, the assessment of the biosafety of the C_4F_7N gas mixture and its decomposition products is also crucial considering the safety of the relevant personnel during the actual operation of the equipment.

At present, domestic and foreign research on the decomposition characteristics and mechanism of C_4F_7N gas mixture under different fault conditions and different influencing factors is still insufficient, mainly including the research on the characteristics of the macroscopic level and the reaction mechanism at the microscopic level is not comprehensive and in-depth. At the same time, the composition and content of the decomposition products of C_4F_7N gas mixture under different fault conditions and the correlation between the change rule and different influencing factors are the important basis for the assessment of the operating status of the equipment. Therefore, it is necessary to carry out a systematic study on the decomposition characteristics of C_4F_7N gas mixtures under different fault conditions, and to consider the biological safety of C_4F_7N gas mixtures and their decomposition products under fault conditions, so as to comprehensively assess the feasibility and safety of C_4F_7N gas mixtures applied to equipment.

1.2 Current status of research on eco-friendly insulating medium C_4F_7N gas mixture

1.2.1 Insulation and arc extinguishing properties of C_4F_7N gas mixtures

Insulation and arc extinguishing performance is an important indicator to evaluate whether the environmentally friendly gas insulating medium has the potential for application, excellent gas insulating medium needs to be able to withstand the equipment operating voltage or overvoltage and has a certain current breaking capacity.

(1) C_4F_7N gas mixture insulation performance

The current research on the insulation performance of C_4F_7N gas mixtures mainly focuses on the AC and DC breakdown characteristics, lightning impact characteristics, PD characteristics, etc. In 2016, 3M Owens et al. used plate-plate electrodes to simulate a quasi-uniform electric field to carry out the AC breakdown test of C_4F_7N-N_2, C_4F_7N-CO_2 and C_4F_7N-Air gas mixtures for the first-time. The results showed that the insulation breakdown strength of all three gas mixtures increased with the increase of air pressure and C_4F_7N content, which was most obvious in the C_4F_7N-CO_2 gas mixture; the three gas mixtures containing 20% of C_4F_7N could reach the insulation strength of SF_6 under the same conditions [44]. Zhang et al. of Xi'an Jiaotong University found that C_4F_7N-CO_2 gas mixtures containing 15% C_4F_7N could obtain the equivalent insulation strength of SF_6 at 100 kPa air pressure under the breakdown voltage of C_4F_7N-CO_2 gas mixtures under different air pressures and different types of electrodes (plate-plate, ball-plate, rod-plate, and pin-plate) and found that gas mixtures containing 15% C_4F_7N could obtain the equivalent insulation strength of SF_6 at 100 kPa air

pressure, and the gas mixtures with a C_4F_7N content of 15% C_4F_7N. The critical breakdown field strength of the gas mixture with 15% C_4F_7N was 98.8% of that of SF_6 under the same conditions, respectively, and the test results confirmed that the C_4F_7N gas mixture has the potential to replace SF_6 for medium-voltage equipment in terms of insulation performance [45].

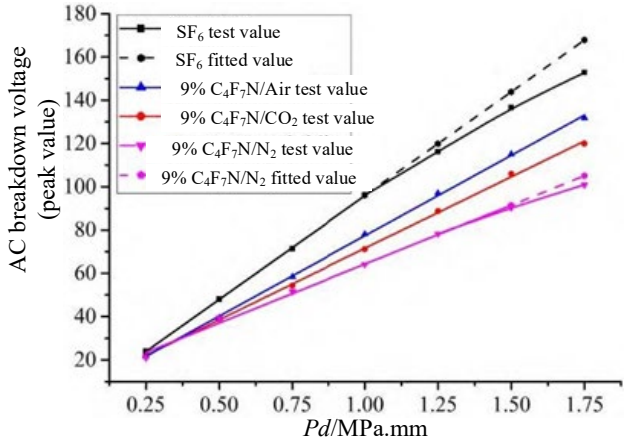

Fig 1.2 SF_6 and C_4F_7N gas mixture frequency breakdown voltage versus *pd* [47]

Nechmi et al. tested the frequency breakdown performance of C_4F_7N-CO_2 gas mixtures containing 3.7%-96.3% C_4F_7N at different air pressures and electrode gaps and compared it with SF_6, and found that gas mixtures containing 20% C_4F_7N could achieve the equivalent insulation strength of SF_6 at an air pressure of 0.1 MPa, and gas mixtures containing 3.7% C_4F_7N could meet the ambient operating temperature of -30°C and reach 72% of the breakdown voltage of pure SF_6 at an absolute air pressure of 0.55 MPa. The gas mixture containing 3.7% C_4F_7N can meet the ambient operating temperature of -30°C and reach 72% of the breakdown voltage of pure SF_6 under 0.55MPa absolute air pressure, indicating that the C_4F_7N gas mixture can meet the insulation requirements of high-voltage equipment while meeting the liquefaction temperature requirements [46]. By testing the AC breakdown characteristics of C_4F_7N gas mixtures with different background gases (CO_2, N_2, and Air), Wuhan University's team of Zhou Wenjun pointed out that the breakdown voltages of 5%-20% C_4F_7N-N_2 gas mixtures in the air pressure range of 0.3-0.7 MPa are lower than those of C_4F_7N-CO_2 and C_4F_7N-Air gas mixtures under the same conditions (shown in Figure 1.2) and carbon precipitates on the electrode surface after the test, confirming that the C_4F_7N-CO_2 and C_4F_7N-Air gas mixtures have more potential for application compared to the C_4F_7N-N_2 gas mixtures [47].

In order to evaluate the sensitivity of C_4F_7N-CO_2 gas mixture to uneven electric field, Yan et al. of China Electric Power Research Institute firstly deduced the calculation formula of the excellent value of the gas mixture and the control value of electrode surface roughness at the theoretical level, and then carried out the AC breakdown test under the rough electrode,

the results showed that the C_4F_7N-CO_2 gas mixture with 4%-20% C_4F_7N has the same insulation performance as SF_6, and the control value of 6.3μm of electrode surface roughness in SF_6 equipment is also applicable to C_4F_7N-CO_2 gas mixture equipment [48]. Deng et al. of Yunnan Electric Power Research Institute used three electrode models (plate-plate, ball-plate and needle-plate) to simulate different types of electric fields to study the effect of electric field uniformity on the AC breakdown performance of C_4F_7N-Air gas mixture, and found that under the condition of lower electric field inhomogeneity, the AC breakdown voltage of the C_4F_7N-Air mixture increases linearly with the increase of the barometric pressure, and increases saturated with the increase of electric field uniformity; under the condition of low electric field inhomogeneity, the AC breakdown voltage of C_4F_7N-CO_2 mixture increases linearly with the increase of barometric pressure, and increases saturated with the increase of electric field uniformity. Under the condition of low electric field inhomogeneity, the AC breakdown voltage of C_4F_7N-Air gas mixture increases linearly with the increase of air pressure, and the trend of saturation growth with the increase of electric field homogeneity; in the very inhomogeneous electric field, the breakdown voltage of C_4F_7N-Air gas mixture appears hump phenomenon with the increase of air pressure, and the sensitivity of C_4F_7N-Air gas mixture to the electric field is slightly higher than that of SF_6 gas [49]. Zhang et al. of Wuhan University experimentally studied the AC breakdown characteristics of C_4F_7N-CO_2 and C_4F_7N-N_2 gas mixtures under a very inhomogeneous electric field (needle-plate electrodes), and found that the AC breakdown voltage of gas mixtures containing 2-8% C_4F_7N showed a saturated growth trend with the increase of the air pressure and the mixing ratio, and that the insulating strength of C_4F_7N gas mixtures in a very inhomogeneous electric field was weaker than that of SF_6 in a very inhomogeneous electric field. slightly inhomogeneous electric field, and the sensitivity of C_4F_7N gas mixture to electric field inhomogeneity is higher than that of SF_6 [50, 51]. The results for the C_4F_7N gas mixture AC breakdown synergistic effect show that the AC breakdown voltages of C_4F_7N-CO_2 and C_4F_7N-N_2 gas mixtures containing 5%-20% C_4F_7N under quasi-uniform electric field conditions of 0.1-0.7 MPa show synergistic effect with the change of C_4F_7N content, and the quantitative description of the synergistic effect by the normalization factor h finds that C_4F_7N-CO_2 gas mixture has better synergistic effect than C_4F_7N-N_2 gas mixture, which is the optimal choice for environmentally friendly gas-insulated equipment [52].

For the DC breakdown characteristics of C_4F_7N gas mixture, Tu et al. from North China Electric Power University carried out DC breakdown tests on C_4F_7N-CO_2 gas mixtures containing 4% and 8% C_4F_7N in the range of 304.7kPa to 717.83kPa. The results of the study

showed that the breakdown field strength of the gas mixtures in the homogeneous field increased with the increase of the air pressure, and the breakdown field strength of the positive polarization was higher than that of the negative polarization at 717.83kPa and reached the maximum value. The breakdown field strength was higher than that of the negative polarity at 717.83 kPa and reached the maximum value. The breakdown voltage of the negative polarity of the C_4F_7N-CO_2 gas mixture showed an increasing trend with the increase of air pressure in a non-uniform field, while the opposite was true for the positive polarity, which showed a strong acute effect [53]. The negative polarity DC breakdown field strengths of C_4F_7N-CO_2 gas mixtures containing 4% and 8% C_4F_7N at 0.7 MPa gas pressure can reach 81.21% and 96.48% of SF_6 at 0.5 MPa gas pressure, respectively [54]. Li et al. from North China Electric Power University investigated the DC breakdown characteristics of 4%C_4F_7N-96%CO_2 gas mixture, SF_6-N_2 gas mixture and pure SF_6 gas under the influence of particles, and found that the insulation strength of 4%C_4F_7N-96%CO_2 gas mixture was comparable to that of 30%SF_6-70%N_2 under the condition that no particles were present in the discharged air gap; when there existed the influence of particles, the insulation strength of 4%C_4F_7N-96%CO_2 gas mixture has a lower Discharge Sensitivity by Particles (DSP) than that of 30% SF_6-70%N_2 gas mixture and higher than that of 20% SF_6-80%N_2 gas mixture, and C_4F_7N-CO_2 gas mixture has a lower sensitivity to particles [55].

The above studies on the frequency and DC breakdown behavior of C_4F_7N gas mixtures under different field uniformity conditions show that C_4F_7N gas mixtures have excellent insulating properties, especially C_4F_7N-CO_2 gas mixtures have the best synergistic effect. However, compared with SF_6, C_4F_7N gas mixtures are more sensitive to electric field inhomogeneities, so insulation defects should be avoided as much as possible during the manufacture and transportation of gas-insulated equipment.

Partial discharge characteristics reflect the insulating properties of gas insulating media under defective conditions, and are also an important aspect in assessing the strength of gas insulation. The team of Zhang et al. from Wuhan University studied the effect of gas pressure and mixing ratio on partial discharge inception voltage (PDIV) of C_4F_7N-CO_2 gas mixture, and found that the PDIV of C_4F_7N-CO_2 gas mixture containing 2%~12% C_4F_7N compared with SF_6 decreases and then stabilizes with the increase of gas pressure (Fig. 1.3(a)). It was found that the PDIV of C_4F_7N-CO_2 mixture containing 2%~12% C_4F_7N relative to SF_6 decreased and then stabilized with the increase of air pressure (shown in Fig. 1.3(a)), and increased rapidly and then saturated with the increase of the C_4F_7N content (shown in Fig. 1.3(b)). The PDIV of the 12% C_4F_7N-88%CO_2 mixture under the air pressure of 0.6MPa was

comparable to that of SF_6 under the air pressure of 0.3MPa, and the synergy effect coefficient of the localized discharges of C_4F_7N and CO_2 was obtained. coefficient of synergistic effect, we obtained that C_4F_7N and CO_2 have strong synergistic effect [51]; PDIV- and PDIV+ of C_4F_7N-N_2 gas mixture containing 2%~12% C_4F_7N increase with the increase of air pressure, and the PDIV of C_4F_7N-N_2 gas mixture relative to that of SF_6 under the air pressure of 0.5~0.6MPa shows a saturated growth with the increase of the content of C_4F_7N trend, increasing the content of C_4F_7N in the gas mixture under low air pressure can effectively improve the insulation strength [56].

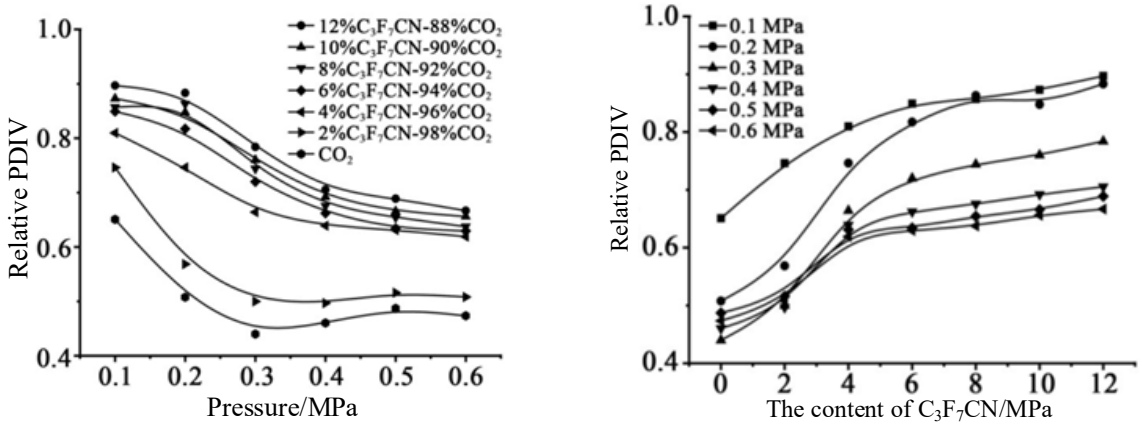

(a) (b)

Fig 1.3 Variation of PDIV of C_4F_7N-CO_2 gas mixture relative to SF_6 with gas pressure and C_4F_7N content [51]

Wang et al. used metal conductor protrusions to simulate the extremely inhomogeneous electric field in the equipment to carry out partial discharge tests, and analyzed the discharge parameters such as PDIV, PD pulse time and frequency, and phase resolved partial discharge (PRPD) mapping of the 4% C_4F_7N-96% CO_2 gas mixture. The results showed that the PDIV of C_4F_7N gas mixture was 76%-84% of that of SF_6, and the electrode type and air pressure were the key factors affecting the PDIV; the PD pulses of C_4F_7N gas mixture had longer rise time, pulse width, and Fast Fourier Transform (FFT)) relative amplitude compared to that of SF_6. The conclusion obtained from the average values extracted from the 10 PRPDs is that the average apparent discharges and the number of discharges for both SF_6 and 4%C4F7N-96%CO_2 gas mixtures increase with the applied voltage (shown in Fig.1.4), and that both the discharges and the number of discharges for the C_4F_7N gas mixtures are higher than that for SF_6 under the same conditions, but that the PDs occur at lower applied voltage conditions with lower frequency [57].

Zhang et al. from Xi'an Jiaotong University investigated the PD characteristics of 20%C_4F_7N-80%CO_2 gas mixture and SF_6 at 0.1~0.2 MPa, tested the PDIV and plotted the

PRPD maps. It was found that the PDIV of 20%C_4F_7N-80%CO_2 gas mixture was basically the same as that of SF_6, and the number of PD pulses in the statistical time of SF_6 and C_4F_7N-gas mixture increased with the increase of the applied voltage, but the saturation growth tendency was shown for the C_4F_7N gas mixture; the average PD discharge of SF_6 showed the change rule of increasing first and then decreasing with the increase of the applied voltage SF_6 has more PDs with lower discharges, while the number of PDs in the 20%C_4F_7N-80%CO_2 gas mixture is less than that of SF_6, but the individual PD discharges will be larger. an increase in the proportion of C_4F_7N in the C_4F_7N gas mixture can effectively inhibit the generation of PDs mainly due to the strong electrophilicity of C_4F_7N, which has a high degree of electrophilicity and a high level of saturation. has a strong electron affinity [45]. Toigo et al. from the French Supergrid Institute investigated the local discharge characteristics of C_4F_7N gas mixtures under the defects of high-voltage DC conductor protrusions, and found that the PD pulse amplitude of C_4F_7N-CO_2 gas mixtures was greater than that of SF_6 under positive polarity and less than that of SF_6 under negative polarity conditions, and the PD repetition rate of C_4F_7N-CO_2 gas mixtures was higher than that of SF_6 [58]. The team of Tu from North China Electric Power University investigated the DC PD characteristics of C_4F_7N-CO_2 gas mixtures and found that the positive polarity DC PDIV of C_4F_7N-CO_2 gas mixtures was lower than the negative polarity; the PDIV (negative polarity DC) of C_4F_7N-CO_2 gas mixtures containing 8% C_4F_7N was higher than that of the mixtures containing 4% C_4F_7N, whereas the positive polarity DC PDIV of mixtures containing 4% C_4F_7N was higher than that of mixtures containing 8% C_4F_7N [59].

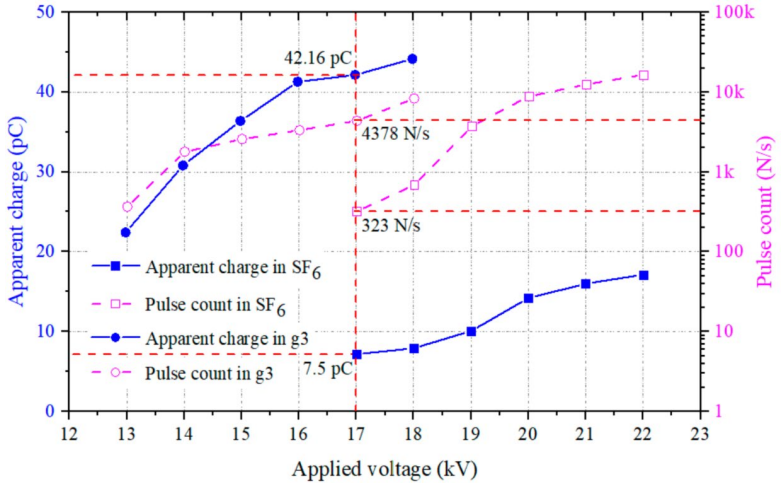

Fig 1.4 Average apparent discharges and number of discharges for SF_6 and C_4F_7N gas mixtures at different voltages [57]

The results of the above PD characterization studies for C_4F_7N gas mixtures under AC and DC conditions show that the mixed gas PD characteristics are affected by factors such as

electrode type, applied voltage, mixing ratio, and air pressure, etc., and that the repetition rate of the PD for C_4F_7N gas mixtures is higher than that for SF_6 under the same conditions, and that the PD for C_4F_7N gas mixtures exhibits an obvious polarity effect under DC conditions.

With regard to the study on the lightning impact characteristics of C_4F_7N gas mixture, Jiang of Xidian Switch Electric Co., Ltd. experimentally investigated the lightning impact characteristics of C_4F_7N-CO_2 gas mixture under the condition of extremely inhomogeneous electric field (needle-plate electrodes), including the effects of air pressure, mixing ratio and electrode spacing, and pointed out that the positive lightning impact voltage of C_4F_7N-CO_2 gas mixture containing 5%-10% C_4F_7N showed a trend of saturation growth with the increase of air pressure, and there was a clear "hump" effect, and the negative lightning impact voltage also saturated at a higher air pressure; the negative lightning impact voltage containing 5% C_4F_7N also saturated. It is pointed out that the positive lightning impulse voltage of C_4F_7N-CO_2 gas mixture containing 5%-10% C_4F_7N is saturated with the increase of air pressure, and there is an obvious "hump" effect, and the negative lightning impulse voltage will be saturated at higher air pressure; the lightning impulse voltage of C_4F_7N-CO_2 gas mixture containing 5% C_4F_7N (positive polarity) can be up to 80% of that of SF_6, C_4F_7N content increased to 10% can reach 90% of the equivalent conditions SF_6, lightning shock voltage response of the C_4F_7N gas mixture relative to SF_6 insulation performance of positive polarity is slightly higher than negative polarity. Overall, the C_4F_7N-CO_2 gas mixture has a significant polarity effect, and the breakdown voltage is significantly lower in positive polarity than in negative polarity [60]. The team of Zhang from Xi'an Jiaotong University tested the lightning impact characteristics of C_4F_7N-CO_2 gas mixture under the conditions of slightly inhomogeneous electric field and very inhomogeneous electric field, and found that in the case of C_4F_7N-CO_2 gas mixture in the slightly inhomogeneous electric field environment and high air pressure, the breakdown voltage will tend to saturation, and the breakdown voltage of the C_4F_7N-CO_2 gas mixture with 5%-20% C_4F_7N will reach 0.8% with respect to that of SF_6 [61]. The lightning impact strength of the C_4F_7N-CO_2 gas mixture containing 5% to 20% C_4F_7N is more than 0.8, but the insulation strength relative to SF_6 decreases when the air pressure is greater than 0.5 MPa. By introducing the electric field sensitivity coefficient S to represent the decrease in breakdown voltage of gas insulating media in an inhomogeneous electric field environment, it was obtained that the sensitivity of the C_4F_7N gas mixture to the electric field inhomogeneity under the action of lightning shock is greater than that of SF_6 and CO_2 [61, 62].

(2) Arc extinguishing performance of C_4F_7N gas mixture

The research on the arc extinguishing performance of C_4F_7N gas mixture mainly focuses

on two aspects, experimental research and simulation, on the one hand, through the load switch or circuit breaker to carry out different conditions of the C_4F_7N gas mixture of the opening test, testing including arc voltage, current and current zero-zone characteristics and post-arc breakdown characteristics and other characteristics of the evaluation of its breaking capacity; on the other hand, through the establishment of the opening current process of the magnetohydrodynamic model to evaluate the opening capacity under different conditions. On the other hand, by establishing a magnetohydrodynamic model of the breaking current process, the breaking capacity of the interrupting medium under different conditions is evaluated by calculating the arc temperature, air pressure in the interrupting chamber, and airflow field distribution.

In terms of experimental research, Li's team of Xi'an Jiaotong University's designed a test device that can simulate the arc ignition process of direct-acting and compressed-air high-voltage load switches, and used the device to study the arc ignition characteristics of the C_4F_7N-CO_2 gas mixture under the conditions of pulling and blowing arcs, including the arc voltage, current, and current-zero zone characteristics and the post-arc breakdown characteristics. The results show that gas blowing can effectively enhance the energy dissipation of small-current arcs, and the thermal breaking capacity of the C_4F_7N-CO_2 gas mixture in the arc-pulling test is comparable to that of SF_6 under the same conditions, while that of the C_4F_7N-CO_2 gas mixture in the arc-blowing test can reach 91% of that of SF_6 [63]. Yan et al. of the China Electric Power Research Institute (CEPRI) used a synthetic test circuit to test the arc extinguishing performance of a 12kV ring main unit filled with C_4F_7N-CO_2 gas mixture under micro-positive voltage, measured the voltage characteristics and dielectric recovery strength of the gas mixture, and compared it with SF_6. The test results show that under micro-positive pressure (0.14 MPa absolute air pressure), the arc voltage of the C_4F_7N-CO_2 gas mixture is similar to that of SF_6, but the peak voltage is lower than that of SF_6, the arc column is wider than that of SF_6, and the arc of the C_4F_7N-CO_2 gas mixture is more easily reversed and commutated. The dielectric recovery strength of C_4F_7N-CO_2 gas mixture is about 34% of that of SF_6 at the same breaking current. The breaking capacity of C_4F_7N-CO_2 gas mixture can meet the requirements of IEC standard for load. In addition, the breaking capacity of C_4F_7N-CO_2 gas mixture can be further improved by optimizing the arc extinguishing structure [64]. Lin Xin et al. of Shenyang University of Technology studied the arc quenching characteristics of C_4F_7N-CO_2 gas mixture, and the results showed that with the increase of the content of C_4F_7N in the gas mixture, the peak arc quenching value of the arc voltage and the arc conductance were gradually close to that of SF_6 gas, which showed excellent arc quenching

characteristics [65].

Meyer et al. from GE used 6%C_4F_7N-5%O_2-89%CO_2 gas mixture as insulation and arc extinguishing medium to develop and type test circuit breakers (145kV/40kA) according to IEC standards, with the minimum pressure set at 0.75MPa for insulation and breaking, and the results showed that the addition of 5%O_2 could increase the circuit breaker electrical life to improve the opening performance by inhibiting the generation of gas and solid decomposition products [66]. The results showed that the addition of 5% O_2 could improve the electrical life of the circuit breaker by inhibiting the formation of gases and solid decomposition products to improve the opening performance, especially for the opening test with higher current, and the obvious improvement effect was observed after adding 5% O_2 [66]. Zhang et al. from Xi'an Jiaotong University carried out short-circuit current breaking test on 40.5 kV porcelain column circuit breaker filled with C_4F_7N-CO_2-O_2 gas mixture and analyzed its breaking capacity by obtaining the zero-zone characteristics of short-circuit current under different conditions. The results show that under the premise of not changing the switch structure, appropriately increasing the gas pressure of 6%C_4F_7N-5%O_2-89%CO_2 gas mixture can make it improve the ability to break large currents; C_4F_7N gas mixture containing 20% O_2 can break a short-circuit current of 31.5kA under the breaking condition, but it cannot be successfully opened under the reclosing condition, and increasing the content of O_2 can improve the breaking performance of the mixture by 10%, and the breaking performance of the mixture can be improved by 10%, and the breaking performance of the mixture can be improved by 10%. Increasing the O_2 content can improve the breaking performance of the gas mixture by 10%, but there is still a certain gap compared with the breaking performance of SF_6 [67].

In terms of simulation calculation, Zhang et al. constructed a real gas model according to the physical parameters of C_4F_7N gas mixture and SF_6, carried out a magnetohydrodynamic simulation study on the arc process of breaking short-circuit currents, obtained the arc time constants and energy dissipation coefficients based on the Mayr model, and quantitatively analyzed the thermal breaking capacity of C_4F_7N gas mixture, and found that the arc of the gas mixture containing 5% C_4F_7N has a stronger diffusion capacity along the axis, but the arc generated by SF_6 has a stronger radial diffusion capacity. It was found that the arc diffusion ability of the gas mixture containing 5% C_4F_7N was stronger in the axial direction, but the radial diffusion ability of the arc generated by SF_6 was stronger. 20% O_2 was added to the C_4F_7N gas mixture to reduce the temperature of the arc past the zero point, and the heating ability of the gas in the expansion chamber was increased at the peak of the current. In addition, the simulation results showed that the thermal breaking capacity of C_4F_7N gas mixture with

20% O_2 at 0.6 MPa gas pressure was only 58.5% of that of SF_6 under the same conditions [68].

Overall, the conclusions of the current domestic and international experimental studies on the AC and DC breakdown characteristics, PD characteristics and lightning impact characteristics of C_4F_7N gas mixtures confirm the excellent insulating properties of C_4F_7N gas mixtures and their potential for use as insulating media in equipment. In addition, C_4F_7N gas mixture has a certain arc extinguishing ability, but there is still a certain gap compared with SF_6, which needs to be further improved by optimizing the switch structure and changing the gas formula and gas pressure. Although the addition of O_2 as the second buffer gas can improve the arc extinguishing performance of the gas mixture, the existing research has only considered the effect of O_2 on the arc breaking ability of the gas mixture, the lack of O_2 on the C_4F_7N gas mixture insulation properties (breakdown, PD) of the influence of the law and mechanism of research.

1.2.2 Failure decomposition characteristics of C_4F_7N gas mixtures

Electron collision ionization and photoionization in discharge faults and high temperatures in overheating faults can lead to decomposition and inter-particle reorganization of gas insulating media, generating a variety of gases and solid by-products. Replacement of SF_6 environmentally friendly gas insulation medium not only need to have excellent insulation and arc extinguishing performance, but also need to have a certain degree of chemical stability, that is, in the discharge and overheating fault conditions of the main insulating medium will not be seriously decomposed, the overall insulation strength of the gas mixture and arc extinguishing ability will not be seriously affected by the decomposition of the gas and solid by-products, so the decomposition characteristics of the gas mixture of C_4F_7N in the electric and thermal fault conditions are examined. Therefore, it is necessary to investigate the decomposition characteristics of C_4F_7N gas mixture under electric and thermal fault conditions. In addition, the correlation between the decomposition characteristics of the gas mixture under different influencing factors and the type and severity of faults can provide a basis for the construction of equipment fault diagnosis methods.

(1) Decomposition characteristics of C_4F_7N gas mixture under overheating failure condition

In 2016, Kieffel et al. from GE carried out thermal decomposition tests on a C_4F_7N-CO_2 mixture containing 400-600 ppm C_4F_7N using a tube-heated furnace to simulate a superheat failure inside the device, ramping up to 1000 °C at 10 °C per minute, and qualitatively detecting the changes in decomposition products with temperature by Fourier Transform-Infrared Spectroscopy (FTIR). Infrared Spectroscopy (FTIR) to qualitatively detect the

changes of decomposition products with temperature. The results showed that C_4F_7N started to decompose at 650 °C and CO was first detected at this temperature; C_2F_6 and HF were detected when the superheated temperature increased to 700 °C, and the three products, C_2F_6, CF_3CN, C_2F_5CN, and COF_2 were detected when the temperature was higher than 800 °C, but the concentration of C_2F_6 was lower; when the temperature reached 880 °C, all of the C_4F_7N decomposed. However, under long-term thermal aging conditions (120°C, 200 days) C_4F_7N showed better thermal stability [38].

Zhang's team from Wuhan University used local heat source to simulate the POF inside the equipment to carry out 12h thermal decomposition test of C_4F_7N-CO_2 (6% C_4F_7N) gas mixture under different temperatures (350℃-550℃) and gas pressures (0.15MPa-0.6MPa) and detected and analyzed the thermal decomposition products by Gas Chromatography-Mass Spectrometry (GC-MS), and found that the thermal decomposition of 6%C4F7N-94%CO_2 gas mixture started to generate C_3F_6 and CO. Spectrometry (GC-MS) was used to detect and analyze the thermal decomposition products, and it was found that the onset temperature of thermal decomposition of the 6%C_4F_7N-94%CO_2 gas mixture to generate C_3F_6 and CO was 350°C (0.15 MPa), and these two by-products could be used as characteristic products to characterize the early superheated failure. In addition, CF_4, C_3F_6, C_2F_6 could be detected, CF_3CN, COF_2, and $(CN)_2$ decomposition products, among which the production of C_3F_6 and $(CN)_2$ increases with increasing temperature (below 450°C) and then decreases at 500°C. The decomposition products of C_3F_6, C_3F_8, and $(CN)_2$ are also detected. The generation of CO, C_3F_8, COF_2 and CF_3CN increased with increasing temperature; CF_4 and C_2F_6 started to be generated at temperatures higher than 500°C, and these two products can be used as the characteristic products to characterize the severe overheating faults; increasing the air pressure can reduce the decomposition of C_4F_7N in the gas mixture to a certain extent, and the generation of most of the by-products decreased with the increase of the air pressure. The C_4F_7N-CO_2 gas mixture at high gas pressure (>0.3 MPa) shows better thermal stability and decomposition characteristics [69]. Zhang' s team at the Institute of Electrical Engineering, Chinese Academy of Sciences (IEEE, CAS) carried out thermal decomposition tests on a 10% C_4F_7N-90% CO_2 gas mixture (0.3 MPa) at 200°C-700°C (6 h), and found that C_4F_7N started to decompose at 550°C, and CHF_3, C_2F_4, CF_3CN, and CNCN were generated; in addition, HF is one of the main thermal decomposition byproducts of C_4F_7N-CO_2 gas mixture, and a large amount of HF is one of the major thermal decomposition byproducts of C_4F_7N-CO_2 mixture. In addition, HF is one of the main thermal decomposition by-products of C_4F_7N-CO_2 gas mixture, and a large amount of HF gas will react with the inner wall of the stainless-steel gas

chamber, which may reduce the service life of gas-insulated electrical equipment. Therefore, the inner wall of the gas chamber of GIL or GIS needs to be sprayed with an anticorrosive coating or an adsorbent capable of adsorbing HF is placed inside the gas chamber, and the moisture content inside the equipment should be strictly controlled in order to prevent the generation of excessive HF gas in case of overheating faults in C_4F_7N-CO_2 gas mixture equipment [70].

(2) Decomposition characteristics of C_4F_7N gas mixture under discharging fault conditions

Typical discharging faults include insulation breakdown (spark discharge), partial discharge (PD) and switching arc discharge. Zhang et al. from Xi'an Jiaotong University conducted 2000 breakdown tests on a 13.3%C_4F_7N-86.7%CO_2 gas mixture under a defective pin-plate electrode insulation, recorded the breakdown voltage values, and analyzed the gases and solid by-products generated during the discharge process. It is found that the main gas by-products generated from the decomposition of C_4F_7N-CO_2 gas mixture under multiple frequency breakdown conditions are CF_4, C_2F_4, C_2F_6, C_2F_8, C_3F_6, C_4F_6, C_4F_{10}, HF, CO, CF_3CN, C_2F_3CN, C_2F_5CN, C_2N_2, and HCN, and the insulation strength of most of the decomposition products is lower than that of C_4F_7N. So, the breakdown voltage of the C_4F_7N-CO_2 mixture decreased after multiple breakdowns. By quantitatively measuring CF_4, C_2F_6, C_3F_8 and CO, it was found that the amount of all four products increased with the increase of the number of breakdowns, and the amount of CO was the highest, which reached 4200 ppm after 2000 breakdown tests. 2000 breakdowns resulted in the generation of yellowish powders in the inner wall of the gas and on the surface of the electrodes, and the main compositions of these solid products were Si, Cu, F, and N [71]. The team of Zhang from Wuhan University used a ball-ball electrode to simulate a quasi-uniform electric field to carry out an AC breakdown test on a C_4F_7N-N_2 gas mixture, and found that the products that could be quantitatively analyzed had a high generation of CF_4 and C_2F_6, and black solid material precipitated from the electrode surface [72]. Technicians from Siemens also found solid precipitates on the electrode surface after breakdown of the C_4F_7N-N_2 gas mixture, but no solid precipitates appeared after discharge of the C_4F_7N gas mixture with CO_2 as the background gas [73].

Gao 's team from China Electric Power Research Institute (CEPRI) conducted tests on the breakdown and partial discharge decomposition characteristics of 9%C_4F_7N-91%CO_2 gas mixture under suspended potential partial discharge conditions with different contents of microwater (0ppm, 300ppm, 600ppm, 900ppm, 1200ppm, 1500ppm). The results show that the breakdown voltage of C_4F_7N-CO_2 gas mixture increases with the increase of air pressure

and decreases with the increase of micro water content, and the insulating performance of the gas mixture can be ensured by increasing the air pressure and strictly controlling the water content in the equipment in practical engineering applications [74]. The main decomposition products under the condition of different contents of microwater are CO, CHF_3, CF_4, C_2F_6, C_3F_8, C_2F_4, C_3F_6, C_4F_8, $(CN)_2$, and CF_3CN; when the microwater content is less than 1219 ppm, the generation of all the decomposition products increases with the increase of the microwater content; when the microwater content reaches 1647 ppm, the CF_4, $(CN)_2$, CHF_3 production increased exponentially with the increase of microwater content; the effective gas production rates of CF_4, C_2F_6, C_2F_4, C_3F_6, CHF_3, CNCN and CF_3CN were positively correlated with the microwater content, and the microwater in the equipment promoted the decomposition of the C_4F_7N-CO_2 gas mixture. In addition, the ratio of the production of decomposition products under different contents of microwater can be used as an evaluation index of the severity of discharge faults [75]. Tu 's team at North China Electric Power University also used suspended potential simulation equipment within the PD to carry out discharge decomposition tests on a 5%C_4F_7N-95%CO_2 gas mixture at 0.25 MPa gas pressure, and among the several major decomposition products of CF_4, C_2F_6, C_3F_8, and CF_3CN, the relative amount of generation of C_2F_6 remained basically unchanged with the increase of discharge time, and the amount of generation of C_2F_6 and C_3F_8 showed a nonlinear increase [74]. generation showed a nonlinear increase [76].

Simka, a technical expert from ABB, carried out a partial discharge decomposition test on a C_4F_7N-CO_2 gas mixture containing 4% C_4F_7N at 0.1 MPa gas pressure for 23 days, and analyzed the decomposition products qualitatively and quantitatively by combining two detection methods, GC-MS and FTIR, and the decomposition under the action of the PD resulted in the formation of various by-products such as CO, CF_4, C_2F_6, C_3F_8, C_3F_6, C_4F_6, C_4F_{10}, 2-C_4F_8, COF_2, C_2F_4O, CF_3H, CF_3CN, and C_2F_5CN, and many other by-products [77]. Zhang 's team at the Institute of Electrical Engineering, Chinese Academy of Sciences mixed C_4F_7N with three different background gases (CO_2, N_2, and Air) to carry out an IF partial discharge test, and qualitatively and quantitatively analyzed the correlation properties of the buffer gases with the decomposition components, and found that the main products of the decomposition of the binary gas mixture discharge of C_4F_7N include CO, CF_4, C_2F_6, C_3F_8, C_3F_6, and C_2F_4, C_4F_{10}, CO_2, C_2N_2, CF_3CN, and C_2F_5CN, and the C_4F_7N-CO_2 gas mixture discharge decomposition generates the O product $C_2F_6O_3$, and the generation of CO_2 after the discharge of the C_4F_7N gas mixture with Air as the background gas is much higher than that of the binary mixture with N_2 as the background under the same conditions, and the generation

of more CO under the condition of CO_2 as the background needs to be close attention; compared with other binary gas mixtures, C_4F_7N-N_2 gas mixtures generate more fluorocarbons and nitrile gas products, and the generation of these two types of products has a smaller correlation with the C_4F_7N content [78, 79].The generation of saturated halogenated hydrocarbons in the C_4F_7N-Air gas mixtures under the action of PD increases with the externally applied voltage and the C_4F_7N content, which showing a positive correlation; CHF_3 can be used as a characteristic product to characterize the severity of discharge faults [80]. The results of the PD test for C_4F_7N-N_2 gas mixture under micro-hydraulic conditions showed that with the increase of the water content in the gas mixture, the generation of CO_2 gradually increased and saturated, the generation of fluorocarbon gas products firstly decreased and then increased, and the total generation of several products that can be quantitatively analyzed increased slowly and continuously, and solid precipitates were found on the surface of the electrodes at the end of the discharge test, whose main components were C, N, and CHF_3. Solid precipitates were found on the surface of the electrode at the end of the discharge test, whose main constituent elements were C, N and F. Fe and Cr elements appeared in the solid precipitates when the moisture content was further increased [81].

For the decomposition of C_4F_7N gas mixture under the action of switching arc, Radisavljevic, a technical expert of ABB, carried out arc opening and its decomposition characterization tests on C_4F_7N-O_2-CO_2 gas mixture containing 9.5% C_4F_7N (9.5% O_2) on a high-voltage circuit breaker with a filling pressure of 0.5 MPa, and the gas mixture increased by 0.15 MPa (of which 0.11 MPa increase in air pressure comes from the decomposition of C_4F_7N) after 18 current opening tests. After 18 breaking tests, the arc extinguishing chamber of the air pressure increased by 0.15MPa (of which 0.11MPa increase in air pressure comes from the decomposition of C_4F_7N); from the gas chromatogram obtained from the GC-MS analysis given in Figure 1.5 can be seen that the C_4F_7N mixture of gases after the opening of the CO will be generated, CF_4, C_2F_4, C_2F_6, C_3F_6, C_3F_8, CF_3CN, C_2F_5CN and C_2N_2 products, and COF_2 was detected by FTIR supplementation [82].

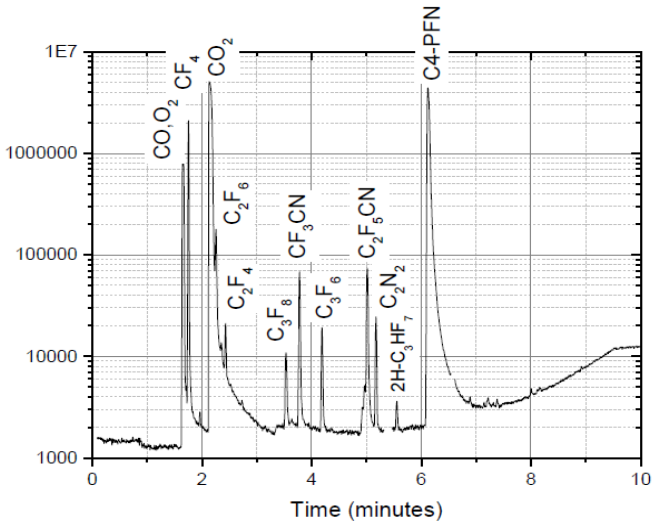

Fig 1.5 Gas chromatogram of C_4F_7N-CO_2-O_2 gas mixture after arc extinguishing [82]

Table 1.2 Analysis of gas components after breaking of 145kV GIS [66]

Components	CAS	Percentage (%)	Concentration (ppm)
CO_2	124-38-9	88.05	880500
$(CF_3)_2CFCN$	42532-60-5	5.52	55200
O_2	7782-44-7	4.25	42500
CO	630-08-0	1.91	19100
C_nF_{2n+2}(CF_4, C_2F_6, C_3F_8)	-	0.2228	2228
CF_3-CF_2-CF_2-CN	375-00-8	0.0037	37
CF_3-CF_2-CN	442-04-08	0.0035	35
CF_2=CF_2	116-14-3	0.0011	11
CF_2=CF-CF_3	116-15-4	0.0022	22
CF_3-NH-CO-CN	NA	0.0015	15
CF_3-CN	353-85-5	0.012	120
CN-CN	460-19-5	0.002	20
COF_2	353-50-4	0.0166	166
CF_2=CF-CN	433-43-2	0.0038	38
$(CF_3)_2C$=CF_2	382-21-8	0.00012	1.2

Meyer et al. developed a test circuit breaker (145kV/40kA) with 6%C_4F_7N-5%O_2-89%CO_2 gas mixture as insulation and arc extinguishing medium according to IEC standard to study the arc extinguishing and decomposition characteristics of C_4F_7N-CO_2-O_2 mixture [66], the test circuit breaker was used to insulate and disconnect with the minimum pressure set at 0.75MPa. The results show that the addition of 5% O_2 can inhibit the generation of gas and solid by-products of the C_4F_7N gas mixture under the action of high-energy arc to a certain extent. The gas decomposition by-products generated after the 40 kA short-circuit current test are CO, CF_4, C_2F_6, C_3F_8, CF_3CN, C_2F_5CN, $(CN)_2$, COF_2, C_2F_4, and C_3F_6, except CO, CF_4, C_2F_6, and C_3F_8, the gas by-products range from 1 ppm to 200 ppm (shown in Table 1.2), and this type of GIS was piloted in Switzerland and Francis in 2017-2018 [83], which also

confirmed the potential of the 6%C_4F_7N-5%O_2-89%CO_2 gas mixture in high-pressure equipment. Zhang et al. found through his research that the generation of decomposition products of the 5%C_4F_7N-6%O_2-89%CO_2 gas mixture after switching off a 25kA current increases with the number of switching off, and that an increase in switching off current leads to an increase in the generation of decomposition products, but the type of products does not change; in addition, it was also found that the O_2 inhibits to a certain extent the decomposition of the C_4F_7N, the Cyanide production also decreases, but CO_2 production increases, and the addition of O_2 can inhibit carbon deposition at the nozzle [67].

At present, experimental studies on the decomposition characteristics of C_4F_7N gas mixture under discharge and overheating faults have shown that the decomposition of C_4F_7N gas mixture under fault conditions generates many by-products, and the addition of O_2 can inhibit the generation of gases and solid by-products in the process of arc breaking to a certain extent. However, little research has been done on the influence of O_2 on the decomposition characteristics of C_4F_7N gas mixture under discharge fault (breakdown, PD) and overheating fault (POF) conditions, and the correlation between different influencing factors and fault severity and decomposition characteristics is not yet clear.

(3) Decomposition mechanism of C_4F_7N gas mixture

When studying the discharge plasma composition of a gas insulating medium, it is necessary to use minimum Gibbs free energy calculations to obtain the discharge plasma composition, considering that the reactive system is in a local thermodynamic equilibrium state under the high temperature conditions generated during the high-current turn-on and turn-off process [84]. The team of Rong of Xi'an Jiaotong University calculated the thermophysical parameters such as the components, thermodynamic properties, transport coefficients and net radiation coefficients of the plasma in the localized thermodynamic equilibrium state of the C_4F_7N and C_4F_7N-CO_2 gas mixtures in the range of 300 K-30,000 K [85]. In addition, the rapid decay of the arc temperature and the low-temperature region at the arc boundary will deviate from the thermodynamic and chemical equilibrium states, and the dynamic properties of the plasma components in the non-thermodynamic equilibrium state need to be investigated by chemical kinetics methods [86, 87]. Li et al. used a chemical kinetic model for the C_4F_7N arc plasma in the arc boundary region to further refine the decomposition paths and transition states of C_4F_7N, and calculated the reaction rate constants according to the variational transition state theory, which showed that the relaxation time of the decomposition of C_4F_7N depended on the temperature, and that the reaction barriers limited the reaction when the temperature was lower than 1000 K. This proved that chemical kinetic calculations are

necessary to study the C_4F_7N plasma composition at lower temperatures or in the arc boundary region [88]. Zhong et al. from Southeast University calculated the arc plasma properties, including equilibrium components, thermodynamic properties, transport parameters, and net radiation coefficients, of C_4F_7N binary gas mixtures with CO_2 and N_2 as the background gases, respectively, and found that the decomposition of C_4F_7N gas mixtures in a high-temperature arc could not be recovered by either background gas, and the addition of the background gases gradually eliminated the peaks of the constant-pressure specific heat capacity and mass density product peak, and the C_4F_7N gas mixture with CO_2 added had a greater pre-dielectric recovery than the mixture with N_2 added [89]. Yokomizu et al. from Nagoya University, Japan, calculated the equilibrium state components of the C_4F_7N-CO_2-O_2 gas mixture in the range of 300K-20000K, and analyzed the generation mechanism of solid by-products during the discharge process [90].

The study of the decomposition mechanism of C_4F_7N gas mixture under fault conditions can also be calculated by quantum chemical methods, firstly, the reaction system of the system is constructed according to the fault conditions and different influencing factors, and then the microscopic parameters of the individual particles in the reaction system and their constitutive reaction paths are calculated based on the Density Functional Theory (DFT) and Transition State Theory (TST) to calculate the microscopic parameters of the individual particles in the reaction system and their constitutive reaction paths [91-93], and to study the effects of different influencing factors on the decomposition of the C_4F_7N gas mixture and the generation paths of its characteristic products. Alternatively, the distribution and evolution laws of particles in the reaction system under different influences can be obtained based on the reactive molecular dynamics approach, which describes the breaking and formation of molecular chemical bonds by using the bond levels of the chemical bonds in the reactive force field [94].

Zhang et al. from Wuhan University calculated the decomposition mechanism of C_4F_7N in the presence of trace moisture based on density functional and transition state theories, including the enthalpies, Gibbs free energies, and activation energies of different dissociation paths of C_4F_7N, and revealed the generation of the decomposition products and the mechanism of the influence of trace moisture on the decomposition of C_4F_7N. The results show that the C-C and C-F bonds connected with the C atom at the center of the C_4F_7N molecule are easily broken under the action of high-energy electric field or superheat fault, and the particles generated from the dissociation of C_4F_7N can be partially recovered to generate C_4F_7N molecules, which ensures that the insulating properties of the mixture of gases will not change significantly; under the condition of trace moisture, the presence of H and OH accelerates the

reaction of the decomposed particles of C_4F_7N and generate by-products such as CF_3H, CF_2O, C_3F_7H, C_3F_7OH, CF_3CFHCN and CH_2FCN, thus inhibiting the recovery process of C_4F_7N. The ionization parameters of products such as CF_3OH and CF_2O are relatively weak, and the formation of these by-products will further reduce the dielectric strength of the medium in the defective region, and under long-term operating conditions, the large generation of these by-products may lead to serious insulation failures [95]. Fu et al. from Xi'an University of Science and Technology constructed a reaction system through 16 possible dissociation paths of C_4F_7N, and studied the decomposition mechanism of C_4F_7N by using the B3LYP/6-311G (d, p) method combined with the transition state theory, and calculated the reaction rate constants of all the paths from 300 K to 3500 K. It was found that the dissociation of C_4F_7N through one transition state generates the reaction rate constants for the formation of FCN and CF_2CFCF_3 is the most dominant reaction process leading to the dissociation of C_4F_7N at less than 600 K [91].

For larger reaction systems composed of molecules with complex structures, molecular dynamics methods are suitable to calculate their chemical reaction processes. Zhang's team from Wuhan University studied the distribution of decomposed particles of C_4F_7N-CO_2 gas mixture based on the combination of the ReaxFF reaction molecular dynamics (MD) and quantum chemistry, and pointed out that the decomposition rate and decomposition amount of C_4F_7N increased with the increase of temperature, in which the three types of radical particles, namely CF_3, CN and F, had the highest content, and the addition of CO_2 had a certain buffering effect, which could reduce the decomposition rate of C_4F_7N in the system. It was pointed out that the decomposition rate and amount of C_4F_7N increased with the increase of temperature, in which the content of CF_3, CN and F radical particles was the highest, and the addition of CO_2 had a certain buffering effect, which could reduce the decomposition rate of C_4F_7N in the system [96]. Wang 's team carried out MD simulations of C_4F_7N-CO_2 gas mixture around 3000 K. The results showed that the buffer gas CO_2 consumed the F and CF_3 radicals, which led to a significant difference in the time evolution of CF_4 and FCN. Based on the MD simulations of the C_4F_7N-CO_2-H_2O system, it was found that the species of the main products remained unchanged, but the amount of CO was affected by the OH and H radicals, and several hydrides such as HF, CHF_3, and C_3HF_3 were generated simultaneously [97].

On the whole, some progress has been made on the decomposition characteristics and mechanism of C_4F_7N-CO_2 gas mixture, and the experimental study mainly includes the decomposition characteristics under electric and thermal failure conditions, and the change rule of decomposition products with the influencing factors; and the simulation calculation

mainly includes the construction of the decomposition paths, the calculation of reaction thermodynamic parameters, and the simulation calculation of plasma components and molecular dynamics of the arc discharge, etc. However, after considering the addition of O_2, the decomposition characteristics and mechanism of C_4F_7N-CO_2-O_2 mixture are relatively scarce. However, the decomposition characteristics and mechanism of C_4F_7N-CO_2-O_2 gas mixture after considering the addition of O_2 is relatively scarce, including the composition of the decomposition products under electric and thermal faults and the change rule of the amount of generation with the content of O_2 and other influencing factors, the kinetic analysis of the influence of O_2 on its decomposition of the particle distribution characteristics and the rate of production, and the construction of the path of the decomposition of C_4F_7N and the generation of the products under the conditions of the reaction with the participation of O_2 and the calculation of its thermodynamic parameters. and its thermodynamic parameters calculation.

1.2.3 Biosafety of C_4F_7N gas mixture

Considering that equipment production, operation and maintenance personnel inevitably need to come into contact with the gases in the equipment during installation and maintenance, and that electrical and thermal failures of the equipment can induce the decomposition of the gases to produce a variety of products, and some of the decomposition products have strong toxicity. Therefore, it is necessary to carry out an in-depth study on the biosafety of the C_4F_7N gas mixture and its decomposition products before large-scale popularization and application, to determine the types of toxicity products that need to be monitored in the engineering application and the safety threshold, and to put forward effective public health protection measures, so as to avoid public safety problems caused by the leakage of harmful gases in the equipment or the non-safe exposure of personnel.

The acute and repeated dose inhalation toxicity of C_4F_7N was investigated by 3M, which indicated that the 4h acute inhalation LC50 of C_4F_7N in rats ranged from 10,000-15,000 ppm; the repeated dose inhalation toxicity: 6 hours of inhalation per day in a 4-week (1 week, 5 days) test No observed adverse effect level (NOAEL) of 500 ppm and occupational exposure limits (OEL) of 65 ppm were obtained [38]. Kieffel et al. indicated that C_4F_7N content of 4%, 10% of the C_4F_7N/CO_2 gas mixtures with 4% and 10% C_4F_7N content had LC50s (rat, 4 h) of 190000 and 100000 ppm, respectively [38]. In 2018, Zhang 's team at Wuhan University took the lead in conducting toxicity tests on rats with 4h and 12h acute inhalation of C_4F_7N gas, and analyzed the effects of the gas on the target organs of the organism through the key symptoms, blood cell counts, and pathology sections of the rats after the contamination. The results showed that inhalation of C_4F_7N gas may cause abnormal blood cell counts and damage

to lungs, kidneys, intestines and brain tissues in rats [98].

The conclusions of related studies confirm the acute toxicity of pure C_4F_7N gas to rats, but few toxicity data related to the acute inhalation of pure C_4F_7N gas in mice have been reported. In order to protect the safety and health of people exposed to pure C_4F_7N gas, an accurate and comprehensive assessment of the biosafety of C_4F_7N gas is needed, which requires the use of different strains of animals (at least two or more) for biosafety studies, and it is not sufficient to assess the data from acute inhalation experiments in rats alone. Meanwhile, the acute inhalation toxicity study of C_4F_7N is not comprehensive enough, such as the effects of gender differences on LC50, mortality and time to death of the test animals after exposure, the recovery characteristics of the surviving test animals, and the duration of the toxic effects of C_4F_7N in the test animals are still lacking in the relevant reports.

In addition, due to the more complex molecular structure of C_4F_7N, its stability and recovery characteristics are weaker than SF_6, the high-energy arc discharge generated in the process of arc breaking will cause C_4F_7N decomposition to generate a large number of gases and by-products. On the one hand, the arc extinguishing and insulating properties of the decomposition products are weaker than those of C_4F_7N, which will affect the arc extinguishing and insulating properties of the C_4F_7N gas mixture after arc breaking, on the other hand, some of the products are more acutely toxic than C_4F_7N, and a large number of gaseous by-products generated by the decomposition of C_4F_7N will lead to significant changes in the toxicity of the mixed gases, which will pose a threat to the health of the operation and maintenance personnel. Therefore, it is necessary to study the acute toxicity of the decomposition products of C_4F_7N gas mixture after arc extinguishing, to determine its toxicity classification, and to propose the necessary emergency protective measures. However, few studies have been reported on the biosafety of C_4F_7N gas mixture after arc opening.

1.2.4 The engineering application examples of C_4F_7N gas mixture

For engineering applications, General Electric (GE) introduced new 145 kV GIS, 420 kV GIL and 245 kV CT with C_4F_7N gas mixture as insulation medium in 2016 [41]. Among them, the new GIS is designed and manufactured according to IEC 62271-203 standard and has passed the type test, in addition, the isolation switch and earthing switch have also passed the special test; the 420 kV GIL and 245 kV CT with C_4F_7N gas mixture have also successfully passed the relevant tests of IEC 62271-102 and IEC 61869. Currently, the above equipment has been tested and commissioned in Frankfurt, Wright, and other European regions. In 2017, Axpo Power AG, together with distribution system operator EKZ, installed the world's first 123kV GIS filled with a C_4F_7N-CO_2-O_2 gas mixture near Lake Zurich, Switzerland, and

passed the on-site acceptance test (shown in Fig. 1.6) [83].

Fig 1.6 123kV C_4F_7N-CO_2-O_2 gas mixture GIS substation [83]

Comprehensively, the current domestic and international research on the insulation, arc extinguishing and decomposition characteristics of C_4F_7N gas mixture has achieved certain results, which basically confirms that the C_4F_7N gas mixture has good performance and can meet the application requirements of various types of medium- and high-voltage gas-insulated equipment. Meanwhile, it has been shown that the addition of O_2 as a second buffer gas to C_4F_7N-CO_2 gas mixtures can improve their arc breaking capacity and reduce the generation of gas and solid by-products (carbon particles) [66]. Although the addition of O_2 can bring the aforementioned advantages for the application of C_4F_7N gas mixtures in switchgear, the effect of O_2 on the stability of C_4F_7N gas mixtures under electrical and thermal fault conditions must be re-examined and evaluated, considering that O_2 is strongly oxidizing and C_4F_7N gas mixtures should be chemically stable under actual operating conditions. However, at this stage, there are fewer reports on the effects of O_2 on the insulating properties and the electrical and thermal decomposition of C_4F_7N-CO_2 gas mixtures, and the biosafety of C_4F_7N gas mixtures and their decomposition products, and the optimal amount of O_2 added to the C_4F_7N-CO_2-O_2 gas mixture has yet to be investigated; at the same time, the effect of O_2 on the stability of the C_4F_7N-CO_2-O_2 gas mixture in the presence of different fault conditions and different influencing factors has yet to be investigated. At the same time, there is a lack of systematic research on the decomposition characteristics of C_4F_7N-CO_2-O_2 gas mixture under different fault conditions and influencing factors, and the correlation between fault conditions and influencing factors and the type, content and gas production rate of the decomposition products are not yet clear. In addition, residents in the production, operation and maintenance of the equipment and the installation area are exposed to the risk, and the decomposition of the gas to generate a variety of by-products can be induced by electrical and thermal faults in the

equipment, so it is urgent to clarify the biosafety of the C_4F_7N gas mixture before its large-scale popularization and application in order to avoid the public safety problems caused by the leakage of hazardous gases in the equipment or the unsafe exposure of the personnel.

Although foreign electrical equipment manufacturers have designed, manufactured and test run some of the equipment with C_4F_7N-CO_2-O_2 gas mixture as the insulating medium, it is still in the stage of testing and optimization, and our country's current design experience for environmentally friendly gas-insulated equipment is relatively weak. In order to break the monopoly of foreign technology and realize the localization and manufacture of environmentally friendly gas insulating equipment, it is necessary to thoroughly study the insulating properties, fault decomposition characteristics and biological safety of C_4F_7N-CO_2-O_2 gas mixture, and to provide important theoretical and practical support for the design, material selection, optimization and safe application of C_4F_7N-CO_2-O_2 gas mixture insulating equipment, so as to reduce the SF_6 emission in various industries. The researchers will contribute to the manufacture and upgrading of environmentally friendly gas-insulated equipment to curb global warming.

1.3 Thesis research content and chapter organization

1.3.1 Main contents

At present, researchers at home and abroad for the environmental protection insulation gas C_4F_7N-CO_2 related properties of the research has been more perfect, but with the gas insulation equipment safety and stable operation requirements gradually improved, environmental protection insulation gas C_4F_7N-CO_2-O_2 has become the optimal choice to replace the SF_6 used in various types of medium and high voltage gas insulation equipment, about the C_4F_7N-CO_2-O_2 gas mixture of insulating properties and decomposition characteristics under different fault conditions and the mechanism and safety applications need to be further researched. The insulating properties of C_4F_7N-CO_2-O_2 gas mixture and the decomposition characteristics under different fault conditions, as well as the mechanism and safety applications need to be further studied. This paper focuses on the insulation and decomposition characteristics of C_4F_7N-CO_2-O_2 gas mixture under different influencing factors and electrical and thermal faults, as well as biosafety, and the main research contents are as follows:

(1) The thermal decomposition model of C_4F_7N-CO_2-O_2 gas mixture was constructed to simulate the ReaxFF reaction molecular dynamics, to obtain the composition, distribution and generation rate of the thermal decomposition particles of the mixture with different O_2 contents

and temperatures; at the same time, the thermal decomposition simulation platform was utilized to experimentally explore the thermal stability of the mixture, and the effects of temperature and O_2 content on the composition of the thermal decomposition products of the mixture and their generation amount were analyzed. O_2 content on the composition of the thermal decomposition products and their production rate. The combination of simulation and experimental results reveals the thermal decomposition mechanism of the C_4F_7N-CO_2-O_2 gas mixture and the influence of O_2 on the evolution characteristics of the thermal decomposition particles of the mixture.

(2) A test platform for PD and its decomposition characteristics, to carry out tests on the PD and decomposition characteristics of C_4F_7N-CO_2-O_2 gas mixture under different O_2 contents and applied voltages, to summarize the influences of different factors on the PD statistical characteristics of C_4F_7N-CO_2-O_2 gas mixture, and to analyze the influences of O_2 and applied voltage on the PD and decomposition characteristics of C_4F_7N-CO_2-O_2 gas mixture. The influence mechanism of O_2 and externally applied voltage on the PD and decomposition characteristics of C_4F_7N-CO_2-O_2 gas mixture. The composition and content of solid precipitates generated during the PD process were tested at the microscopic level to analyze the generation mechanism and the influence of O_2 on their generation.

(3) An industrial frequency breakdown and decomposition test platform was constructed to test the AC breakdown voltage of C_4F_7N-CO_2-O_2 gas mixtures with different O2 contents as well as the changes in the composition and content of decomposition products, and the mechanisms of the influence of O_2 on the insulating strength and breakdown and decomposition characteristics of the gas mixtures were discussed. The additional reaction path of C_4F_7N due to the addition of O_2 is proposed, and the related reaction enthalpies and activation energies are calculated based on the density-functional theory (DFT) and the transition state theory (TST), to further analyze the discharge decomposition mechanism of C_4F_7N and the generation mechanism of O-containing products under the conditions of O_2 participation in the reaction.

(4) Summarize the effects of different O_2 contents on the decomposition characteristics of C_4F_7N-CO_2-O_2 gas mixture under insulation and electrical and thermal faults, and propose the optimal O2 additions of C_4F_7N-CO_2-O_2 gas mixture for medium-voltage gas-insulated equipment. On the basis of the decomposition characteristics, the characteristic quantities that can characterize the type and severity of faults within the equipment are extracted, which can provide a reference for the fault diagnosis and operation and maintenance strategy of C_4F_7N-CO_2-O_2 gas mixture equipment. The toxicity test of C_4F_7N and its arc decomposition products

was carried out in mice by acute inhalation, and its biological safety was evaluated by obtaining its LC50, toxicity classification, and effects on the mice's body. Based on the relevant simulation and test results, the feasibility and safety of C_4F_7N-CO_2-O_2 gas mixtures applied to equipment were comprehensively evaluated.

1.3.2 Research ideas and technical lines

The technology roadmap adopted in this paper is shown in Figure 1.7, and the specific research ideas are as follows:

Aiming at the mechanism of thermal decomposition of C_4F_7N-CO_2-O_2 gas mixture, firstly, we constructed a model of the reaction system of C_4F_7N-CO_2-O_2 gas mixture, and carried out the simulation of thermal decomposition process under different O_2 contents and different temperatures based on the molecular dynamics method of the ReaxFF reaction, and analyzed the effects of O_2, temperature, and simulation time on the composition, distribution, and reaction rate of the particles of the thermal decomposition of C_4F_7N-CO_2-O_2, to reveal the evolution mechanism of the kinetic process of thermal decomposition and its product particles under different conditions. Analyze the influence of O_2 and simulation time on the composition, distribution and reaction rate of C_4F_7N-CO_2-O_2 thermal decomposition particles, and reveal the kinetic process of C_4F_7N-CO_2-O_2 thermal decomposition and the evolution mechanism of its product particles under different conditions. A thermal decomposition test platform was built to carry out the thermal decomposition test of C_4F_7N-CO_2-O_2 gas mixture, to obtain the composition of the decomposition products and the rule of change of the amount of decomposition products under different O_2 content and superheating temperature. Finally, the mechanism of thermal decomposition of C_4F_7N-CO_2-O_2 gas mixture was clarified by combining simulation and experimental results.

For the insulation and discharge decomposition characteristics of C_4F_7N-CO_2-O_2 gas mixture, we set up an AC breakdown and partial discharge decomposition test platform to carry out the discharge and decomposition characteristics test of the gas mixture. For the frequency breakdown test, the influence of O_2 content and the number of breakdowns on the breakdown voltage of the gas mixture, its dispersion and the composition and content of the decomposition products are analyzed; for the partial discharge decomposition test, the characteristic coefficients of the PD signals are extracted by using MATLAB, and the phase resolved partial discharge (PRPD) maps are constructed, and the discharge repetitions are statistically calculated. To analyze the influence mechanism of O_2 and applied voltage on the PD characteristics and the composition and content of decomposition products of C_4F_7N-CO_2-O_2 gas mixture by counting the parameters of discharge repetition rate, average apparent

discharge and cumulative discharge per unit time, to characterize the microscopic morphology and elemental composition of solid precipitates generated in the PD process, and to summarize and analyze the correlation between PD and decomposition characteristics, and to reveal the influence of O_2 content on the composition and content of decomposition products of C_4F_7N-CO_2-O_2 gas mixture by using MATLAB to extract the characteristic parameters of PD signal and construct PRPD (Phase resolved partial discharge). We summarize and analyze the correlation between PD and decomposition properties, and reveal the mechanism of O_2 content on the generation and inhibition of gas and solid by-products during the discharge decomposition of C_4F_7N-CO_2-O_2 gas mixture. Based on the density functional theory (DFT) and transition state theory (TST), the relevant reaction enthalpies and activation energies were calculated to further analyze the discharge decomposition mechanism of C_4F_7N and the generation mechanism of O-containing products under the conditions of O_2 participation.

Finally, based on the simulation and experimental results, we summarize and analyze the influence of O_2 content on the insulation and decomposition characteristics of C_4F_7N-CO_2-O_2 gas mixture under discharge and overheating faults, and propose the optimal O_2 additive amount of C_4F_7N-CO_2-O_2 gas mixture for medium-voltage gas-insulated equipment, taking into account the actual operating conditions of the equipment as well as the safety of operation and maintenance personnel. The correlation between the fault conditions and influencing factors and the types and contents of decomposition products is summarized, and the characteristic products that can characterize the types of equipment faults and their severity are extracted, which can be used as a reference for the diagnosis of faults and operation and maintenance strategies of C_4F_7N-CO_2-O_2 gas mixture equipment. The toxicity test of C_4F_7N and its arc decomposition products was carried out in mice by acute inhalation, and its biological safety was evaluated by obtaining its LC50, toxicity classification, and effects on the mouse body. Finally, the feasibility and safety of C_4F_7N-CO_2-O_2 gas mixtures applied to equipment were jointly evaluated by synthesizing the insulation and fault decomposition properties and biosafety.

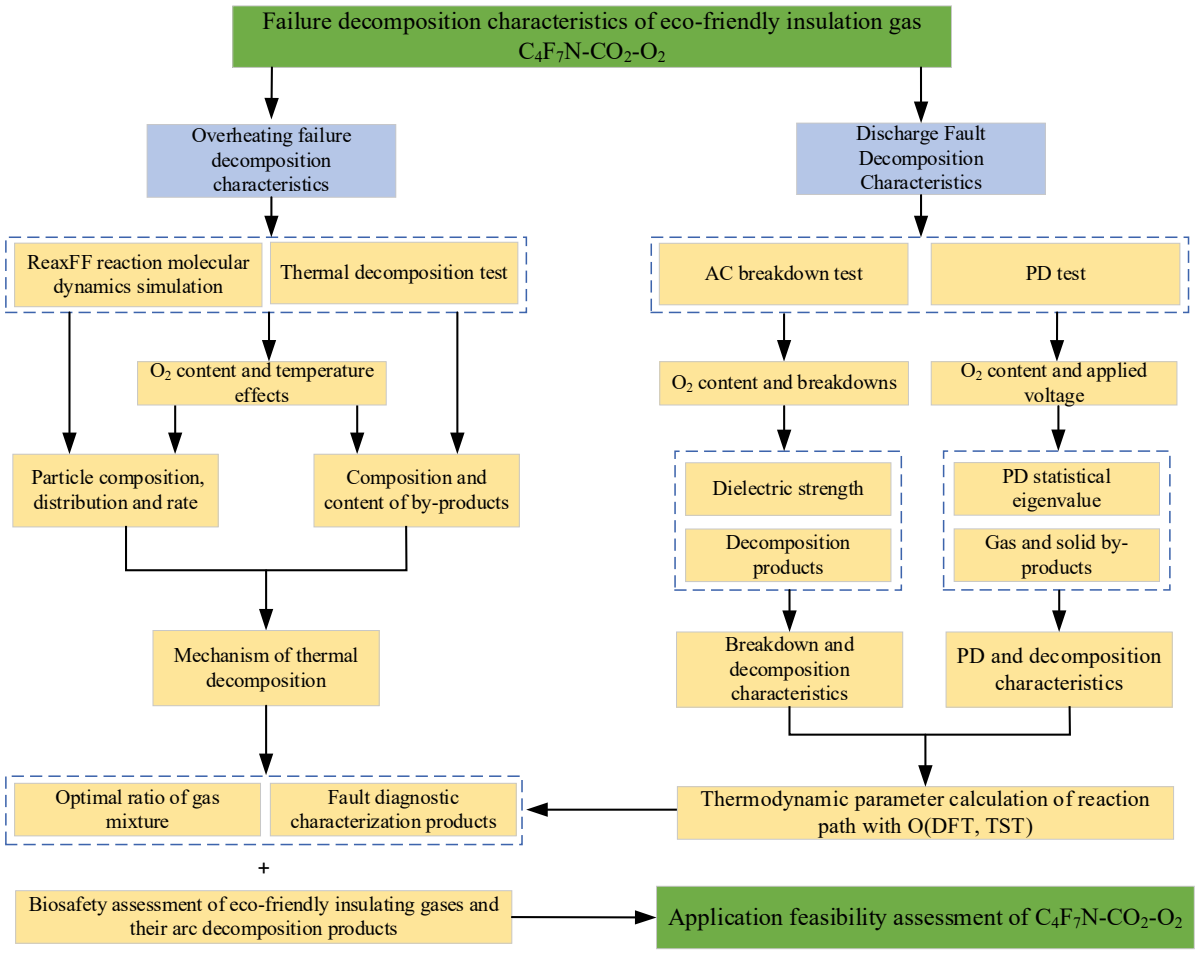

Figure 1.7 Technical roadmap for this article

1.3.3 Thesis structure and chapter organization

The main contents of this paper include the following six chapters:

Chapter 1 introduces the research background and significance of eco-friendly insulating gases, reviews the current research status of eco-friendly insulating gases, focuses on the insulation and arc extinguishing performance, fault decomposition characteristics, biosafety and engineering application cases of C_4F_7N gas mixture, and puts forward the main research contents and technical routes of this paper.

Chapter 2 constructs a model of C_4F_7N-CO_2-O_2 gas mixture reaction system, carries out the simulation of thermal decomposition process based on the reaction molecular dynamics method with different O_2 content and different temperatures, and analyzes the influence of O_2, temperature and simulation time on the composition, distribution and reaction rate of C_4F_7N-CO_2-O_2 thermal decomposition particles. Carry out the thermal decomposition test of C_4F_7N-CO_2-O_2 gas mixture under different O_2 contents and temperatures, and reveal the thermal decomposition mechanism of C_4F_7N-CO_2-O_2 gas mixture by combining the simulation results.

In Chapter 3, the PD and decomposition characteristics of C_4F_7N-CO_2-O_2 gas mixture

under different O_2 contents and applied voltages are carried out to summarize the influence mechanisms of different influencing factors on the PD statistical parameters of C_4F_7N-CO_2-O_2 gas mixture, analyze the correlation characteristics of the influencing factors with the PD of the mixture and its decomposition characteristics, and test the components and contents of the solid precipitates produced in the process of the discharge at the micro level to analyze the solid precipitates produced in the process. The components and contents of the solid precipitates generated during the discharge process are tested at the microscopic level, and the mechanism of their generation and the influence of O_2 on their generation are analyzed.

In Chapter 4, the AC breakdown voltage of C_4F_7N-CO_2-O_2 gas mixtures with different O_2 contents and the composition and content of their decomposition products are tested to analyze the influence of O_2 on the insulation strength, breakdown voltage dispersion and decomposition product generation of the gas mixtures. The additional reaction path of C_4F_7N due to the addition of O_2 is proposed, and the related reaction enthalpies and activation energies are calculated based on the density functional and transition state theories, to further analyze the discharge decomposition and O-containing product generation mechanism of C_4F_7N under the conditions of O_2 participation in the reaction.

Chapter 5 summarizes and analyzes the influence of O_2 content on the insulation and decomposition characteristics of C_4F_7N-CO_2-O_2 gas mixture based on the simulation and experimental results under discharge and overheating faults, and proposes the optimal O_2 additive amount of the C_4F_7N-CO_2-O_2 gas mixture for medium-voltage gas-insulated equipment as well as the characteristic products that characterize the type of faults and their severity. The toxicity test of C_4F_7N and its arc decomposition products was carried out in mice by acute inhalation, and its biological safety was evaluated by obtaining its LC50, toxicity classification and effects on the mice's body. The feasibility of applying the C_4F_7N-CO_2-O_2 gas mixture in equipment is comprehensively evaluated by combining its insulation, electrothermal decomposition properties and biosafety results, and recommendations for safe application are given.

Chapter 6 summarizes the research work of this paper and gives an outlook on the subsequent research work.

Chapter 2. Characteristics of thermal decomposition of C_4F_7N-CO_2-O_2 and mechanism of product evolution

When there are defects such as poor contact, magnetic saturation or overloading faults within gas-insulated electrical equipment, the thermal stability of the defective parts will be destroyed, which will lead to partial overthermal fault in gas-insulated equipment. These early partial overheating faults can damage the insulation material to varying degrees, accelerating the deterioration of the insulation material, which may ultimately lead to insulation breakdown or ablatio. Therefore, the examination of the thermal stability and thermal decomposition characteristics of gas insulating media is an important part of the assessment of their reliability in application.

In this chapter, the molecular dynamics simulation of the ReaxFF reaction was carried out through the constructed thermal decomposition model of C_4F_7N-CO_2-O_2 gas mixture, and the composition, distribution and generation rate of the particles of thermal decomposition of the gas mixture were obtained at different O_2 contents and temperatures, so as to reveal the mechanism of thermal decomposition of the C_4F_7N-CO_2-O_2 gas mixture and the influence of O_2 on the thermal decomposition of the gas mixture; At the same time, the thermal decomposition characteristics of C_4F_7N-CO_2-O_2 mixture were investigated by using the thermal decomposition test platform, and the effects of temperature and O_2 content on the composition and amount of thermal decomposition products of the mixture were analyzed. Through the combination of simulation and experimental results, the thermal decomposition mechanism of C_4F_7N-CO_2-O_2 mixture was clarified.

2.1 Kinetic modelling of the evolutionary properties of C_4F_7N-CO_2-O_2 thermal decomposition particles

2.1.1 ReaxFF reaction molecular dynamics and force field methods

For reactive systems consisting of large molecules (systems with more than 100 atoms), the reaction process is usually studied using molecular dynamics. The flow chart of the molecular dynamics simulation process is shown in Fig. 2.1, which firstly analyses the initial state of the reaction system, then calculates the interactions of the particles in the reaction system, calculates the velocity and position of the particles in space by solving the Newtonian mechanics equations, and then obtains the relevant parameters of the system and makes macroscopic adjustments to them, and analyses the trajectory evolution of the reaction system [99].

In the molecular dynamics simulation process, the initial structure of the molecule is first

created, then an initial velocity is applied to each atom, and the force, initial coordinates and acceleration of the atoms under this condition are calculated, and then the Newtonian mechanical equations are solved using the finite difference method based on these parameters to obtain the new parameters such as configuration, velocity, and energy, and the cyclic process is executed based on the results of the calculations. The selection of the computational time step is closely related to the nature of the reaction system under study. In general, for simple atomic systems and rigid molecules, the selected time step is 5 to 10 fs; For the reaction system with non-rigid molecules and the breaking and formation of chemical bonds, a time step of 0.1 to 2 fs is suitable. For the modelling of molecular dynamics reaction systems, a certain number of molecules are usually placed in a cubic reaction system with a side length of L. In this way, the density of the reaction system can be obtained based on the mass of the molecules. In order to keep the density of the system constant during the simulation, periodic boundary conditions need to be used.

Although quantum chemical methods can calculate the relevant parameters of chemical reactions relatively accurately, their computational losses are large and unsuitable for large reaction systems, so it is necessary to solve the chemical reaction process of the system by means of an accurate force field. The potential energy between particles in a reacting system is the central parameter for solving the equations of mechanics, and the force field is the conversion of the potential energy into a mathematical expression that can be computed, and the accuracy of the force field depends on the accuracy of the test or calculation. Classical force fields show deficiencies when the particles deviate from the equilibrium position by a large distance during their motion, i.e., when the reaction system particles are involved in bonding and bond breaking processes. In order to accurately describe such chemical reaction processes, reaction force fields such as COMB, MEAM and ReaxFF were created. Compared to the classical force field, the ReaxFF reactive force field proposed by Van Duin et al. 2001 has similarities in energy calculations, but the ReaxFF reactive force field is more complex in describing bonding interactions [100], It is suitable for modelling chemical reaction processes and their thermodynamic and kinetic properties at mesoscopic scales, and is currently widely used in the fields of thermal decomposition of gases, combustion of substances and research and development of new materials. [101]。

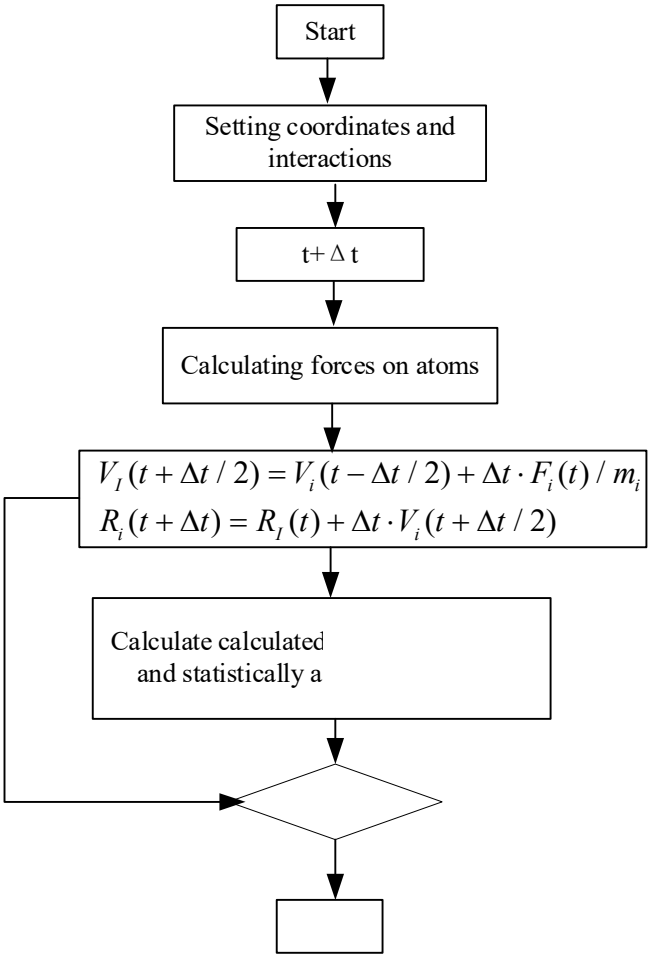

Fig. 2.1 Flow chart of the molecular dynamics simulation process

Conventional force fields describe chemical bonding primarily through bond connectivity，ReaxFF Reaction Molecular Dynamics, it is a method of molecular dynamics simulation using a reactive force field centred on bond levels, and establishes an energy calculation system for reactive systems mainly by describing the correspondence between bond levels and bond energies, and bond levels and bond distances. ReaxFF reaction force field in the bond level BO on the basis of the interaction between atoms in the reaction system is expressed as a function of the bond level, that is, the internal parts of the molecule interaction energy in the form of bond poles to express the energy of the system is expressed as [102]:

$$E_{system} = E_{bond} + E_{over} + E_{angle} + E_{torsion} + E_{vdWaals} + E_{coulomb} + E_{specific} \quad (2.1)$$

in equation (2.1)，E_{system} is the total energy of the system; E_{bond} is the bond energy term between atoms; E_{angle} and $E_{torsion}$ denote the three-bond modified energy term and four-body energy action term, respectively; E_{over} is an over-coordination energy correction term； $E_{vdwaals}$ and $E_{coulomb}$ is Van der Waals action term and Coulomb action term, respectively，The electrostatic and dispersive interactions in the interaction can be described as non-bonding

terms; $E_{specific}$ Usually used for system-specific energy terms such as lone pair electrons, conjugated electrons, hydrogen bonding and C2 correction terms.

The composition and connection of the total energy of the ReaxFF reaction system is shown in Fig.2.2, where the total energy of the system consists of two parts: the energy term related to the bond level and the energy term not related to the bond level. To get the bond energy term E_{bond}， Firstly, the bond level BO_{ij} needs to be calculated, which can be expressed as a function of the interatomic distance r_{ij}, and can be divided into three parts according to the three different types of chemical bonds: σ, π and ππ bonds (shown in Eq. 2.2). In Eq. 2.2, BO_{ij} is the bond level between atoms i and j, r_{ij} is the distance between atoms i and j, the r0 term is the bond length term at equilibrium for different types of bonds, and the pbo term is an empirical parameter term.

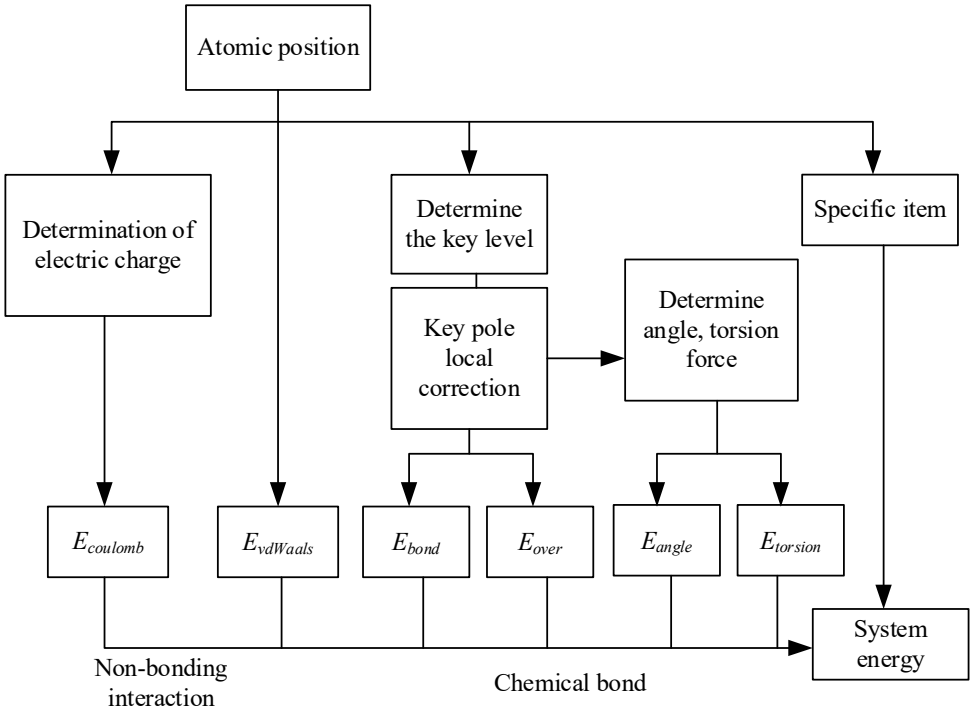

Fig.2.2 Schematic diagram of the components of the total energy composition of ReaxFF

$$BO_{ij}^{'}=BO_{ij}^{'\sigma}+BO_{ij}^{'\pi}+BO_{ij}^{'\pi\pi}$$
$$=\exp\left[p_{bo1}\left(\frac{r_{ij}}{r_0^{\sigma}}\right)^{p_{bo2}}\right]+\exp\left[p_{bo3}\left(\frac{r_{ij}}{r_0^{\pi}}\right)^{p_{bo4}}\right]+\exp\left[p_{bo5}\left(\frac{r_{ij}}{r_0^{\pi\pi}}\right)^{p_{bo6}}\right] \quad (2.2)$$

The actual equilibrium positions of different bonding levels can deviate in the calculation process, and other surrounding atoms can have an effect on their bonding process. At this point it is possible to use the uncorrected atomic over-coordination function $\Delta^{'}$, as shown below：

$$\Delta_i^{'}=-Val_i+\sum_{j=1}^{nerghbours(i)}BO_{ij}^{'} \quad (2.3)$$

Eq. (2.3) where is the uncorrected bond level where Vali is the number of outermost electrons of the i atom.

In order to make the calculated values of bond energies more accurate, it is necessary to further correct the calculated initial bond levels, So the second coordination function that makes the correction process more accurate is introduced $\Delta_i^{'boc}$ (as shown in equation (2.4)),

The specific calibration steps are shown in equations (2.5)-(2.8).

$$\Delta_i^{'boc}=\text{-}Val_i^{boc}+\sum_{j=1}^{nerghbours(i)} BO_{ij}^{'} \tag{2.4}$$

$$BO_{ij}^{\sigma}=BO_{ij}^{'\sigma}\cdot f_1\left(\Delta_i^{'},\Delta_j^{'}\right)\cdot f_4\left(\Delta_i^{'},BO_{ij}^{'}\right)\cdot f_5\left(\Delta_j^{'},BO_{ij}^{'}\right) \tag{2.5}$$

$$BO_{ij}^{\pi}=BO_{ij}^{'\pi}\cdot f_1\left(\Delta_i^{'},\Delta_j^{'}\right)\cdot f_1\left(\Delta_i^{'},\Delta_j^{'}\right)\cdot f_4\left(\Delta_i^{'},BO_{ij}^{'}\right)\cdot f_5\left(\Delta_j^{'},BO_{ij}^{'}\right) \tag{2.6}$$

$$BO_{ij}^{\pi\pi}=BO_{ij}^{'\pi\pi}\cdot f_1\left(\Delta_i^{'},\Delta_j^{'}\right)\cdot f_1\left(\Delta_i^{'},\Delta_j^{'}\right)\cdot f_4\left(\Delta_i^{'},BO_{ij}^{'}\right)\cdot f_5\left(\Delta_j^{'},BO_{ij}^{'}\right) \tag{2.7}$$

$$BO_{ij}=BO_{ij}^{\sigma}+BO_{ij}^{\pi}+BO_{ij}^{\pi\pi} \tag{2.8}$$

$$f_1\left(\Delta_i^{'},\Delta_j^{'}\right)=\frac{1}{2}\left(\frac{Val_i+f_2\left(\Delta_i^{'},\Delta_j^{'}\right)}{Val_i+f_2\left(\Delta_i^{'},\Delta_j^{'}\right)+f_3\left(\Delta_i^{'},\Delta_j^{'}\right)}+\frac{Val_j+f_2\left(\Delta_i^{'},\Delta_j^{'}\right)}{Val_j+f_2\left(\Delta_i^{'},\Delta_j^{'}\right)+f_3\left(\Delta_i^{'},\Delta_j^{'}\right)}\right) \tag{2.9}$$

$$f_2\left(\Delta_i^{'},\Delta_j^{'}\right)=\exp(-p_{boc1}\cdot\Delta_i^{'})+\exp(-p_{boc1}\cdot\Delta_j^{'}) \tag{2.10}$$

$$f_3\left(\Delta_i^{'},\Delta_j^{'}\right)=\ln\left\{\frac{1}{2}\left[\exp(-p_{boc2}\cdot\Delta_i^{'})+\exp(-p_{boc2}\cdot\Delta_j^{'})\right]\right\} \tag{2.11}$$

$$f_4\left(\Delta_i^{'},BO_{ij}^{'}\right)=\frac{1}{1+\exp(-p_{boc3}\cdot(p_{boc4}\cdot BO_{ij}^{'}\cdot BO_{ij}^{'}-\Delta_i^{'boc})+p_{boc5})} \tag{2.12}$$

$$f_5\left(\Delta_j^{'},BO_{ij}^{'}\right)=\frac{1}{1+\exp(-p_{boc3}\cdot(p_{boc4}\cdot BO_{ij}^{'}\cdot BO_{ij}^{'}-\Delta_{ij}^{'boc})+p_{boc5})} \tag{2.13}$$

The number of new over-allocations can be calculated by equations (2.5)-(2.13). Δ_i, as shown below:

$$\Delta_i=\text{-}Val_i+\sum_{j=1}^{nerghbours(i)} BO_{ij} \tag{2.14}$$

In equations (2.10)-(2.13), p_{boc1}~p_{boc5} is the force field parameter. The resulting expression for E_{bond} is as follows:

$$E_{bond}=-D_e^{\sigma}\cdot BO_{ij}^{\sigma}\cdot\exp\left[p_{be1}\left(1-\left(BO_{SF}^{\sigma}\right)^{p_{be2}}\right)\right]-D_e^{\pi}\cdot BO_{ij}^{\pi}-D_e^{\pi\pi}\cdot BO_{ij}^{\pi\pi} \tag{2.15}$$

Eq. (2.15) where D_e^{σ} 、 D_e^{π} 、 $D_e^{\pi\pi}$ are the force field parameters derived from the σ-bonding, π-bonding and double-π-bonding levels, respectively. p_{be1} and p_{be2} is the provisional parameter of the force field.

E_{over} is the over-coordination energy correction term calculated as follows：

$$E_{over} = p_{over1} \cdot \Delta_i^1 \cdot \left(\frac{1}{1+\exp\left(p_{over2} \cdot \Delta_i^1 \right)} \right) \tag{2.16}$$

Eq. (2.16) where p_{kov1} and p_{kov2} are the over-coordination energy correction force field parameters, respectively.

The bond angle energy term E_{angle} is also expressed in the Reax FF reaction force field as a function of bond level by the following equation:

$$E_{angle} = f_7\left(BO_{ij}\right) \cdot f_7\left(BO_{jk}\right) \cdot f_8\left(\Delta_j\right) \cdot \left\{ p_{angle1} - p_{angle1} \cdot \exp\left[-p_{angle2} \cdot \left(\Theta_0\left(BO\right) - \Theta_{ijk} \right)^2 \right] \right\} \tag{2.17}$$

$$f_7\left(BO_{ij}\right) = 1\text{-}\exp\left(-p_{angle3} \cdot BO_{ij}^{p_{angle4}} \right) \tag{2.18}$$

$$f_8\left(\Delta_j\right) = p_{angle5} - \left(p_{angle5} - 1 \right) \cdot \frac{2+\exp\left(p_{angle6} \cdot \Delta_j^{angle} \right)}{1+\exp\left(p_{angle5} \cdot \Delta_j^{angle} \right) + \exp\left(-p_{angle7} \cdot \Delta_j^{angle} \right)} \tag{2.19}$$

Equation (2.17) where Θ_0 s the equilibrium bond angle，determined by SBO as a function of the sum of bond levels of the π-bonds, the hybridisation state of the atom at the centre of the bond angle can be determined by the following equation:

$$SBO = \sum_{\text{n=1}}^{nerghbours(j)} \left(BO_{jn}^{\pi} + BO_{jn}^{\pi\pi} \right) + \left[1 - \prod_{n=1}^{nerghbours(j)} \exp\left(-BO_{jn}^{8} \right) \right] \cdot \left(-\Delta_j^{angle} - p_{angle8} \cdot n_{lp,j} \right) \tag{2.20}$$

$$\Delta_i^{angle} = -Val_i^{angle} + \sum_{\text{j=1}}^{nerghbours(i)} BO_{jn} \tag{2.21}$$

$$\begin{aligned} &SBO2 = 0 && \text{if} \quad SBO \le 0 \\ &SBO2 = SBO^{p_{angle9}} && \text{if} \quad 0 < SBO < 1 \\ &SBO2 = 2 - \left(2 - SBO\right)^{p_{angle9}} && \text{if} \quad 1 < SBO < 2 \\ &SBO2 = 2 && \text{if} \quad SBO > 2 \end{aligned} \tag{2.22}$$

$$\Theta_0\left(BO\right) = \pi - \Theta_{0,0} \cdot \left\{ 1 - \exp\left[-p_{angle10} \cdot \left(2 - SBO2 \right) \right] \right\} \tag{2.23}$$

The four-body energy action term $E_{torsion}$ denotes the energy of the dihedral angle and is given by the following equation:

$$\begin{aligned} E_{tors} &= f_{10}\left(BO_{ij}, BO_{jk}, BO_{kl}\right) \cdot \sin\left(\Theta_{ijk}\right) \cdot \sin\left(\Theta_{jkl}\right) \\ &\cdot \left[\begin{array}{l} \frac{1}{2} \cdot V_1 \cdot \left(1+\cos\omega_{ijkl}\right) + \frac{1}{2} \cdot V_2 \cdot \\ \exp\left\{ p_{tor1} \cdot \left(BO_{JK}^{\pi} - 1 + f_{11}\left(\Delta_j, \Delta_k\right)^2 \right) \right\} \left(1+\cos\omega_{ijkl}\right) + \frac{1}{2} \cdot V_3 \left(1+\cos 3\omega_{ijkl}\right) \end{array} \right] \end{aligned} \tag{2.24}$$

$$\begin{aligned} f_{10}\left(BO_{ij}, BO_{jk}, BO_{kl}\right) &= \left[1 - \exp\left(-p_{tor2} \cdot BO_{ij} \right) \right] \\ &\cdot \left[1 - \exp\left(-p_{tor2} \cdot BO_{jk} \right) \right] \cdot \left[1 - \exp\left(-p_{tor2} \cdot BO_{kl} \right) \right] \end{aligned} \tag{2.25}$$

$$f_{11}\left(\Delta_j,\Delta_k\right)=\frac{2+\exp\left[-p_{tor3}\cdot\left(\Delta_j^{angle}+\Delta_k^{angle}\right)\right]}{1+\exp\left[-p_{tor3}\cdot\left(\Delta_j^{angle}+\Delta_k^{angle}\right)\right]+\exp\left[p_{tor4}\cdot\left(\Delta_j^{angle}+\Delta_k^{angle}\right)\right]} \tag{2.26}$$

$E_{valwaals}$ is the van der Waals role term, for system energy discontinuities that tend to occur in conventional molecular dynamics calculations, the Taper function can be taken in account in the van der Waals action term energy calculation as follows:

$$\begin{aligned} Tap &= Tap_7\cdot r_{ij}^7+Tap_6\cdot r_{ij}^6+Tap_5\cdot r_{ij}^5+Tap_4\cdot r_{ij}^4 \\ &+Tap_3\cdot r_{ij}^3+Tap_2\cdot r_{ij}^2+Tap_1\cdot r_{ij}^1+Tap_0 \end{aligned} \tag{2.27}$$

$$\begin{aligned} Tap_7 &= 20/R_{cut}^7 \\ Tap_6 &= \text{-}70/R_{cut}^6 \\ Tap_5 &= =84/R_{cut}^5 \\ Tap_4 &= \text{-}35/R_{cut}^4 \\ Tap_3 &= Tap_2=Tap_1=0 \\ Tap_0 &= 1 \end{aligned} \tag{2.28}$$

Eq. (2.28) where R_{cut} is the truncation radius of the non-bonding term.

The use of the Morse function in ReaxFF simulations allows the combination of chemical bonding interactions and non-bonding interactions for more accurate calculations, The resulting van der Waals interaction term $E_{valwaals}$ is derived as follows:

$$E_{valwaals}=Tap\cdot D_{ij}\left\{\exp\left[\alpha_{ij}\cdot\left(1-\frac{f_{13}\left(r_{ij}\right)}{r_{vdW}}\right)\right]\right\}-2\exp\left[\frac{1}{2}\cdot\alpha_{ij}\cdot\left(1-\frac{f_{13}\left(r_{ij}\right)}{r_{vdW}}\right)\right] \tag{2.29}$$

$$f_{13}\left(r_{ij}\right)=\left[r_{ij}^{p_{vdW1}}+\left(\frac{1}{\gamma_w}\right)^{p_{vdW1}}\right]^{1/p_{vdW1}} \tag{2.30}$$

In equation (2.29), D_{ij} and α_{ij} are the parameters required to calculate the van der Waals forces, r_{vdW} is the van der Waals radius.

$E_{coulumb}$ is the Coulomb interaction term, calculated as follows：

$$E_{coulomb}=Tap\cdot C\cdot\frac{q_i\cdot q_j}{\left[r_{ij}^3+\left(\frac{1}{\gamma_{ij}}\right)^3\right]^{1/3}} \tag{2.31}$$

In Eq. (2.31), C is the Coulomb interaction term parameter and qi is the charge of atom i. The charge of the atom at different moments is calculated using the change in interatomic distance as a parameter.

The range of interatomic covalent bonding in the ReaxFF force field is 5 Å, which satisfies the weakest interaction distance of most interatomic covalent bonds. However, for atoms with large valence bond radii, bond level corrections need to be applied to remove

spurious bonding properties between unbonded neighbouring atoms. The calculation process starts with determining the bond levels of each neighbouring atom in the system and calculating E_{bond}, E_{over}, E_{angle} and $E_{torsion}$ in the total energy based on the results of the bond level calculations; Then, the charge balance method is introduced in the iterative calculations to solve for the charges of the acquired partial atoms, which are used in the calculation of the Coulomb interaction term; finally, the van der Waals correction term is introduced to calculate the total energy of the acquired system.

The ReaxFF force field is capable of accurately modelling chemical reactions in polyatomic systems and has a wide range of applications in the fields of combustion, surface catalysis and thermal decomposition of gases. [99-101] In this paper, the thermal decomposition of C_4F_7N-CO_2-O_2 mixture with different content of O_2 and different temperatures was simulated based on the ReaxFF-MD method, and the effects of temperature and O_2 content on the composition of the particles and the amount of production of thermal decomposition of the mixture were analysed.

2.1.2 C_4F_7N-CO_2-O_2 thermal decomposition reaction model creation

The occurrence of a chemical reaction is related to the size of the reaction system, the concentration of the reactants, the temperature and the reaction time, etc., and the speed of the same reaction occurs at different temperatures is not the same, while the temperature does not have an effect on the sequence of the occurrence of the different reactions and the reaction mechanism of the system, so in order to reveal the reaction mechanism of the system in a more complete manner while taking into account the cost of the calculations, it is possible to use the "Temperation Accelerated Dynamics，TAD" In order to reveal the reaction mechanism more completely and consider the computational cost, the "Temperature Accelerated Reaction Kinetics" method can be used to carry out MD simulations at higher temperatures than the actual temperatures by increasing the temperature so that the simulation time scale can be extended by an order of magnitude [103].

The time scale of the MD simulation process (ps level) is much smaller than that of the actual test (up to tens of hours), so this paper adopts the "warming" method in the simulation process, i.e., the simulation of the gaseous decomposition process is carried out at higher temperatures, which speeds up the reaction rate and extends the time scale of the simulation at the same time. The temperature at which a superheated fault occurs inside a gas-insulated device is about 260°C to 660°C [3],the content of the characteristic decomposition products generated by the decomposition of C_4F_7N in this temperature range is low (about 10-6 to 10-9 mol/L), so it is necessary to increase the simulation temperature in order to accelerate the

rate of the reaction and to promote the generation of the products. In addition, the results of literature [96] show that the type and content of the products generated from the decomposition of C4F7N at the simulation temperature of 1900 K are less and the initial dissociation reaction occurs at 615 ps (the total simulation time is 1000 ps). In order to better reflect the influence of O2 on the distribution of particles of the thermal decomposition of the C4F7N-CO2 -O2 mixture and to save the cost of the calculations, this paper carries out the MD simulation of the thermal decomposition of the C4F7N-CO2-O2 mixture at the simulation temperatures of 2000K-3000K.

Firstly, a 260Å*260Å*260Å cubic periodic reaction system was constructed in this paper, and the whole reaction system contained 500 molecules with 75 C4F7N molecules (15%) inside, and the ReaxFF-MD simulations were carried out by varying the O2 content (0%, 2%,, 4%, 6%, 8%, and 10%) and simulated temperatures (2000K, 2200K, 2400K, and 2600K, 2800K, 3000K) to carry out ReaxFF-MD simulations of C4F7N-CO2-O2 gas mixture at different O2 contents and temperatures, the particle composition of the reactants in the simulated system, the temperature settings and the system density are shown in Table 2.1. The ratios of the gas mixtures in the simulation system of this paper are kept consistent with the experiments, and the results of the simulation calculations can be compared and analysed with the experimental results.

Table 2.1 Particle composition of reactants for the simulated system

NO.	C_4F_7N		CO_2		O_2		simulated temperature (K)	system density (g/cm^3)
	number of molecules	viscosity	number of molecules	viscosity	number of molecules	viscosity		
1	75	15%	425	85%	0	0%	2600	0.0031
2	75	15%	415	83%	10	2%	2600	0.0031
3	75	15%	405	81%	20	4%	2600	0.0031
4	75	15%	395	79%	30	6%	2600	0.0031
5	75	15%	385	77%	40	8%	2600	0.0031
6	75	15%	375	75%	50	10%	2600	0.0030
7	75	15%	395	79%	30	6%	2000	0.0031
8	75	15%	395	79%	30	6%	2200	0.0031
9	75	15%	395	79%	30	6%	2400	0.0031
1	75	15%	395	79%	30	6%	2800	0.0031
11	75	15%	395	79%	30	6%	3000	0.0031

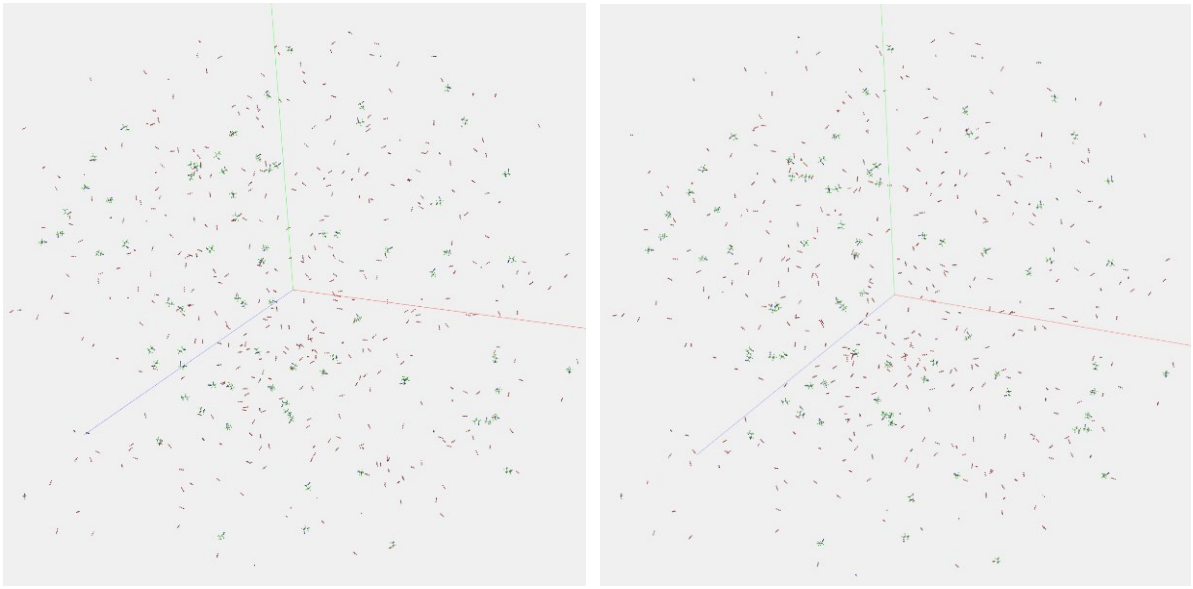

(a) (b)

Fig.2.3 Optimised reaction system model (a) 15%C_4F_7N-85%CO_2 (b) 15%C_4F_7N-79%CO_2-6%O_2

When analysing the particle composition of the products of a simulation process, it is considered that a chemical bond is formed if the bond level between two atoms is greater than a certain threshold (typically 0.3), otherwise it is considered that no chemical bond is formed [103]. The Reax FF MD simulation uses the velocity-verlet method to update the coordinates and velocities of atoms at each reaction time point in real time. Before the molecular dynamics simulation, the geometry of the system was optimised based on the NVE system (with constant values for the number of atoms, the size and energy of the reaction system) for 10 ps at 20 K (closed system with no heat exchange with the outside world) to establish a more reasonable initial structure of the reaction, and the reaction structure was optimised based on the NVE system (with constant values for the number of atoms, the size and the energy of the reaction system). The optimised reaction systems of 15% C_4F_7N-85% CO_2 and 15% C_4F_7N-79% CO_2-6% O_2 are shown in Fig.2.3; Subsequently, equilibrium calculations based on the NVT system (with constant values for the number of atoms, the size of the reaction system, and the temperature) were carried out for the system for 10 ps at 1000 K temperature. Finally, ReaxFF-MD was carried out for the C_4F_7N-CO_2-O_2 gas mixture system at different O_2 contents (0%-10%) and temperature intervals of 2000K-3000K, with a total simulation duration of 500 ps and a sampling step of 0.25fs. The NVT system was used for simulation and the Berendsen temperature control method was chosen for the temperature control procedure. All Reax FF-MD simulations in this paper are based on the Reax FF module in the cross-scale computational chemistry platform AMS (Amsterdam Density Functional), and the force-field files have been optimised using Monte Carlo methods based on NiCH.ff developed by Mueller et al. in conjunction with the properties of the C_4F_7N molecule [104].

2.2 Particle evolutionary properties of C_4F_7N-CO_2-O_2 thermal decomposition

2.2.1 Kinetic analysis of the effect of O_2 on the thermal decomposition particles of C_4F_7N-CO_2-O_2

The simulation temperature selected in this paper is 2000K-3000K, and it is mentioned above that the temperature will not have any effect on the sequence of the reaction and the reaction mechanism, but in order to make the chemical reaction process in the simulation system fully carried out, the temperature of 2600K in the middle section is selected to carry out the kinetic analysis of the effect of O_2 on the thermal decomposition particles of C_4F_7N-CO_2-O_2. Fig.2.4 gives the variation of C_4F_7N and various types of decomposed particles in the C_4F_7N-CO_2-O_2 reaction system with different content of O_2 at 2600 K simulation temperature with simulation time, and the number of each particle at the end of the simulated reaction. In the reaction process, there will be some fluctuations between the actual simulation temperature and the set temperature, and the sampling interval in the simulation parameter setting is small, which leads to the fluctuation phenomenon of the decomposition of the particle generation curve, but this fluctuation phenomenon will not have a greater impact on the qualitative analysis of the particle distribution law.

From Fig.2.4, it can be seen that CF_3, CF_2, CF, F, CF_3CF_2(C_2F_5), CF_2CF_2(C_2F_4), C_2F_2, $(CF_3)_2CF$, C_2F, CF_2CN, CF_3CFCN(C_3F_4N), CFN, CNO, CN, CO, O, C, and C_2 were produced in the 15% C_4F_7N-85% CO_2 system. 18 particles, and the number of decomposed particle species in the reaction system after the addition of O_2 was 14 (2% O_2), 15 (4% O_2), 16 (6% O_2), 13 (8% O_2) and 11 (10% O_2), respectively. It can be seen that after the addition of O_2, the number of particle species in the reaction system basically shows a decreasing trend with the increase of O_2 content, indicating that the addition of O_2 can inhibit the generation of some particles to a certain extent. From the generation of various types of particles in the system, the main several decomposition particles under different contents of O2 are CF3, CF2, CF, F, CN and C2F5 (the number of particles is greater than 5), which need to be investigated in spite of the low number of O-containing particles, since the influence of O2 on the distribution law of the particles of the thermal decomposition of C4F7N-CO2-O2-O2 is mainly considered in this chapter. It can be seen that COF2 (carbonyl fluoride) is the hallmark product of O2 addition and is generated only with the addition of 6% O2 and 8% O2, both with particle number 1.

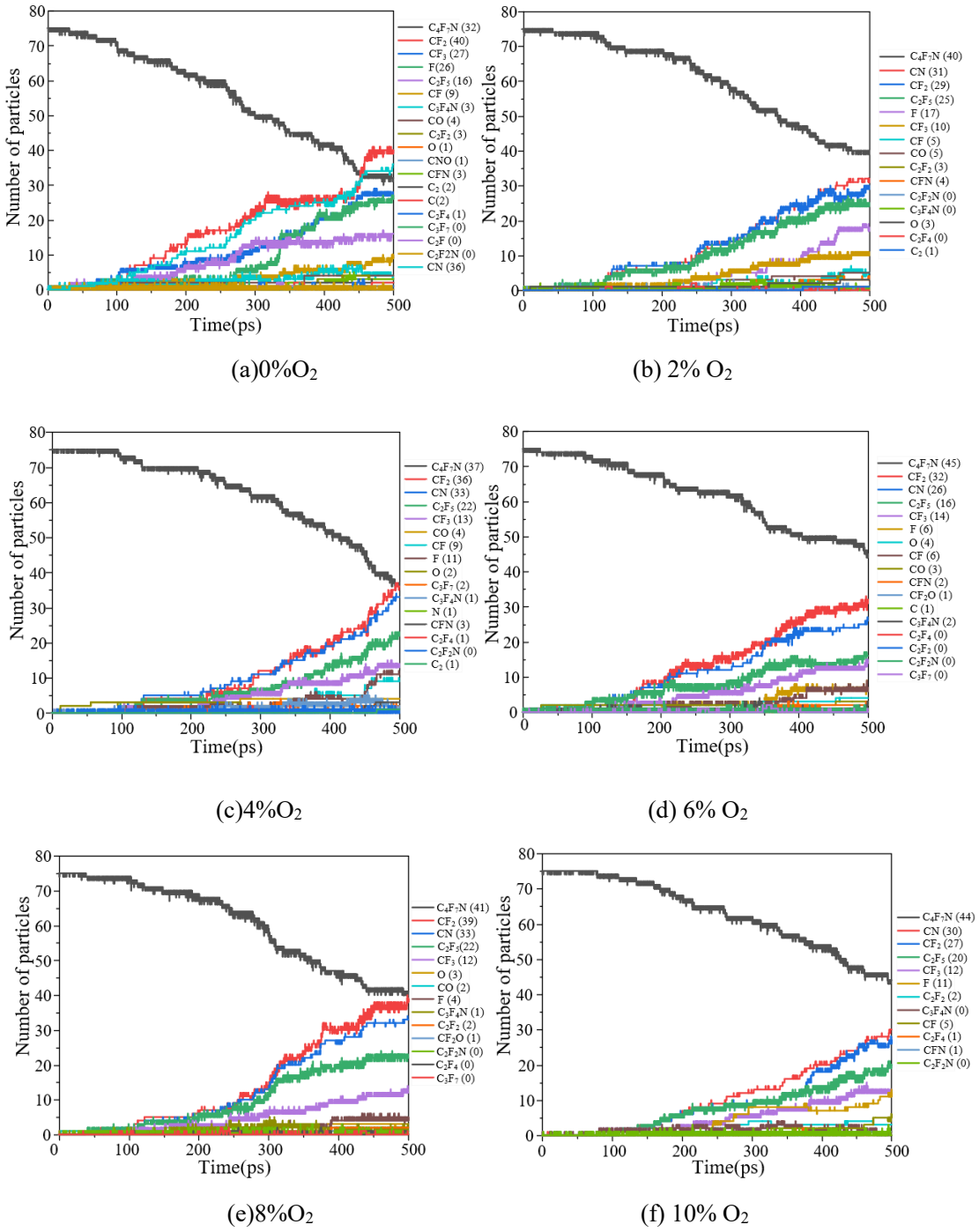

Fig.2.4 Particle distribution pattern of C_4F_7N-CO_2-O_2thermal decomposition at 2600k temperature with different content of O_2

In the 15% C_4F_7N-85% CO_2 system, the decomposition of C_4F_7N begins at 1.4 ps to form CF_3 and CF_3CFCN, and at 4.7 ps to form C_3F_7 and CN. The decomposition of C_4F_7N to form CF_3CF_2 and CF_2CN at a reaction time of 5.8 ps is not a simple one-time dissociation reaction, and there is a certain number of transition states in the middle, so this reaction is more difficult to occur compared to the dissociation reactions that occur at 1.4 ps and 4.7 ps. With the increase of simulation time, CF_3CFCN will be further decomposed to form CF_3, CF and CN,

and CF_3 will be further decomposed to form CF_2 and F. Therefore, the maximum number of particles of CF_3CFCN (C_3F_4N) at the end of the reaction is only 3 and decreases after the addition of O_2, which suggests that the addition of O_2 may accelerate the decomposition of CF_3CFCN, resulting in the dominant number of particles of several particles are CF_3, CF_2, CF, F, CN, and C_2F_5, respectively.

Upon addition of 2% O_2 to the C_4F_7N-CO_2 system, the decomposition of C_4F_7N started at 0.75 ps to form CF_3CF_2 and CF_2CN, and at 1.1 ps to form CF_3 and CF_3CFCN, and these two reactions occurred simultaneously at the simulation time of 1.1 ps. Compared to the case without O_2, both reactions occurred earlier, and it can be seen that O_2 can advance the initial dissociation time of C_4F_7N. Since the decomposition of C_4F_7N to form CF_3CF_2 and CF_2CN, a reaction that involves a transition state, suggests that the addition of O_2 makes the decomposition process of C_4F_7N more complex from the early stage of the reaction.

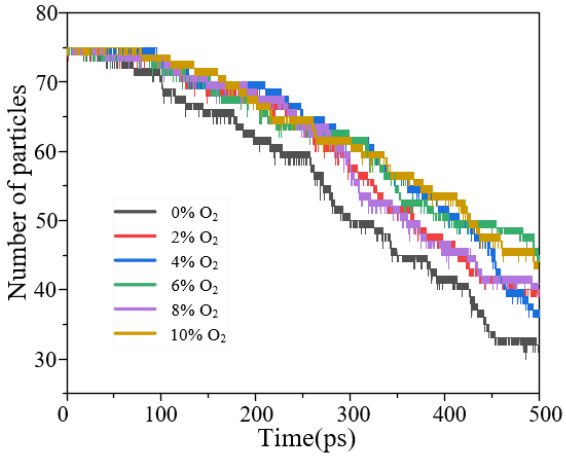

Fig.2.5 Variation in the number of C_4F_7N particles with simulation time for different contents of O_2 in the reaction system

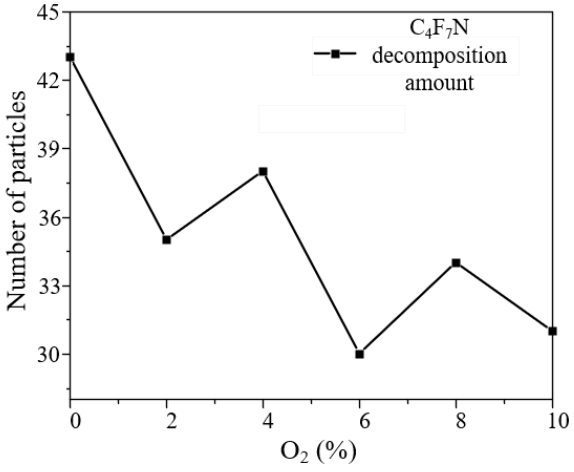

Fig.2.6 Variation of C_4F_7N decomposition with O_2 content in the system at the end of the reaction

Fig.2.5 gives the variation of the number of C_4F_7N particles in the reaction system with reaction time for different contents of O_2, and it can be seen that with the increase of simulation time, the decomposition of C_4F_7N with different O_2 contents gradually increases, so the number of C_4F_7N particles in the reaction system decreases. It can be clearly seen that the decomposition rate (slope of the particle number versus time curve) accelerates at simulation times greater than 250 ps, especially at O_2-free conditions. The variation of C_4F_7N decomposition with O_2 content in the system at the end of the reaction is given in Fig. 2.6, and it can be seen that the amount of C_4F_7N decomposition decreases significantly after the addition of O_2 and shows an overall decreasing trend with the increase of O_2 content, The decomposition of C_4F_7N under the condition of 6% O_2 was the least, and only 30 C_4F_7N molecules were decomposed, which was 30.2% less compared with the decomposition of 43 C_4F_7N molecules before the addition of O_2, indicating that the addition of a certain content of O_2 can effectively inhibit the decomposition of C_4F_7N.

Fig.2.7 gives the distribution law of the main decomposition particles of CF_3, CF_2, CF, F, C_2F_5, CN, O and CO under different contents of O_2. Combined with the main thermal decomposition particles of C_4F_7N-CO_2-O_2 gas mixture with different contents of O_2 at the end of the reaction at the simulated temperature of 2600K given in Table 2.2, it can be seen that the addition of 2% O_2 to the mixture of gas CF_3, CF_2, CF, F and CN particles were significantly reduced, and the generation of these particles was less than that without O_2 under the condition of 4%-10% O_2, and CN particles were generated the least under the condition of 6% O_2.The addition of a certain content of O_2 to the C_4F_7N-CO_2 gas mixture can inhibit most of the particles, mainly due to the strong oxidative property of O_2, and with the increase of O_2 content, the O particles can be inhibited by the addition of O_2. O_2 content increases, the number of O particles also increases, which is easy to combine with these more reactive particles, resulting in a decrease in their number.

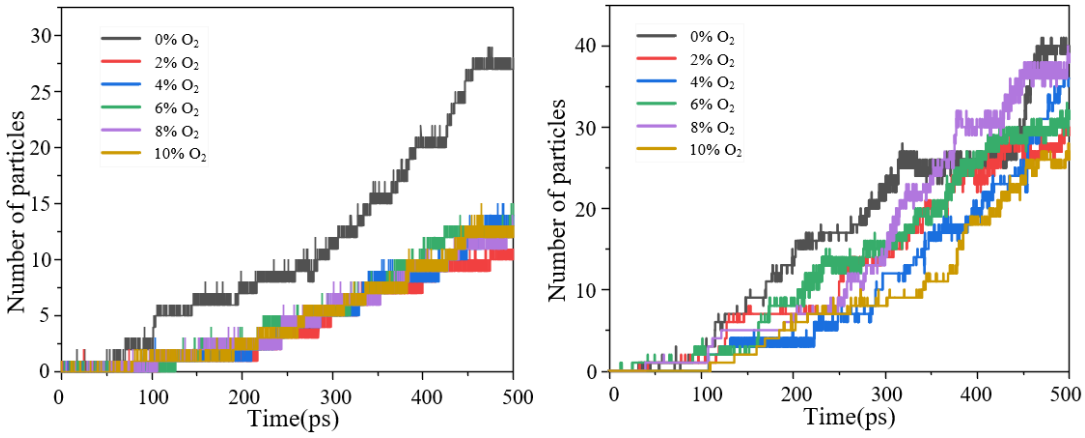

(a) CF_3 (b) CF_2

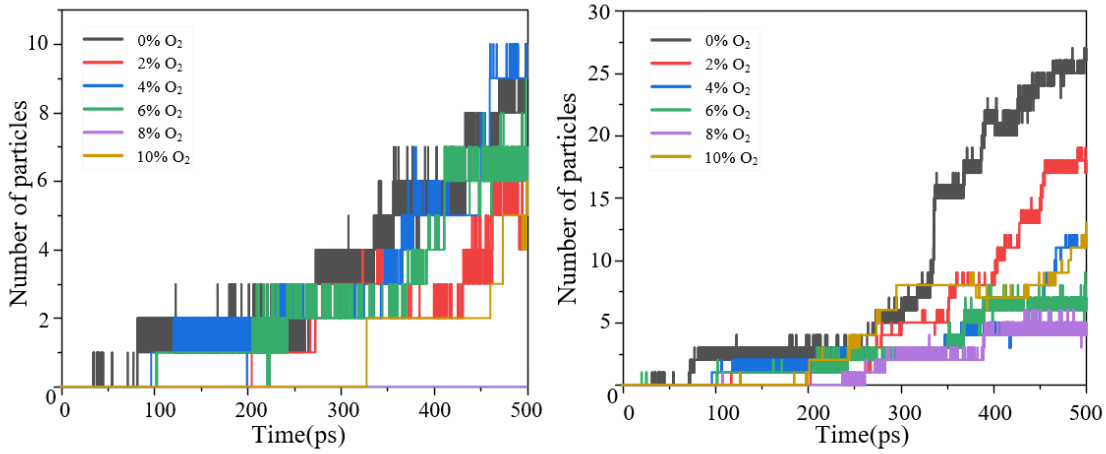

(c) CF (d) F

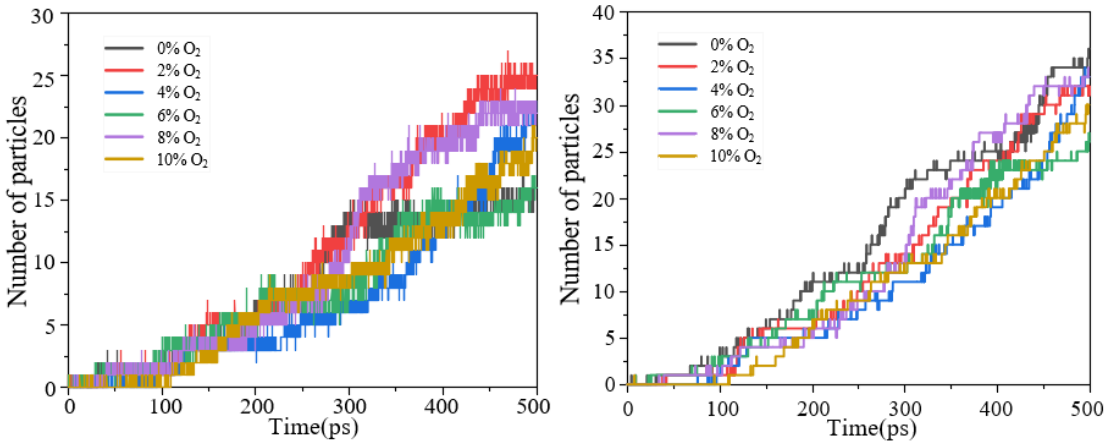

(e) C_2F_5 (f) CN

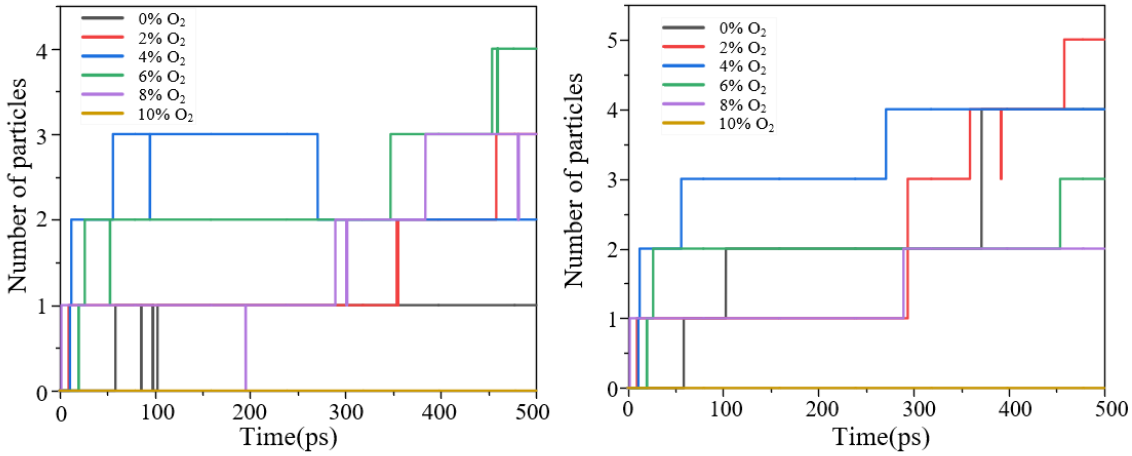

(g) O (h) CO

Fig.2.7 Variation of major decomposed particles with simulation time for different contents of O_2

Table 2.2 Major thermal decomposition particle generation at different O2 contents (2600K)

O_2 (%)	Particle Type							
	CF_3	CF_2	CF	F	C_2F_5	CN	O	CO
0	27	40	9	26	16	36	1	4
2	10	29	5	17	25	31	3	5
4	13	36	9	11	22	33	2	4
6	14	32	6	6	16	26	4	3
8	12	39	0	4	22	33	3	2
10	12	27	5	11	20	30	0	0

The generation of CF_3 particles does not show a significant trend with O_2 content in the range of 2%-10% O_2, and increases only smoothly with simulation time; However, at 0% O_2, the CF_3 generation is much larger than the case of adding O_2, and its generation rate increases rapidly at simulation times greater than 300 ps, indicating that the simulation time has a large effect on the CF_3 generation rate when no O_2 is added to the gas mixture. The generation of F particles has a similar trend to that of CF_3 particles. However, for CF_2, CF and CN, the effect of O_2 content change on their overall distribution pattern is not obvious, and the generation increases steadily with simulation time. At simulation times greater than 300 ps, C_2F_5 particle production increased after O_2 addition, and C_2F_5 was mainly derived from the decomposition of C_4F_7N to form C_2F_5 and C_2F_2N, and this reaction occurred earlier after 2% O_2 addition compared to the other initial dissociation reactions, suggesting that O_2 addition contributes to the occurrence of this reaction. In addition, C_2F_5 particles are more stable than other particles and do not easily combine with O_2 and O to form other products.

In order to further investigate the effect of O_2 on the reaction rate of the system, the reaction rate constants k were calculated for some of the reaction paths involved in several of the main decomposing particles given in Table 2.2, and the results are shown in Table 2.3. As an important physical quantity in kinetic analysis, the rate constant k directly reflects the speed of the rate and is the main basis for the study of the reaction mechanism. It can be seen that the reaction rates for reaction paths 1-3 in Table 2.3 tend to decrease at 0%-4% O_2 content in the reaction system, and start to increase at O_2 contents greater than 6%; The reaction rate of reaction path 3 at 10% O_2 content has an order of magnitude change compared to other O_2 contents. The reaction rate of path 4 decreases at 0%-8% O_2 content in the reaction system and increases at 10% O_2 content. In addition, the addition of O_2 accelerates the reaction path 6. Overall, the addition of 0%-4% O_2 reduces the reaction rates of most decomposition reactions, but O_2 levels greater than 8% accelerate these reactions.

Table 2.3 Rate constants for major decomposition reactions at different levels of O_2 (2600 K)

NO.	Reaction path	Rate constant k ($cm^3 \cdot mol^{-1} \cdot s^{-1}$)					
		0% O_2	2% O_2	4% O_2	6% O_2	8% O_2	10% O_2
1	$C_4F_7N \rightarrow CF_2CN+CF_3CF_2$	2.75E+09	2.04E+09	1.83E+09	1.92E+09	2.02E+09	2.83E+09
2	$C_4F_7N \rightarrow CF_3+ CF_3CFCN$	2.03E+09	1.48E+09	1.47E+09	1.73E+09	1.71E+09	2.21E+09
3	$CF_2CN \rightarrow CF_2+CN$	8.35E+11	7.63E+11	4.47E+11	4.66E+11	5.91E+11	6.15E+12
4	$CF_2CF \rightarrow F+CFCF$	1.30E+12	1.03E+12	9.94E+11	5.76E+11	3.08E+11	1.33E+12
5	$CF_3CF_2 \rightarrow CF_2+CF_3$	4.84E+09	3.25E+09	4.47E+09	9.18E+09	8.40E+08	5.45E+09
6	$CO_2 \rightarrow CO+O$	9.47E+06	9.69E+06	1.51E+07	1.53E+07	1.05E+07	-

2.2.2 Kinetic analysis of the effect of temperature on the thermal decomposition particles of C_4F_7N-CO_2-O_2

Based on the results of the kinetic analysis of the effect of O_2 on the thermal decomposition particles of the C_4F_7N-CO_2-O_2 mixture in 2.2.1, under the condition of 6% O_2, the decomposition amount of C_4F_7N is the least and the generation amount of main decomposition particles is low, so the C_4F_7N-CO_2-O_2 gas mixture containing 6% O_2 is selected to carry out the kinetic simulation of thermal decomposition process at different temperatures. Fig.2.8 gives the variation of C_4F_7N and various types of decomposed particles in the 15% C_4F_7N-79%CO_2-6%O_2 reaction system with simulation time at different temperatures and the number of each particle at the end of the simulated reaction. The number of particle species generated in the reaction system at different temperatures were 10 (2000 K), 8 (2200 K), 14 (2400 K), 16 (2600 K), 18 (2800 K) and 19 (3000 K), respectively, and it can be seen that there is an overall increasing trend in the number of species and number of decomposed particles in the reaction system with the increase in simulation temperature. At 2000K-2400K, the reaction time for the onset of decomposition of C_4F_7N is concentrated at 11-13 ps, and when the simulated temperature is at 2600K-3000K, the reaction time for the onset of decomposition of C_4F_7N is concentrated at 0.5-0.8 ps, which suggests that the initial time for the decomposition of C_4F_7N is advanced at simulated temperatures greater than 2600K, and the number of generated particles is also significantly increased.

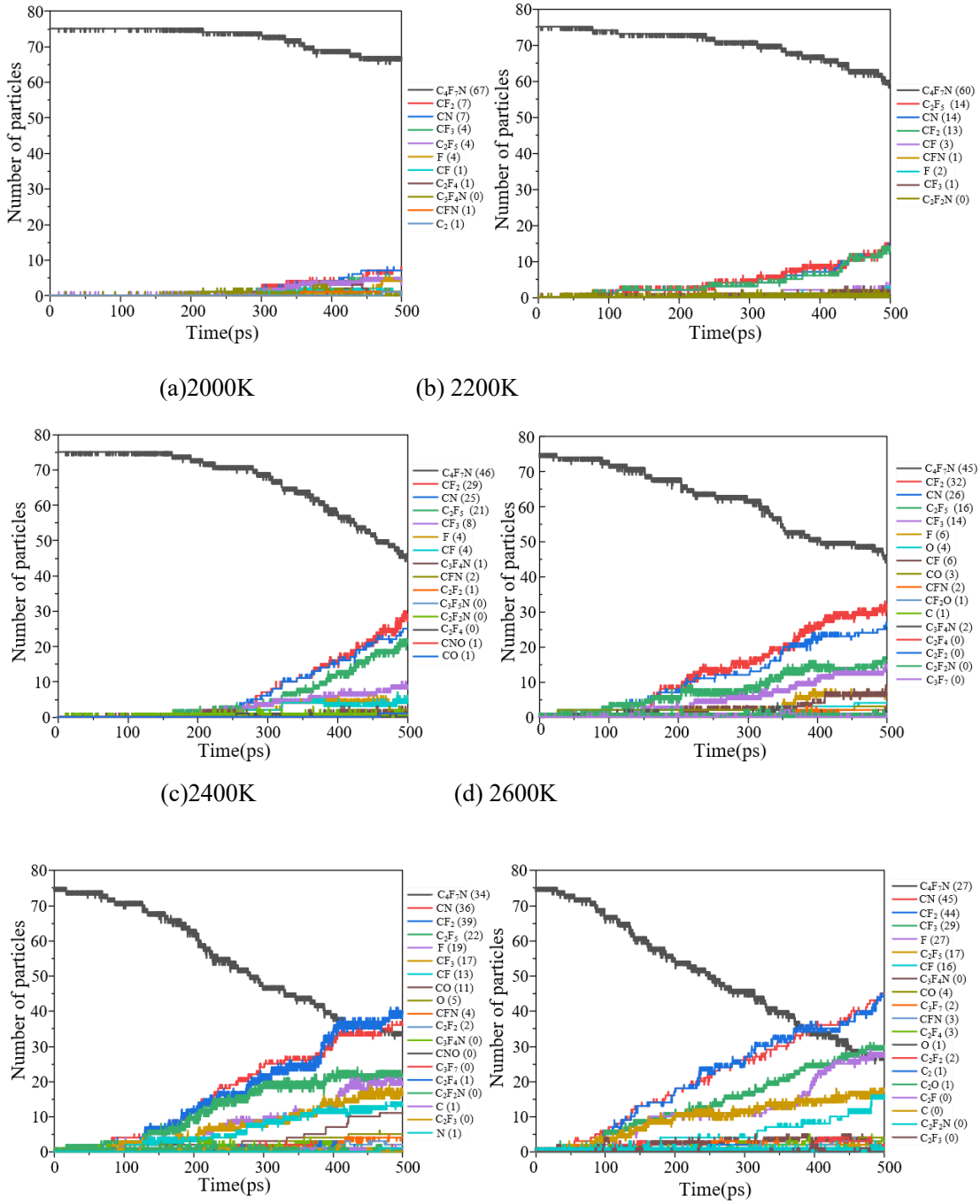

(a)2000K (b) 2200K

(c)2400K (d) 2600K

(e)2800K (f) 3000K

Fig.2.8 Particle distribution pattern of thermal decomposition of C_4F_7N-CO_2-O_2 with 6% O_2 at different simulation temperatures

Fig.2.9 gives the variation of the number of C_4F_7N particles in the reaction system with simulation time at different temperatures, and it can be seen that the decomposition rate of C_4F_7N accelerates significantly with the increase of simulation temperature. Fig.2.10 gives the variation of the amount of C_4F_7N decomposition in the system at the end of the reaction with the simulation temperature, the number of particle species generated by the decomposition of

C_4F_7N at different temperatures are 8 (2000K), 15 (2200K), 29 (2400K), 30 (2600K), 41 (2800K), and 48 (3000K), which shows that the simulation temperature in the range of 2200K-2400K, the decomposition rate of C_4F_7N is faster, with little change between 2400K and 2600K, and continues to increase when it is greater than 2600K, indicating that the decomposition of C_4F_7N will reach saturation when the simulated temperature increases to a certain interval, and that it is necessary to continue to increase the temperature in order to promote the decomposition of C_4F_7N.

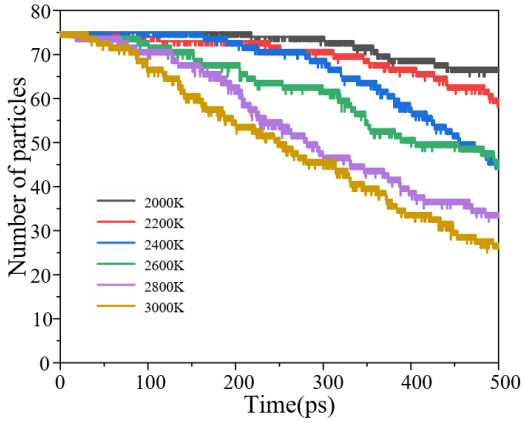

Fig.2.9 Variation of the number of C_4F_7N particles in the reaction system with simulation time at different simulation temperatures

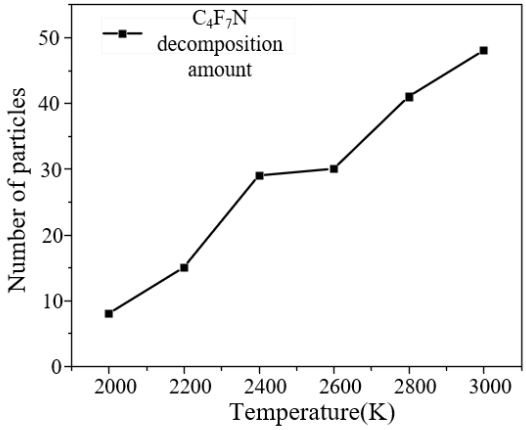

Fig.2.10 Variation of C_4F_7N decomposition in the system at the end of the reaction with simulated temperature

The distribution patterns of the main decomposition particles, CF_3, CF_2, CF, F, C_2F_5, CN, O and CO, at different simulation temperatures are given in Fig. 2.11, and the main thermal decomposition particles produced by C_4F_7N-CO_2-O_2 with 6% O_2 at different simulation temperatures are given in Table 2.4. It can be seen that at different simulation temperatures,

the two particles CF_2 and CN have the highest generation, followed by CF_3 and F. The generation of C_2F_5 and CN shows a trend of uniform growth with temperature and simulation time. It can be seen that the amount and rate of generation of CF_3 particles at the simulated temperature of 3000K is much larger than other temperatures. CF_3 particles come from direct dissociation reactions of C_4F_7N, CF_3CFCN and C_2F_5 particles on the one hand, and recombination of CF_2 and F particles on the other hand, and these dissociation and recombination reactions are intensified by an increase in the energy of the reaction system when the simulated temperature reaches 3000 K. The production of CF_2 is slow at the simulated temperatures of 2000K and 2200K, with a large increase in the production rate at simulation times greater than 450 ps and a significant acceleration of the production rate at temperatures greater than 2200K. The CF and F particles follow the same trend with temperature, and their production starts to increase rapidly at simulated temperatures greater than 2400K.

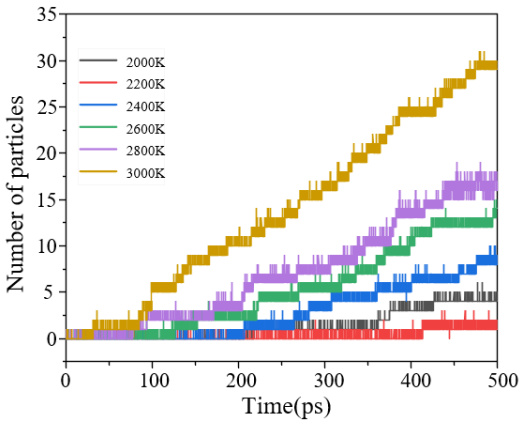

(a) CF_3

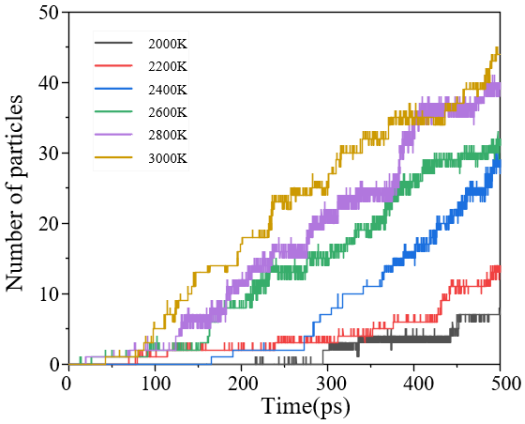

(b) CF_2

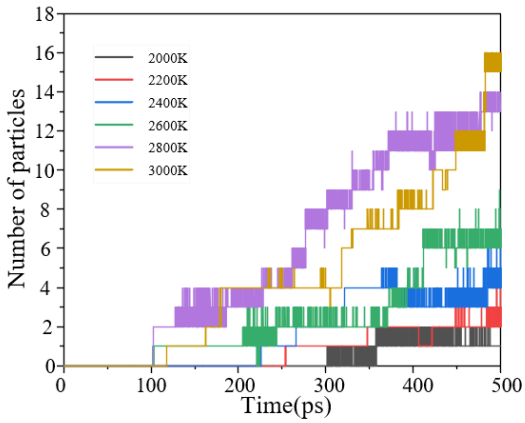

(c) CF

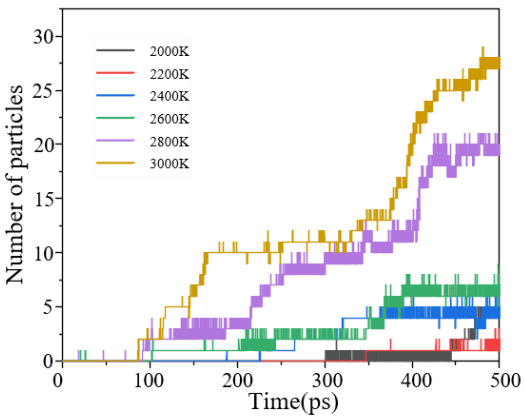

(d) F

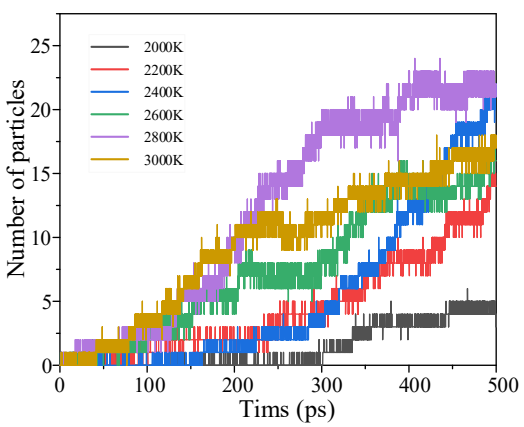

(e) C_2F_5

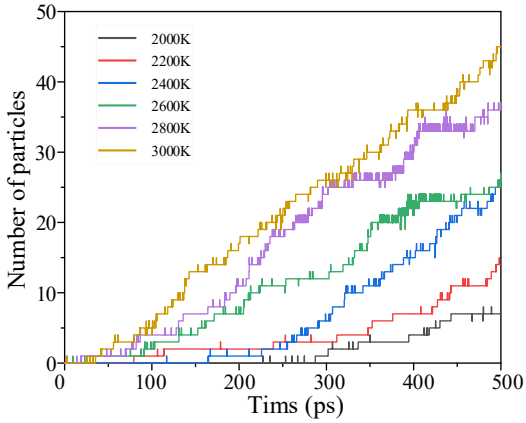

(f) CN

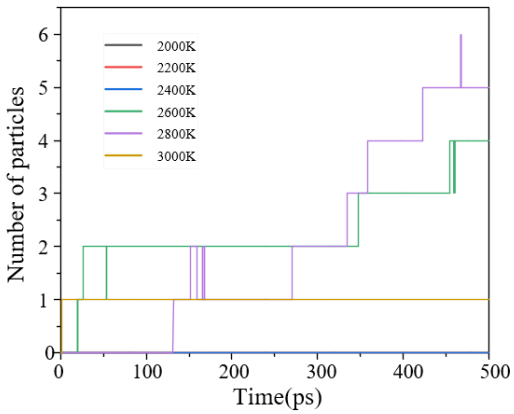

(g) O

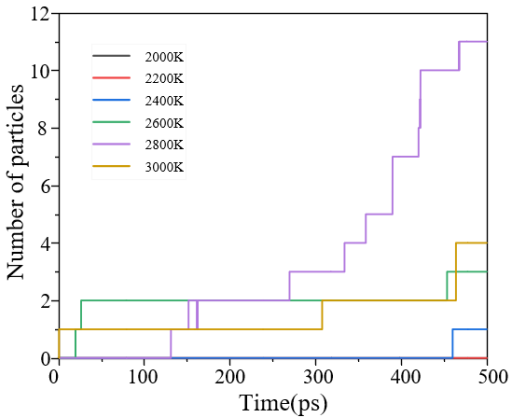

(h) CO

Fig.2.11 Variation of major thermal decomposition particle generation with simulation time at different simulation temperatures

The decomposition of O_2 to produce O particles requires high energy, so O particles do not appear until the simulation temperature rises to 2600 K. The O particles are not visible until the simulation temperature increases to 2600 K. CO originates from the dissociation of CO_2 or the reaction of O particles with C particles, so no CO particles are found in the system at simulated temperatures less than 2400K.

Table 2.4 Major thermal decomposition particle generation at different simulation temperatures (6% O2)

temperature	Particle Type							
(K)	CF_3	CF_2	CF	F	C_2F_5	CN	O	CO
2000	4	7	1	4	4	7	0	0
2200	1	13	3	2	14	14	0	0
2400	8	29	4	4	21	25	0	1
2600	14	32	6	6	16	26	4	3
2800	17	39	13	19	22	36	5	11

3000	29	44	16	27	17	45	1	4

Overall, the results of ReaxFF-MD simulations of the thermal decomposition process of the C_4F_7N-CO_2-O_2 mixture show that although the addition of O_2 to the C_4F_7N-CO_2 mixture decreases the initial decomposition time of C_4F_7N, the amount of decomposition and most of the particles generated can be effectively reduced, and the least amount of decomposition of C_4F_7N is particularly observed at an O_2 content of 6%. In addition, the addition of 0%-4% O_2 decreases the reaction rates of the major decomposition reactions in the reaction system, but O_2 levels greater than 8% accelerate these reactions. At simulated temperatures greater than 2600 K, the initial decomposition time of C_4F_7N is significantly reduced and the rate of decomposition particle generation is accelerated. From the simulation results at different contents of O_2 and at different temperatures, it can be seen that the two particles, CF_2 and CN, have the highest amount of generation, followed by CF_3 and F.

2.3 Thermal decomposition properties of C_4F_7N-CO_2-O_2

2.3.1 Thermal decomposition test platform and method

In order to accurately simulate the decomposition process of gas insulating medium when local overheating faults occur in gas insulated equipment in engineering practice, this paper adopts the C_4F_7N-CO_2-O_2 mixed gas thermal decomposition test platform shown in Fig. 2.12 to carry out the test，the platform is mainly composed of stainless steel airtight chamber, power supply, heat source (POF defect model), temperature control system and barometer. The POF physical defect model is used to simulate localised heat sources inside gas-insulated electrical equipment and is placed in the centre of a stainless steel gas chamber. The power supply provides DC power to the heat source with a rated voltage of 24V and a rated power of 120W. Temperature control system includes controller, sensor and relay three parts, using proportional-integral-derivative (PID) temperature control method, through the temperature sensor on the surface of the heat source for real-time detection and monitoring of the temperature of the heat source surface in contact with the gas, using the PID control method to set the value of the actual measured value compared with the output results of the relay to give a fault signal, to determine whether the heat source needs to continue to work, in order to achieve precise control of the temperature of the heat source. The sealed air chamber is made of 304 stainless steel with a volume of approximately 10L and can withstand an upper air pressure limit of 0.7MPa; Sampling and inlet ports are fitted on the outer wall of the gas chamber and connected to a gas line for filling the test gas and collecting the sample gas.

The filling pressure of medium-voltage gas-insulated switchgear generally does not

exceed 0.20 MPa, and the absolute air pressure of most medium-voltage equipment is 0.12 MPa [51]. To meet the minimum ambient operating temperature of -25℃, the content of C_4F_7N in the C_4F_7N-CO_2 gas mixture should not exceed 18% within the range of 0.1-0.2MPa, and it has been demonstrated that under quasi-uniform electric field, the insulating ability of the C_4F_7N-CO_2 gas mixture is comparable to that of the pure SF_6 of 0.12MPa at 0.14MPa gas pressure [51]. So all the experimental studies in this paper are centred around a C_4F_7N-CO_2-O_2 gas mixture containing 15% C_4F_7N at 0.14 MPa gas pressure.

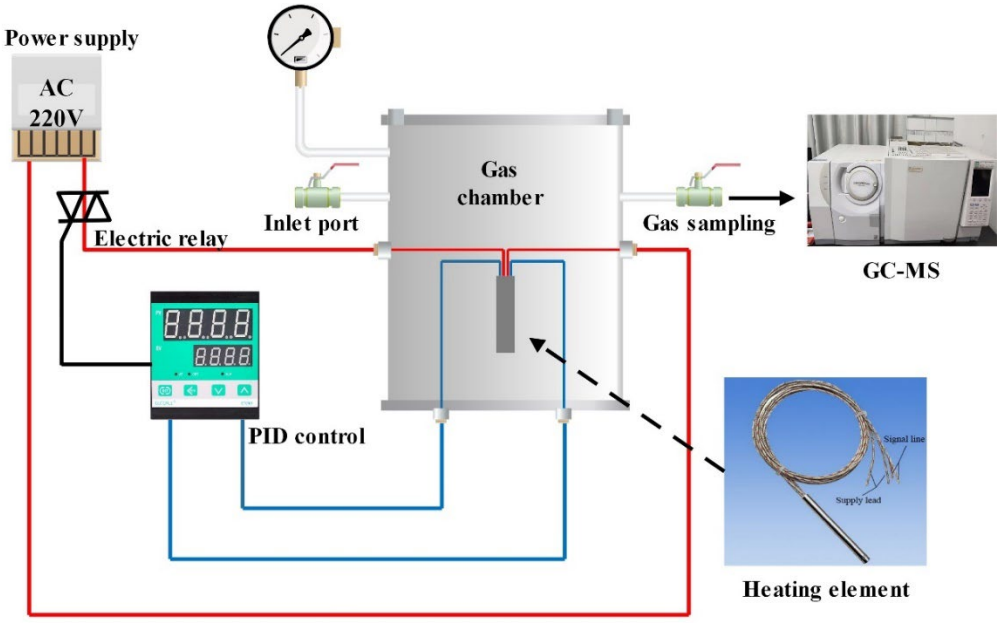

Fig 2.12 Schematic diagram of POF decomposition characteristic test platform

In this paper, the POF decomposition characteristics of a gas mixture containing 15% C_4F_7N at 0.14 MPa gas pressure are investigated at different O_2 contents (0%-10%) and different temperatures (400°C-525°C). Through a number of tests found that C_4F_7N-CO_2-O_2 gas mixture at 400 ℃ below only a few decomposition products generated, and the amount of generation is relatively small, is not conducive to the study of mixed gases in the local superheat fault decomposition of components of the law of change, so in the study of O_2 on the local superheat decomposition of mixed gases of decomposition characteristics of the influence of the properties of the temperature is set to 450 ℃, the mixing into the content of O_2 for the 2%, 4%, 6%, 8%, and 10%, respectively; According to the results of ReaxFF-MD simulation, the decomposition of C_4F_7N was the least when the O_2 addition was 6%, so in the study of the effect of temperature on the local superheated decomposition characteristics of the gas mixture, the O_2 content of the gas mixture was set to 6%, and the experimental temperatures were 400 °C, 425 °C, 450 °C, 475 °C, 500 °C, and 525 °C, respectively, and the upper limit of the temperature was selected to be 525 °C, taking into consideration of the

tolerance of the heat source to high temperatures.

The specific test steps are as follows:

(1) Place the heat source in the centre of the test gas chamber, with the signal and power lines facing upwards, to facilitate the dissipation of the magnesium oxide part of the wiring, and to avoid local overheating leading to the accumulation of carbon and conductivity at the wiring. The heat source and the inner wall of the stainless steel gas chamber were wiped with a dust-free cloth dipped in anhydrous ethanol to remove the influence of impurities on the test results, and then left for 1 h to allow the ethanol to evaporate completely. A vacuum pump was used to evacuate the stainless steel gas chamber and leave it for 6h, the air pressure inside the sealing tank was measured and read by a digital barometer to ensure a good airtightness, and then the buffer gas CO_2 of C_4F_7N gas mixture was filled to 0.14 MPa and then evacuated, and the process was repeated for 3 times to remove the impurity gases inside the gas chamber.

(2) According to Dalton's law of partial pressure, C_4F_7N, O_2 and CO_2 were introduced into the gas chamber sequentially, firstly, 15% C4F7N (21kPa) gas was slowly introduced into the tank, and then different contents of O_2 and CO_2 were introduced, and the O_2 content and the corresponding partial pressures of O2 were 0% (0kPa), 2% (2.8kPa), 4% (5.6kPa), 6% (8.4kPa), 8% (11.2kPa) and 10% (14kPa), and the CO_2 content and the corresponding partial pressures were 85% (119kPa) and 10% (14kPa), respectively. (11.2kPa), 8% (11.2kPa) and 10% (14kPa), and the filled CO_2 content and the corresponding partial pressures were 85% (119kPa), 83% (116.2kPa), 81% (113.4kPa), 79% (110.6kPa), 77% (107.8kPa) and 75% (105kPa), respectively. The air pressure in the sealed tank was monitored by a barometer during the filling process, and the gas was allowed to stand for 12 h after completion of the filling process to allow for homogeneous gas mixing.

(3) Connect the test circuit and turn on the power supply, set the PID thermostat to the test temperature, and carry out the thermal decomposition test with different content of O2 and different temperatures.

(4) The duration of each group of tests was 12h, and the gas samples were collected inside the gas chamber every 2h, and the components and contents of the pyrolysis gases were analysed by gas chromatography-mass spectrometry (GC-MS), and at the end of the test, the heat source was removed to observe the surface morphology, and the inner wall of the gas chamber was cleaned with anhydrous ethanol, and the heat source was replaced again in the next test.

In this paper, the decomposition components of a C_4F_7N-CO_2-O_2 gas mixture under fault conditions were analysed by combined gas chromatography-mass spectrometry (GC-MS)

detection. The selected GC-MS instrument was a Shimadzu QP2010 Ultra (shown in Fig. 2.13), and its main components included the carrier gas system, the injection system, the column box, the chromatographic columns, the detection system, and the recording system. The equipment selects high-purity He gas with purity higher than 99.999% as the carrier gas, combines a packed column and a special capillary column, and employs a double-pulsed He ion detector (PDHID) with a detection accuracy of 0.01 μL/L. The PDHID is a high performance liquid chromatography (HPLC) system with a high purity and low cost of ownership. From the earlier findings, it was observed that the main gaseous by-products generated from the decomposition of C_4F_7N gas mixture under different conditions (discharge, superheat) were CF_4, $C2F_6$, C_3F_6, C_3F_8, CO, CF_3CN, C_2F_5CN, COF_2, $(CN)_2$ and $C_2F_6O_3$, and the selected chromatographic column model CP-Sil5CB (60m*8μm*0.32mm) could effectively separate these decomposition products. 0.32 mm), which can effectively separate these decomposition products.

The warming procedure for the chromatographic column is as follows:

(1) The chromatographic column was kept at 32°C for 10 min.

(2) Heat to 150°C at a ramp rate of 60°C/min for 2 minutes.

(3) Both the inlet temperature and the ion source temperature were set to 200°C.

In this paper, the decomposition products of five standard gases, CF_4, C_2F_6, C_3F_8, C_3F_6 and CO, were analysed in absolute amounts by the external standard method [69]. For other decomposition characteristic components for which standard gases were not available, relative quantitative analyses were performed using a manual peak area integration method based on the results of analyses from the National Institute of Standards and Technology (NIST 14.0) database. Several of the identified compounds were matched against the compound database within GC/MS and were fluorocarbons (CF_4, C_3F_8, C_2F_6, and C_3F_6), oxygenates (CO, CF_2O, and $C_2F_6O_3$), and nitriles (CF_3CN, C_2F_5CN, and $(CN)_2$). In this paper, the single ion monitoring (SIM) method was used to detect possible decomposition products, and the mass-to-charge ratios (m/z) of the decomposition products under fault conditions for the C_4F_7N gas mixture are given in Table 2.5.

Fig. 2.13 Gas Chromatography Mass Spectrometer

Table 2.5 Mass-to-charge ratios of characteristic decomposition products of the C_4F_7N gas mixture

Gas decomposition products	mass-to-charge ratio (m/z)
CF_4	**69**
C_2F_6	**69**, 119
C_3F_8	**119**, 69, 169
C_3F_6	**69**, 131, 100
CF_3CN	**76**, 69
C_2F_5CN	**76**, 126, 69
$(CN)_2$	**52**
$C_2F_6O_3$	**50,** 69
CO	**12**
COF_2	**66**, 50

2.3.2 Characteristics of thermal decomposition of C_4F_7N-CO_2-O_2 with different O_2 contents

The main products of the thermal decomposition test of the C_4F_7N-CO_2-O_2 gas mixture are CF_4, C_3F_8, C_3F_6, CO, COF_2, CF_3CN, C_2F_5CN and C_2N_2. Fig. 2.14 shows the variation of CF4, C3F8, C3F6 and CO production after POF decomposition test (450°C, 12 hours) at different O2 content. It can be found that among the four decomposition products, the highest amount of CO is generated and the lowest amount of CF4 is generated.At 0%-4% O2 content, the four products are CO, C3F6, C3F8 and CF4 in descending order. All possible decomposition paths and product generation paths for the C4F7N-CO2-O2 mixture under the POF test are given in Table 2.6. The main particles produced by decomposition are CF3, CF2,

CF2, C2F5, C3F7, CF, F, C, O, and CN (see D1-D14), and most of the products are produced by complexation of these particles (see R1-R14).

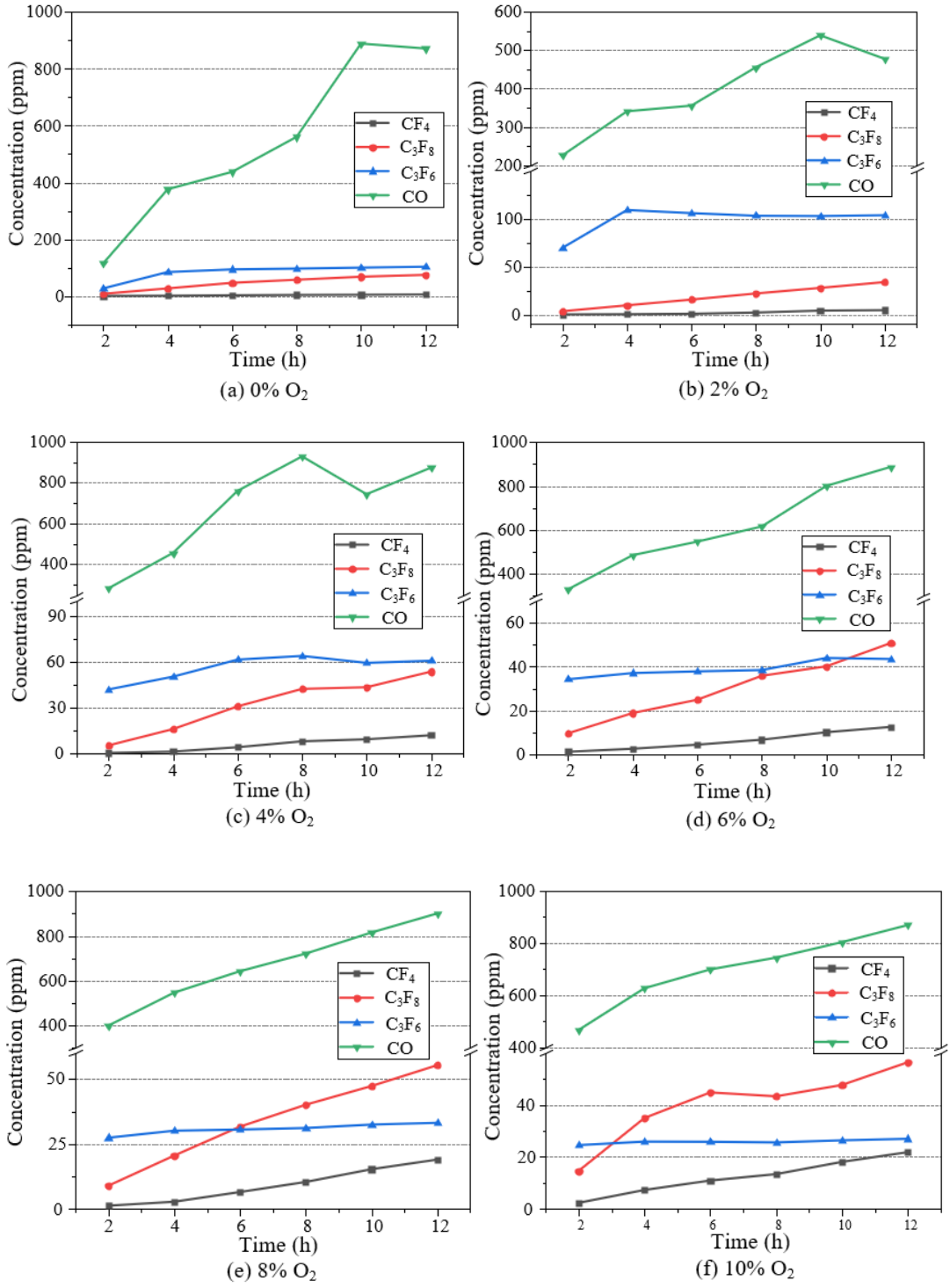

Fig. 2.14 Generation of C_4F_7N-CO_2-O_2 POF decomposition products at different O_2 contents

Studies have shown that the decomposition products of C_4F_7N-CO_2 gas mixture after 2000 times of AC breakdown test in the highest generation of CF_4 (greater than 4000 ppm),

followed by the generation of CO [71], these two decomposition products in the POF decomposition test under the generation of much lower than the breakdown of the breakdown test, resulting in this difference may be the main reason is that the electrical equipment discharge failure, discharge The main reason for this difference may be that when the electrical equipment discharge fault occurs, the temperature of the discharge centre can reach 2000K-12000K, and the high-energy arc instantly generates huge energy, which makes the chemical bond of the C_4F_7N molecules in the gas mixture break, and produces a large number of particle fragments, and the complex chemical reaction between the particles results in the generation of the decomposition products. The generation of CF_4 comes from the recombination of two particles that require CF_3 and F. Calculations in the literature have shown that these two particles are easier to produce compared to other particles, so the generation of CF_4 is the highest among the discharge decomposition products [91].

Table 2.6 Possible dissociation and complexation reaction pathways for C_4F_7N-CO_2-O_2 gas mixtures under POF conditions

Path	Decomposition reaction	Path	Recombination reaction
D1	$C_4F_7N \rightarrow (CF_3)_2CF+CN$	R1	$CF_3+F \rightarrow CF_4$
D2	$C_4F_7N \rightarrow (CF_3)_2C(CN)+F$	R2	$CF_2+CF_2 \rightarrow C_2F_4$
D3	$C_4F_7N \rightarrow CF_3CFCN+CF_3$	R3	$(CF_3)_2CF+F \rightarrow C_3F_8$
D4	$C_4F_7N \rightarrow CF_3CF_2CFCN+F$	R4	$CF_2=C\text{-}CF_3+F \rightarrow C_3F_6$
D5	$(CF_3)_2CF \rightarrow (CF_3)_2C+F$	R5	$CF_3+CN \rightarrow CF_3CN$
D6	$(CF_3)_2C \rightarrow CF_2=C\text{-}CF_3+F$	R6	$CF_3CFCN+F \rightarrow C_2F_5CN$
D7	$CF_2=CF\text{-}CF_3 \rightarrow CF_2=CF+CF_3$	R7	$CN+CN \rightarrow C_2N_2$
D8	$CF_3CFCN \rightarrow CFCN+CF_3$	R8	$CF_2+O \rightarrow COF_2$
D9	$CF_3CFCN \rightarrow CN+CF_3CF$	R9	$CF_3+O \rightarrow COF_2+F$
D10	$CF_3CF \rightarrow C\text{-}CF_3+F$	R10	$C_2F_4+O_2 \rightarrow 2COF_2$
D11	$CF_3 \rightarrow CF_2+F$	R11	$CF+F+O \rightarrow COF_2$
D12	$CF_2 \rightarrow CF+F$	R12	$2C+O_2 \rightarrow 2CO$
D13	$CO_2 \rightarrow CO+O$	R13	$C+O_2 \rightarrow CO_2$
D14	$O_2 \rightarrow O+O$	R14	$2CO+O_2 \rightarrow 2CO_2$

The overheating temperature set in the test was 400°C-525°C, which is low compared to the energy released by a discharge fault. Therefore, the generation of CF_4 and CO from decomposition under overheating faults is much smaller than that of discharge faults. In fact, the wave functions of the C_4F_7N frontline analysis orbitals are mainly distributed on the carbon atoms attached to the CN group and their neighboring carbon atoms [89], and the more reactive chemistry of the CN group may lead to the interaction of the C_4F_7N molecule with the metal

heating element at high temperatures to generate C_3F_7 and CN particles (as shown in Table 2.6(D1)). C_3F_7 particles can combine with F particles to form C_3F_8 (see Table 2.5 (R3)) or can be further decomposed to form C_3F_6 and F particles. It has been shown that the C_4F_7N-CO_2 gas mixture can react with copper at 220°C to first form C_3F_6 [105]. Therefore, under POF decomposition conditions, the content of C_3F_6 and C_3F_8 is higher than that of CF_4. As shown in Table 2.6, CO is mainly from the following sources: (1) activated C and O in the stainless steel of the heating element combined at high temperatures; (2) decomposition of CO_2 at high temperatures; and (3) reduction reactions of CO_2 and C particles at high temperatures. Therefore, the POF decomposition test had the highest CO

In addition, it can be found that the generation of CF_4 and C_3F_8 increases with the increase of superheating time. In the 12 h continuous test, CF_4 production was low and started mainly at 4 h of superheating time. The maximum generation of CF4 was 21.84 ppm at 10% O_2. The maximum generation of C_3F_8 was 103.51 ppm (2% O_2, 12h). The change in C_3F_6 production began to stabilize after 6 hours of POF testing with a maximum increment of no more than 3.5 ppm, suggesting that C_3F_6 production saturates with POF time. The difference between the maximum and minimum values of C_3F_6 generation during the 12h continuous POF test was 76.39ppm (0% O_2), 33.86ppm (2% O_2), 18.77ppm (4% O2), 9.22ppm (6% O_2), 5.74ppm (8% O_2), and 2.42ppm (10% O_2), which can be seen that the higher the O_2 content, the smaller the trend of C_3F_6 generation, indicating that the addition of O_2 is detrimental to the generation of C_3F_6. (8% O_2), 5.74ppm (8% O_2) and 2.42ppm (10% O_2), it can be seen that the higher the O_2 content, the smaller the trend of C_3F_6 generation, indicating that the addition of O_2 is not conducive to C_3F_6 generation. The generation of CO showed a significant increase with test time, with a maximum level of 928.26 ppm (4% O_2, 12h).

Partial overheating faults within gas-insulated equipment begin as potential faults of low energy and can develop further into serious faults if appropriate measures are not taken. In fact, it is inaccurate to judge the severity of equipment failure based only on the trend of decomposition product generation with different factors, and it is necessary to consider the rate of gas production, which can be a more intuitive description of the severity of failure and its trend [106]. As defined in equation (2.32), R_i is the absolute rate of gas production, $C_{i1}$and C_{i2} can be described as the amount (ppm or peak area) of decomposition product i measured for the first and second time, and Δt is the time interval between two sample collections.

$$R_i = \frac{C_{i1} - C_{i2}}{\Delta t} \tag{2.32}$$

It is more statistically significant to use the effective rate of gas production, RRMS, to describe the trends of the different decomposition products with respect to the influencing

factors [106]. Equation (2.33) gives the formula for R_{RMS}, where R_{ij} is the absolute gas production rate of decomposition component i at hour j (j = 2,4,6,8,10,12) and n is the number of samples. The duration of each set of pyrolysis tests was 12 hours and samples were collected every 2 hours, resulting in an n-value of 6.

$$R_{RMS} = \sqrt{\frac{\sum_{j=1}^{n} R_{ij}^2}{n}} \tag{2.33}$$

The effective gas production rate equation (2.34) used herein can be derived from Eq. (2.32) and Eq. (2.33), where C_2、C_4、C_6、C_8、C_{10}、C_{12} represent the production of the decomposition components for 2h, 4h, 6h, 8h, 10h, and 12h, respectively.

$$R_{RMS} = \sqrt{\frac{\left(\frac{C_2}{2}\right)^2 + \left(\frac{C_4 - C_2}{2}\right)^2 + \left(\frac{C_6 - C_4}{2}\right)^2 + \left(\frac{C_8 - C_6}{2}\right)^2 + \left(\frac{C_{10} - C_8}{2}\right)^2 + \left(\frac{C_{12} - C_{10}}{2}\right)^2}{6}} \tag{2.34}$$

Fig. 2.15(a) gives the variation of CF4 production and effective gas production rate with O_2 content. The CF4 production was 5.3 ppm (12h), 4.58 ppm (12h) and 11.17 ppm (12h) when 0%O_2, 2%O_2 and 4%O_2 were added to the C_4F_7N-CO_2 mixture, respectively. In the C_4F_7N-CO_2 mixture the generation and effective gas production rate tended to increase with increasing O_2 content. In addition, the CF_4 production and the effective gas production rate remained stable with the addition of 4-6% O_2 to the C_4F_7N-CO_2 mixture, and started to increase sharply at O_2 contents higher than 6%. CF_4 generation was positively correlated with O_2 content.

The C_4F_7N-CO_2 gas mixture produced 74.38 ppm of C_3F_8 after the 12 h POF test, while the decomposition of the gas mixture containing 2% O_2 produced only 33.82 ppm of C_3F_8 (shown in Fig. 2.15(b)), which inferred that the addition of 2% O_2 could inhibit the production of C_3F_8. The amount of C_3F_8 generated and the effective rate of gas production remained stable at O_2 levels of 4-8 per cent and started to increase when the oxygen content was higher than 8 per cent. The generation of C_3F_8 at 10% O2 addition to the C_4F_7N-CO_2 mixture was 56.32 ppm (12 h), which is still lower than the case without O_2. As can be seen from Table 2.6, C_3F_8 is mainly composed of C_3F_7 and F particles. From the above analysis, it can be seen that the addition of a certain amount of O_2 will cause C_3F_7 to react with O particles or further decompose to form other products, which will lead to a decrease in the amount of C_3F_8 produced.

Fig. 2.15(c) shows the trend of C_3F_6 generation and effective gas production rate under different O_2 content conditions at 450°C. When 2% O_2 was added to the C_4F_7N-CO_2 mixture, the production of C_3F_6 increased from 26.69 ppm (2h) and 84.2 ppm (4h) to 69.65 ppm (2h)

and 108.98 ppm (4h), at which time the increase of C_3F_6 was 42.96 ppm (2h) and 24.78 ppm (4h), respectively. There was no significant change in the amount of C3F6 generated after adding 2% O_2 from 6h to 12h, which shows that the promotion effect of O_2 on the generation of C_3F_6 was more significant in the first 4h of the 12h test. When the O_2 content is higher than 4%, the generation of C_3F_6 and the effective gas production rate decrease sharply, which is mainly due to the unsaturated C=C bond contained in C_3F_6, and the further increase of O_2 may lead to the formation of other products in the presence of O_2, which will reduce the generation of C_3F_6.

From Fig. 2.15(d), it can be seen that when 2% O_2 was added to the C_4F_7N-CO_2 mixture, the CO production decreased from 871.61 ppm (12h) to 477.25 ppm (12h), and there was a trend of increase in the CO production at 4%-10% O_2 content. CO is mainly produced by the decomposition of CO_2 in the C_4F_7N-CO_2 gas mixture. Upon addition of a small amount of O_2 (2%) to the C_4F_7N-CO_2 gas mixture, some of the CO and O particles reacted to form CO_2, resulting in a decrease in CO production. In addition, the C particles in the stainless-steel heat generator and O_2 may also react at high temperatures to generate CO, so CO generation increases when the O_2 content is greater than 2%. The distribution law of CO particles with O_2 content in section 2.2.1 shows that the trend of CO particles is not obvious at 0%-4% O_2 content, and the CO particles start to decrease when O_2 is greater than 6%, which is somewhat different from the results of the experimental study, mainly due to the fact that there are no C particles from stainless steel heaters in the reaction system constructed by MD simulation study.

Fig. 2.16(a) shows the trend of COF_2 production and effective gas production rate under different O_2 content conditions at 450°C. The generation and effective gas production rate of COF_2 showed a decreasing trend after the addition of 2% O_2 to the C_4F_7N-CO_2 mixture, whereas the generation and effective gas production rate of COF_2 increased when the O_2 content was higher than 2%, and started to increase significantly when the O_2 content was higher than 8%. The generation of COF_2 requires the combination of CFx particles with O particles. The results of the MD simulation study in Section 2.2.1 show that the generation of CFx decreases with the addition of 2% O_2, and the generation of some CFx particles increases when the O_2 content is greater than 4%, which better explains the variation of the COF_2 generation with the O_2 content.

Fig. 2.16(b) and Fig. 2.16(c) show the trends of CF_3CN and C_2F_5CN generation and effective gas production rates at different O_2 contents at 450°C. The amount of CF_3CN and C_2F_5CN produced and the effective gas production rate decreased sharply when 2%O_2 was

added to the C_4F_7N-CO_2 gas mixture. The amount of CF_3CN and C_2F_5CN produced and the effective gas production rate increased when the O_2 content was higher than 2%. In fact, CF_3CN comes mainly from the composite of CF_3 and CN particles, and C_2F_5CN comes mainly from the composite of CF_3CFCN and F particles. The decomposition of C_4F_7N accelerates and generates CF_3 particles at higher O_2 content, so when the O_2 content is higher than 6%, the generation of CF_3CN increases sharply, and the generation of C_2F_5CN remains essentially unchanged. In addition, it can be seen from Fig. 2.16(d) that when 2% O_2 is added, the amount of C_2N_2 generation and effective gas production rate decrease significantly and continue to decrease with the increase of O_2 content, indicating that the addition of O_2 can significantly inhibit the generation of C_2N_2.

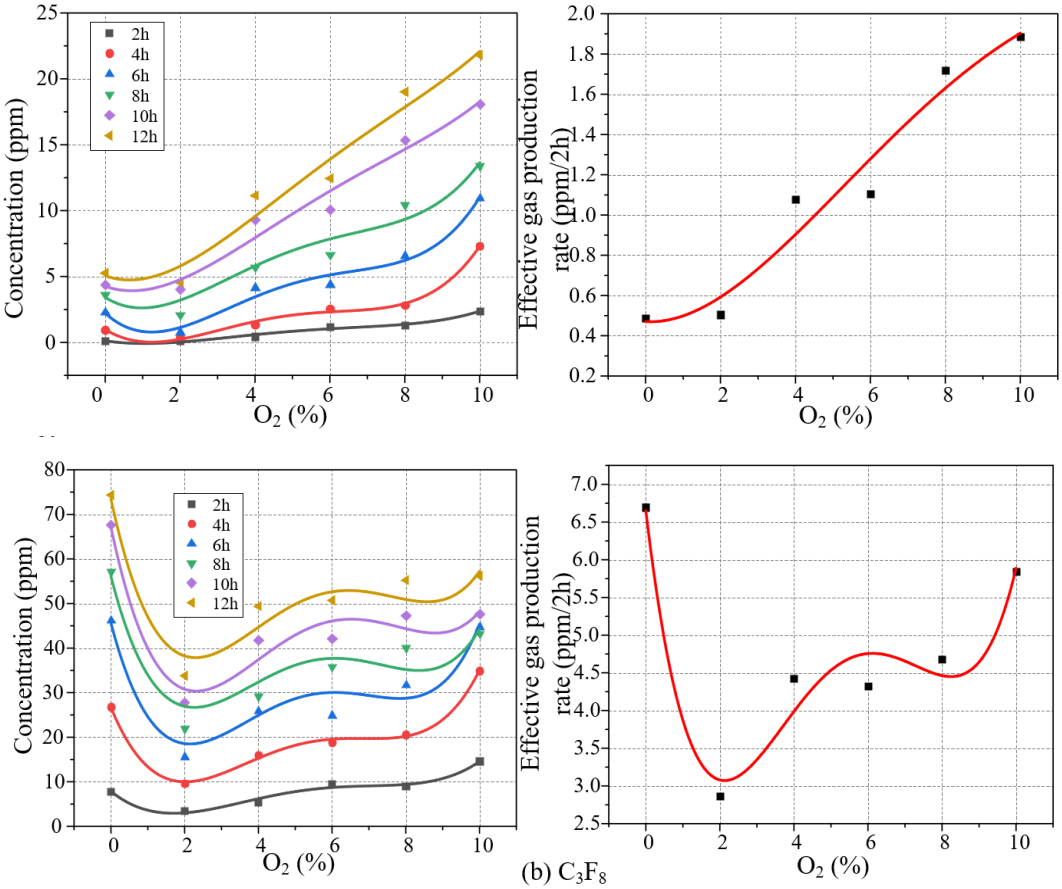

(b) C_3F_8

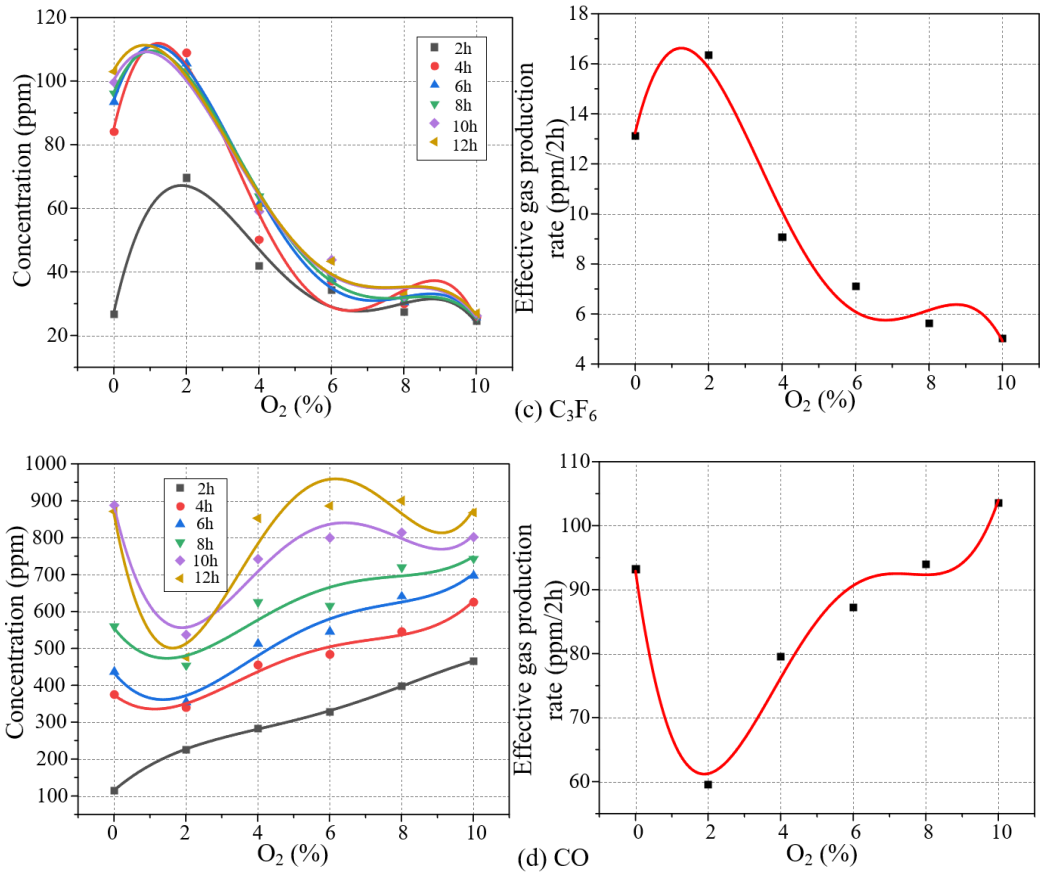

Fig 2.15 Variation of the production of C_4F_7N-CO_2-O_2 POF decomposition products and effective gas production rate with O_2 content

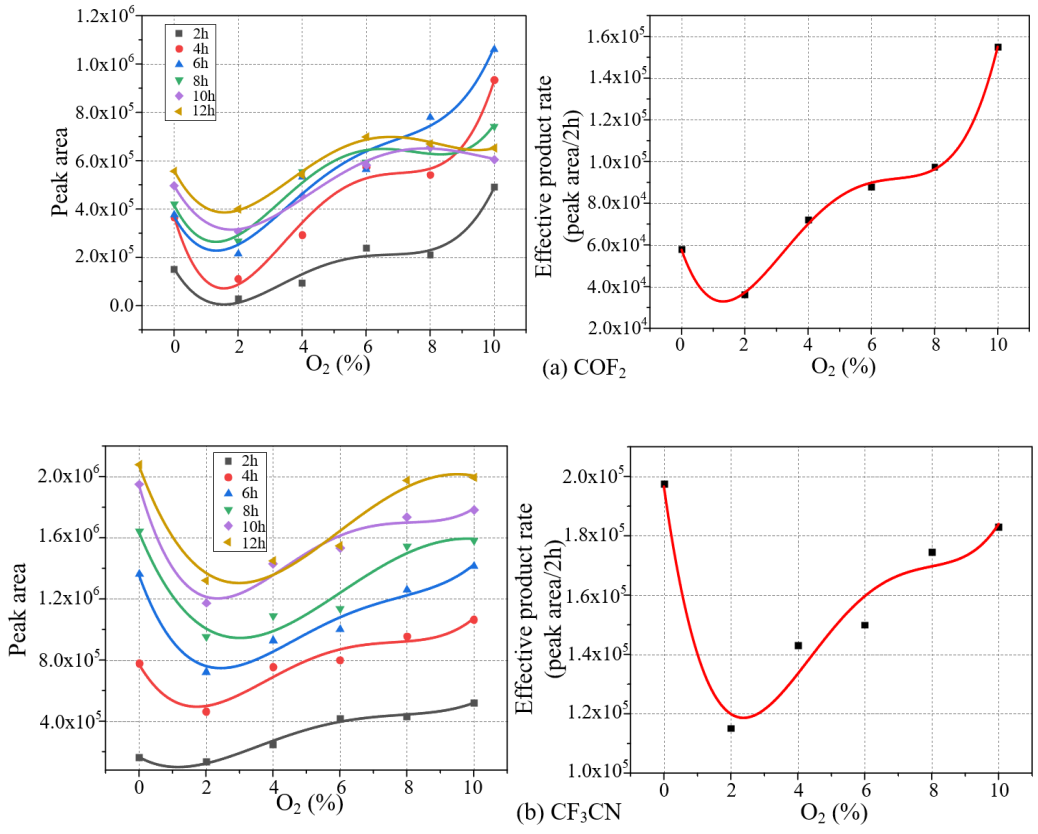

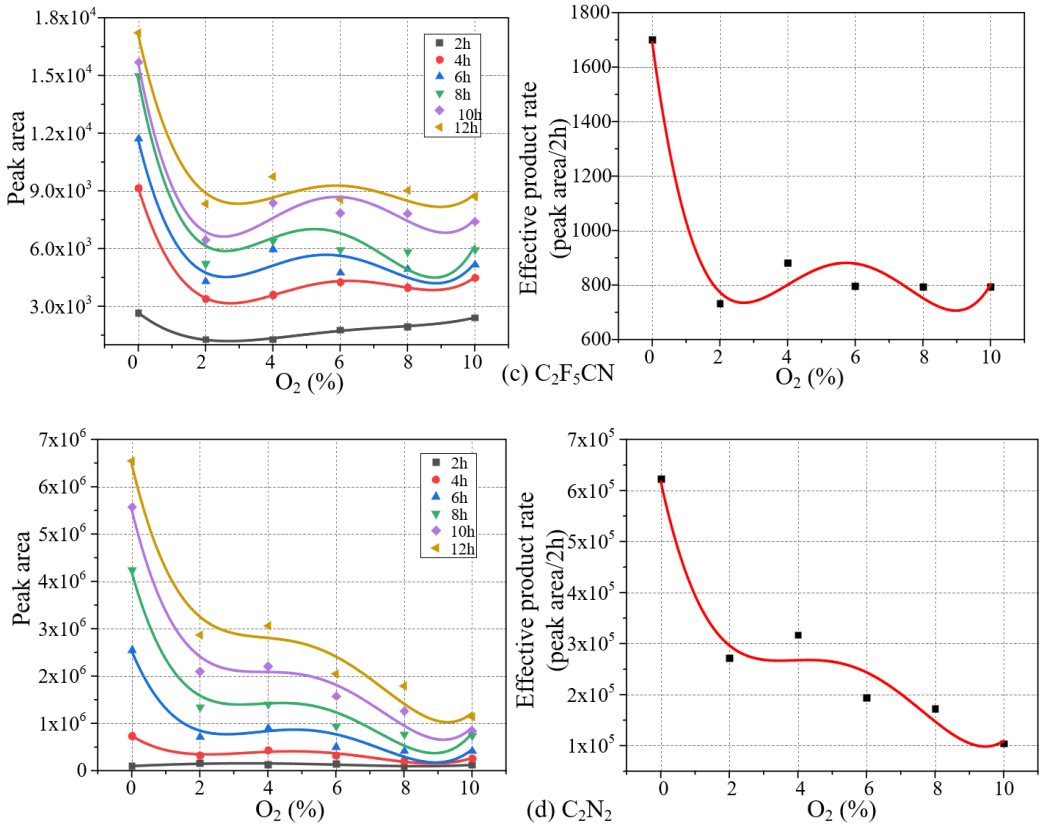

Fig 2.16 Variation of the production of C_4F_7N-CO_2-O_2 POF decomposition products and effective gas production rate with O_2 content

2.3.3 Thermal decomposition characteristics of C_4F_7N-CO_2-O_2 at different temperatures

Fig. 2.17 gives the variation of CF_4, C_3F_8, C_3F_6 and CO production with time for a C_4F_7N-CO_2-O_2 gas mixture containing 6% O_2 after POF tests at different temperatures. At 400°C-525°C, the production of CO is the highest of all quantifiable decomposition products, followed by C_3F_6 and C_3F_8. The production of CF_4 is much lower than the other decomposition products.

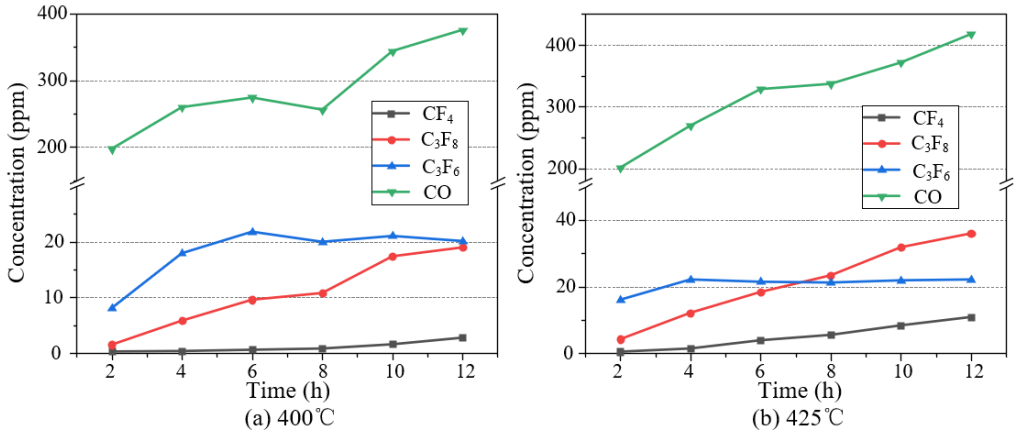

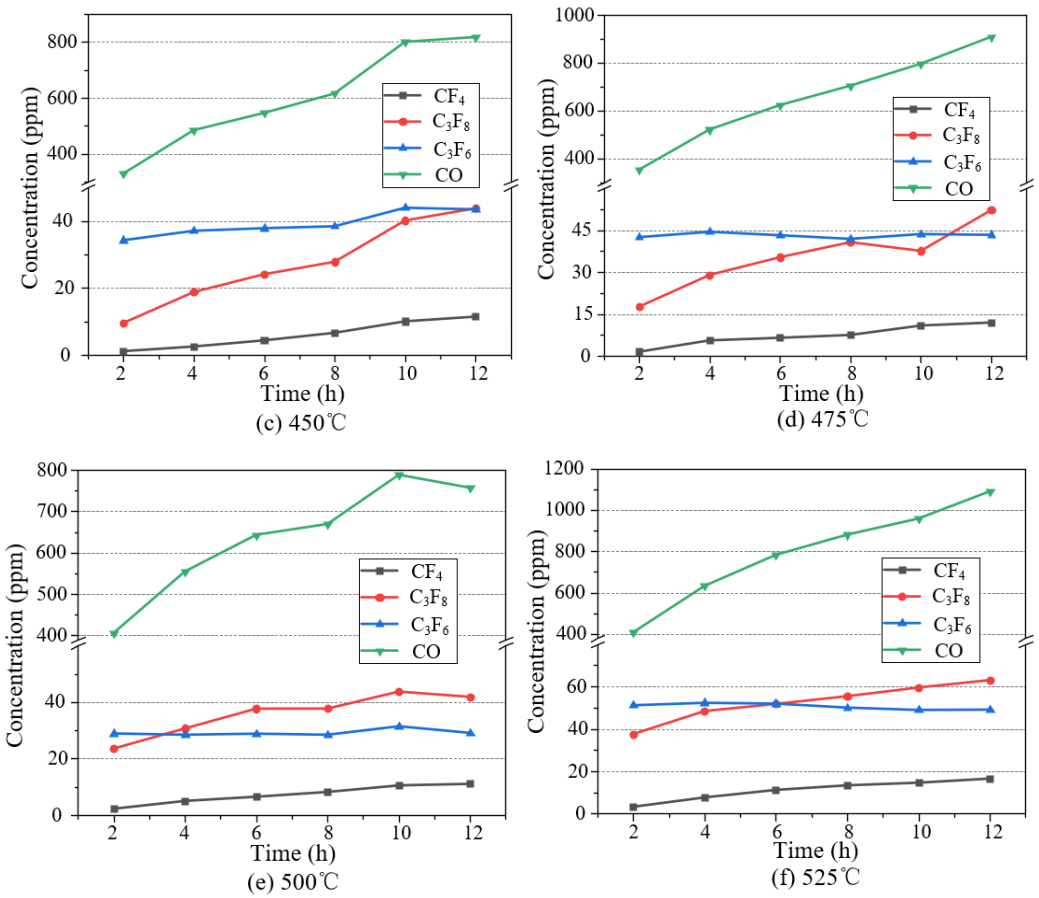

Fig. 2.17 Generation of C_4F_7N-CO_2-O_2 POF decomposition products at different temperatures

According to the trend of the generation of major decomposition products with superheating time at different temperatures, the generation of CF_4 at 525 °C was 3.22 ppm (2h), 16.56 ppm (12h); and the generation of C_3F_8 was 37.53 ppm (2h), 63.03 ppm (12h); The production of C_3F_6 was 51.13 ppm (2h), 49.09 (12h); the production of CO was 408.07 ppm (2h), 1092.27 ppm (12h). It can be seen that the production of C_3F_6 hardly changes with the increase of superheating time, while the production of the remaining decomposition products changes significantly with the increase of superheating time. C_3F_6 is mainly generated by the interaction between C_4F_7N and metal heaters, and the increase of O_2 content will accelerate the interaction between C_4F_7N and metal heaters, while the active metal particles produced by heaters at high temperatures are limited, so the changes in the amount of C_3F_6 generated will be stabilized in a short period of time.

Fig 2.18(a) shows the trend of CF_4 generation and effective gas production rate with temperature. The generation of CF_4 was 2.7 ppm (12h), 10.88 ppm (12h), 11.85 ppm (12h) and 16.56 ppm (12h) at 400°C, 425°C, 500°C and 525°C, respectively. The effective gas production rate of CF_4 increased sharply at 400°C-425°C and 500°C-525°C, respectively, with insignificant trends between 425 and 500°C. The production of CF_4 at 400 °C was 2.7 ppm,

indicating that the initial temperature for the decomposition of the C_4F_7N-CO_2-O_2 gas mixture POF to produce CF_4 was about 400 °C. When the temperature is higher than 400°C, the number of CF_3 and F particles increases, leading to a rapid increase in CF_4 production. Among several decomposition products CF_4 was generated in the smallest amount and did not show a correlation between temperature and generation, so CF_4 could not be used as a characteristic product to characterize the severity of overheating faults.

The amount of C_3F_8 produced and the effective gas production rate increased with temperature from 400 °C to 475 °C, decreased slightly at 500 °C, and increased sharply above 500 °C (shown in Fig. 2.18(b)). In the range of 400°C-475°C, the amount and effective gas production rate of C_3F_6 increased with the increase of temperature, and the amount of C_3F_6 at 475°C and 500°C were 43.34 ppm (12h) and 29.1 ppm (12h), respectively. When the temperature reaches 500°C, the amount of C_3F_6 and the effective gas production rate decreased slightly, and part of the C_3F_6 was generated by the interaction between C_4F_7N and the metal. Part of the C_3F_6 is generated by the interaction between C_4F_7N and the metal heat generator, when the temperature reaches 500°C, the metal heat generator is destroyed leading to a significant decrease in the amount of C_3F_6 generated, and when the temperature continues to increase (higher than 500°C), the chemical bond of the C_4F_7N molecule is broken leading to an increase in the amount of C_3F_6 generated (shown in Fig. 2.18(c)). The amount of CO production and the effective gas production rate varied little from 400-425°C, increased sharply from 425°C-450°C, showed a saturating growth trend from 450°C-500°C, and increased rapidly above 500°C (shown in Fig. 2.18(d)).

Fig. 2.19(a) shows the trend of COF_2 production and effective gas production rate at different temperatures. It can be seen that the effective gas production rate of COF_2 is positively correlated with temperature, increasing essentially linearly with temperature. Therefore, COF_2 is able to characterize to a large extent the degradation of the C_4F_7N-CO_2-O_2 mixture in the presence of POF. Figures 2.19 (b), 2.19 (c) and 2.19 (d) show the trends of the production and effective gas production rates at different temperatures for CF_3CN, C_2F_5CN and C_2N_2, respectively. The effective gas production rates of CF_3CN and C_2F_5CN increased dramatically between 400 °C and 450 °C, with a saturating trend at 450 °C and 500 °C, and continued to increase exponentially when the temperature exceeded 500 °C. The generation and effective gas production rate of C_2F_5CN showed a small temperature dependence trend at 400°C-500°C and increased sharply above 500°C. Therefore, C_2F_5CN can be used as a signature decomposition product of a leap in the nature of POF faults and must be given high priority when performing troubleshooting. The effective gas production rate of C_2N_2 increases

essentially linearly with increasing temperature, and thus C_2N_2 can be used as a characteristic product to characterize the degradation of the C_4F_7N-CO_2-O_2 mixture in the presence of POF.

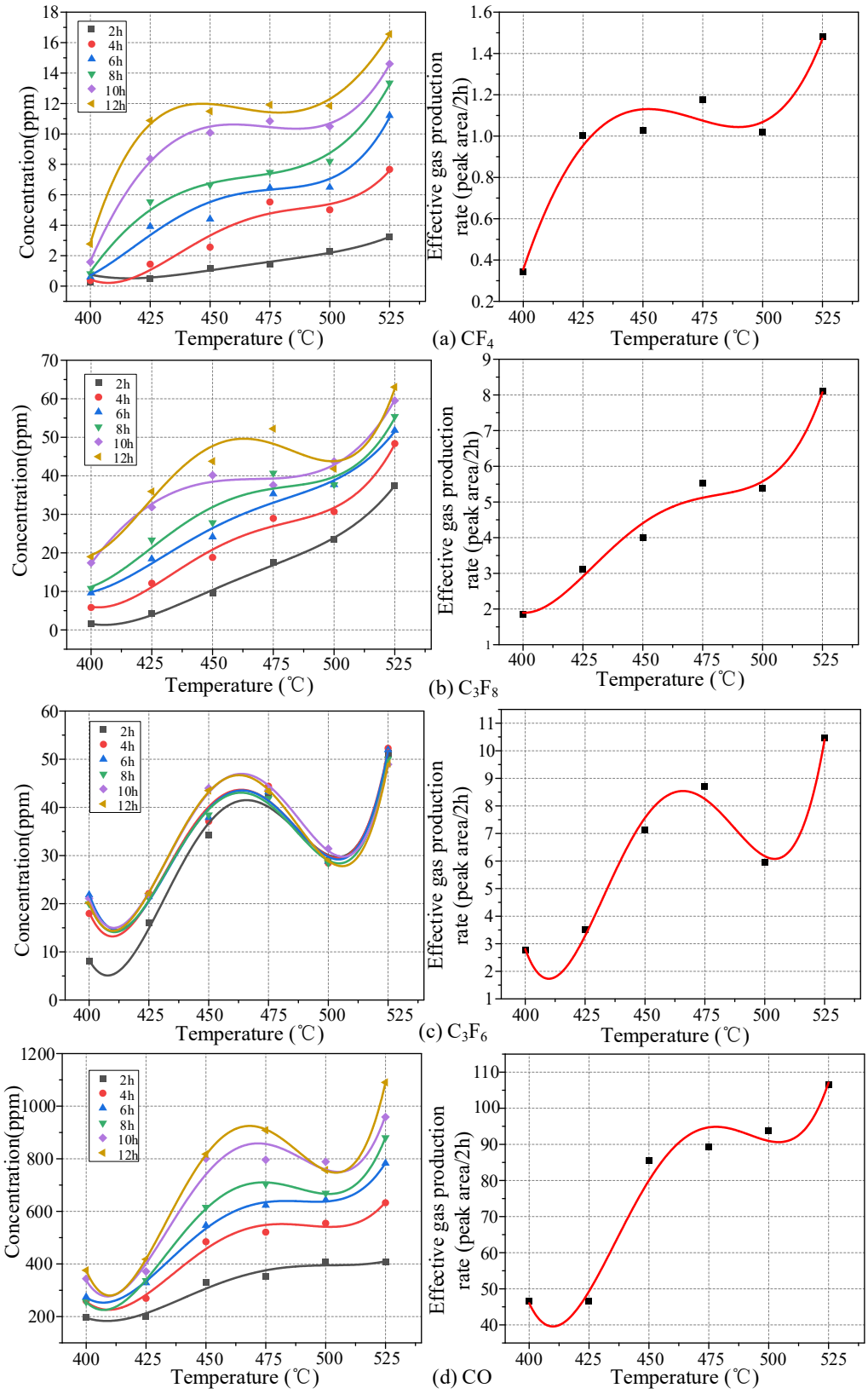

Fig. 2.18 Variation of C_4F_7N-CO_2-O_2 POF decomposition product generation and effective gas production rate with temperature

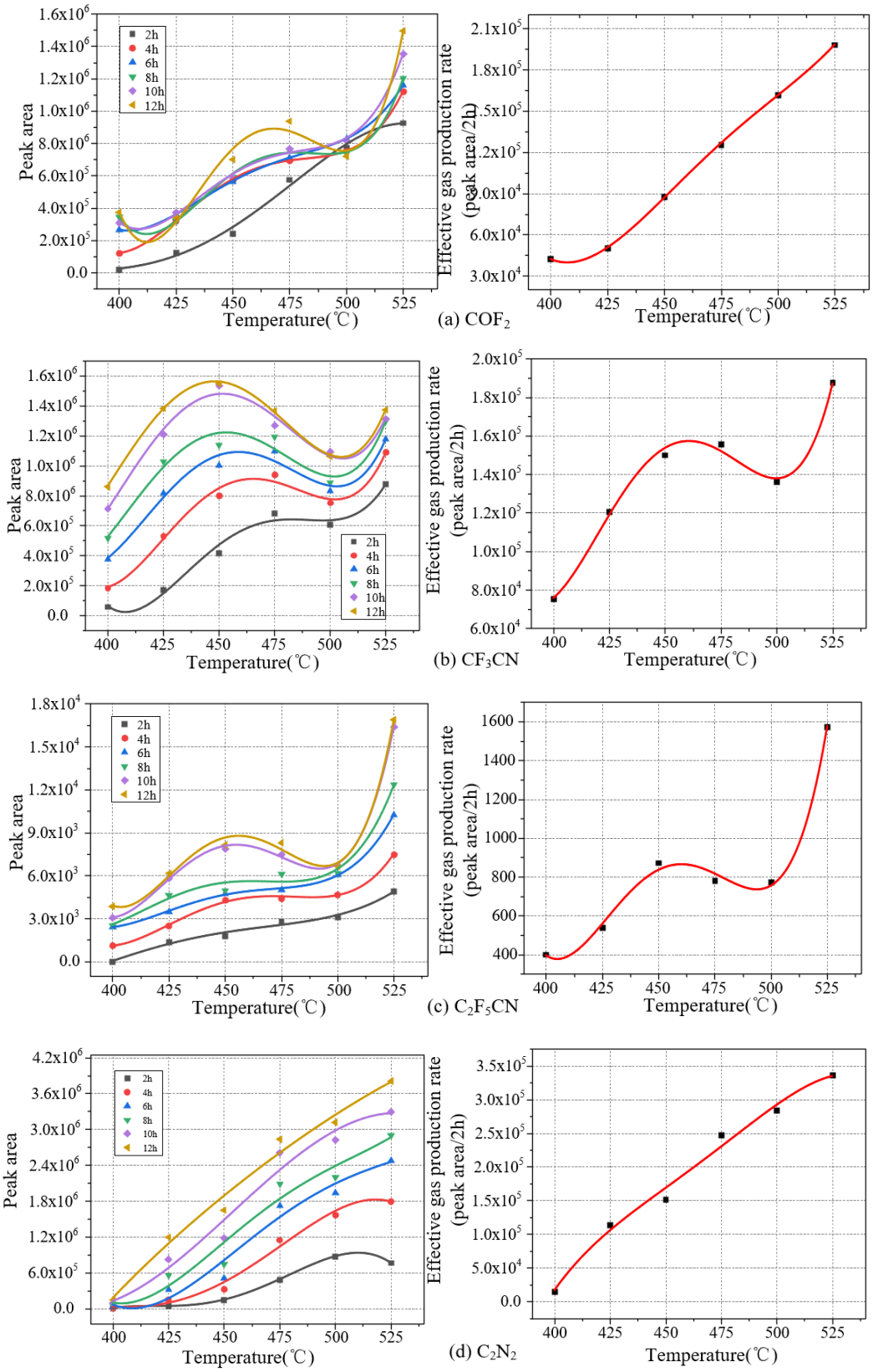

Fig. 2.19 Variation of C_4F_7N-CO_2-O_2 POF decomposition product generation and effective gas production rate with temperature

2.4 Summary of the chapter

In this chapter, the molecular dynamics simulation of the ReaxFF reaction was carried out by means of the constructed thermal decomposition model of C_4F_7N-CO_2-O_2 gas mixture, and the composition, distribution and generation rate of thermal decomposition particles of the mixture were obtained at different O_2 contents and temperatures, so as to reveal the thermal decomposition mechanism of the C_4F_7N-CO_2-O_2-O_2 mixture and the influence of O_2 on the thermal decomposition of the mixture; meanwhile, the thermal stability of the C_4F_7N-CO_2-O_2 mixture was investigated by means of the constructed superheated fault decomposition test platform. At the same time, the thermal stability of C_4F_7N-CO_2-O_2 mixture was investigated by using the superheated fault decomposition test platform, and the effects of temperature and O_2 content on the composition of the thermal decomposition products of the mixture and their generation amount were analysed. The main conclusions are as follows:

(1) The ReaxFF-MD simulation results show that the thermal decomposition of the C_4F_7N-CO_2-O_2 gas mixture mainly generates particles such as CF_3, CF_2, CF, F, C_2F_5, C_2F_4, C_2F_2, C_3F_7, C_2F_2N, C_3F_4N, CFN, CN, CO, O, and C, with the highest amount of the two types of particles CF_2 and CN, followed by CF_3 and F. Although the addition of O_2 to the C_4F_7N-CO_2 mixture decreases the initial decomposition time of C_4F_7N, it is effective in reducing the amount of decomposition of C_4F_7N and the generation of most of the particles, and in particular, the least amount of decomposition of C_4F_7N is achieved at an O_2 content of 6%. The addition of 0%-4% O_2 decreases the reaction rate of the main decomposition reaction in the reaction system, and the reaction rate increases at O_2 levels greater than 8%. At simulated temperatures greater than 2600 K, the initial decomposition time of C_4F_7N is significantly reduced and the rate of decomposition particle generation is accelerated.

(2) The main products of the thermal decomposition test of the C_4F_7N-CO_2-O_2 gas mixture are CF_4, C_3F_8, C_3F_6, CO, COF_2, CF_3CN, C_2F_5CN and C_2N_2. At an O_2 content of 2%, the production of all products decreased to varying degrees, except for C_3F_6 production, which increased; On further increase in O_2 content, the content of C_3F_6 decreased and the production of the remaining products increased; The rate of CF_4, C_3F_8, CO and COF_2 generation was accelerated at O_2 additions greater than 8%. The larger the addition of O_2 to the C_4F_7N-CO_2-O_2 mixture, the more pronounced is the saturation trend of C_3F_6 generation with the increase of local superheating failure time, and all other product generation shows a positive correlation with the superheating time.

(3) The production and effective gas production rates of CF_4, C_3F_6, C_3F_8, CF_3CN, and C_2F_5CN all decreased to varying degrees at 500 °C and continued to grow at temperatures

greater than 500 °C. The trend of C_2F_5CN generation and effective gas production rate with superheating temperature is small at 400°C-500°C, and increases rapidly when the temperature is greater than 500°C, which can be used as a signature decomposition product of the POF failure property jump. The effective gas production rates of both COF_2 and C_2N_2 show a strong positive correlation with the superheating temperature, which can be used as a characteristic product to characterise the degradation of the C_4F_7N-CO_2-O_2 mixture under the action of POF.

Chapter 3 C_4F_7N-CO_2-O_2 PD and its decomposition properties

Partial Discharge is one of the most common faults of gas-insulated electrical equipment, if the electrical equipment in the operation of the voltage under the continuous occurrence of partial discharge, the cumulative effect of the energy generated by these weak discharge will make the dielectric properties of the insulation medium gradually deteriorate and make the local defects to expand, and finally lead to the breakdown of the entire insulation; On the other hand, partial discharges will cause the decomposition of the gas insulating medium to form a number of by-products that have poor insulation properties and are hazardous to human health. Although the addition of a certain content of O_2 to the C_4F_7N-CO_2 mixture can improve the open-break performance and inhibit the generation of some by-products [66], the influence of the O_2 content on the PD and its decomposition characteristics of the C_4F_7N-CO_2-O_2 mixture is still unclear due to the strong oxidative property of O_2 itself, so it is necessary to further investigate the influence of different factors on the PD and its decomposition characteristics of the C_4F_7N-CO_2-O_2 mixture and its mechanism of action.

In this chapter, based on the partial discharge decomposition test platform, experiments on the PD and decomposition characteristics of C_4F_7N-CO_2-O_2 gas mixture with different O_2 contents and applied voltages are carried out, and the characteristic coefficients of the PD signals are extracted using MATLAB and the phase resolved partial discharge (PRPD) map is constructed to summarize the influence of different influencing factors on the PD statistical characteristic coefficients of C_4F_7N-CO_2-O_2 mixture through the parameters such as discharge repetition rate, average apparent discharge and cumulative discharge per unit time. The statistical parameters such as discharge repetition rate, average apparent discharge and cumulative discharge per unit time were used to summarize the effects of different influencing factors on the statistical parameters of the PD of the C_4F_7N-CO_2-O_2 mixture, and to analyze the influences of O_2 and applied voltage on the PD and decomposition characteristics of the C_4F_7N-CO_2-O_2 mixture. Finally, the components and contents of the solid precipitates produced during the PD process were tested at the microscopic level to analyse the generation mechanism and the influence law of O_2 on its generation.

3.1 PD decomposition test platform and method

3.1.1 Test platforms

The C_4F_7N-CO_2-O_2 gas mixture PD decomposition test bed is given in Fig 3.1. The test

transformer (0-100kV, 50kVA) generates an industrial frequency high voltage which is applied to the insulation defects (pin-plate electrodes) through a protective resistor (10kΩ), and a capacitive voltage divider (500pF, 100kV) is used to measure the test voltage applied to the ends of the insulation defects. Based on the pulsed current method recommended by the IEC 60270 standard, a coupling capacitance (500 pF, 100 kV) and a non-inductive detection impedance (50 Ω) were used to measure the pulsed signals of insulation defect PDs [107]. Tektronix DPO5104B is used to acquire PD signals with an analogue bandwidth of 1GHz, a sampling rate of 20GS/s, an A/D conversion accuracy of 8 bits and a memory depth of 48M. The test gas chamber is a homemade stainless steel tank with a volume of about 29L, which can withstand a maximum pressure of 1MPa and is well sealed.

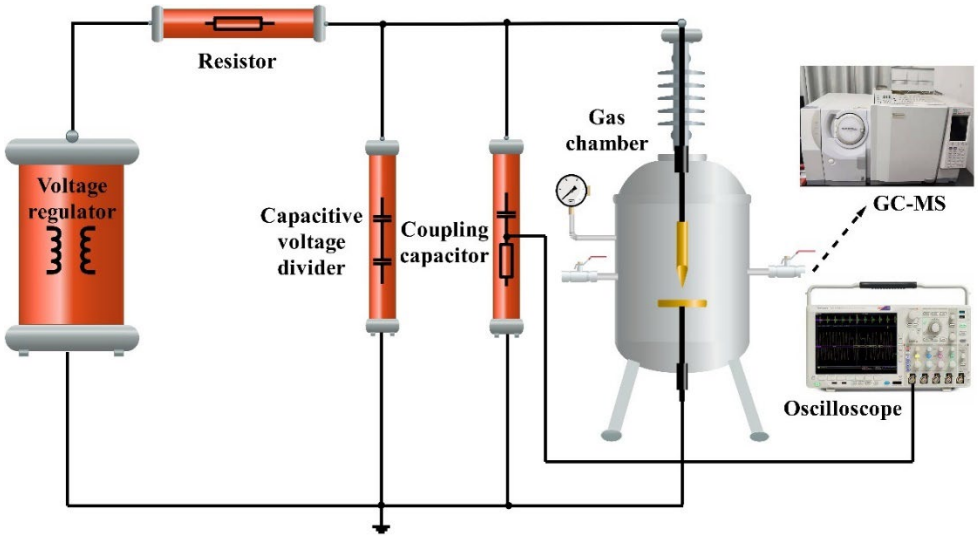

Fig. 3.1 Schematic diagram of PD decomposition characteristic test platform

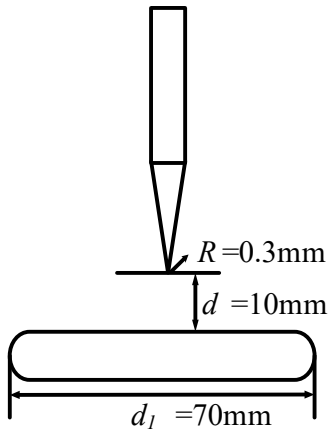

Fig. 3.2 Needle-plate electrode

Fig.3.3 JZF-9 type calibration pulse generator

Fig.3.4 Tektronix DPO 5104B Oscilloscope

Metal protrusion defects within equipment are usually caused by poor workmanship, damage during transport or assembly. The small radius of curvature of the tip of the protrusion causes an increase in the intensity of the local electric field, which forms a stable PD during the operation of the equipment and affects the safe operation of the equipment and the power system. The test uses a needle-plate electrode as shown in Fig.3.2 to simulate metal protrusion defects inside the device, the needle-plate electrode spacing is set to 10mm, the electrode material is brass, the needle electrode and the plate electrode are connected to the high-voltage conductor and the grounding conductor inside the tank, respectively. The radius of curvature of the tip end of the needle is 0.3 mm and the plate electrode has a diameter of 70 mm and a thickness of 8 mm.

3.1.2 PD signal detection system

The test adopts the pulse current method recommended by IEC60270 for the detection of PD signals and the correction of the discharge amount, using the JZF-9 calibration pulse generator shown in Fig. 3.3 to output pulse signals of known charge, the coupling capacitor provides a high-frequency low-impedance channel for the pulse signals, and the detection impedance will be converted from the pulse signals to the voltage signals, which are then displayed and stored by the oscilloscope (shown in Fig. 3.4), and finally the stored voltage signals under different charges are obtained from the discharge correction curve by the forced-

over-zero linear fitting method, and the pulse generator can output four kinds of pulse signals with charges of 5pC, 50pC, 100pC and 500pC. The calibration curves of the discharge of C_4F_7N-CO_2-O_2 gas mixtures with different contents of O_2 under metallic protrusion defects (needle-plate electrodes) are shown in Fig. 3.5.

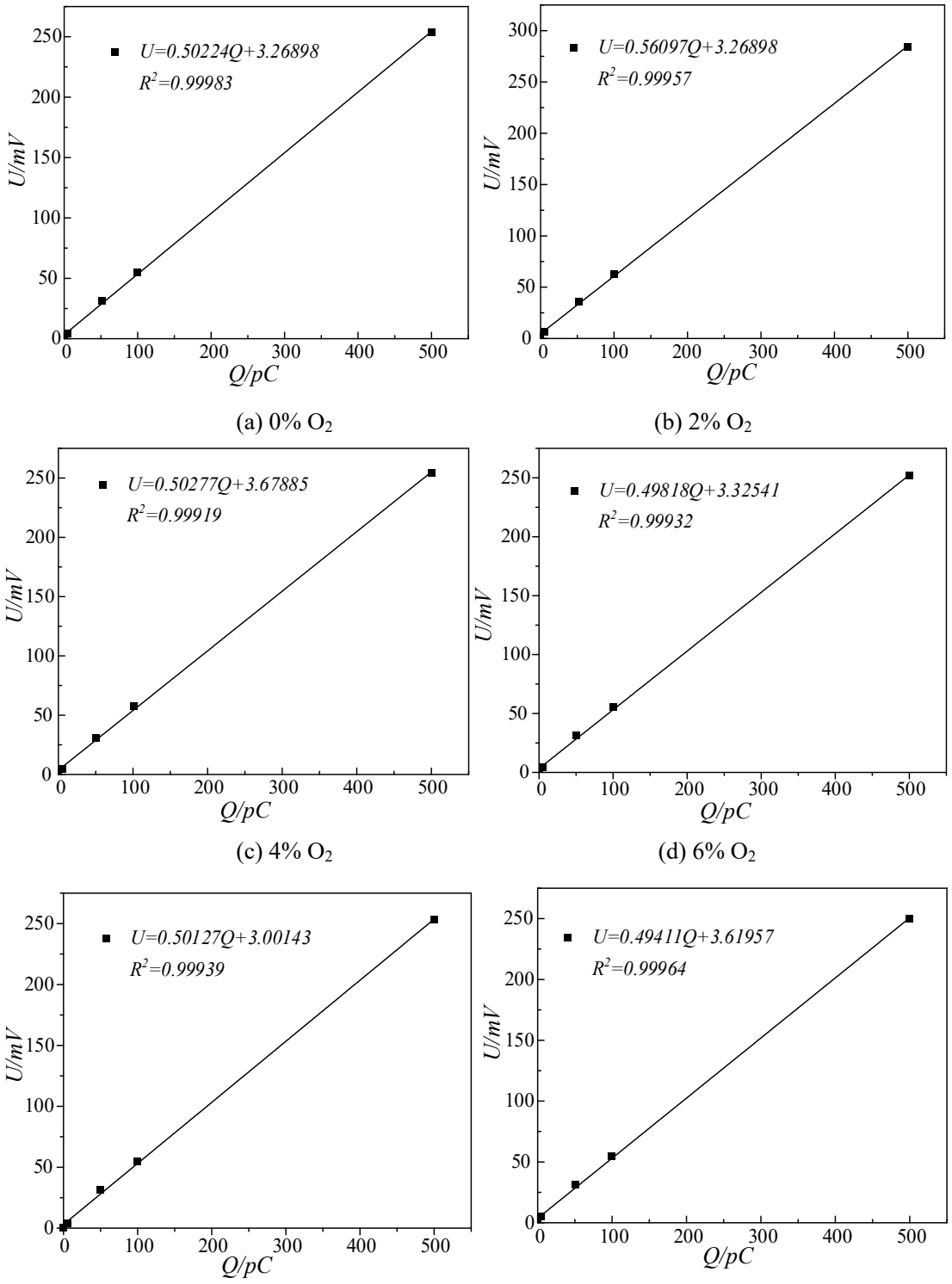

(a) 0% O_2 (b) 2% O_2

(c) 4% O_2 (d) 6% O_2

(e) 8% O_2 (f) 10% O_2

Fig.3.5 Calibration curves of insulation dielectric discharge at different O_2 contents

3.1.3 Test content and method

In this paper, the PD decomposition characteristics of C_4F_7N-CO_2-O_2 gas mixture containing 15% C_4F_7N at 0.14 MPa gas pressure were investigated at different O2 contents (0%, 2%, 4%, 6%, 8%, and 10%) and different applied voltages (21 kV, 24 kV, and 27 kV) in the following experimental steps:

(1) The test circuit was connected according to the schematic diagram of the test platform shown in Fig. 3.1, and the metal protrusion model (needle-plate electrode) was arrived inside the stainless steel canister, and then the interior of the stainless steel canister was cleaned, air-dried, and tested for airtightness according to the steps of the POF decomposition test.

(2) According to Dalton's law of partial pressure, C_4F_7N, O_2 and CO_2 were sequentially introduced into the gas chamber, and the corresponding partial pressures of the three gases in the different test groups were kept the same as that of the POF decomposition test method, and then left to stand for 12h to make the gases fully mixed uniformly.

(3) Adopt the step-by-step method to apply the required test voltage to the needle-plate electrode, and carry out the PD decomposition test with a discharge length of 96 hours continuously for each group of tests. Considering that the PD signals are more stable for 12 hours in the discharge process with a total length of 96h, and the decomposition of the gas insulating medium is less at this time, and the ablation of the electrode tip due to the discharge is less serious, it is more favorable for the study of the effects of O_2 content and applied voltage on the PD characteristics of the gas mixture. It is more advantageous to study the influence of O_2 content and applied voltage on the PD characteristics of the gas mixture. Therefore, the PD signal of 12 hours of discharge was collected by oscilloscope for statistical analysis, and then the decomposed gas was collected every 12h, and the type and content of the decomposed gas was detected by GC-MS, so as to analyse the influence of different influencing factors on the PD decomposition characteristics of the gas mixture.

3.2 C_4F_7N-CO_2-O_2 PD characteristics

3.2.1 Effect of O_2 on the properties of C_4F_7N-CO_2-O_2 PD characteristics

Due to the uncertainty of the PD generation process, the amplitude and phase of the PD signals as well as the time interval between two adjacent discharges have a certain degree of randomness, so a single PD signal is not representative. In addition, the electronegativity and strong oxidation of O_2 also lead to a large dispersion of the PD of the C_4F_7N-CO_2-O_2 mixture, so the influence law of the O_2 content on the partial discharge characteristics of C_4F_7N-CO_2-O_2 is analysed in detail here by means of the PD statistical characteristic coefficients.

Firstly, the partial discharge inception voltage (PDIV) of the gas mixture with different O2 contents were measured on the experimental setup as 15.2kV (0% O_2), 16kV (2% O_2), 17kV (4% O_2), 15.8kV (6% O_2), 15.9kV (8% O_2) and 16.3kV (10% O2), and the average partial discharge inception voltage was about 16kV, so the externally applied voltage of the test group with different O_2 contents was set to be 16kV. O_2), 15.8kV (6% O_2), 15.9kV (8% O_2) and 16.3kV (10% O_2), the average partial discharge onset voltage is about 16kV, so the applied voltage of the test group is set to be 1.5PDIV, i.e., 24kV, for the different O_2 contents, to ensure that the PD signals are stable and the insulation breakdown will not occur. In order to investigate the influence law of O_2 content on the PD characteristics of C_4F_7N-CO_2-O_2 gas mixture, the PD signals were continuously collected for 1 s at different O_2 contents (repeated the test for five times), and the PD characteristic quantities, such as the number of discharges, the amount of discharges and phases, were extracted to construct the PRPD profiles of the number of discharges-phase (n-φ) and the amount of discharges-phase (q-φ). One of the data sets was selected for analysis because of the good reproducibility of the statistical characteristics of PD in the repeated trials.

The PRPD profiles of the C_4F_7N-CO_2-O_2 mixture at different O_2 contents are shown in Fig.3.6. It can be seen that the PD for the different conditions is mainly concentrated in the positive half-period of the IF. The negative half-period discharge disappeared after the addition of 2%-4% O_2 to the C_4F_7N-CO_2 gas mixture, indicating that the addition of a certain content of O_2 can inhibit the generation of negative half-period discharge.

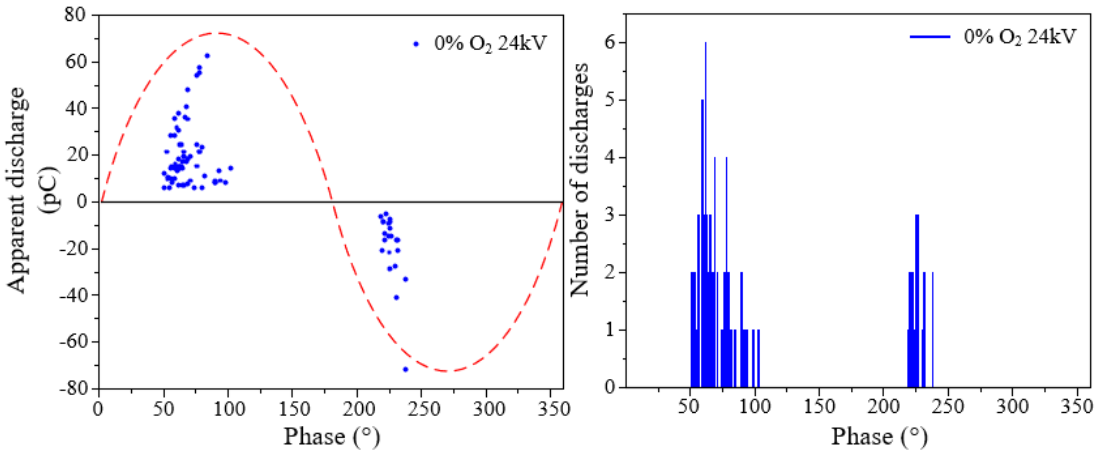

(a) 0% O_2

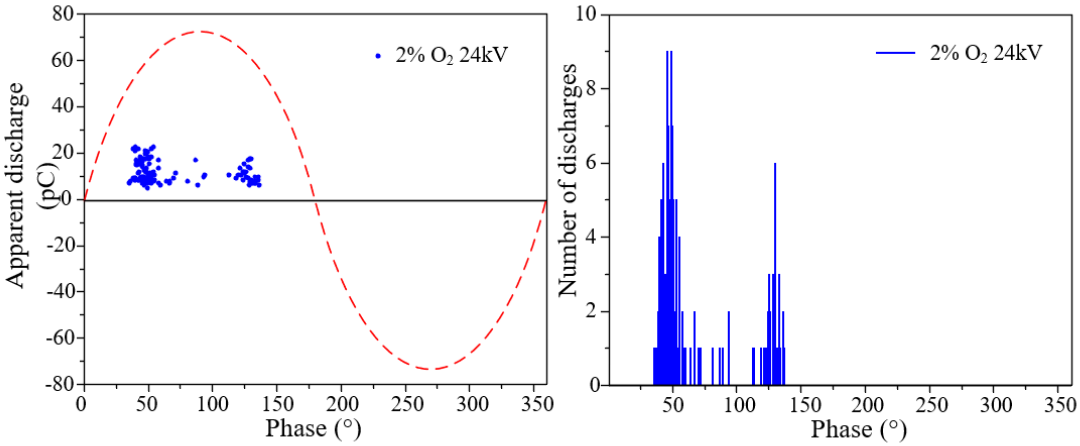

(b) 2% O_2

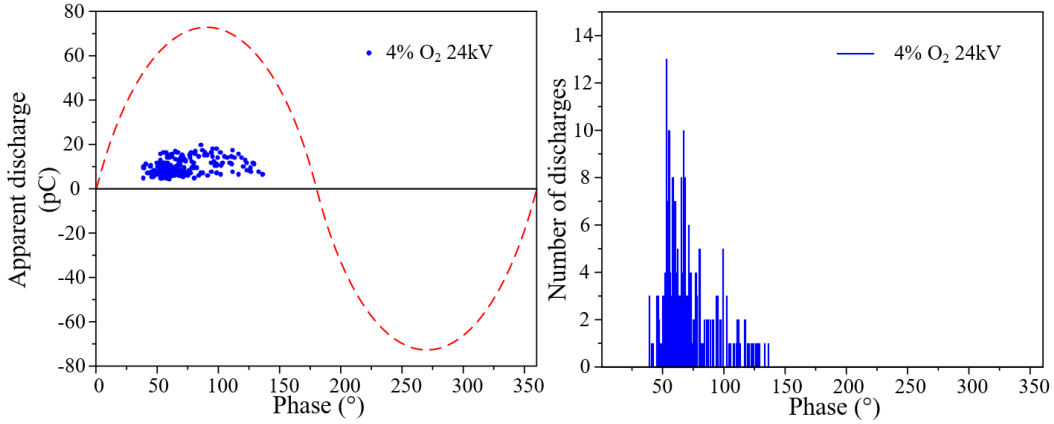

(c) 4% O_2

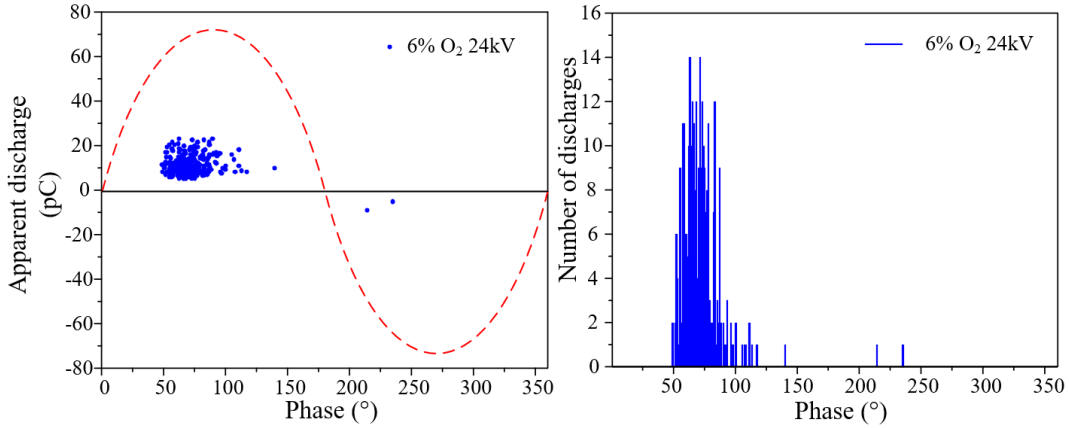

(d) 6% O_2

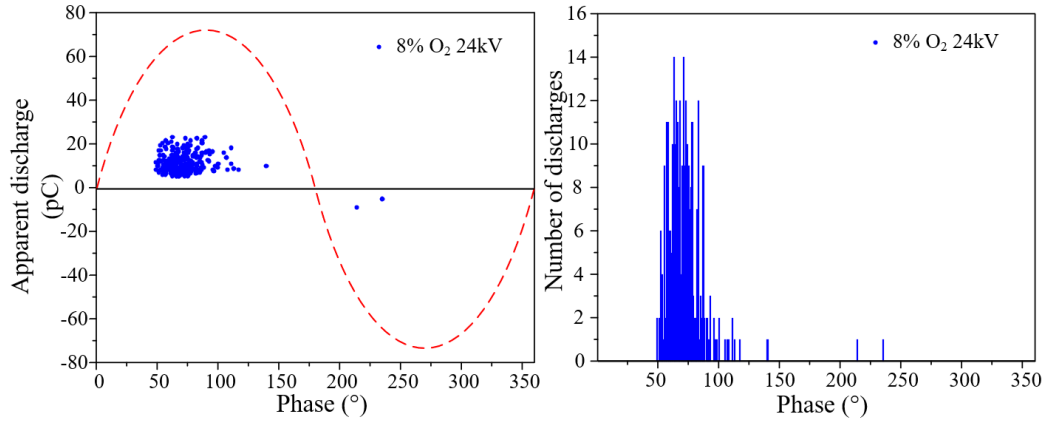

(e) 8% O_2

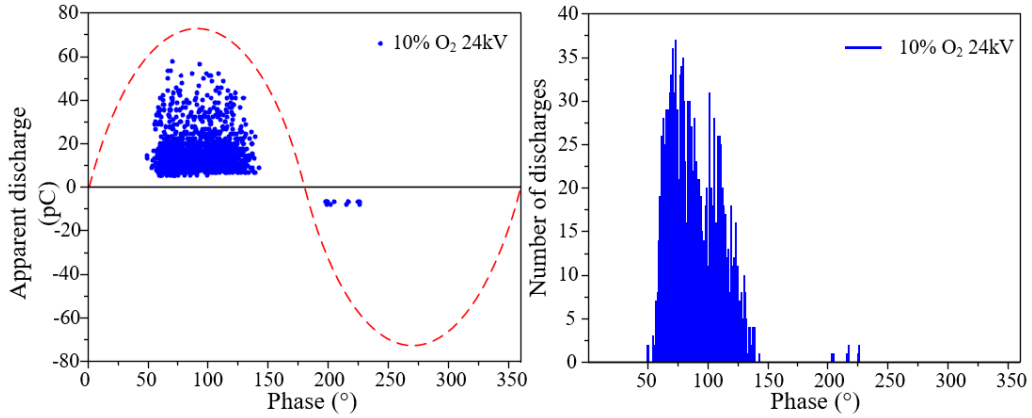

(f) 10% O_2

Fig.3.6 PRPD maps of C_4F_7N-CO_2-O_2 gas mixtures at different O_2 contents

The PRPD mapping profiles differed greatly at different O_2 contents, with a positive half-period discharge phase interval of 76° for the C_4F_7N-CO_2 mixture, and the discharge intervals after the addition of O_2 were 101° (2% O_2), 97° (4% O_2), 88° (6% O_2), 91° (8% O_2), and 93° (10% O_2), respectively. It can be seen that the intervals of the discharge phase distribution in the positive half of the periphery increase significantly after the addition of O_2. However, regardless of the O_2 content, the positive half-period discharge is mainly concentrated at 50°-120°, and the negative half-period discharge is mainly concentrated at 200°-240°. The C_4F_7N-CO_2 gas mixture had the highest number of discharges at 24 kV in a phase of 62°, with a total of 6 discharges; The phase with the highest number of discharges after the addition of 2% O_2 was advanced to 46°, with a total of nine discharges; When the O_2 content was greater than 2%, the phases with the highest number of discharges gradually shifted backwards to 4% O_2 (53°, 13 times), 6% O_2 (63°, 14 times), 8% O_2 (62°, 40 times) and 10% O_2 (74°, 37 times).

With the increase of O_2 content, the phase where the peak number of discharges is located shows a trend of decreasing and then increasing, the peak number of discharges increases gradually, and the peak number of discharges increases sharply when the O_2 content is greater than 6%, and the peak number of discharges reaches saturation when the O_2 content is greater than 8%.

It can also be seen from Fig. 3.6 that the maximum single-pulse discharges of the PD single-pulse of the C_4F_7N-CO_2-O_2 gas mixture with different O_2 contents were 62.4 pC (0% O_2), 22.5 pC (2% O_2), 19.9 pC (4% O_2), 23.3 pC (6% O_2), 50 pC (8% O_2), and 57.8 pC (10% O_2), and that the maximum single-pulse discharges of C4F7N-CO_2 gas mixture with 2%-6% O_2 decreased substantially, suggesting that the addition of O_2 can reduce the maximum single-pulse discharges of C_4F_7N to a certain extent. CO_2 gas mixtures with 2%-6% O_2, the maximum single-pulse discharges were drastically reduced, indicating that the addition of O_2 can reduce the maximum single-pulse discharges to a certain extent. There were 13 PDs with discharges greater than 30 pC without O_2; PDs with discharges exceeding 30 pC disappeared when 2%-6% O_2 was added; The PDs with discharges greater than 30 pC were 50 and 138 at O_2 contents of 8% and 10%, respectively, suggesting that the addition of 2%-6% O_2 can inhibit the PDs with larger discharges, and the PDs with larger discharges increased sharply when the O_2 content was greater than 6%, suggesting that the insulating properties of the gas mixture may be degraded by the addition of O_2 greater than 6% to the C_4F_7N-CO_2 gas mixture.

The PRPD maps better reflect the stochastic distribution characteristics of the PD characteristic quantity. In order to better reveal the influence law of the O_2 content on the PD characteristics of the C_4F_7N-CO_2-O_2 mixture, the discharge repetition rate (number of discharges), the cumulative discharges per second, and the average discharges at different O_2 contents were further extracted in this paper, and the trends of the three typical characteristic quantity with the O_2 content are shown in Fig. 3.7, Fig. 3.8 and Fig.3.9, and the related parameters are shown in Table 3.1.

From Fig. 3.7, it can be seen that the discharge repetition rate in the positive half of the PD of the C_4F_7N-CO_2-O_2 gas mixture is much higher than that in the negative half, and the negative half discharge disappears with the addition of 2%-4% O_2 to the C_4F_7N-CO_2 gas mixture, and reappears with a further increase in the O_2 content. The positive semi-periodic discharge repetition rate increased slowly under 0%-6% O_2 conditions, and both positive and negative semi-periodic discharge repetition rates increased sharply when the O_2 content was greater than 6%.

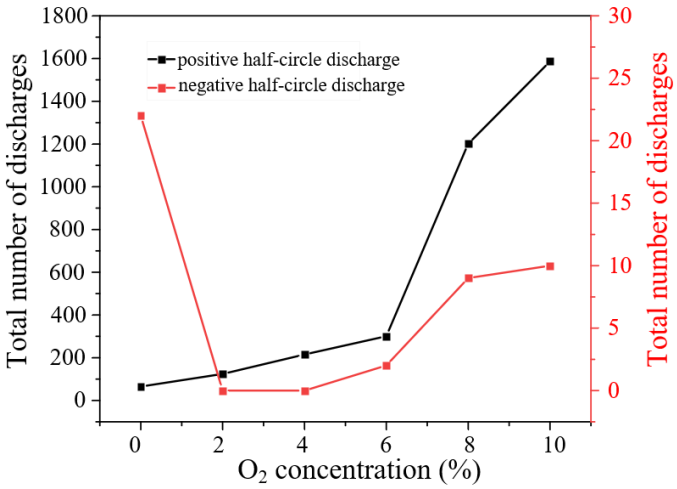

Fig.3.7 Total number of discharges of C_4F_7N-CO_2-O_2 gas mixtures at different O_2 contents

The cumulative PD discharges of the C_4F_7N-CO_2-O_2 mixture at different O_2 contents were 1716.18 pC (0% O_2), 1429.48 pC (2% O_2), 2176.51 pC (4% O_2), 3372.26 pC (6% O_2), 16625.536 pC (8% O_2) and 24616.34 pC (10% O2) (shown in Fig.3.8). It can be seen that the cumulative discharge decreases with the addition of 2% O_2 to the C_4F_7N-CO_2 gas mixture, and increases slowly at 2%-6% O_2. When the O_2 content is greater than 6%, the cumulative discharge increases sharply, indicating that the addition of O_2 to the C_4F_7N-CO_2 gas mixture at a level greater than 6% may lead to insulation degradation of the gas mixture.

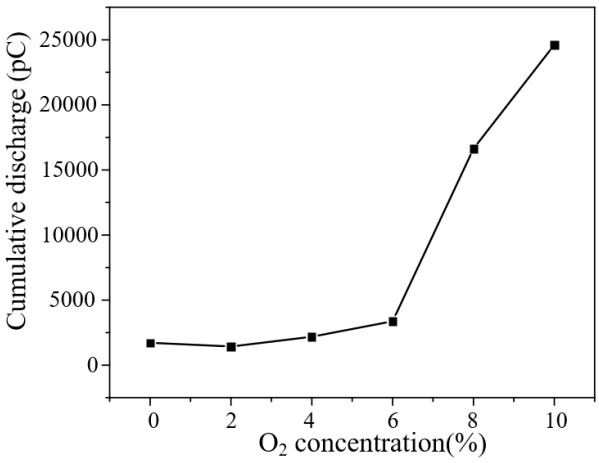

Fig.3.8 Cumulative discharge of C_4F_7N-CO_2-O_2 gas mixtures at different O_2 contents

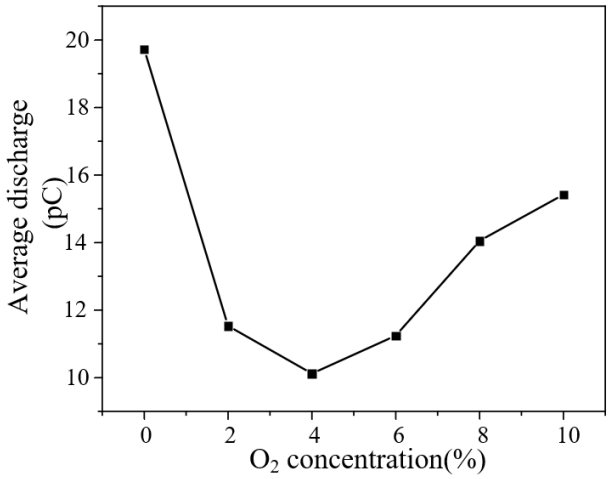

Fig.3.9 Average discharge of C_4F_7N-CO_2-O_2 gas mixtures at different O_2 contents

The average discharges at different O_2 contents can be seen in Fig.3.9 as 19.72pC (0% O_2), 11.53pC (2% O_2), 10.12pC (4% O_2), 11.24pC (6% O_2), 14.05pC (8% O_2), and 15.42pC (10% O_2). After adding a certain content of O_2 to the C_4F_7N-CO_2 gas mixture, the average discharge decreased, especially the average discharge of the PD of the gas mixture with O_2 addition of 4% decreased by 41% compared with the case without O_2, and the average discharge started to increase with 4% O_2 content, but it was always lower than the case without O_2, so the addition of a certain content of O_2 to the gas mixture can reduce the average discharge.

Table 3.1 Statistical characteristic parameters of C_4F_7N-CO_2-O_2 PD with different O_2 contents

O_2 content	Discharge Repetition Rate (1s)			Cumulative Discharge	Average
(%)	positive	negative	all	(pC)	Discharge (pC)
0%	65	22	87	1716.18	19.72
2%	124	0	124	1429.48	11.53
4%	215	0	215	2176.51	10.12
6%	298	2	300	3372.26	11.24
8%	1174	9	1183	16625.53	14.05
10%	1586	10	1596	24616.34	15.42

3.2.2 Effect of externally applied voltage on the properties of C_4F_7N-CO_2-O_2 PD characteristics

The C_4F_7N-CO_2-O_2 PRPD maps at different externally applied voltages are given in Fig.3.10, with discharge phase intervals of 48° (21 kV), 99° (24 kV) and 97° (27 kV). When the applied voltage increases from 21kV to 24kV, it can be seen that the discharge phase

interval increases by about one times, and the discharge repetition rate per second and the cumulative amount of discharge also increase by about one time. When the voltage increases from 24kV to 27kV, the discharge phase interval is basically unchanged, but the discharge repetition rate per second and the amount of discharge decrease, which may be due to the fact that the applied voltage increases to a certain degree will lead to the increase of the local electric field strength near the needle electrode, and the intense discharge near the needle electrode for a short period of time will lead to the ablation of the tip part of the needle electrode, which will lead to the decrease of the local electric field strength near the needle electrode. This may be due to the fact that an increase in the externally applied voltage to a certain extent will cause the local electric field strength near the needle electrode to increase, and the intense discharge near the needle electrode for a short period of time will result in the tip of the needle electrode being partially ablated, which will lead to an increase in the radius of curvature of the needle electrode, and the local electric field strength near the needle electrode to decrease, which will lead to a reduction in the number of electrons collapsing near the needle electrode, and thus the cumulative amount of discharge and the rate of repetitions of the discharge decrease.

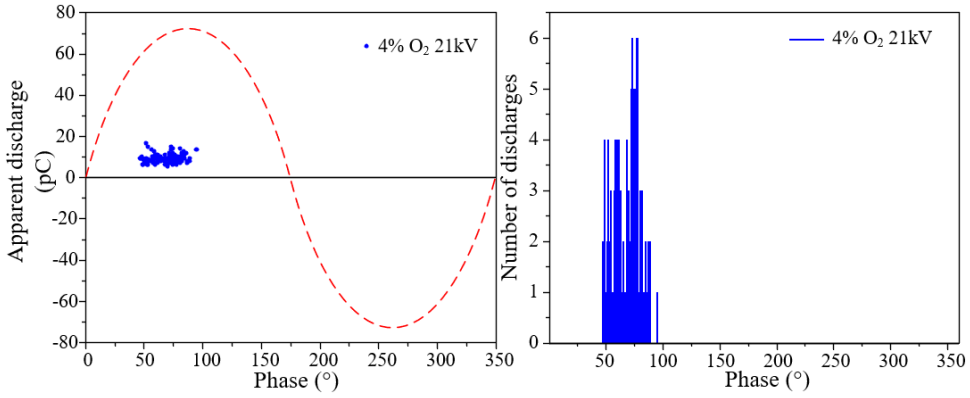

(a) 21kV

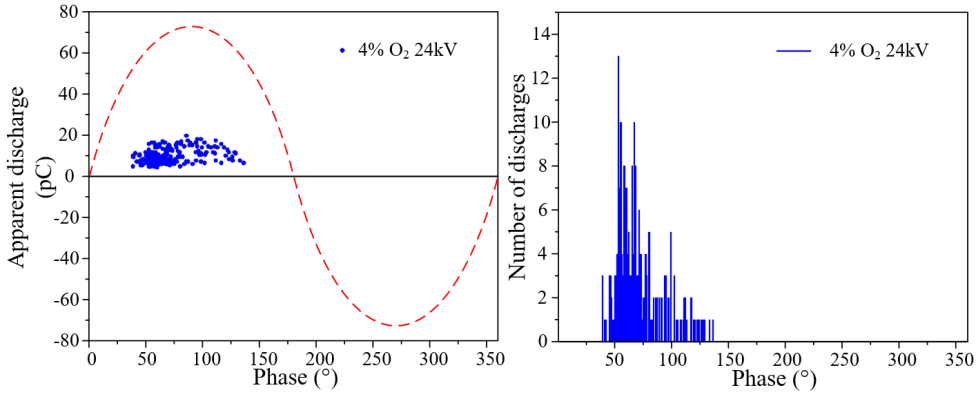

(b) 24kV

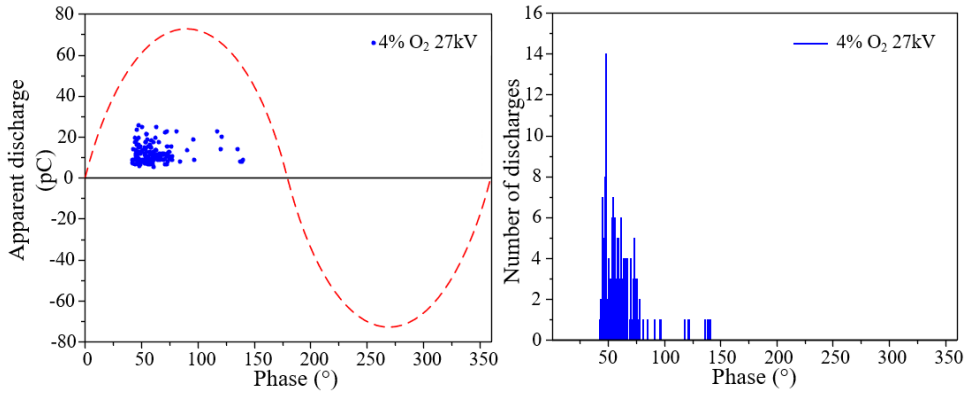

(c) 27kV

Fig.3.10 PRPD maps of C_4F_7N-CO_2-O_2 gas mixtures at different externally applied voltages

The parameters of the statistical characteristics of the C_4F_7N-CO_2-O_2 PD at different externally applied voltages are given in Table 3.2. The number of PDs with discharges exceeding 15 pC in the C_4F_7N-CO_2-O_2 gas mixture containing 4% O_2 at different applied voltages were 3 (21 kV), 27 (24 kV), and 31 (27 kV), respectively, and the number of PDs with larger discharges increased gradually with the increase of the applied voltage. The number of discharges per second and the cumulative discharge of the C_4F_7N-CO_2-O_2 gas mixture reached a maximum at 1.5 PDIV (24 kV), and the number of discharges per second and the cumulative discharge decreased when the applied voltage was further increased to close to the breakdown voltage (27 kV), but the average discharge of a single pulse increased with the increase of the applied voltage.

Table 3.2 Parameters of statistical characteristics of C_4F_7N-CO_2-O_2 PD under different externally applied voltages

applied voltage (kV)	discharge repetition rate (1s)	cumulative discharge (pC)	average discharge (pC)
21	114	1071.1	9.4
24	215	2176.51	10.12
27	149	1804.92	12.22

3.3 C_4F_7N-CO_2-O_2 PD decomposition characteristics

3.3.1 Decomposition characteristics of C_4F_7N-CO_2-O_2 PD at different O_2 contents

The decomposition of gas insulating media is mainly caused by the accumulation effect of PD, which is mainly affected by factors such as PD pulse intensity, cumulative discharge and discharge repetition rate, etc. From the above, it can be seen that O_2 has a greater influence

on factors such as PD pulse intensity, cumulative discharge and discharge repetition rate of the gas mixture, which in turn also affects the PD decomposition characteristics of the gas mixture. Typically, the arc plasma generated by the discharge causes complex physical and chemical reactions that result in the decomposition of gas molecules and the production of a variety of by-products. The main products of PD decomposition of the C_4F_7N-CO_2-O_2 gas mixture are CF_4, C_2F_6, C_3F_8, C_3F_6, CO, COF_2, $C_2F_6O_3$, CF_3CN, C_2F_5CN and C_2N_2. The characteristic curve of the effect of O_2 content on the PD decomposition products of the C_4F_7N-CO_2-O_2 mixture is given in Fig.11. From Fig.11(a), it can be seen that the trend of CF_4 generation with O_2 content is not obvious when the discharge length is 12h-48h, and the addition of 4% O_2 to the C_4F_7N-CO_2 mixture can obviously inhibit the generation of CF_4 in the discharge from 48h-96h, and the content of CF_4 starts to increase when the O_2 content is greater than 4%. It can be seen that 4%-6% O_2 has a certain inhibitory effect on the amount of CF_4 generation, but this inhibitory effect needs to reach a certain length of discharge to reflect more obvious.

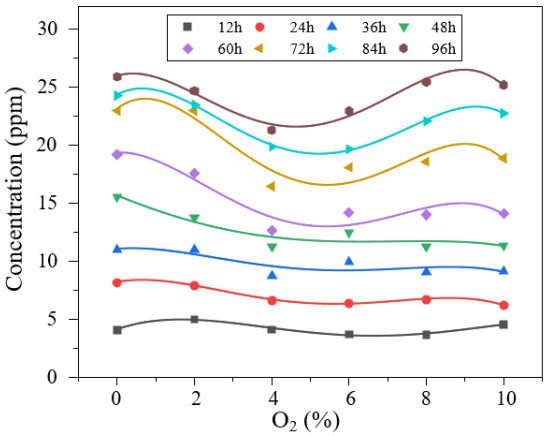

(a) CF_4

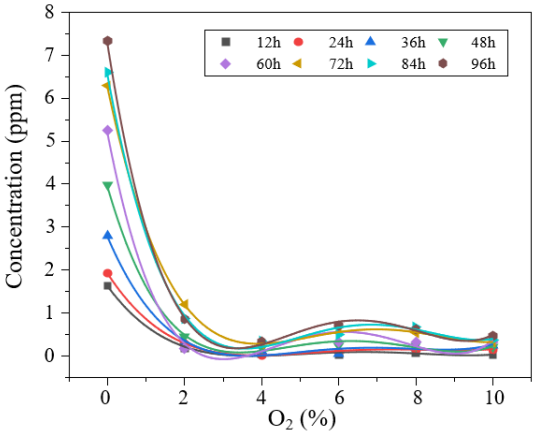

(b) C_2F_6

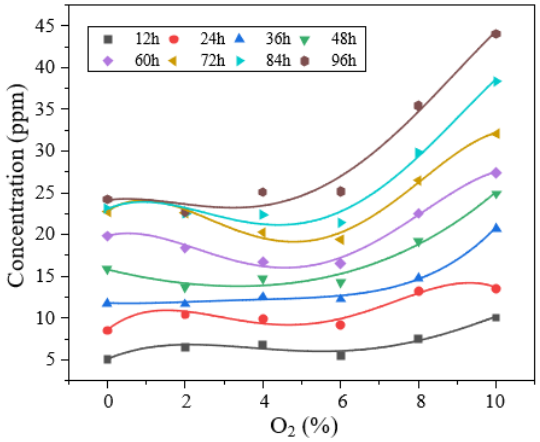

(c) C_3F_8

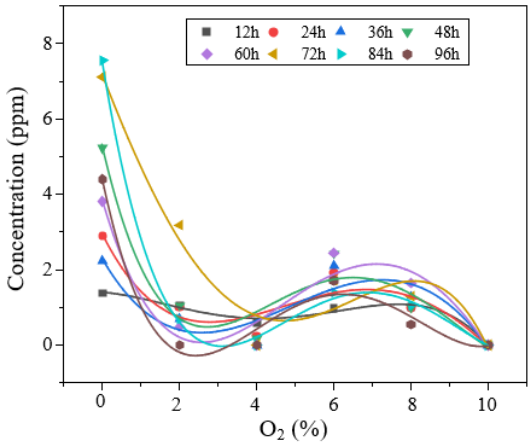

(d) C_3F_6

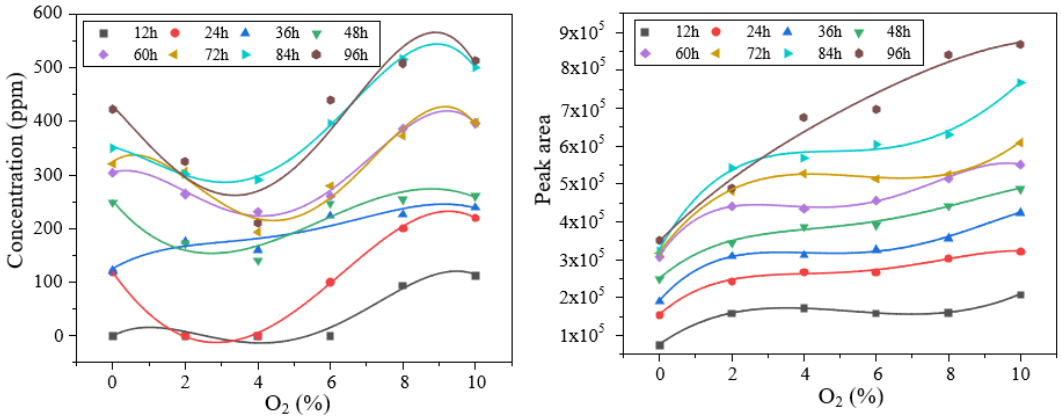

(e) CO (f) COF_2

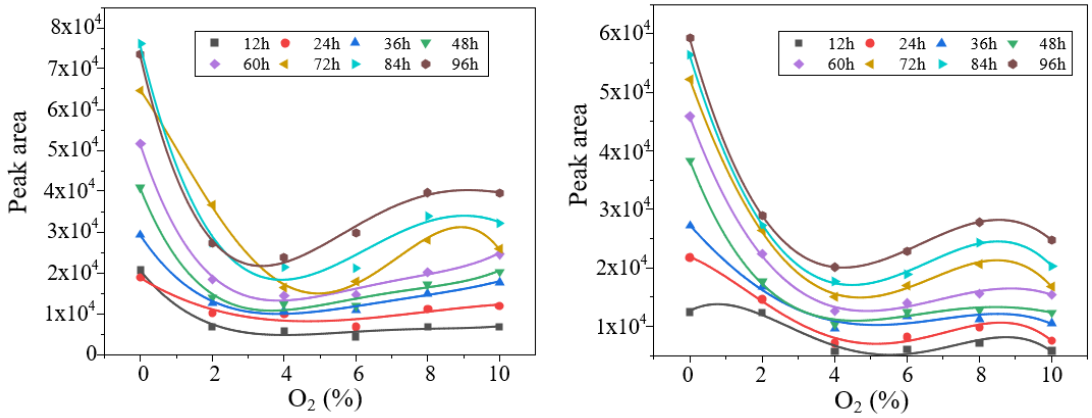

(g) $C_2F_6O_3$ (h) CF_3CN

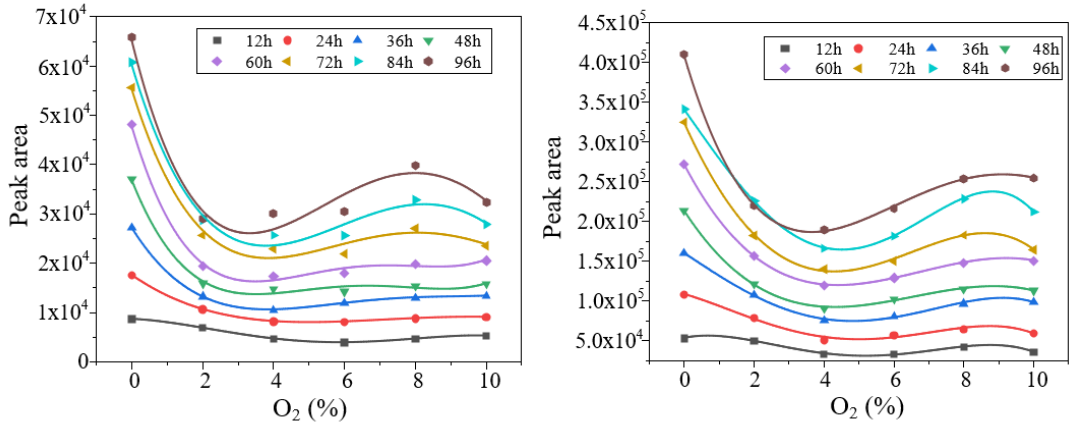

(i)C_2F_5CN (j) C_2N_2

Fig 3.11 Variation of PD decomposition products of C_4F_7N-CO_2-O_2 gas mixture with O_2 content

The C_2F_6 generation reached a maximum value of 7.4 ppm under the condition of no O_2 and the discharge time reached 96 h (shown in Fig. 3.11(b)), and the C_2F_6 generation decreased sharply after the addition of O_2, with the maximum generation not exceeding 1.2 ppm, and the change trend of the C_2F_6 generation under the condition of O_2 content of 2%-10% was not

obvious, and it can be seen that the addition of O_2 can inhibit the C_2F_6 generation significantly. It can be seen that the addition of O_2 can significantly inhibit the generation of C_2F_6.

The addition of 0%-6% O_2 did not have a significant effect on C_3F_8 production (shown in Fig.3.11(c)), but when the O_2 content was greater than 6%, the production of C_3F_8 increased significantly. The generation of C_3F_6 was maximum (7.55 ppm) at a discharge time of 84 h and O_2 content of 0%, and the addition of 2% O_2 led to a decrease in the generation of C_3F_6 to 0 ppm (shown in Fig. 3.11(d)), and with a further increase in the O_2 content, the trend of changes in the generation of C_3F_6 was small, which indicated that the addition of O_2 would inhibit the generation of C_3F_6. The generation of C_3F_6 under PD failure is lower than other by-products, on the one hand, due to the unsaturated C=C in C_3F_6 which leads to the easy oxidation of C_3F_6, and on the other hand, C_3F_6 mainly arises from the interfacial reaction between C_4F_7N and metals under high temperature conditions [105]. CO is produced in the highest amount among several by-products, and CO originates from the decomposition of CO_2 on the one hand, and from the reaction between C monomers and O atoms produced during the discharge of C_4F_7N on the other hand. It can be seen that the addition of 2%-4% O_2 inhibits CO production, with the lowest CO production at 4% O_2 (210 ppm), and an increase in CO production at O_2 levels greater than 4% (shown in Fig.3.11(e)). The production of COF_2 increases with increasing O_2 content, mainly because O_2 decomposes into O particles when collisional ionisation occurs or at high temperatures, and O particles combine with CF_2 to produce COF_2, so the addition of O_2 can contribute to the production of COF_2 (shown in Fig.3.11(f)).

The generation of C_2F_6O3, CF_3CN, C_2F_5CN and C_2N_2 followed approximately the same trend with O_2 content (shown in Fig. 3.11(g)(h)(i)(j)), decreasing sharply at O_2 contents of 2%-4%, with a minimum of the four by-products at 4% O_2, and a saturating trend of growth in the generation of the four by-products at O_2 contents of greater than 4 %. Taken together, the addition of 2%-4% O_2 to the C_4F_7N-CO_2 mixture significantly reduces the generation of most of the by-products, but the generation of these by-products starts to increase slowly at O_2 contents of 6%-10%, and this trend is basically in line with the trend of the average discharge of the PDs of the C_4F_7N-CO_2-O_2 mixture with O_2 content (shown in Fig.3.9).

3.3.2 Decomposition characteristics of C_4F_7N-CO_2-O_2 PD under different applied voltages

From Fig.3.11, it is seen that after the addition of 2%-4% O_2 to the C_4F_7N-CO_2 mixture, except for C_3F_8 and COF_2, the content of all the by-products showed a decreasing trend to different degrees, and it reached the lowest at 4% O_2, which indicates that 2%-4% O_2 can

effectively inhibit the decomposition of the mixture. Therefore, in this paper, the decomposition characteristics of C_4F_7N-CO_2-O_2 mixture containing 4% O_2 under different externally applied voltages are investigated to clarify the correlation between the PD characteristic covariates and the product generation. Fig.3.12 reflects the variation of PD decomposition product generation with PD time and externally applied voltage for the C_4F_7N-CO_2-O_2 gas mixture. It can be seen that except for C_3F_6, the content of all the by-products increases with increasing PD time. C_3F_6 contains unsaturated C=C, so as the PD time increases, C_3F_6 decomposes or is oxidised to other products due to the energy accumulation effect, which results in the generation of C_3F_6 decreasing or becoming saturated with the increase in discharge time. Among all decomposition by-products, the generation of CF_4 basically increased linearly with the increase of discharge time and applied voltage. Combined with the characteristic parameters of C_4F_7N-CO_2-O_2 PD under different applied voltages given in Table 3.2, it can be seen that the PD characteristics are the fundamental cause of the differences in decomposition characteristics, when the applied voltage is increased from 21 kV to 24 kV, the repetition rate of the discharge per second and the cumulative discharge increase by about a factor of 1, and the average discharge increases by 7.6%, and most of the product generation shows an obvious growth trend, and the CO trend is not significant, mainly due to the weak degree of PD at this time, the C atoms produced by electron impact on the metal as well as the C atoms precipitated by C_4F_7N under the action of PD are relatively small. When the applied voltage was increased from 24 kV to 27 kV, the average discharge increased by 20.75 per cent, although the discharge repetition rate per second and the cumulative discharge decreased by 30 per cent and 17 per cent, respectively.

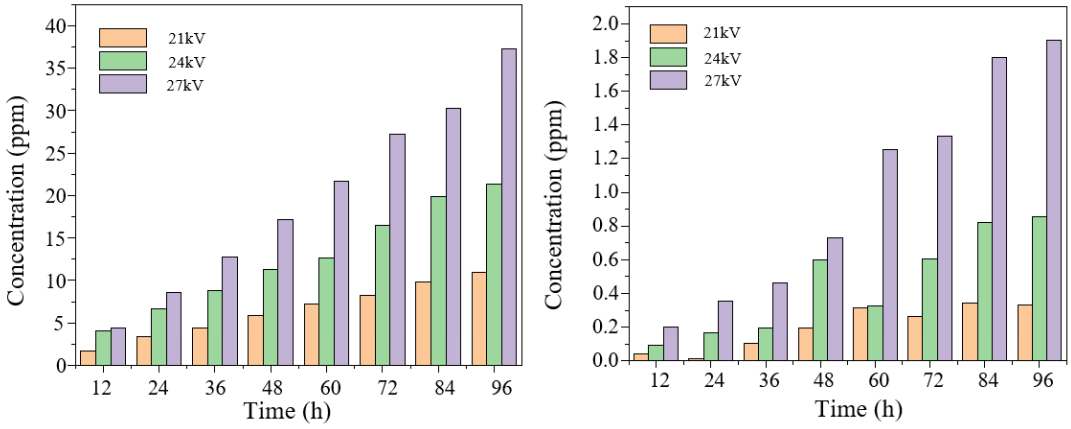

(a)CF_4 (b) C_2F_6

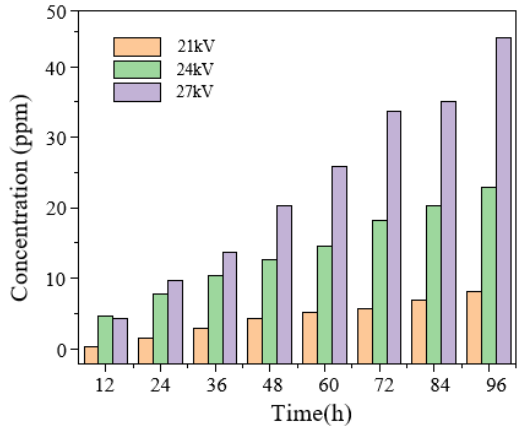

(c) C_3F_8

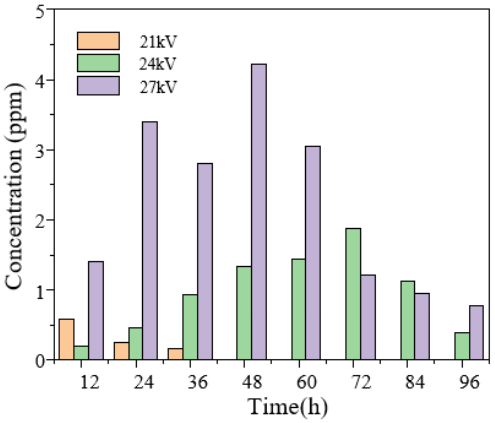

(d) C_3F_6

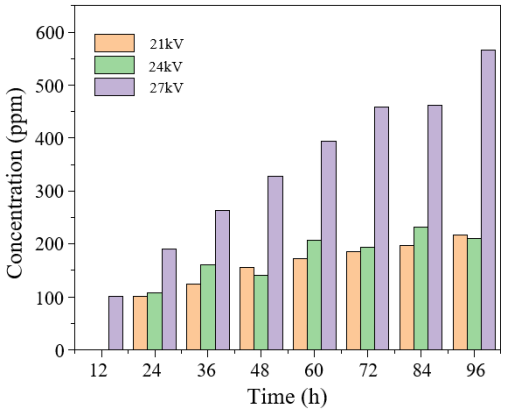

(e) CO

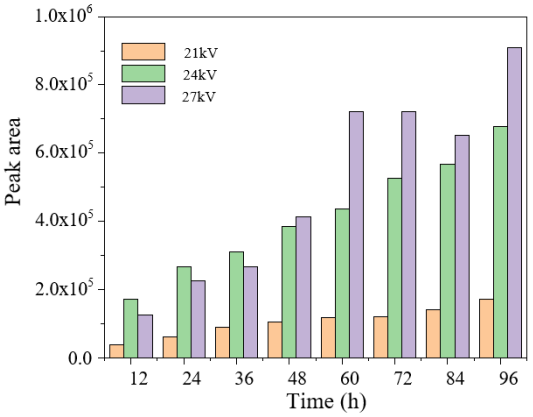

(f) COF_2

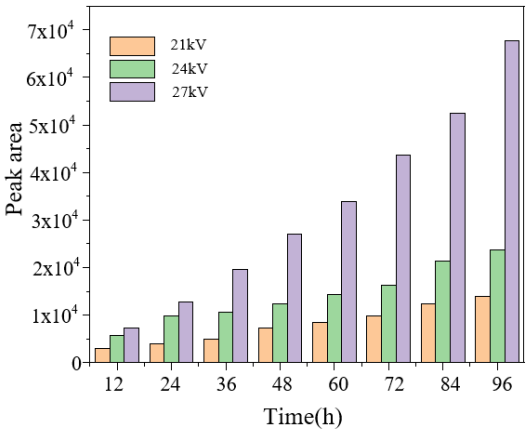

(g) $C_2F_6O_3$

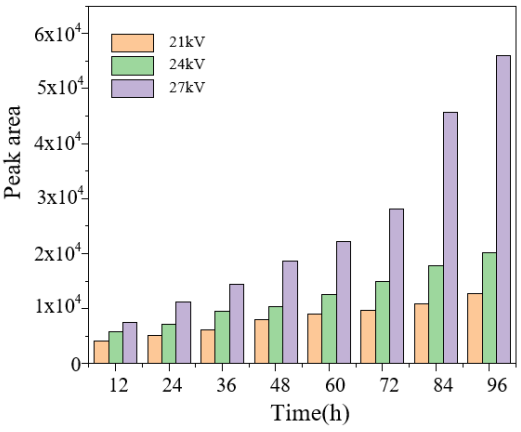

(h) CF_3CN

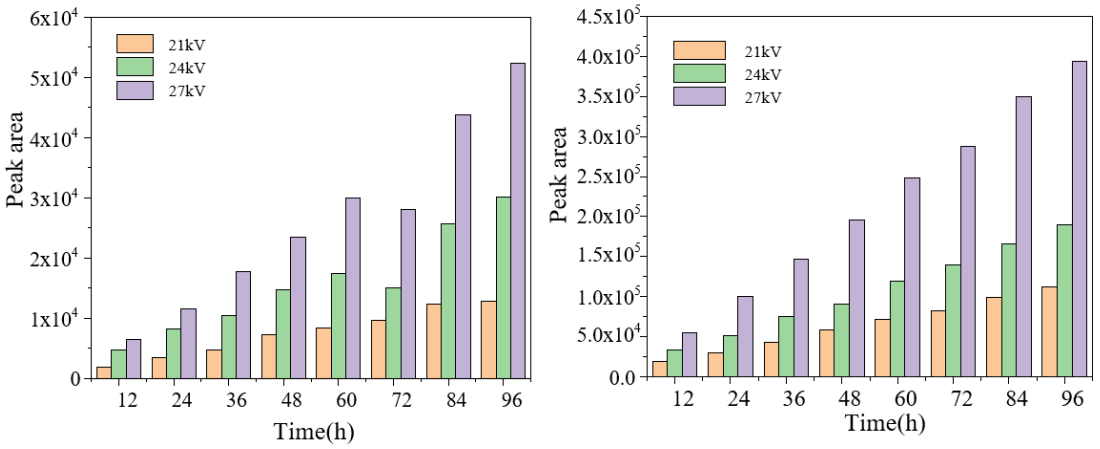

Fig.3.12 Variation of decomposition products of C_4F_7N-CO_2-O_2 gas mixture with applied voltage

The magnitude of the average discharge is the dominant factor for the decomposition of the gas mixture to occur, which can be verified from the trend of the PD and its decomposition characteristics of the gas mixture with the O_2 content, the average discharge of the C_4F_7N-CO_2 gas mixture shows a trend of decreasing and then increasing with the O_2 content under the externally applied voltage of 24 kV and reaches a minimum at 4% O_2, and the trend of the most of the by-product yields with the O_2 content is the same as the trend of the average discharge with the O_2 content, so that it can be deduced that the content of the decomposition components of the PD of the C_4F_7N-CO_2 -O_2 mixture has a positive correlation with the average discharge.

3.4 Mechanism of O_2 effect on C_4F_7N-CO_2-O_2 PD and its decomposition characteristics

3.4.1 Mechanism of O_2 effect on C_4F_7N-CO_2-O_2 PD characteristics

The PRPD spectra can better reflect the distribution law of PD, and from the above test results, it can be seen that the PD of C_4F_7N-CO_2-O_2 mixture under different test conditions is mainly concentrated in the positive half-period of the industrial frequency. According to the polarity effect of air gap discharge in a very inhomogeneous electric field, when the voltage is relatively small, the discharge occurs first in the negative half of the periphery, which is due to the fact that the presence of a positive space charge strengthens the strength of the electric field in the vicinity of the surface of the tip of the needle, which makes the development of the discharge easier; However, the positive space charge in the vicinity of the needle electrode weakens the electric field in the space outside the needle electrode in the direction of the plate electrode, making it less likely that the corona zone will spread outward, leading to a more difficult development of the discharge. Therefore, when the needle electrode is positive

polarity, with the further increase of the externally applied voltage (1.5PDIV), the corona discharge region extends outward, and the strong electric field region will also gradually advance toward the plate electrode, and the electric field between the plate electrode and the plate electrode is further strengthened, and some electrons collapsed to form a flow injection, and develops rapidly to the depth of gap, so that the positive half-weekly of the C_4F_7N-CO_2-O_2 mixture under 1.5PDIV condition has a significantly higher The discharge amplitude is significantly higher than that in the negative half week, and the discharge repetition rate is also significantly higher than that in the negative half week, and the breakdown occurs in the positive half week when the applied voltage reaches the breakdown voltage.

The O_2 content has a large influence on the PD characteristics of the C_4F_7N-CO_2-O_2 mixture, and the negative half-period discharge disappears after 2%-4% O_2 is added to the C_4F_7N-CO_2 mixture, indicating that the addition of a certain content of O_2 can inhibit the generation of the negative half-period discharge. O_2 is an electronegative gas, in front of the electron collapse, O_2 molecules absorb relatively slow electrons to form negative ions, so the negative space charge is formed by the development of these heavy particles and slow ions, which leads to a reduction in the electric field strength over a short distance at the tip of the negative electrode, which can prevent the further development of the electron collapse process, so the addition of 2%-4% O_2 makes the discharge in the negative half of the periphery disappear, and the negative space charge is reduced when the O_2 content is greater than 6%, the strong oxidative property of O_2 promotes the decomposition of C_4F_7N molecules, which leads to a decrease in the electronegativity of the gas mixture and a decrease in the negative space charge near the needle electrode, which leads to a slight increase in the electric field strength near the tip of the negative electrode, so that the negative half-weekly discharge reappears.

Since the concentration of C_4F_7N was fixed during the experiment, the PD characteristics of the C_4F_7N-CO_2-O_2 mixture mainly depended on the variation of the CO_2 and O_2 content in the mixture. Xi'an Jiaotong University Mingzhe Rong et al. investigated the effect of O_2 content on the electron energy distribution function (EEDF) of CO_2-O_2 gas mixtures, and found that under the conditions of 0.01 MPa, 3000 k, and an approximate electric field strength E/N of 80 Td, the average electron energy of the gas mixture will increase with the further increase of the O_2 content of the gas mixture (greater than 6%), which will be more likely to undergo ionisation. Table 3.3 gives the ionisation potential energy of different particles [108], and it can be seen that CO_2 and its decomposition product CO have a greater ionisation potential energy than O_2 and O. Therefore, the addition of excess O_2 leads to a decrease in the

content of CO_2 and its decomposition products, and the C_4F_7N-CO_2-O_2 gas mixture is more prone to ionisation, which is macroscopically manifested in the number of discharges per second of the gas mixture PD when the O_2 content is greater than 6%, Accumulated discharges per second and average discharges all show a sharp increase trend.

Table 3.3 Ionisation potentials for different particles

particles	O_2	CO_2	CO	O
ionisation potential (eV)	12.06	13.30	14.2	13.62

3.4.2 Mechanism of O_2 effect on the decomposition properties of C_4F_7N-CO_2-O_2 PDs

The PD characteristics of gas mixtures are greatly affected by the amount of O_2 added, and the decomposition of gas mixtures is mainly caused by the accumulation effect of PD, and there is a strong correlation between the decomposition characteristics of gas mixtures and their PD characteristic quantities, and their decomposition characteristics can also be used to identify the severity of PD faults in engineering applications. The C_4F_7N-CO_2-O_2 gas mixture decomposes under the action of PD to form free radicals such as CF_3, CF_2, F, CN and O. The recombination of these free radicals produces perfluoroalkane gases (CF_4, C_2F_6, C_3F_8, and C_3F_6), nitrile gases (C_2N_2, CF_3CN, and C_2F_5CN) and oxides (CO, COF_2, and $C_2F_6O_3$). Except for COF_2, the content of all the by-products showed different decreasing trends after the addition of 2%-4% O_2 and reached the lowest at 4% O_2.

The formation pathways of several O-containing compounds in the PD decomposition products are given in Table 3.4. Without adding O_2, the trace O_2 mixed in the inflation process will generate O_3 under the discharge conditions, O_3 has higher oxidability than O_2, and can generate $C_2F_6O_3$ with chemically stable C_2F_6, and CF_3 is easily oxidised to generate COF_2 after O_2 is added, and the relevant literature has shown that C_4F_7N requires the least amount of energy for generating CF_3 among the four preliminary dissociation reactions [71], therefore, CF_3 is continuously produced during the discharge process, and with the increase of O_2 content, CF_3 easily reacts with O atoms to generate COF_2, so the COF_2 content tends to increase when the O_2 content varies between 0% and 10%, while the yield of $C_2F_6O_3$, which also requires CF_3 particles, tends to decrease between 0% and 4% of O_2, and when the O_2 content is greater than 6% of O_2 The number of discharges per second, the cumulative discharges per second and the average discharges of the mixed gas PD show a sharp increase trend, which will lead to a sharp decomposition of the mixed gas thus generating a large number of free radicals,

especially free radicals such as CFx and F, so that most of the by-products content will increase under the condition that the O_2 content is greater than 6%. In order to avoid the serious insulation degradation caused by the massive decomposition of the gas mixture under PD fault conditions, the O_2 addition should not exceed 6%.

Table 3.4 Generation pathways of O-containing by-products under PD action

decomposition product	reaction path
COF_2	$CF_3+O \rightarrow COF_2+F$
	$CF_2+O \rightarrow COF_2$
	$CF+F+O \rightarrow COF_2$
$C_2F_6O_3$	$3O_2 \rightarrow 2O_3$ (discharging condition)
	$CF_3+CF_3+O_3 \rightarrow C_2F_6O_3$
CO	$2C+O_2 \rightarrow 2CO$
	$2CO+O_2 \rightarrow 2CO_2$

3.5 Solid precipitates under the action of C_4F_7N-CO_2-O_2 PD

At the end of the C_4F_7N-CO_2-O_2 gas mixture 96h PD discharge decomposition test, the test electrodes were removed and corrosion phenomena and solid precipitates were observed on the surface of the plate electrodes. According to the conclusion of the above study, it is more appropriate to add 4% of O_2 to the C_4F_7N-CO_2-O_2 gas mixture under the comprehensive consideration of PD and its decomposition characteristics, so the corrosion phenomena and solid precipitates appeared on the surface of the electrode after 96h of discharge under the conditions of 0% O_2 and 4% O_2 are selected for analysis in this section.

Fig.3.13 gives the macroscopic morphology of the electrode surface before and after 96h partial discharge of C_4F_7N-CO_2-O_2 gas mixture, it can be seen that compared with the electrode before the test, the surface of the electrode after the test in the central region of the electrode surface appeared to be more obvious circular solid precipitates, and the closer to the centre of the electrode, the darker the colour. This phenomenon indicates that the C_4F_7N-CO_2-O_2 gas mixture produces solid precipitates and causes corrosion of the plate electrodes under prolonged partial discharge conditions. In this paper, a needle-plate electrode model is placed in a stainless steel tank (test gas chamber) to carry out partial discharge decomposition tests, and the whole test model can be divided into three areas, including the main gas chamber area, the ion diffusion area and the glow discharge area. Glow discharge region is located near the needle electrode, the electric field strength is higher in this region, the discharge process will

generate a large number of high-energy electrons, the resulting collision ionisation process will lead to the dissociation of the C_4F_7N-CO_2-O_2 gas mixture and the complex reaction generates a large number of gases and solid by-products, the gas by-products will be uniformly diffused to the stainless steel gas chamber, the solid by-products due to the effect of gravity will be attached to the electrode The solid by-products will be attached to the electrode surface due to gravity, the projection of the electric field distribution of the needle-plate electrode on the plate electrode is circular, so the surface of the plate electrode will produce circular solid precipitates, the closer to the tip of the needle electrode, the higher the electric field strength, the more intense the collision ionisation, and the more by-products are produced, so the closer the plate electrode, the darker the central region of the solid precipitates.

(a) Pre-testing (b) 0% O_2 (c) 4% O_2

Fig.3.13 Macroscopic morphology of electrode before and after 96h partial discharge of C_4F_7N-CO_2-O_2 gas mixture

In order to further investigate the interaction characteristics of the C_4F_7N-CO_2-O_2 gas mixture with the copper electrode under prolonged PD and the effect of O2 on the solid precipitates of the C_4F_7N-CO_2 gas mixture, this paper employs Scanning Electron Microscopy (SEM), Energy Dispersive Spectrometer (EDS), and X-ray photoelectron spectra (XPS) to analyse the micromorphology and the elemental composition and content of solid precipitates in the region of the solid precipitates. Fig.3.14 gives the SEM morphology at different magnifications, and it can be found that the surface structure of the copper electrode before the test is flat, and the fine texture-like cut section is clearly visible (shown in Fig. 3.14(a)), and on the surface of the copper after 96 h of discharge in a 15% C_4F_7N-85% CO_2 gas mixture, dense scale-like corrosion can be seen (shown in Fig. 3.14(b)), and after the addition of 4% O_2 can be seen spherical and cubic crystal-like corrosives distributed in various regions of the copper surface (shown in Fig. 3.14(c)). Both of the above cases indicate that the microstructure of the copper electrode surface has changed significantly, and the high-magnification image shows the particle delamination, which suggests that the textured cut cross section on the surface of the copper has completely disappeared under the prolonged discharge conditions,

and the microstructure of the copper surface has been severely damaged. The region of distribution of solids and the density of distribution show that the generation of solid products without O_2 is significantly larger than that with the addition of O_2, suggesting that O_2 may inhibit the generation of solid by-products while inhibiting gaseous by-products.

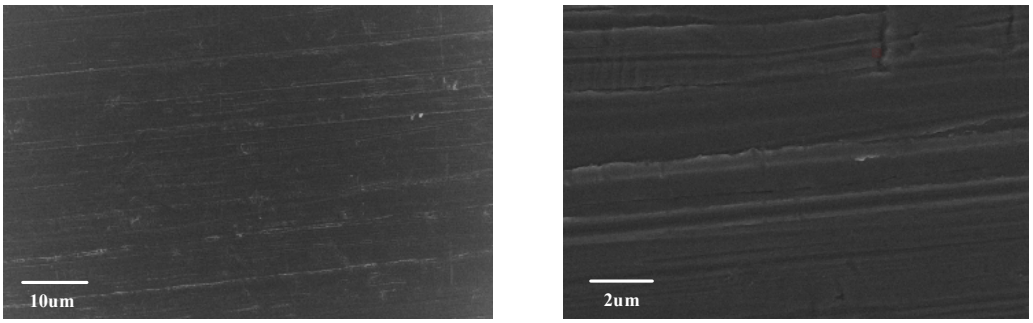

(a) control group

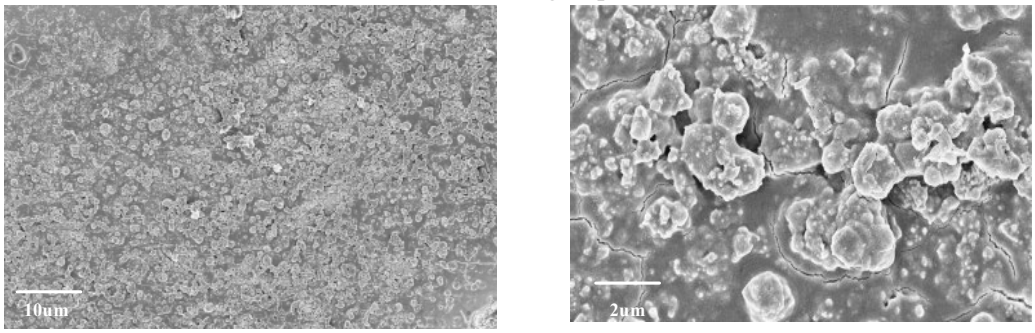

(b) 0% O_2

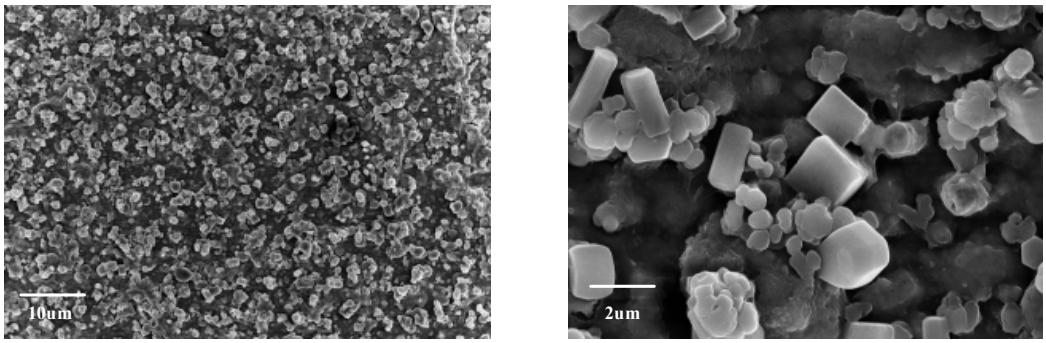

(c) 4% O_2

Fig.3.14 SEM of electrode surface before and after 96h partial discharge of C_4F_7N-CO_2-O_2 gas mixture

Table 3.5 EDS elemental analysis of electrode surface after discharge

elemental	apparent concentration		Wt (%)	
	0% O_2	4% O_2	0% O_2	4% O_2
C	7.69	8.14	14.91	15.43
N	5.58	7.27	7.03	9.24
O	17.00	18.24	19.25	22.19
F	23.90	15.89	26.49	19.51

Si	3.45	1.95	2.49	1.43
Cu	27.22	30.36	29.83	32.20

EDS is mainly used in conjunction with SEM to detect the elemental composition and content of the sample by selecting a tiny location area. Table 3.5 gives the results of the qualitative and quantitative analysis of EDS on the surface of the electrode after discharge, and the solid precipitates on the surface of the electrode are mainly made up of five elements: C, N, O, F and Si, and Si is mainly originated from the SiO2, which is the main constituent of the observation window on the side of the stainless steel gas chamber. The quantitative analysis results of EDS are usually expressed in mass percentage (Wt%), and the largest change in the mass percentage of the five elements in the gas mixture after the addition of 4% O_2 was element F, which decreased by 26.3% compared with that before the addition of O_2, and the element F was mainly originated from the fluoride in the solid by-products generated on the surface of the electrodes, so that the solid material distribution area and the distribution density of solid material after the addition of O_2 was significantly less than that of the case of no addition of O_2. Therefore, the distribution area and density of the solid material after the addition of O_2 is obviously smaller than that without O_2, which further indicates that O_2 can inhibit the generation of by-products to a certain extent.

In order to further investigate the chemical state of the elemental composition of the solid precipitates on the electrode surface after partial discharge, five elements, Cu, F, O, N and C, were selected for XPS spectroscopy based on the results of EDS spectroscopy. The XPS spectrum of the electrode surface after 96h partial discharge of C_4F_7N-CO_2-O_2 gas mixture at 0% O_2 and 4% O_2 is given in Fig. 3.15,the horizontal coordinates in the XPS spectrum are the atomic orbital binding energies (B.E.), and the vertical coordinates are the peak intensities, which were fitted to the peaks using Gaussian method. Under 0% O2 conditions, the Cu element mainly consists of three characteristic peaks located at 935.01 eV, 943.95 eV and 954 eV, which correspond to the three compositions of $CuSiO_3$ $2p_{3/2}$, CuO $2p_{3/2}$ and CuF, respectively (shown in Fig. 3.15(a)); The characteristic peaks of element F located at 684.15 eV and 688.36 eV correspond to CuF2 and CFx (fluoride), respectively (shown in Fig.3.15(b)); The characteristic peak of element O located at 532.02 eV corresponds to CuO (shown in Fig.3.15(c)); Elemental N consists mainly of two characteristic peaks located at 399.63 eV and 407.23 eV, corresponding to N1_s and NOx (nitrogen oxides), respectively (shown in Fig. 3.15(d)); The three characteristic peaks of element C located at 284.81 eV, 288.92 eV and 293.13 eV correspond to C_1S, O-C=O and CFx, respectively (shown in Fig. 3.15(e)).

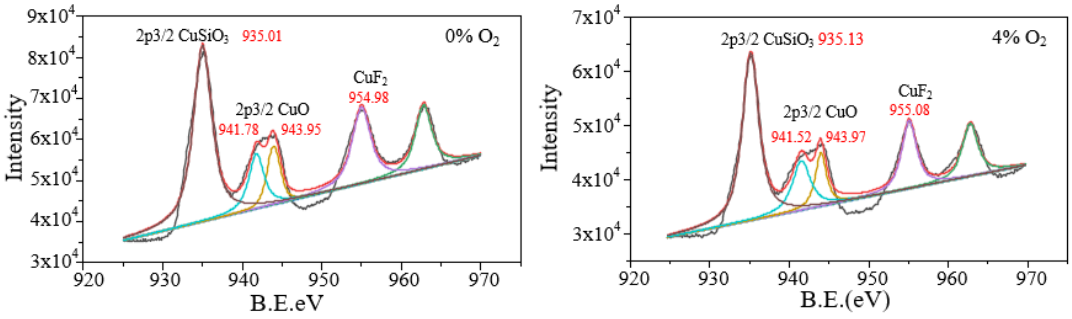
2p3/2 CuSiO3 935.01
0% O2
2p3/2 CuO
941.78
943.95
CuF2
954.98
Intensity
B.E.eV
2p3/2 CuSiO3 935.13
4% O2
2p3/2 CuO
941.52
943.97
CuF2
955.08
B.E.(eV)

(a) Cu

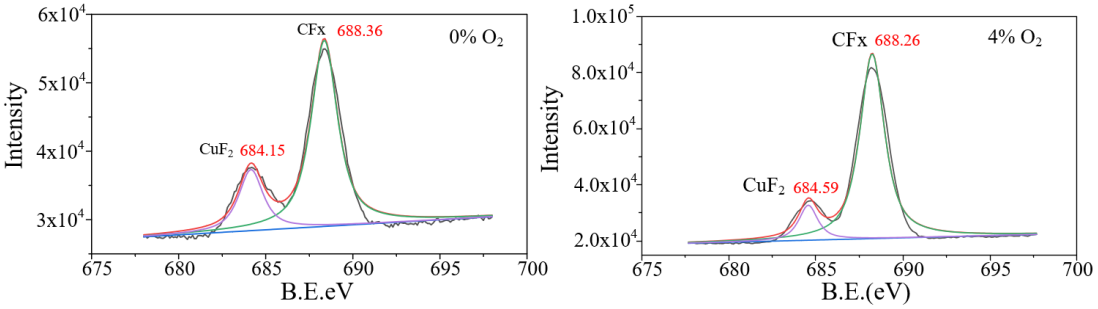
CFx 688.36
0% O2
CuF2 684.15
Intensity
B.E.eV
CFx 688.26
4% O2
CuF2 684.59
B.E.(eV)

(b) F

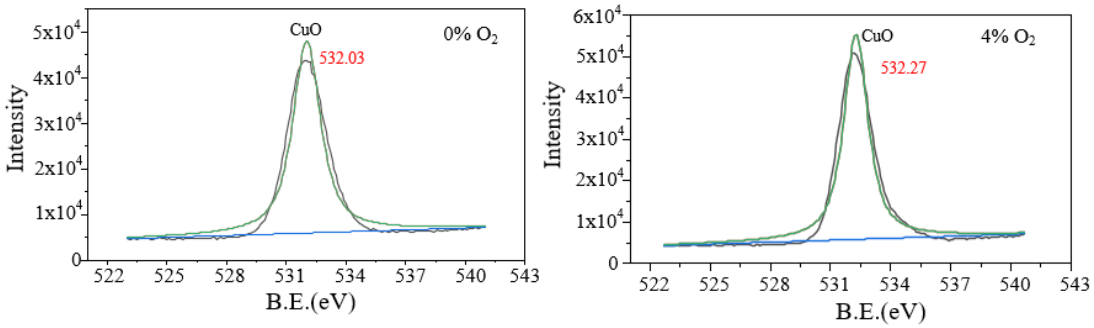
CuO
532.03
0% O2
Intensity
B.E.(eV)
CuO
532.27
4% O2
B.E.(eV)

(c) O

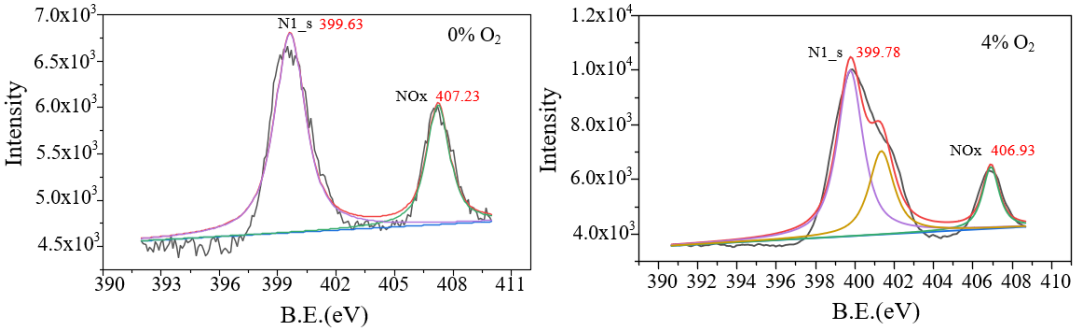
N1_s 399.63
0% O2
NOx 407.23
Intensity
B.E.(eV)
N1_s 399.78
4% O2
NOx 406.93
B.E.(eV)

(d) N

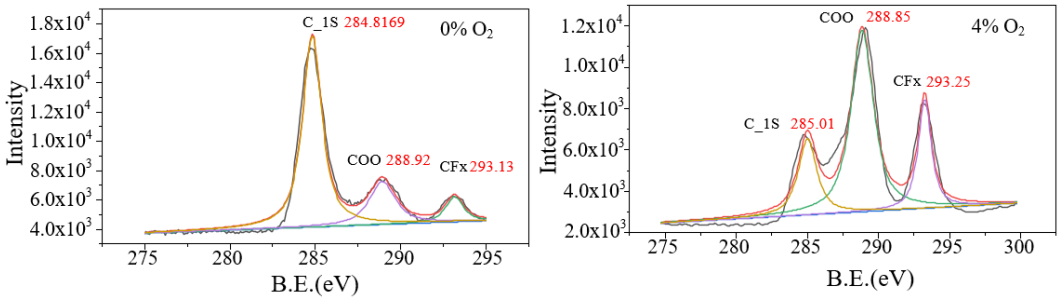

(e) C

Fig.3.15 XPS spectrum of electrode surface after 96h partial discharge of C_4F_7N-CO_2-O_2 gas mixture

It can be seen that the substances corresponding to the different characteristic peaks after the addition of 4% O_2 are basically the same as those without O_2, which means that the addition of O_2 does not have a large effect on the components of the solid products, mainly in the differences in the content of the components. From the intensity of the characteristic peaks, it can be seen that the O-C=O content is significantly higher than that of CFx and C_1S at 4% O_2, suggesting an increase in the production of carbon and oxygen compounds in the by-products after the addition of O_2. Taken together, the main substances leading to electrode surface corrosion after 96h partial discharge of C_4F_7N-CO_2-O_2 gas mixture are metal oxides, silicates, fluorides and carbon oxides. The generation of solid by-products is mainly generated by the cumulative effect of the energy of the discharge process, the size of the cumulative energy is positively correlated with the length of the discharge, so the generation of solid by-products should be avoided as much as possible during the long discharge process to the detrimental effect on the metal conductors and insulating parts in the equipment. On the one hand, solid precipitates adhering to the surface of a metal conductor can change the electric field distribution around the conductor, which can lead to partial discharges or even breakdowns; On the other hand, solid precipitates may be attached to the insulating parts inside the equipment, and the conductive components contained in these solid precipitates will affect their insulating properties, leading to a series of insulation failures in the equipment, so it is necessary to monitor and control the partial discharge faults inside the equipment in real time, to avoid the impact of prolonged discharges and serious failures to produce solid products on the safe and stable operation of the equipment.

In addition, in conjunction with the quantitative analysis of the EDS energy spectra given in Table 3.5, the decrease in the content of element F after the addition of O_2 is mainly due to the fact that a portion of the fluorocarbon compound combines with O_2 to form COF_2. In

addition, there is an increase in the O elemental content, which is due to the combination of C and O produced during the decomposition of the C_4F_7N discharge to form carbon-oxygen compounds. It can be seen that the addition of O_2 can effectively inhibit the generation of some solid by-products, but it will also generate some harmful gaseous by-products, such as COF_2 and CO, so it is necessary to strictly control the amount of O_2 added while satisfying the insulation and decomposition characteristics in the actual equipment.

3.6 Summary of the chapter

This chapter carries out the experimental study of partial discharge and decomposition characteristics of C_4F_7N-CO_2-O_2 gas mixture based on the PD decomposition characteristics test platform built for gas insulating dielectrics, reveals the partial discharge characteristics of C_4F_7N-CO_2-O_2 gas mixture and the change rule of the amount of by-products generated under different contents of O_2 and applied voltages, and discusses the influence mechanism of O_2 content on the PD characteristics and the correlation relationship between PD and decomposition characteristics of C_4F_7N-CO_2-O_2 gas mixture. The influence mechanism of O_2 content on the PD characteristics of C_4F_7N-CO_2-O_2 gas mixtures and the correlation relationship between PD and decomposition characteristics were discussed, and the components and contents of solid precipitates produced in the PD process were tested at the microscopic level, and their generation process and the influence law of O_2 on their generation amount were analysed. The main findings are as follows：

(1) The PD of the C_4F_7N-CO_2-O_2 mixture is mainly concentrated in the positive half-period of the IF, and the discharge phase distribution intervals in the positive half-period increase significantly after the addition of O_2. The addition of 2%-4% O_2 to the C_4F_7N-CO_2 gas mixture significantly suppresses the negative half-week discharge and reduces the maximum single-pulse discharge. The addition of 2%-6% O_2 can inhibit the PD with larger discharges, and a large increase in the number of discharges per second, cumulative discharges per second, and average discharges of the mixed-gas PD occurs when the O_2 content is greater than 6%, and the addition of more than 6% O_2 to the C_4F_7N-CO_2 gas mixture may lead to the insulation degradation of the gas mixture.

(2) With the increase of applied voltage, the number of PDs of C_4F_7N-CO_2-O_2 gas mixture discharging a larger amount increases gradually, and the number of discharges per second and the cumulative amount of discharges decreases when the applied voltage is further increased to close to the breakdown voltage, and the average amount of discharges in a single pulse increases with the increase of applied voltage.

(3) The main products of PD decomposition are CF_4, C_2F_6, C_3F_8, C_3F_6, CO, COF_2,

$C_2F_6O_3$, CF_3CN, C_2F_5CN and C_2N_2. The addition of 2%-4% O_2 to the C_4F_7N-CO_2 gas mixture resulted in a decreasing trend in by-product generation to varying degrees, except for C_3F_8 and COF_2, which reached a minimum at 4% O_2. At O_2 contents greater than 6%, an increase in all by-products generation occurs to varying degrees. The generation of the PD decomposition component of the C_4F_7N-CO_2-O_2 gas mixture is positively correlated with the average discharge.

(4) Solid precipitates appeared on the electrode surface after 96h PD of C_4F_7N-CO_2-O_2 gas mixture, and the microscopic morphology was that of scaly or cubic crystalline corrosives, and the main compositions included metal oxides, silicates, fluorides, and carbon-oxygen compounds, and the addition of 4% O_2 had less influence on the elemental composition of the solid precipitates of the PD and its valence state, but it could reduce its generation to some extent.

Chapter 4 C_4F_7N-CO_2 -O_2 frequency breakdown and its decomposition characteristics

The frequency breakdown characteristic is the basic basis for judging the insulating strength of gas insulating media, which can provide a reference for improving the insulating structure of the equipment and exploring the optimal ratio of the gas mixture. The addition of O_2 may affect the insulating properties of the C_4F_7N-CO_2-O_2 gas mixture, such as the breakdown voltage. On the other hand, considering the strong oxidising property of O_2 itself, the addition of O_2 may also have a certain influence on the stability and decomposition characteristics of the C_4F_7N-CO_2-O_2 gas mixture after a breakdown fault occurs, and the study of the decomposition characteristics of the gas mixture discharge and the mechanism of the product generation after considering the addition of O_2 may help to clarify the correlation characteristics between the decomposition characteristics and the influencing factors.

In this chapter, the insulation and decomposition characteristics of C_4F_7N-CO_2-O_2 gas mixtures used in medium-voltage equipment are investigated using a constructed test rig for industrial frequency breakdown characteristics. Firstly, the industrial frequency breakdown voltage of C_4F_7N-CO_2-O_2 gas mixture and its dispersion under different O_2 contents were tested, and then the variation rule of breakdown decomposition product generation with O_2 content and breakdown times was analysed, and the mechanism of the influence of O_2 on the insulating and its decomposition properties of C_4F_7N-CO_2-O_2 gas mixture was discussed. Finally, the additional reaction path of C_4F_7N due to the addition of O_2 is proposed, and the enthalpies and activation energies of the relevant reactions are calculated based on the density-functional theory (DFT) and the transition state theory (TST), to further analyse the discharge decomposition of C_4F_7N and the product generation mechanism under the conditions of O_2 participation in the reaction.

4.1 Industrial Frequency Breakdown Test Platform and Methods

4.1.1 Test platforms

Figure 4.1 shows the C_4F_7N-CO_2-O_2 gas mixture frequency breakdown test platform. Industrial frequency breakdown characteristics test platform and partial discharge decomposition characteristics test platform wiring is similar, based on the removal of coupling capacitance (500pF, 100kV) and non-inductive detection impedance (50Ω), the transformer (0-100kV, 50kVA) generated by the high voltage of the industrial frequency through the protection resistor (10kΩ) is applied to the insulation defects (ball-ball electrodes), the

protection resistor can limit the current in the circuit at the time of breakdown, to prevent damage to the test circuit, capacitance divider (500pF, 500kV), preventing damage to the test circuit, capacitance divider (500pF, 500kV), the test circuit to prevent damage to the test circuit. The protective resistor can limit the current in the circuit during the breakdown to prevent the test circuit from being damaged, and the capacitive voltage divider (500pF, 100kV) is used to measure the test voltage applied to both ends of the insulation defect. The test gas chamber is made of a self-made 304 stainless steel tank with a volume of about 29L, which can withstand a maximum pressure of 1MPa and is well sealed.

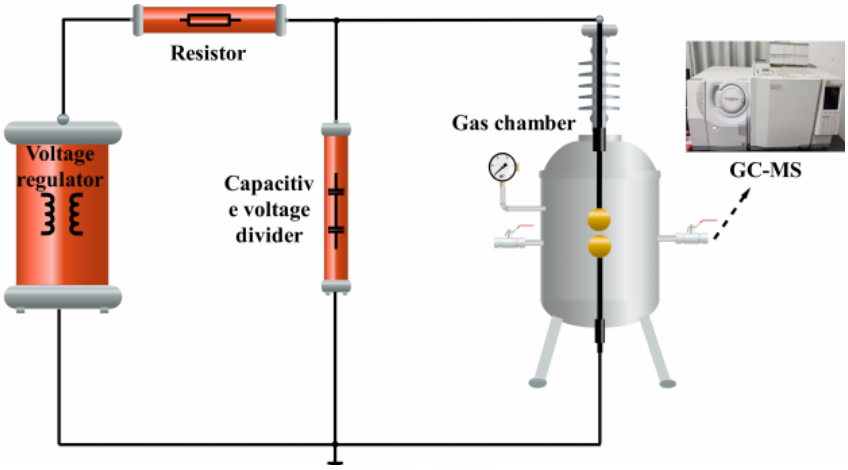

Figure 4.1 Schematic diagram of industrial frequency breakdown characteristics test platform

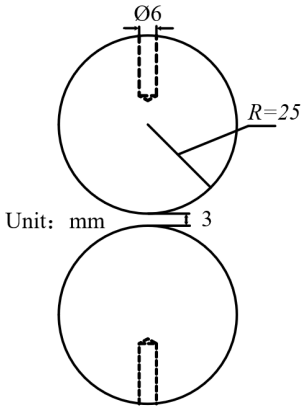

Figure 4.2 Ball-ball electrode

In this paper, the physical model of ball-ball electrodes shown in Fig. 4.2 is used to simulate the quasi-uniform electric field environment inside the equipment, and to carry out the test on the breakdown characteristics of C_4F_7N-CO_2-O_2 gas mixture at work frequency. The ball electrodes are made of brass with a radius of 25mm, two ball electrodes are connected to the high voltage guide rod and the grounding guide rod through threads, and the ball gap can be controlled by adjusting the threads, and the ball-ball electrode spacing is 3mm.

4.1.2 Test content and method

The frequency breakdown decomposition characteristic test can assess the insulation strength of C_4F_7N-CO_2-O_2 gas mixture by testing its breakdown voltage under the condition of different content of O_2 on the one hand, and its decomposition characteristic can be assessed by testing the composition and content trend of decomposition products under different content of O_2 and number of breakdowns on the other hand, and the specific test steps are as follows:

(1) The ball-ball electrode is mounted inside the tank and the interior of the stainless steel tank is cleaned, air-dried, and tested for airtightness in the same manner as the POF and PD disintegration test methods.

(2) According to Dalton's law of partial pressure, C4F7N, O2 and CO2 were sequentially introduced into the gas chamber, and the corresponding partial pressures of the three gases in the different test groups were kept the same as those in the POF and PD decomposition test methods, and then left to stand for 12h to make the gases fully mixed uniformly.

(3) connect the test circuit and turn on the power supply, carry out different O_2 content (2%, 4%, 6%, 8%, 10%) C_4F_7N-CO_2-O_2 gas mixture breakdown characteristics, using step-by-step boosting hair adjusting the test voltage, when the gas insulation dielectric breakdown occurs to record the value of the breakdown voltage of the test, each group of test conditions to carry out 100 times the frequency breakdown, every 20 times to collect gas samples, qualitative and quantitative analysis of gas samples of the characteristics of the decomposition of the components of the generation of the rule of change of the different influencing factors.

4.2 C_4F_7N-CO_2-O_2 frequency breakdown characteristics

4.2.1 Effect of O_2 on the insulation strength of C_4F_7N-CO_2-O_2

Figure 4.3 gives the amplitude of the breakdown voltage of the C_4F_7N-CO_2-O_2 gas mixture under different O_2 content for 100 times at work frequency, and the red colour in the figure is directly the fitted curve of the breakdown voltage value obtained by linear fitting, which reflects the overall trend of the breakdown voltage of the gas mixture with the number of discharges.

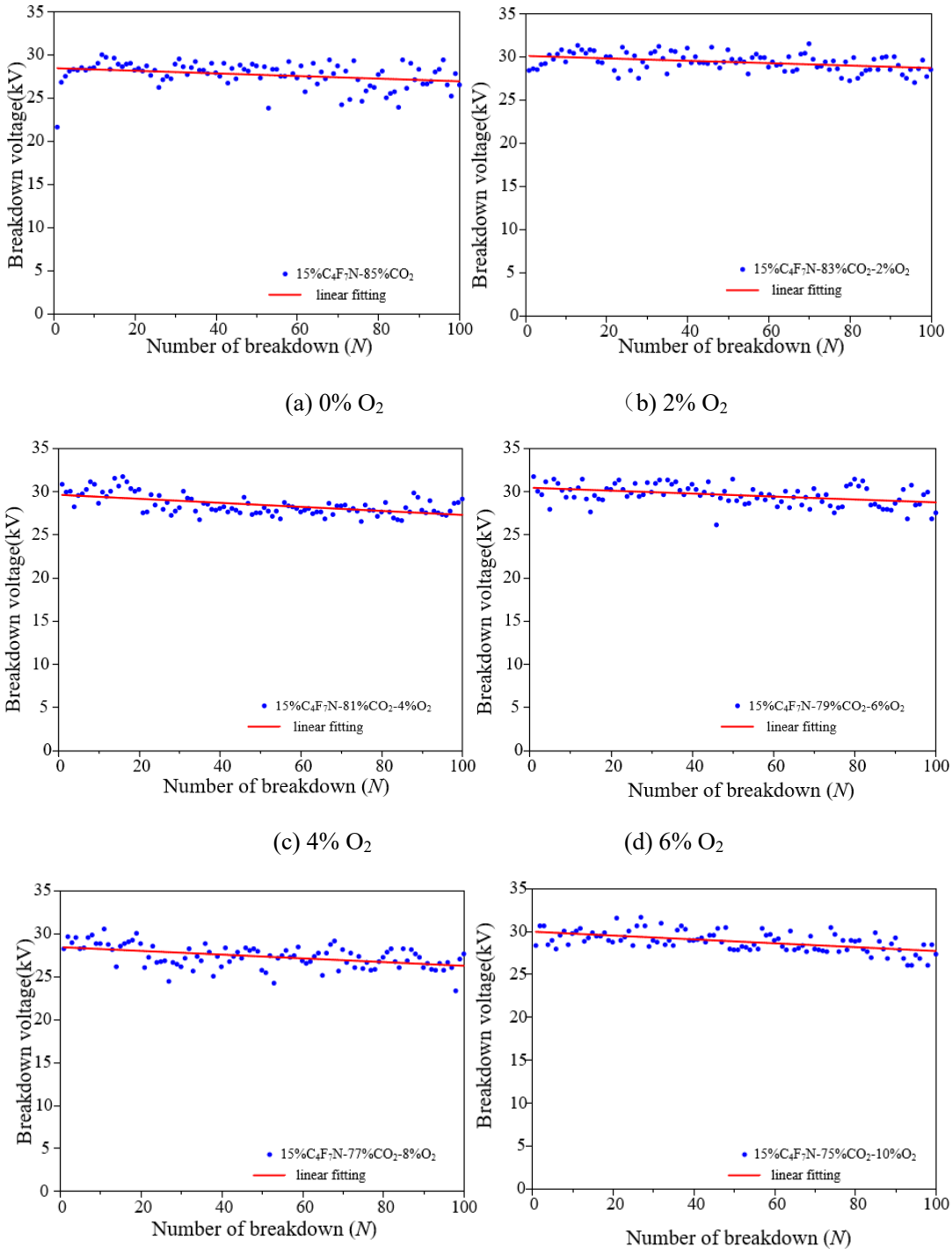

(a) 0% O_2 (b) 2% O_2

(c) 4% O_2 (d) 6% O_2

(e) 8% O_2 (f) 10% O_2

Fig. 4.3 C_4F_7N-CO_2-O_2 frequency breakdown voltage with different O_2 contents

It can be seen that 15% C_4F_7N-85% CO_2 gas mixture of the frequency breakdown voltage is about 28.1kV, with the increase in the number of breakdown, the breakdown voltage decreased, which is mainly due to the breakdown process of electric sparks will erode the electrode surface, so that the roughness of the electrode surface changes, which triggered the ball-ball gap electric field distortion, resulting in the reduction of the insulating strength of the

gas insulating medium. The slopes of the fitted curves of breakdown voltage are given in Table 4.1, and the slopes of the fitted curves are all negative.

Table 4.1 Fitting parameters for different gas mixture breakdown voltages

Gas mixture	Slope of the fit	Standard deviation
15% C_4F_7N-83% CO_2	-0.01524	1.45
15% C_4F_7N-83% CO_2-2% O_2	-0.01395	1.02
15% C_4F_7N-81% CO_2-4% O_2	-0.02339	1.12
15% C_4F_7N-79% CO_2-6% O_2	-0.01700	1.14
15% C_4F_7N-77% CO_2-8% O_2	-0.02173	1.31
15% C_4F_7N-75% CO_2-10% O_2	-0.02251	1.15

The AC breakdown voltages of C_4F_7N-CO_2-O_2 gas mixtures at different O_2 contents are given in Figure 4.4, where the AC breakdown voltage is the average of the first 10 breakdown voltages out of 100 tests for each group. It can be found that the average AC breakdown voltage of C_4F_7N-CO_2-O_2 gas mixture increases and then decreases with the increase of O_2 content. The average breakdown voltage of the C_4F_7N-CO_2 gas mixture is 28.06 kV, and the insulation strength of the C_4F_7N-CO_2-O_2 gas mixture is improved by 4.85% (2% O_2), 6.49% (4% O_2), 7.70% (6% O_2), 3.21% (8% O_2) and 2.74% (10% O_2), compared with that of the C_4F_7N-CO_2 gas mixture.), indicating that the addition of a certain content of O_2 to the C_4F_7N-CO_2 gas mixture can enhance its insulating properties, especially the best insulating properties when the O addition is 6%, but the insulating strength decreases when the O_2 content is greater than 6%.

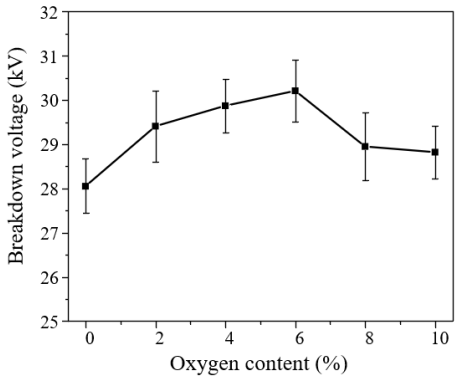

Figure 4.4 Effect of O_2 on C_4F_7N-CO_2-O_2 frequency breakdown voltage

In fact, the critical approximate electric field strength (E/N)crit of CO_2 and O_2 with respect to SF_6 are 0.23 and 0.33, respectively [8], which indicates that O_2 has a higher dielectric strength than CO_2, and the increase of O_2 content in the gas mixture is accompanied by a

decrease of CO_2 content, so that the breakdown voltage of the C_4F_7N-CO_2-O_2 mixture is increased with the increase of O_2 content. When the O_2 content is higher than 6%, the breakdown voltage of the gas mixture shows a decreasing trend, which may be due to the decomposition of C_4F_7N under the action of O_2.

4.2.2 Effect of O_2 on the dispersion of C_4F_7N-CO_2-O_2 breakdown voltage

Electrode surface roughness and other factors will make the gas insulating medium discharge channel formation process has a certain degree of randomness, so the C_4F_7N-CO_2-O_2 gas mixture frequency breakdown voltage will also show a certain degree of dispersion. Gas insulating medium frequency breakdown voltage dispersion size can be characterised by the standard deviation of the breakdown voltage (Standard Deviation), the standard deviation can reflect the degree of dispersion of a data set, this paper uses the standard deviation of the size of the study of the different content of O_2 on the dispersion of the breakdown voltage of the C_4F_7N-CO_2-O_2 gas mixture. The standard deviation is calculated by the following formula:

$$\sigma=\sqrt{\frac{1}{N-1}\sum_{i=1}^{N}(x_i-\bar{x})^2} \tag{4.1}$$

where N is the number of samples (N=100); x_i is the ith breakdown voltage in the test, $\bar{x}$ is the average value, and σ is the standard deviation of the breakdown voltage of the group of tests. The standard deviation of the breakdown voltage of C_4F_7N-CO_2-O_2 gas mixture with different O_2 content was calculated from equation (4.1) as shown in Table 4.1. It can be seen that the standard deviation of the IF breakdown voltage of the C_4F_7N-CO_2 gas mixture is the largest, which indicates that the dispersion of the IF breakdown voltage of the gas mixture under the condition of no O_2 is larger, while the standard deviation of the breakdown voltage is obviously reduced after adding 2%-6% O_2. This is mainly due to the fact that there are some solid precipitates on the electrode surface after multiple breakdowns without O_2, and the generation of these solid precipitates on the one hand makes the electrode surface become rough from smooth, and then changes the electric field distribution in the electrode area. At the same time, the solid material precipitated on the electrode surface, such as carbon particles, has good electrical conductivity itself, which will have a negative impact on the discharge of the gas mixture. The dispersion of breakdown voltage is essentially due to the randomness of the formation of the discharge channel, when the electrode surface precipitates, the generation of the discharge channel will become more irregular, the degree of randomness is greater, the macroscopic manifestation of the breakdown voltage dispersion is greater. the addition of O_2 will be generated with the solid products of the discharge process of C_4F_7N to react, to reduce the adhesion of the solid precipitates on the surface of the electrode, and thus reduce the

breakdown voltage in the discharge process of the electrode, and thus reduce the breakdown voltage in the discharge process of the electrode. dispersion of breakdown voltage during discharge.。

4.3 C_4F_7N-CO_2-O_2 Breakdown Characteristics

4.3.1 C_4F_7N-CO_2-O_2 breakdown product

In order to investigate the influence law of different content of O_2 on the breakdown characteristics of C_4F_7N-CO_2-O_2 mixture, the gas in the gas chamber was collected for qualitative and quantitative analyses of the decomposition components every 20 times in each group of 100 breakdown tests. Figure 4.5 shows the gas chromatogram of 15% C_4F_7N-85% CO_2 gas mixture after 20 times of AC breakdown discharge test. It can be found that there are CF_4, C_2F_6, COF_2, CO, C_3F_8, CO_2, CF_3CN, C_2F_5CN and $(CN)_2$ characteristic peaks, through the generation of these by-products with the content of O_2 and the number of times of breakdown rule of change to explore the C_4F_7N-CO_2-O_2 mixed gas breakdown characteristics. It can be seen that the types of mixed-gas breakdown products are roughly the same as those generated under POF and PD failure conditions, with only some differences in individual products, and the specific differences will be summarised and analysed in Chapter 5 of this paper.

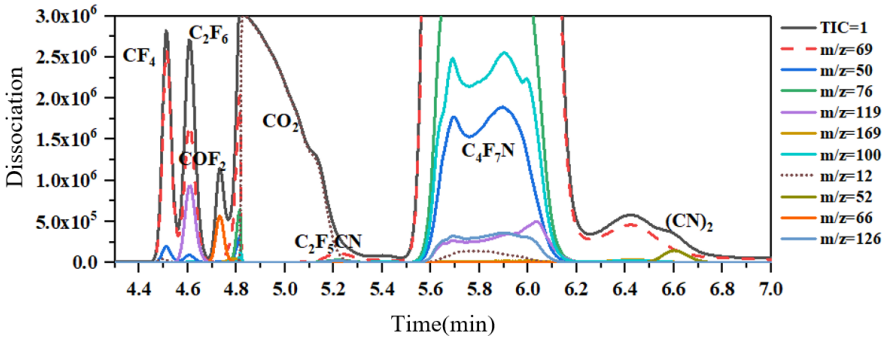

(a) Total Chromatogram

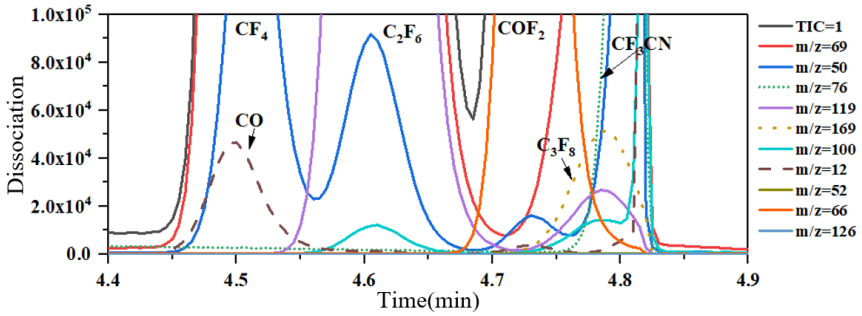

(b) High resolution chromatograms

Figure 4.5 Gas chromatogram of 15%C_4F_7N-85%CO_2gas mixture after 20 breakdown tests

4.3.2 Effect of O_2 on the breakdown properties of C_4F_7N-CO_2-O_2 breakdown

Typically, the arc plasma generated by the discharge induces complex physical and chemical reactions, which lead to the decomposition of the gas insulating medium and the generation of a variety of by-products. In order to investigate the influence of O_2 on the breakdown characteristics of the C_4F_7N-CO_2-O_2 gas mixture, the composition and content of the gas decomposition products in the gas chamber and their changing rules with the influencing factors were analyzed based on GC-MS after carrying out several AC breakdown discharge tests.

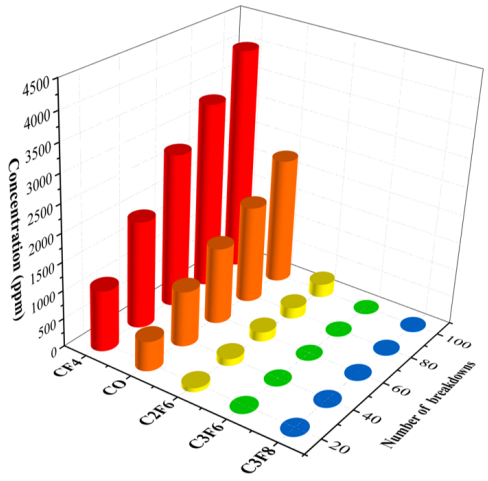

(a) 0% O_2

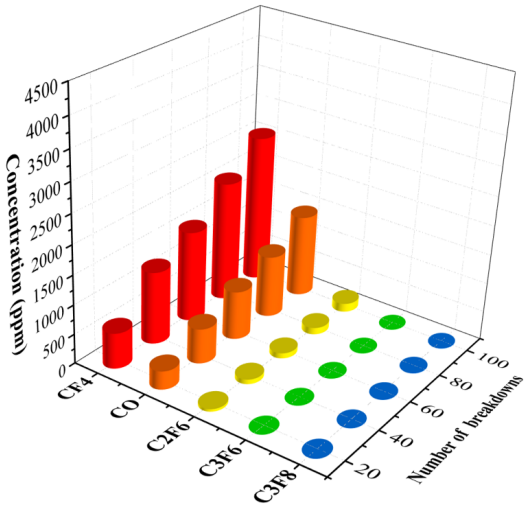

(b) 2% O_2

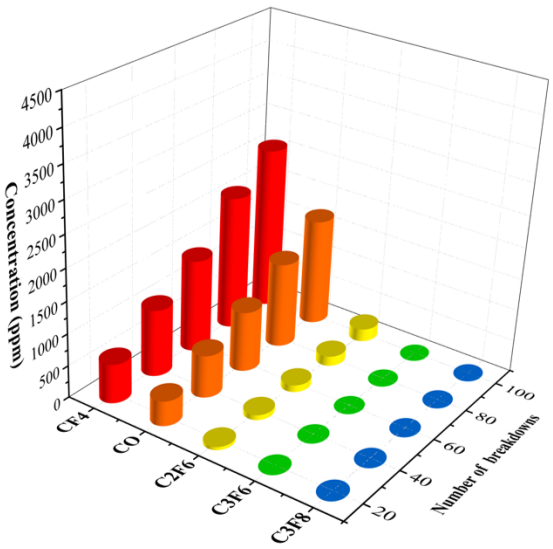

(c) 4% O_2

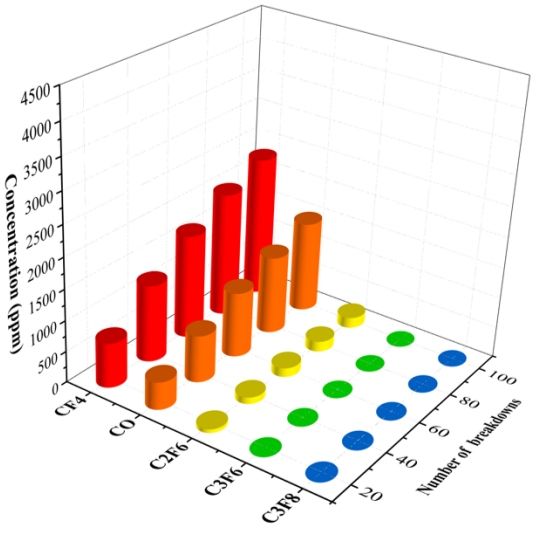

(d) 6% O_2

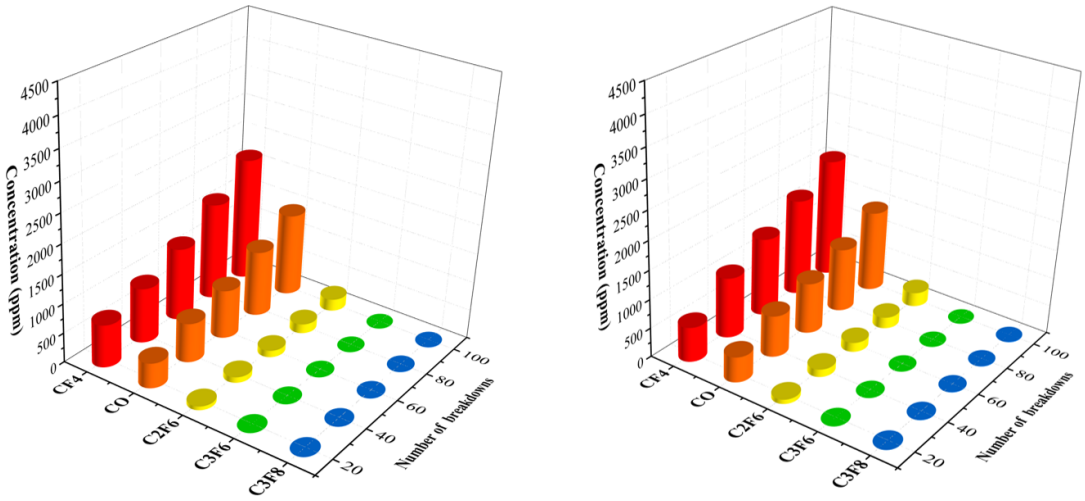

(e) 8% O_2 (f) 10% O_2

Fig. 4.6 Content of CO, CF_4, C_2F_6, C_3F_6 and C_3F_8 at different O_2 contents after the breakdown test

The contents of CO, CF_4, C_2F_6, C_3F_6, and C_3F_8 for the C_4F_7N-CO_2-O_2 gas mixture after several IF breakdown tests are given in Figure 4.6. It can be found that the generation of CF_4 is the highest among all decomposition products that can be quantitatively analyzed, followed by CO, C_2F_6, C_3F_8, and the lowest generation of C_3F_6. In addition, the generation of CO, CF_4, C_2F_6, C_3F_6, and C_3F_8 increases with the number of breakdowns, suggesting that an increase in the number of breakdowns leads to the continued decomposition of the C_4F_7N-CO_2-O_2 mixture.

$$V_P = \sqrt{\frac{\left(\frac{V_{20}}{20}\right)^2 + \left(\frac{V_{40}-V_{20}}{20}\right)^2 + \left(\frac{V_{60}-V_{40}}{20}\right)^2 + \left(\frac{V_{80}-V_{60}}{20}\right)^2 + \left(\frac{V_{100}-V_{80}}{20}\right)^2}{5}} \tag{4.2}$$

The effective production rate can more intuitively analyze the trend of the influence of decomposition O_2 on the production of decomposition products, so this paper uses equation (4.2) to calculate the effective production rate of decomposition products under different O_2 content, where V_P is the effective production rate,V_{20}、V_{40}、V_{60}、V_{80}、V_{100} are the gas content detected after the 20th, 40th, 60th, 80th and 100th breakdowns, respectively. The variation of CF_4, CO, C_2F_6, C_3F_6 and C_3F_8 generation and effective gas production rate with O_2 content after the breakdown test is given in Figure 4.7.

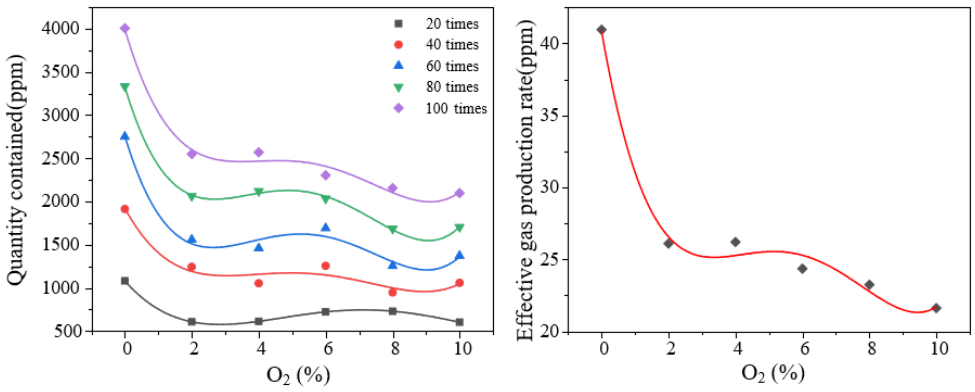

(a) CF_4

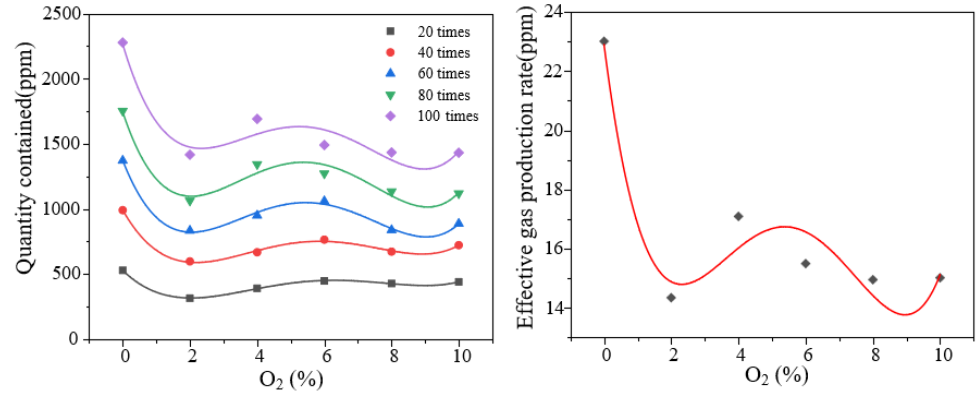

(b) CO

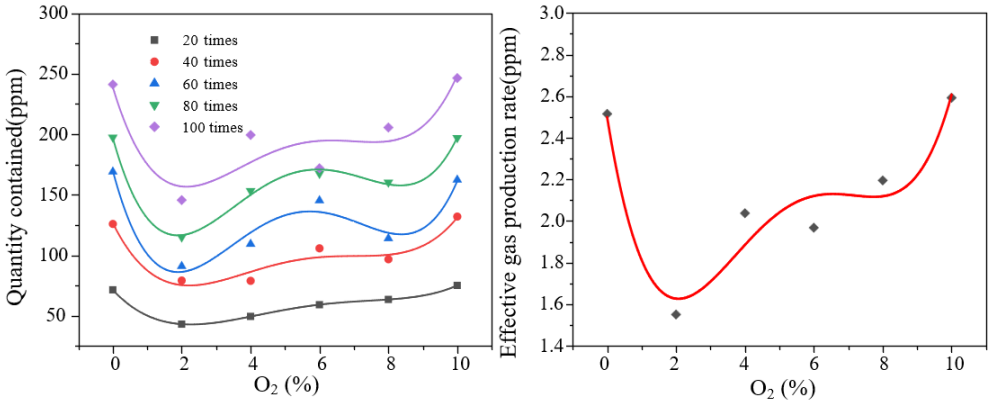

(c) C_2F_6

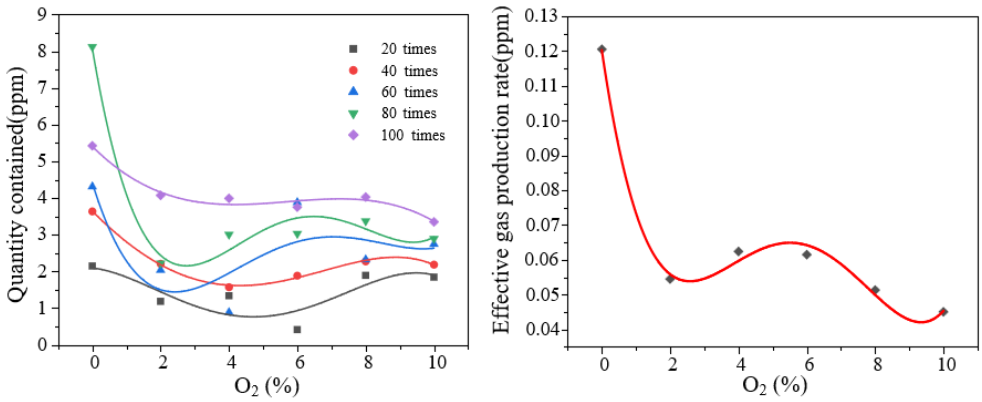

(d) C_3F_6

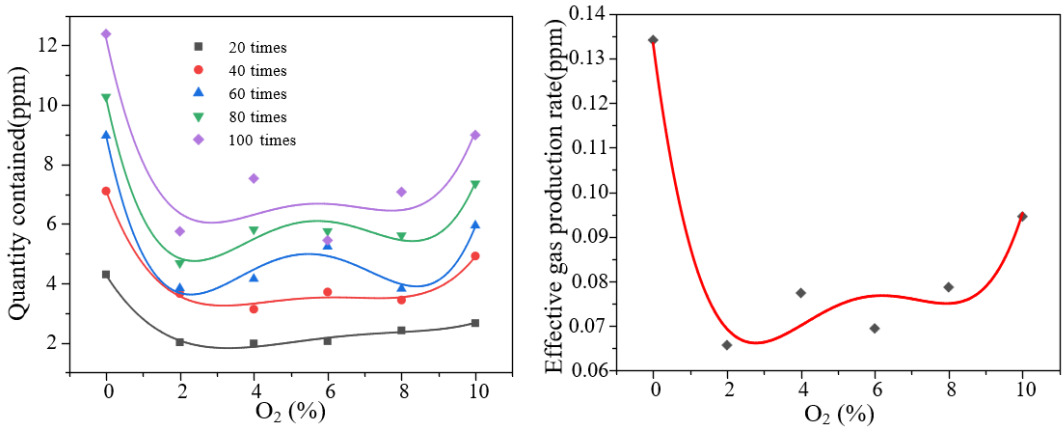

(e) C_3F_8

Figure 4.7 Variation of CF_4, CO, C_2F_6, C_3F_6 and C_3F_8 generation and effective gas production rate with O_2 content after breakdown test

The variation of CF_4 generation and effective gas production rate with O_2 content is given in Figure 4.7(a). It can be seen that the amount of CF_4 generated and the effective production rate decrease gradually with the increase of O_2 content. The generation amount of CF_4 produced by the decomposition of the C_4F_7N-CO_2 gas mixture after 100 breakdown tests was 4004 ppm, and the corresponding value decreased to 2548 ppm when 2% O_2 was added to the gas mixture, so that the addition of 2% O_2 can effectively inhibit the generation of CF_4. In addition, when 2%-4% O_2 was added to the C_4F_7N-CO_2 gas mixture, the amount of CF_4 generation and the effective gas production rate remained stable, however, a decreasing trend was observed when the O_2 content in the C_4F_7N-CO_2-O_2 gas mixture was higher than 6%. As can be seen from Figure 4.4, the breakdown voltage of the C_4F_7N-CO_2-O_2 gas mixture starts to decrease when the O_2 content is greater than 6%, and the energy generated by the discharge also decreases, so that the amount of CF_4 generated and the effective gas production rate decrease at this time.

From Fig. 4.7(b), it can be seen that the CO generation decreases dramatically from 2277 ppm to 1414 ppm (100th breakdown decomposition) with the addition of 2% O_2 to the C_4F_7N-CO_2 gas mixture. In addition, there is a slight increasing trend of CO generation in gas mixtures with 2%-6% O_2 content, while a small decreasing trend can be found when the O_2 content is higher than 6% (6%-10%), and the generation of CO generated from decomposition of the C_4F_7N-CO_2-O_2 gas mixture containing 6%, 8%, and 10% O_2 after the 100th breakdown is 1490.23 ppm, 1433.11ppm and 1430.82ppm, respectively. Therefore, the change rule of CO generation in the gas mixture containing 2%-10% O_2 has a similar trend with the breakdown voltage. For the gas mixture with added O_2, the higher the breakdown voltage is, the higher the energy released from the discharge is, and the decomposition of the C_4F_7N-CO_2-O_2 gas

mixture will be intensified. In addition, the addition of 2% O_2 can effectively reduce the effective gas production rate of CO in the gas mixture. With the increase of O_2 content, the effective gas production rate of CO has a similar trend of breakdown voltage.

The production of C_2F_6 decreases when 2% O_2 is added to the C_4F_7N-CO_2 mixture (shown in Fig. 4.7(c)). The production of C_2F_6 in the C_4F_7N-CO_2 mixture reaches 241 ppm after 100 breakdown tests, whereas this value is only 145 ppm in the 15% C_4F_7N-83%CO_2-2%O_2 gas mixture. The effective gas production rate of C_2F_6 tends to increase with further increase in O_2 content, especially at O_2 content higher than 6%, and its production increases rapidly. The production of C_2F_6 originates from the recombination of CF_3 particles or the complexation of C_2F_5 and F particles, thus indicating that the content of these particles is higher in C_4F_7N-CO_2-O_2 gas mixtures with O_2 content higher than 6%.

The amount of C_3F_6 generated and the effective gas production rate under different O_2 contents are shown in Fig. 4.7(d).The amount of C_3F_6 generated in the C_4F_7N-CO_2 gas mixture after 100 breakdown decomposition tests was only 8.12 ppm, which was lower than that of other byproducts. With the increase of O_2 content, the generation of C_3F_6 shows a decreasing trend. Considering the presence of unsaturated C=C bonds in the C_3F_6 molecule, the addition of O_2 may cause oxidation reactions between them. According to the change characteristics of C_3F_8 given in Fig. 4.7(e), it can be found that the addition of 2% O_2 leads to a decrease in C_3F_8 content after several breakdown tests. The C_3F_8 generation of the C_4F_7N-CO_2 gas mixture after the 100th breakdown is 12.38 ppm, while the value is only 5.74 ppm for the gas mixture containing 2% O_2. In addition, the C_3F_8 generation tends to increase when the O_2 content is higher than 6%.The generation of C_3F_8 is mainly originated from the composite of C_3F_7 and F particles, and the increase of C_3F_8 generation indicates that the decomposition of C_4F_7N is accelerated when the O_2 content in the gas mixture is higher than 6%.

The IF breakdown of the C_4F_7N-CO_2-O_2 gas mixture also produces other by-products, including CF_3CN, C_2F_5CN, $(CN)_2$ and COF_2. Considering that there are no standard gases for these by-products at present, the peak area integration method is used to reveal the effect of O_2 on their production. The peak areas of the characteristic peaks can be used to characterize the relative amount of the measured components produced.

The generation and effective gas production rates of CF_3CN and C_2F_5CN under different O_2 content conditions are given in Figures 4.8(a) and 4.8(b), respectively. It can be found that the generation of CF_3CN and C_2F_5CN has similar characteristics with the change of O_2 content. When 2% O_2 was added to the C_4F_7N-CO_2 mixture, the generation of these two by-products decreased firstly, and then showed an increasing trend with the increase of O_2 content, and the

effective gas production rate was the lowest in the mixture containing 2% O_2, which indicated that the addition of 2% O_2 could increase the effective gas production rate compared with that of the C_4F_7N-CO_2 mixture, which indicated that the addition of 2% O_2 could increase the effective gas production rate. The effective gas production rate was the lowest in the gas mixture with 2% O_2, indicating that the addition of 2% O_2 could effectively inhibit the decomposition of C_4F_7N compared with the C_4F_7N-CO_2 mixture. The effective generation rates of CF_3CN and C_2F_5CN increased with the increase of O_2 content in the gas mixture. When the O_2 content in the C_4F_7N-CO_2-O_2 mixture was higher than 8%, the amount and effective generation rate of CF_3CN and C_2F_5CN reached a level similar to that of the C_4F_7N-CO_2 gas mixture. The generation of CF_3CN and C_2F_5CN requires the participation of several particles including CF_3, CN, and F. The formation of C_2F_5CN and C_2F_5CN was also found to be a significant factor in the formation of C_2F_5CN and CF_3CN. Therefore, the incorporation of higher levels of O_2 (higher than 8%) negatively affects the stability of the C_4F_7N-CO_2-O_2 gas mixture.

The effect of O_2 on $(CN)_2$ production and effective gas production rate is given in Figure 4.8(c). It can be noticed that the $(CN)_2$ production decreases dramatically when 2% O_2 is added to the C_4F_7N-CO_2 gas mixture. The generation of $(CN)_2$ requires CN particles, which come from the decomposition of C_4F_7N. Therefore, the addition of 2% O_2 can effectively inhibit the decomposition of C_4F_7N in the C_4F_7N-CO_2 mixture. In addition, the trend of $(CN)_2$ generation from the decomposition of the C_4F_7N-CO_2-O_2 gas mixture containing 2%-10% O_2 is small, indicating that this range of O_2 addition does not have much effect on the $(CN)_2$ generation.。

The variation of COF_2 under different O_2 content conditions is characterized in Figure 4.8(d). It can be seen that the generation of COF_2 increases with the increase of O_2 content. The COF_2 generation is similar for gas mixtures with O_2 lower than 6%, and a large increasing trend exists when the O_2 content is higher than 6%. As can be seen in Figure 4.4, the breakdown voltage starts to decrease when the O_2 content in the C_4F_7N-CO_2-O_2 gas mixture is 6%-10%, indicating a decrease in the energy released from the discharge and an increase in the generation of COF_2. In fact, the generation of COF_2 originates from the reaction between CFx and O_2, O particles. The increase in COF_2 in gas mixtures with O_2 higher than 6% is due to the strong oxidizing effect of O_2. The higher content of O_2 intensifies the reaction between CFx and O particles to form COF_2, which means that the gas mixture with O_2 content higher than 6% is less stable, and the higher content of O_2 in the gas mixture will have a certain negative impact on the stability of C_4F_7N.

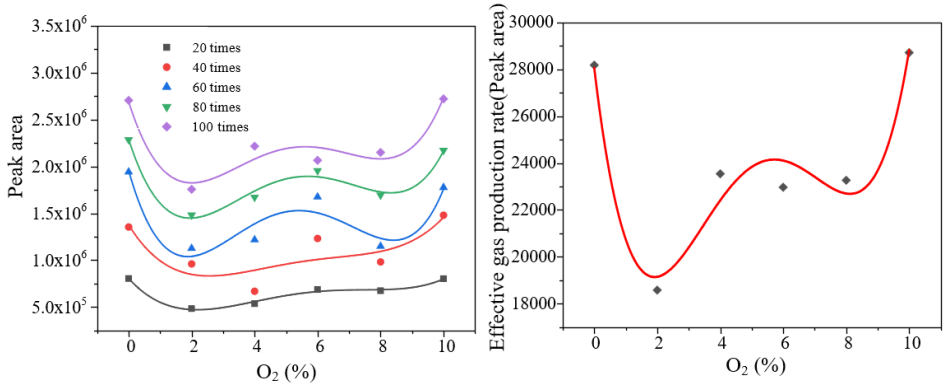

(a) CF_3CN

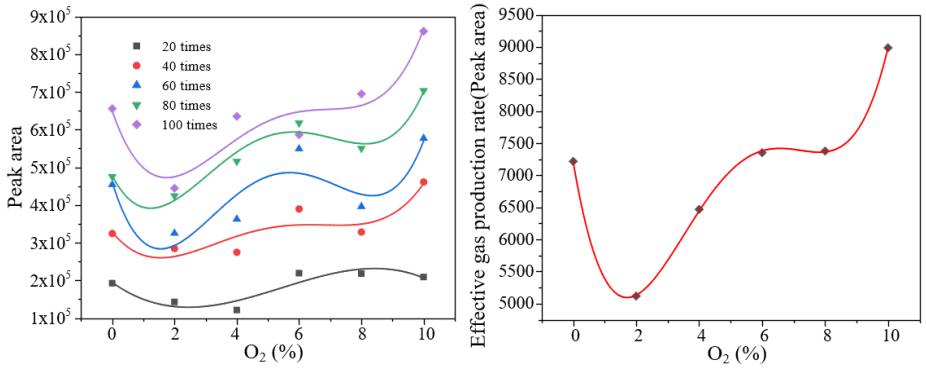

(b) C_2F_5CN

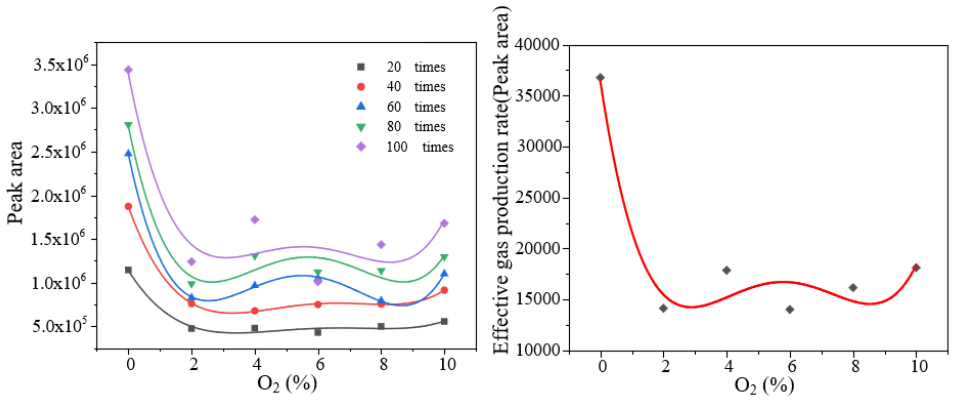

(c) C_2N_2

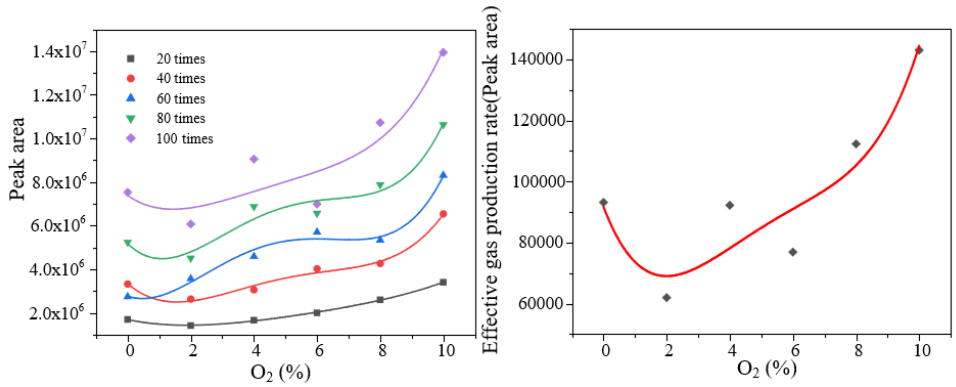

(d) COF_2

Figure 4.8 Variation of CF_3CN, C_2F_5CN, C_2N_2 and COF_2 generation and effective gas production rate

with O_2 content after the breakdown test

4.4 Mechanism of O_2 effect on C_4F_7N-CO_2-O_2 insulation strength and decomposition properties

4.4.1 Mechanism of the effect of O_2 on the insulation strength of C_4F_7N-CO_2-O_2

It can be found that the addition of O_2 to the C_4F_7N-CO_2 gas mixture has a large effect on its insulation strength. Considering that the content of C_4F_7N is fixed at 15% in this paper, the relevant changes may be attributed to the difference in insulation properties between O_2 and CO_2.

In fact, the effect of O_2 on the insulating properties of CO_2-O_2 gas mixtures has been comprehensively investigated. Uchii et al. showed that adding some O_2 to CO_2 improves its insulating strength and brings better thermal breakthrough capability to CO_2 [108]. Xingwen Li et al. investigated the insulation breakdown characteristics of CO_2-O_2 gas mixtures by considering the electron separation of negative ions [109], and calculated the approximate ionization coefficients (α/N), the approximate attachment coefficients (η/N), and the breakdown-approximate electric field strengths (E/N). It was found that the increase of O_2 content in the CO_2-O_2 gas mixture enhances the approximate ionization coefficient and the approximate attachment coefficient. The increase in α/N is due to the fact that the ionization potential energy of O_2 (12.06 eV) is lower than that of CO_2 (13.3 eV), while the increase in η/N is attributed to the strong electronegativity of O_2. In addition, for electron energies around 5-10 eV, the attachment cross-section of O_2 is larger than that of CO_2, which may lead to a decrease in the kinetic energy of electrons [110]. The (E/N)crit of the CO_2-O_2 gas mixture calculated at CO_2 concentrations of 20%, 40%, 60%, 80%, and 100% were 116.3 Td, 111 Td, 104 Td, 94.8 Td, and 77.3 Td, respectively, which confirms that the addition of O_2 improves the dielectric strength of the gas mixture.

Rong et al. investigated the effect of O_2 on the insulating properties of CO_2 under high-temperature discharges and showed that the CO_2-O_2 gas mixture has better dielectric strength than pure CO_2 and air [111]. Since the vibrational cross section of O_2 is smaller than that of CO_2, the electron energy distribution function (EEDF) increases with the increase of O_2 content, α/N below 90 Td increases slightly with the increase of O_2 due to the increase of the average electron energy of excitation, ionization, and attachment reactions, and η/N tends to be more pronounced than α/N with the increase of O_2. Thus, (E/N)crit increases with increasing O_2 content. In addition, the breakdown field strength of pure CO_2 in the temperature range from 300 K to 1500 K is much lower than that of O_2. The breakdown field strength in the

temperature range from 300 K to 3000 K increases significantly with the increase of O_2 content, which is mainly due to the larger attachment cross section of O_2.

As noted above, the insulating properties of CO_2 increase significantly with the addition of O_2. For C_4F_7N-CO_2-O_2 gas mixtures, the amount of C_4F_7N that provides the dielectric strength is fixed, and the difference in dielectric strength is mainly attributed to the change in the ratio of CO_2 to O_2. a larger attachment cross-section of O_2 may result in an increase in the attachment coefficient and a decrease in the critical field strength of the C_4F_7N-CO_2-O_2 gas mixtures. As a result, the breakdown voltage of C_4F_7N-CO_2-O_2 gas mixtures with 2%-10% O_2 added is higher than that of the C_4F_7N-CO_2 gas mixture. In addition, when the O_2 content is higher than 6%, the breakdown voltage shows a decreasing trend. This can be attributed to the strong oxidizing property of O_2. According to the analysis of decomposition characteristics, the production of most of the by-products shows an increasing trend when the O_2 content is higher than 6%.C_4F_7N is difficult to recover after decomposition under the action of high-energy discharge, so its decomposition rate increases with the increase of O_2 content. The relative insulating properties of C_4F_7N and the main decomposition products are given in Table 4.2. It can be noticed that all the generated by-products have lower insulation strength compared to C_4F_7N. Therefore, at higher O_2 content, the decomposition of C_4F_7N is intensified and by-products with lower dielectric strength are generated leading to an overall lower breakdown voltage.

Table 4.2 Dielectric strength of C_4F_7N and its decomposition products

Gas	Insulation strength relative to SF_6	Reference
SF_6	1	[8]
C_4F_7N	2.2	[8]
CO_2	0.23	[8]
O_2	0.33	[8]
CF_4	0.4	[8]
C_2F_6	0.78	[24]
C_3F_8	0.97	[24]
C_3F_6	1.1	[71]
CO	0.4	[71]
CF_3CN	1.46	[72]
C_2F_5CN	1.92	[72]

4.4.2 Mechanism of O_2 influence on the breakdown properties of C_4F_7N-CO_2-O_2 breakdown

The addition of O_2 to the C_4F_7N-CO_2 gas mixture affects its stability and breakdown

characteristics. When 2% O_2 was added to the C_4F_7N-CO_2 gas mixture, the generation of CF_4, CO, C_2F_6, C_3F_6, C_3F_8, CF_3CN, C_2F_5CN, and $(CN)_2$ decreased to some extent, indicating that the addition of O_2 can inhibit the decomposition of C_4F_7N in the C_4F_7N-CO_2 gas mixture to some extent.

The temperature of arc discharge plasma is usually in the range of 300-12000 K. Calculations of the plasma composition of C_4F_7N show that the main particles at temperatures below 3000 K include CF_2, CF_4, C_4F_6, C_2F_3N, C_4F_3N, CO, and CO_2 [85], and that the initial gas, C_4F_7N, is not observed at high concentrations, suggesting that the C_4F_7N at high temperatures arc decomposes and cannot be recovered again, so all byproducts detected after discharge increase with the number of breakdowns.

In fact, the arc time constant of O_2 is known to be less than that of CO_2, 1.5 μs compared to 15 μs for CO_2 [108]. Therefore, O_2 has a better arc extinguishing capability than CO_2.Uchii et al. investigated the arc extinguishing characteristics of pure CO_2 and 85%CO_2-15%O_2 gas mixtures, and found that the post-arc current of the 85%CO_2-15%O_2 gas mixture was much smaller than that of the pure CO_2, suggesting that the addition of O_2 can lead to a more rapid decay of the arc conductivity of the gas mixture. The addition of O_2 can improve the arc extinguishing ability of C_4F_7N-CO_2 gas mixtures, especially the decay rate of arc conductivity [66]. The experimental results in this paper show that the generation of CF_4, CO, C_2F_6, C_3F_6, C_3F_8, CF_3CN, and $(CN)_2$ shows a decreasing trend when 2%-6% O_2 is added to the gas mixture, and the content of some of the by-products starts to increase when 6%-10% O_2 is added. The generation of COF_2 and C_2F_5CN remained relatively stable with the addition of 2%-4% O_2, and tended to increase when the O_2 content was greater than 4%. The formation of these decomposition by-products mainly comes from the compounding of several particles such as CF_3, CN, C_3F_7, F, C_2F_5, CF_2, and O. The generation of these particles decreases when 2%-4% O_2 is added. Relevant theoretical studies on the mechanism of C_4F_7N decomposition have shown that the lowest reaction enthalpy is required for the bond breaking process to produce CF_3 and C_3F_4N, so this reaction is most likely to occur [91]. Although the breakdown voltage is increased when 2%-6% O_2 is added to the reaction system, the energy released from the discharge may not be increased considering that O_2 has a better arc extinguishing ability. Therefore, the addition of 2%-6% O_2 to the C_4F_7N-CO_2 gas mixture can reduce the by-product generation and C_4F_7N decomposition, and when a higher content of O_2 is added (>6%), negative effects such as the breakdown voltage of the gas mixture starts to decrease and some by-products tend to increase with the increase of the O_2 content can be found, which suggests that excessive O_2 can lead to accelerated decomposition of C_4F_7N.

In addition, Meyer et al. investigated the decomposition characteristics of C_4F_7N-CO_2-O_2 gas mixtures for high-voltage equipment [66], using a 6% C_4F_7N-5%O_2-89%CO_2 gas mixture as an insulating and arc-extinguishing medium for the development and type-testing of circuit breakers according to the IEC standard (145 kV/40 kA), with the minimum pressure for insulation and opening set at 0.75 MPa. The results show that the addition of 5% O_2 can improve the electrical life of the circuit breaker by inhibiting the generation of gaseous and solid decomposition products, especially for tests with higher currents, a significant improvement was observed with the addition of 5% O_2. The gaseous decomposition by-products after the 40 kA short-circuit test were CO, CF_4, C_2F_6, C_3F_8, CF_3CN, C_2F_5CN, $(CN)_2$, COF_2, C_2F_4, and C_3F_6. the compounds other than CO, CF_4, C_2F_6, and C_3F_8 were in the concentration range of 1 ppm to 200 ppm, and this type of GIS was piloted in Switzerland and Francis in 2017-2018[83], which also confirmed the 6%C_4F_7N-5%O_2-89%CO_2 gas mixture in high-voltage equipment Potential.。

4.5 Mechanism of C_4F_7N discharge decomposition and product generation under O_2 participation reaction

From the above findings, it can be seen that the addition of O_2 as a background gas to the C_4F_7N-CO_2 gas mixture will have a more significant effect on its decomposition characteristics, so the dissociation of C_4F_7N molecules under the conditions of O particles participating in the reaction and the recombination process of each particle after dissociation and its thermodynamic parameters are of great significance for the study of the effect of O_2 on the decomposition mechanism of the C_4F_7N-CO_2 gas mixture. The density functional theory and transition state theory based on quantum chemistry can provide theoretical support for obtaining the microscopic parameter calculations of the decomposition process under the conditions of O_2 participation in the reaction, and further reveal the decomposition and product generation mechanism of C_4F_7N discharges under the O_2 participation in the reaction.

4.5.1 Density Functional Theory and Transition State Theory

Analyzing chemical reaction processes at the microscopic level requires the use of quantum mechanical methods based on classical physics, which explains the behavior of complex chemical reactions mainly by solving the Schrödinger equation. The Schrödinger equation can be expressed as equation 4.3, with $\hat{H}$ representing the Hamiltonian operator (total energy of the system wave function), ψ the system's stationary wave function (stationary means that the energy has a definite value), and E the system energy. In general, the reaction system under study is a multi-electron system (containing hundreds to thousands

of electrons), and solving the energy and electronic structure of the multi-electron system by the Schrödinger equation becomes extremely complicated.

$$\hat{H}\psi = E\psi \tag{4.3}$$

Hohenberg et al. proposed a quantum chemical method to study the structure of multi-electron systems based on the Thomas-Fermi model [112], i.e., density functional theory (DFT), which is widely used in theoretical calculations. The DFT method is mainly used to study the multi-electron structure through the electron density, and can directly solve the ground state energy and electron density of the system by crossing the intermediate steps in the process of solving the energy and structure of the multi-electron system. structure, in the process of solving the energy and structure of the multielectron system, the intermediate step of the multielectron wave function can be crossed and the ground state energy and electron density of the system can be solved directly. Compared with the traditional Hartree-Fock method, the DFT method is more accurate and has a wider range of applications, and the computational volume is smaller than that of the ab initio method with the same computational accuracy. Hohenberg and Kohn proposed the basic theoretical basis of the DFT method in 1964 [113], which is that firstly, the ground state energy of the multielectronic system is related to only two variables, i.e., the density of electrons and the position of atomic nuclei, and the energy of the atomic nucleus. atomic nucleus positions, i.e., the electron density determines the total energy of the system in the ground state; in addition, the system energy is the minimum value obtained by taking the ground state electron density as the variable to put the system energy through the variational division. Therefore, based on the Hohenberg-Kohn theory, the electron density of the system can be expressed as follows.

$$\rho(r) = \sum_{i=1}^{N} |\psi(r)|^2 \tag{4.4}$$

The virtual kinetic energy of the simulated system can be expressed as:

$$T_s\left[\rho(r)\right] = -\frac{1}{2}\sum_{\sigma}\sum_{i=1}^{N}\left\langle\varphi_i(r)\middle|\nabla^2\middle|\varphi_i(r)\right\rangle = -\frac{h^2}{2m_e}\sum_{i=1}^{N^\sigma}\int\varphi_i(r)\middle|\nabla^2\middle|\varphi_i(r)d^3r \tag{4.5}$$

The external potential energy of the simulated system can be expressed as:

$$U\left[\rho(r)\right] = \frac{1}{2}\sum_{i,j}d^3r_1\int\varphi_i^*(r_1)\varphi_j^*(r_2)\frac{1}{|r_1-r_2|}\varphi_i(r_1)\varphi_j(r_2)d^3r_2 \tag{4.6}$$

The approximate expression for the total energy of the charge density generalization of the system can be obtained from Eqs. (4.4)-(4.6) as:

$$E_{KS}\left[\rho(r)\right]=T_S\left[\rho(r)\right]+\int v_{ext}(r)\rho(r)dr+\frac{e^2}{8\pi\varepsilon}\iint\frac{\rho(r_1)\rho(r_2)}{|r_1-r_2|}dr_1dr_2 + E_{XC}\left[\rho(r)\right] \tag{4.7}$$

Where $E_{XC}\left[\rho(r)\right]$ is the exchange correlation energy, i.e., the difference between the actual total energy and the approximate total energy [113]. The exchange correlation energy can be tabulated as:

$$E_{XC}\left[\rho(r)\right]=(T\left[\rho(r)\right]-T_S\left[\rho(r)\right])+\left(U\left[\rho(r)\right]-U_H\left[\rho(r)\right]\right) \tag{4.8}$$

Where $T\left[\rho(r)\right]$ is the kinetic energy of the real system and $U_H\left[\rho(r)\right]$ is the single-electron potential energy term. If the exchange correlation energy is regarded as a known quantity, the Schrödinger single-electron equation for the simulated system can be derived by the variational principle:

$$\left[-\frac{1}{2}\nabla^2+v(r)+\int\frac{\rho(r_2)}{|r_1-r_2|}dr_2+E_{XC}\left[\rho(r)\right]\right]\varphi_i(r)=\varepsilon_i\varphi_i(r) \tag{4.9}$$

Eq. (4.9) is the core expression of density generalization theory calculations, and the main idea is to transform the multidimensional degree-of-freedom equations into an electron density solving problem to obtain the electronic structure and energy of the system, which can greatly reduce the amount of calculations for the multi-electron system. Solving Eq. (4.9) using the self-consistent field iterative method requires an accurate expression for the exchange-associated potential energy, and the more widely used exchange-energy generalized functions are the local density approximation[114], the generalized gradient approximation[115], and the B3LYP hybridized energy generalized function[116], etc., among which the hybridized generalized function has a higher accuracy in describing the system and the electron energy. Density generalization theory describes the physicochemical properties of substances by calculating the electronic structure and energy of the system, and combines with the transition state theory to reveal chemical reaction mechanisms that cannot be obtained by experimental processes.。

Transition state theory (TST) is a theory proposed on the basis of quantum chemistry and statistical mechanics, which is mainly used to further analyze the mechanism of chemical reactions by calculating the transition states of chemical reactions. Different from the classical molecular collision theory, the transition state theory believes that the products are not generated by simple collision in the process of chemical reaction, when the reactant molecules have enough energy, they will undergo the rearrangement of valence bonds and redistribution

of energy, in the process, the reactant molecules will undergo the configuration corresponding to the highest point of the energy, and the generated transition state corresponds to only one imaginary frequency, at this time, the force vector of the reactive system and the sum of the force vectors is 0, corresponding to the Minimum Energy Pathway (MEP). The reaction energy barriers of the reactants and transition states on the Minimum Energy Pathway are the activation energy ΔE of the reaction (shown in Figure 4.9).

The commonly used methods for searching transition states are the synchronous transfer method and the microperturbation method. Synchronous transfer method mainly searches for transition states by inserting a reaction path between reactants and products, including Linear Synchronous Transit (LST)[117] and Quadratic Synchronous Transit (QST)[118].LST builds a reaction path by interpolating the values between the atoms of reactants and products, and then the structures corresponding to the highest energy points on the constructed path are taken as possible transition states. LST interpolates between the atoms of the reactants and products to build the reaction paths, and then the structures corresponding to the highest energy points on the built paths are used as possible transition states, and the set of ideal configurations connecting the reactants and products is as follows:

$$r^{i}_{ab}(j) = (1-f)r^{R}_{ab} + fr^{p}_{ab} \tag{4.10}$$

Where r^{R}_{ab} and r^{P}_{ab} are the nuclei spacing of the reactants and products, respectively, and f is the interpolation parameter. The molecular structure obtained by inserting Cartesian coordinates between the reactants and products is defined as the LST structure with the minimum value of the objective function:

$$S = \frac{1}{2}\sum_{a\neq b}\frac{[r_{ab} - r^{i}_{ab}(j)]^2}{[r^{i}_{ab}(j)]^4} + 10^{-6}\sum_{a}[x - x^{i}_{a}(j)]^2 \tag{4.11}$$

Where x^{i}_{a} and x_{a} are the Cartesian and real coordinates of the atom, respectively. Different LST reaction paths can be obtained by solving for different values of f. Comparing the potential energy surfaces of different paths, the LST paths with the smallest energy barriers and their corresponding transition state structures can be obtained. In order to solve the error caused by the linear energy change in the LST method, the QST method can be used to construct the quadratic curve of the reaction potential energy surface, and search the molecular configurations in the vertical direction to find the lowest energy point on the basis of the transition state coordinates obtained by LST. The QST maximization calculation is performed to obtain a more accurate transition state structure.

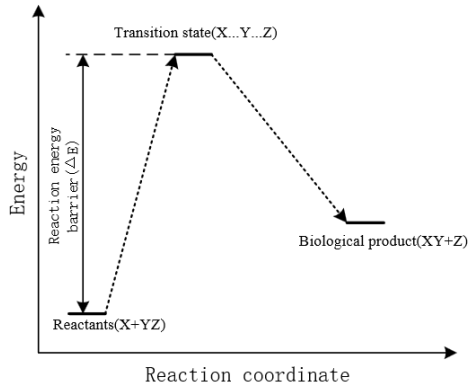

Figure 4.9 Schematic diagram of the transition state reaction process

4.5.2 Decomposition of C_4F_7N and generation of O-containing products under O_2 participation reaction

The decomposition process of C_4F_7N gas mixture is induced by external fault conditions (discharge, overheating), but the reaction process of C_4F_7N molecules is determined by the dissociation mechanism of its molecules themselves. At present, the decomposition mechanism of C_4F_7N has been studied more comprehensively, but few studies have been conducted on the changes occurring in the decomposition process of C_4F_7N after the addition of O_2, so in this section of the study, only the additional dissociation paths of C_4F_7N under the conditions of O_2 participation in the reaction and the generation paths of O-containing products are considered. Firstly, based on the density functional theory and transition state theory, the dissociation paths of C_4F_7N-CO_2-O_2 gas mixture and the generation paths of O-containing particles are constructed on the basis of analyzing the configurations and properties of C_4F_7N, CO_2, and O molecules; then, the structural relaxation and frequency analyses are carried out on the particles involved in the reaction process to obtain the stable configurations and energies of the particles according to the principle of energy minimization. The enthalpies of the reaction paths were calculated by correcting each particle at 298.15 K. Subsequently, the geometrical configurations and reaction energy barriers (activation energies) of the transition states of the reaction process were searched based on the transition state theory. Finally, the reaction mechanism of C_4F_7N-CO_2 gas mixture under the condition of O_2 participation was analyzed by the results of energy calculation of each reaction path. The reaction enthalpy E can be calculated by the following equation:

$$E = (E_{ptotal} + G_{ptotal}) - (E_{rtotal} + G_{rtotal}) \tag{4.12}$$

In Eq. (4.12), E_{ptotal} and G_{ptotal} are the total energy of the product and the zero-corrected energy at a temperature of 298.15 K, and E_{rtotal} and G_{rtotal} are the total energy of the reactant

and the zero-corrected energy at a temperature of 298.15 K, respectively.

In this study, the Dmol^3 module of Materials Studio is used to calculate in order to obtain the energies and enthalpies of reaction for the proposed reaction paths based on the DFT and TS theories. Geometry optimization and harmonic frequency calculations are performed based on the generalized gradient approximation and the Perdew-Burke-Ernzerhof (PBE) (GGA-PBE) method[119], and the dual numerical plus polarization (DNP) is chosen as the basis group. The LST and QST methods were used to search for the transition state (TS)[117] of the proposed pathway to obtain the activation energy of the transition state reaction. Based on the structural characteristics of the C_4F_7N molecule, 13 possible decomposition paths and 10 possible generation paths of O-containing products under the conditions of considering the participation of O particles in the reaction were constructed, which were used to reveal the reaction mechanism of the C_4F_7N-CO_2 mixture under the conditions of O_2 participation. The paths for the dissociation of C_4F_7N under the O-participation reaction are shown in Fig. 4.10 (the molecules involved in the paths are the optimized configurations), and the enthalpies and activation energies under different paths are shown in Table 4.3.

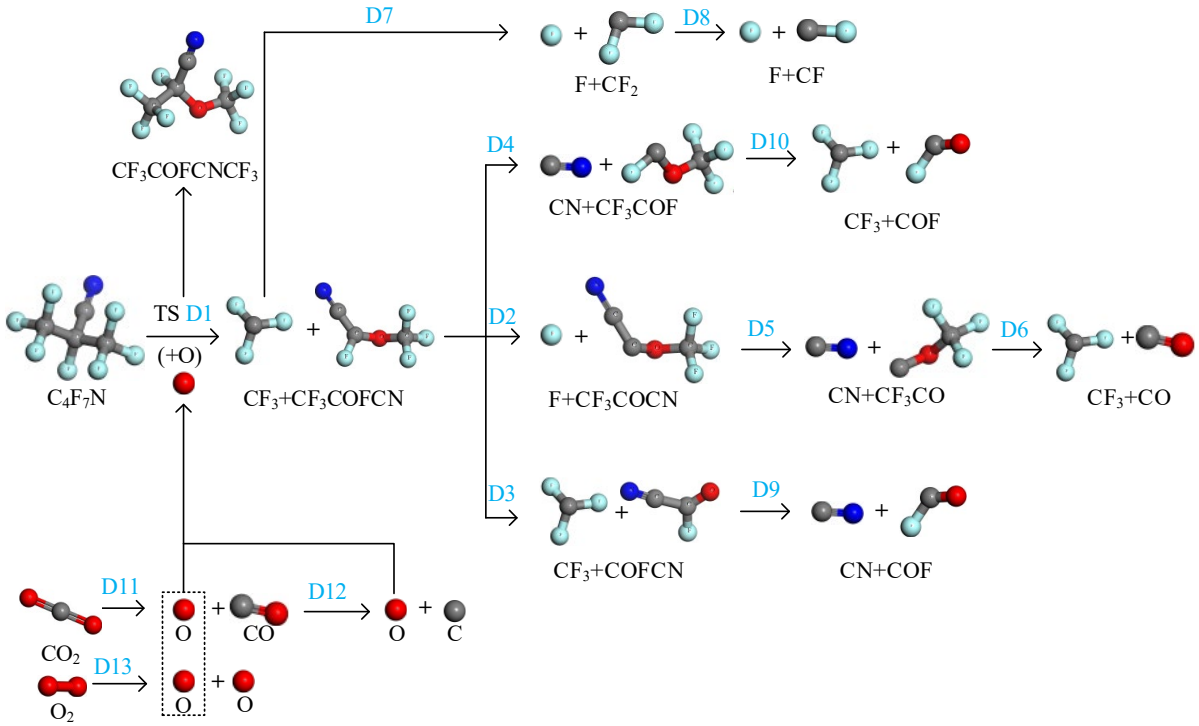

Figure 4.10 C_4F_7N dissociation pathway under O-particle reaction

According to the results of the reaction molecular dynamics simulation in section 2.2, the decomposition process of C_4F_7N under the condition of O_2 participation in the reaction becomes more complicated, especially the initial dissociation process is not a simple one-time dissociation process, but needs to go through a transition state. Firstly, O_2 may react with C_4F_7N in the form of O particles, and the formation process and enthalpy of O particles are

given in Figure 4.11, which shows that O particles originate from the dissociation of CO_2 and O_2 in the gas mixture, and the dissociation of CO_2 to generate O particles requires the absorption of 153.07kcal/mol of energy, which is more likely to occur compared to the dissociation of O_2 to generate O particles (requiring the absorption of 182.29kcal/mol energy), but there will not be a large difference, both are the main source of O particle generation. However, the further generation of C and O particles from CO requires the absorption of 514.60kcal/mol of energy, which only occurs when the external field strength and temperature are high.

Table 4.3 Enthalpies and activation energies of the main dissociation pathways of C_4F_7N under reaction conditions involving O

No.	Reaction path	$\Delta_r H$ (kcal/mol)	ΔH (kcal/mol)
D1	$C_4F_7N+O \rightarrow CF_3+CF_3COFCN$	-106.52	47.51
D2	$CF_3COFCN \rightarrow CF_3COCN+F$	57.17	
D3	$CF_3COFCN \rightarrow CF_3+COFCN$	7.97	-
D4	$CF_3COFCN \rightarrow CF_3COF+CN$	20.54	-
D5	$CF_3COCN \rightarrow CF_3CO+CN$	211.86	
D6	$CF_3CO \rightarrow CF_3+CO$	-41.36	
D7	$CF_3 \rightarrow CF_2+F$	92.96	
D8	$CF_2 \rightarrow CF+F$	131.27	
D9	$COFCN \rightarrow COF+CN$	134.38	-
D10	$CF_3COF \rightarrow CF_3+COF$	85.28	-
D11	$CO_2 \rightarrow CO+O$	153.07	
D12	$CO \rightarrow C+O$	514.60	
D13	$O_2 \rightarrow O+O$	182.29	

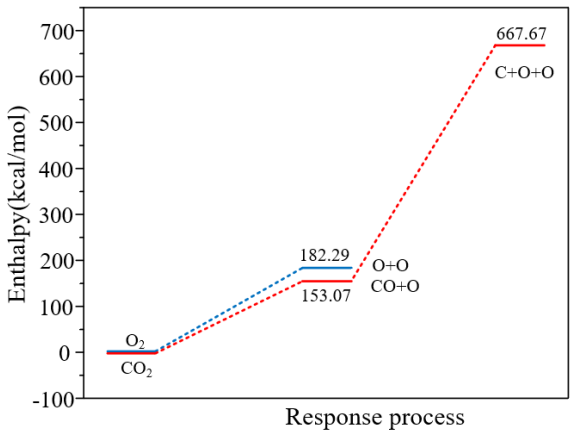

Figure 4.11 Main processes of O particle generation and their enthalpies

Path 1 in Table 4.3 gives the initial dissociation process of C_4F_7N under the condition that O particles are involved in the reaction, i.e., reacting with O particles to form CF_3 and CF_3COFCN particles, and this reaction needs to undergo the transition state structure of $CF_3COFCNCF_3$, with the enthalpy of the reaction of -106.52 kcal/mol, and the need to overcome the 47.51 kcal/mol energy barrier for this reaction to proceed properly. It has been shown that the dissociation of C_4F_7N molecules to form CF_3 and CF_3CFCN particles requires the absorption of 73.14 kcal/mol of energy[91]. The activation energy of pathway 1 is much lower than 73.14 kcal/mol (shown in Figure 4.12), suggesting that the involvement of O particles in the reaction makes the bond breaking process of C_4F_7N more likely to occur. Therefore, O_2 has a negative effect on the stability of C_4F_7N.

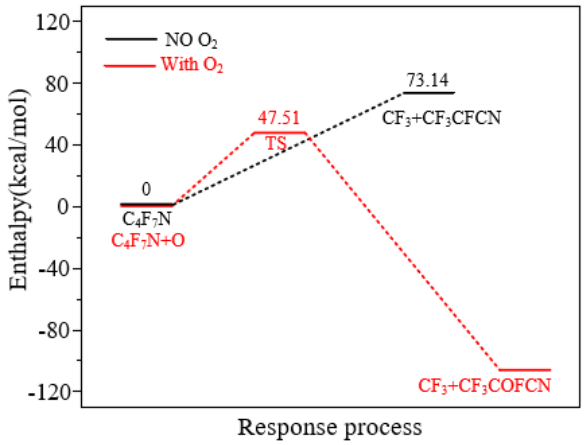

Figure 4.12 Dissociation process and energy change of C_4F_7N under reaction conditions with and without O_2 participation

The CF_3 and CF_3COFCN particles dissociate further and the three primary dissociation paths (D2, D3 and D4) for CF_3COFCN are given in Table 4.3 and the enthalpies of the dissociation paths are given in Figure 4.13. The C=O bond breaking in CF_3COFCN in path D3 to form CF_3 and COFCN requires an energy absorption of 7.97 kcal/mol, which is the lowest among these three paths, indicating that the C=O bond formed between the O atom in the center of the CF_3COFCN molecule and the CF_3 group has the lowest bond energy (shown in D3 in Table 4.3), whereas the CF_3COFCN molecule undergoes the dissociation through path D2 as The energy to be absorbed by the CF_3COCN and F particles is the highest among the three primary dissociation paths (57.17 kcal/mol).

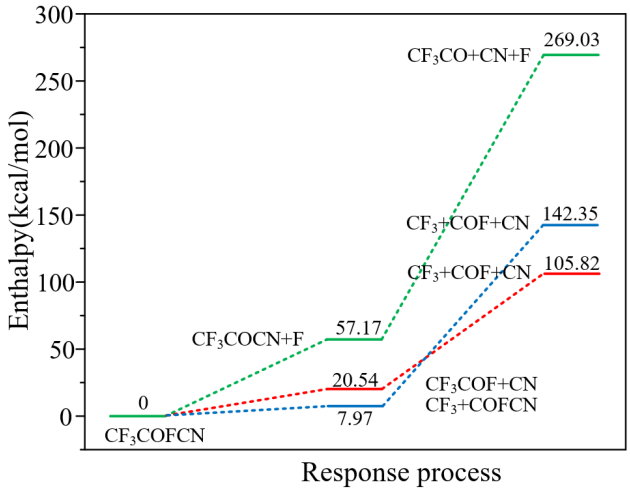

Figure 4.13 Main dissociation processes of CF_3COFCN and their enthalpies

The particles such as CF_3COCN, CF_3COF and COFCN generated by the primary dissociation of CF_3COFCN molecules are still macromolecules, which will be further dissociated under the discharge fault, and the further dissociation paths and enthalpies are also given in Fig. 4.13, which shows that a higher energy is required to further dissociate the CF_3COCN molecules to generate the CF_3CO and CN particles (211.86 kcal/ mol), indicating the high stability of the C-C bond connecting the C atom to the CN group in the CF_3COCN molecule. However, further dissociation of CF_3CO to form CF_3 and CO particles can occur spontaneously and releases 41.36 kcal/mol of energy (shown in Fig. 4.14); the breakage of C=O in the CF_3CO molecule to form CF_3C and O particles is more difficult to occur and requires the absorption of 209.4741.36 kcal/mol of energy. Therefore CF_3COFCN is more likely to break down to form particles such as CF_3, CF and CN under sustained energy, which is in good agreement with the evolutionary pattern of the particles in the results of the molecular dynamics simulations in Section 2.2.

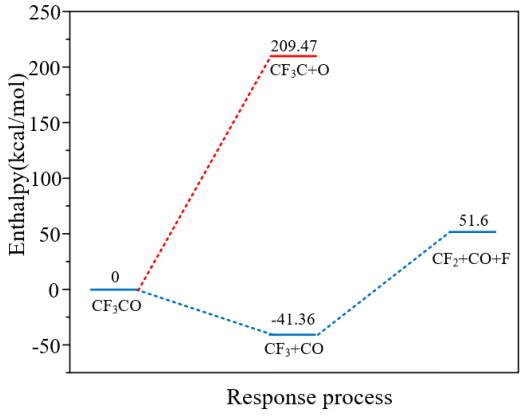

Figure 4.14 Main dissociation processes and their enthalpies for CF_3CO

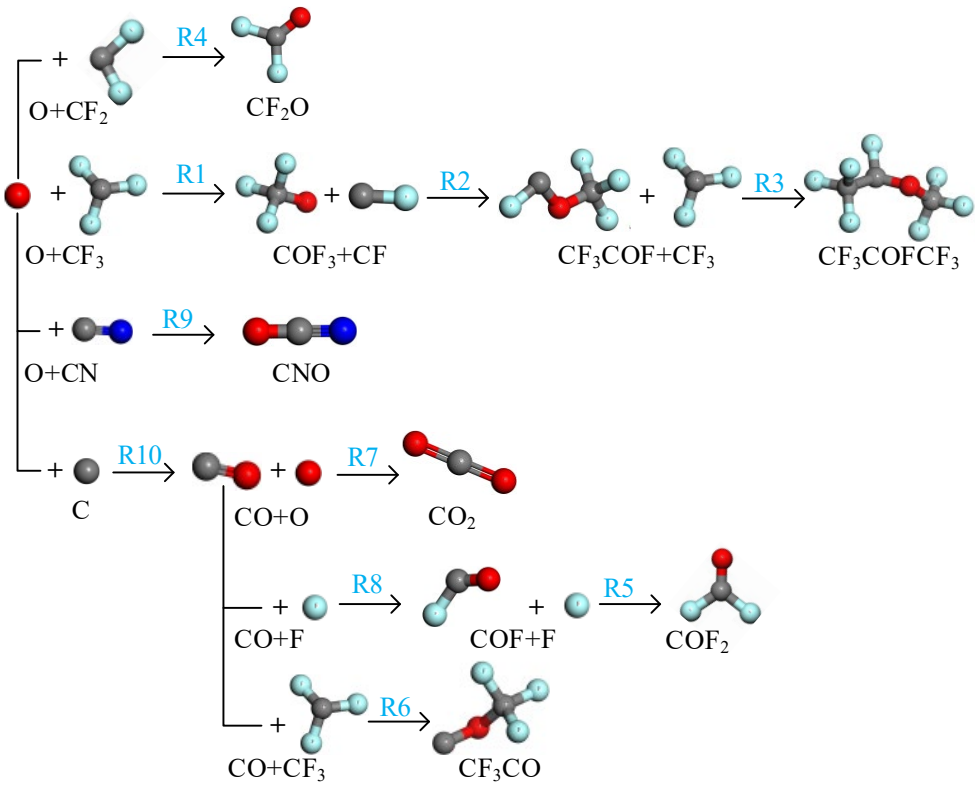

Figure 4.15 Generation pathways of O-containing products

The possible formation pathways of the main O-containing products are given in Figure 4.16 (the molecules involved in the pathways are optimized configurations), and the enthalpies for the different pathways are shown in Table 4.4. It can be seen that the formation of all O-containing products is an exothermic reaction that can proceed spontaneously (negative enthalpy), which may prevent the particles generated by the decomposition of C_4F_7N from recombining to form C_4F_7N or other stable by-products. The process of CO generation from C and O in pathway R10 releases the most energy (-236.4 kcal/mol), which explains why the addition of O_2 can inhibit the production of carbon monomers from C_4F_7N during the discharge process.

Table 4.4 Major O-containing product generation pathways and their enthalpies

No.	Reaction path	$\Delta_r H$ (kcal/mol)	ΔH (kcal/mol)
R1	$CF_3+O\rightarrow COF_3$	-104.05	-
R2	$COF_3+CF\rightarrow C_2F_4O$	-72.59	-
R3	$C_2F_4O+CF_3\rightarrow C_3F_7O$	-161.13	-
R4	$CF_2+O\rightarrow COF_2$	-108.72	-
R5	$COF+F\rightarrow COF_2$	-120.89	-
R6	$CF_3+CO\rightarrow CF_3CO$	-41.36	-
R7	$CO+O\rightarrow CO_2$	-141.99	-

R8	CO+F→COF	-85.33	-
R9	CN+O→CNO	-177.12	-
R10	C+O→CO	-236.4	-

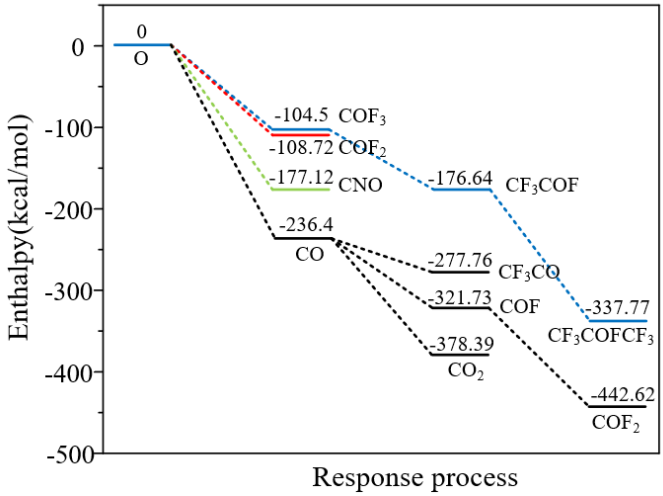

Figure 4.16 Generation processes of major O-containing products and their enthalpies

In summary, the energy released under the discharge fault condition will lead to the simultaneous decomposition of C_4F_7N and O_2 in the gas mixture, generating particles such as CF_3, C_3F_7, CN, CF_2, CF, F, CF_3CF, and O, which interact with each other to generate gaseous byproducts. The addition of O_2 will complicate the dissociation process of C_4F_7N, and the dissociation process of molecules generated by combining C_4F_7N and O is easier to occur compared to the one-time dissociation process of C_4F_7N molecules, indicating that the addition of O_2 will affect the formation process of C_4F_7N decomposition byproducts. The dissociation process of the molecules generated by the combination of C_4F_7N and O is easier than that of the C_4F_7N molecules, which indicates that the addition of O_2 will have an effect on the formation process of C_4F_7N decomposition by-products, and the spontaneous reaction between the O particles and the decomposed particles of C_4F_7N inhibits the generation of some by-products to a certain extent. Therefore, a certain content of O_2 addition can reduce the generation of C_4F_7N decomposition by-products, but the spontaneous reaction between O particles and decomposition particles (e.g., fluorocarbons) generates COF_2 (strong toxicity), so that the generation of part of by-products shows an increasing trend when the amount of O_2 addition is higher.

4.6 Summary of the chapter

In this chapter, based on the constructed gas insulating medium frequency breakdown and decomposition test platform, we carry out the experimental study on the frequency breakdown and decomposition characteristics of C_4F_7N-CO_2-O_2 gas mixture, analyze the

influence mechanism of O_2 content on the insulating and decomposition characteristics of the gas mixture, and through the construction of the reaction paths and based on the results of the DFT and TST calculations, we reveal the discharged decomposition and O-containing product generation mechanism of C_4F_7N under the conditions of the reaction with the participation of O_2 product generation mechanism under the conditions of O_2 participation. The main conclusions are as follows:

(1) The addition of O_2 can improve the insulation strength of C_4F_7N-CO_2 gas mixture. The industrial frequency breakdown voltages of C_4F_7N-CO_2-O_2 gas mixtures containing 2%, 4%, 6%, 8%, and 10% O_2 were increased by 4.85%, 6.49%, 7.70%, 3.21%, and 2.74%, respectively, as compared with C_4F_7N-CO_2, and the addition of 2%-6% O_2 to the gas mixtures can reduce the dispersion of the breakdown voltage.

(2) The C_4F_7N-CO_2-O_2 gas mixture mainly produces CF_4, CO, C_2F_6, C_3F_6, C_3F_8, CF_3CN, C_2F_5CN, $(CN)_2$, and COF_2 in the frequency breakdown decomposition of C_4F_7N-CO_2 gas mixture, and the addition of 2-6% O_2 to the gas mixture of C_4F_7N-CO_2 effectively reduces the amount of most of the by-products produced.

(3) The generation of CO, C_3F_6, CF_3CN, C_2F_5CN, and $(CN)_2$ remained stable or showed little tendency to increase with the addition of 2%-6% O_2 to the C_4F_7N-CO_2 gas mixture. The rate of generation of these by-products increased when the O_2 content was higher than 6%, indicating that higher O_2 additions negatively affected the stability of the C_4F_7N gas mixture under discharge conditions.

(4) The addition of O_2 will complicate the dissociation process of C_4F_7N, which occurs more readily with the combination of C_4F_7N and O compared to the direct dissociation process of the C_4F_7N molecule, with an enthalpy of reaction of -106.52 kcal/mol and an energy of activation of 47.51 kcal/mol. most of the reactions between the O particles and the decomposed particles of C_4F_7N belong to the category of reactions that can be spontaneous exothermic process, which may hinder the recombination of particles generated from C_4F_7N decomposition to form C_4F_7N or other stable by-products. Calculations show that the addition of O_2 affects the discharge decomposition of C_4F_7N gas mixtures and the formation of by-products.

Chapter 5 Feasibility assessment of C_4F_7N-CO_2-O_2 applications considering decomposition and biosafety

The addition of O_2 as the second buffer gas to the C_4F_7N-CO_2 gas mixture can enhance the insulation strength and improve the chemical stability of the gas mixture, but the addition of excessive O_2 will also bring about certain negative effects, so the optimal amount of O_2 added is the key technical indicators of the C_4F_7N-CO_2-O_2 gas mixture in the practical application of the engineering. C_4F_7N-CO_2-O_2 gas mixture in different faults (POF, PD and breakdown) decomposition products of the type and generation of different influencing factors with the change rule of the law can also be reflected to a certain extent the equipment operating state information, can be extracted based on the decomposition characteristics can be characterized by the type of faults within the equipment and its severity of the characteristics of the component. In addition, the gas mixture will generate some toxic and corrosive by-products under fault conditions, which will pose a threat to the safety of equipment operators and maintenance personnel, so it is necessary to evaluate the biosafety of C_4F_7N and its decomposition products before large-scale popularization and application.

In this chapter, by summarizing the influence of different O_2 contents on the decomposition characteristics of C_4F_7N-CO_2-O_2 gas mixture under insulation and electrical and thermal faults, the optimal O_2 additions of C_4F_7N-CO_2-O_2 gas mixture for medium-voltage gas-insulated equipments are proposed. On the basis of the decomposition characteristics, the characteristic quantities that can characterize the types of faults and their severity within the equipment are extracted, which provide a reference for the fault diagnosis method of C_4F_7N-CO_2-O_2 gas mixture equipment. Finally, the biosafety of C_4F_7N and its arc decomposition products was investigated by acute inhalation toxicity test in mice, and based on the relevant conclusions, the feasibility of applying the C_4F_7N-CO_2-O_2 gas mixture in equipment was comprehensively evaluated, and recommendations for safe application were given.

5.1 Optimal C_4F_7N-CO_2-O_2 ratio and characteristic components for equipment fault diagnosis

5.1.1 Optimal ratio of C_4F_7N-CO_2-O_2 for medium pressure equipment

Figure 5.1 shows the stainless steel heating element after a 12-hour localized superheat failure decomposition test under different test conditions. It can be seen that the surface of the heating rod after 12-hour overheating test in C_4F_7N-CO_2 gas mixture without O_2 at 450°C has been completely carbonized (shown in Fig. 5.1(d)), and the carbon on the surface of the

heating rod may originate from two aspects, on the one hand, it may be due to the fact that C_4F_7N belongs to fluorocarbon-based gases, which contain the element of carbon in the molecular structure, and under high temperature, the bond-breaking reaction with the metal heating element will produce C monomers, on the other hand, it may be due to the POF physical defects model stainless steel materials also contain C elements, generated under the action of high temperature in the activated state of C. O_2 content of 6% of the C_4F_7N-CO_2-O_2 gas mixture in the heating rod at 450 ℃ after 12 hours of superheat test surface can also show a certain metallic luster (Figure 5.1 (c) shown), which may be This may be due to the fact that O_2 reacts with the C precipitated on the surface of the metal heating rod to generate CO_2 and thus inhibit carbon deposition. The test results show that under the action of POF, the addition of a certain amount of O_2 can inhibit the precipitation of carbon inside the C_4F_7N-CO_2 gas mixture insulated electrical equipment, thus ensuring the safe operation of the equipment.

At 550°C, the heating rod in the C_4F_7N-CO_2-O_2 gas mixture with 10% O_2 content was severely corroded after 12 hours of overheating experiments (shown in Fig. 5.1(f)), which may be due to the oxidation of the surface of the heating rod exacerbated by the excessively high O_2 content and temperature, indicating that excessively high O_2 additions and severe localized overheating faults will lead to the gas-insulated electrical equipment internal Metal components are seriously corroded, so the C_4F_7N-CO_2 mixture of gas-insulated electrical equipment should not be too high O_2 addition, the specific O_2 addition needs to be combined with the insulating gas mixture and the decomposition characteristics of the fault to be further analyzed.

Figure 5.1 Stainless steel heating elements under different test conditions

The results of the thermal decomposition test of the C_4F_7N-CO_2-O_2 gas mixture show that the addition of a certain content of O_2 to the C_4F_7N-CO_2 gas mixture will have a relatively large effect on the thermal stability of the mixture. When 2% O_2 is added to the C_4F_7N-CO_2 gas mixture, the amount of CF_4, C_3F_8, CO, COF_2, CF_3CN, C_2F_5CN and C_2N_2 products

generated by thermal decomposition of the gas mixture at 450 ℃ decreases to varying degrees, and when the amount of O_2 is added more than 2%, the amount of all other products increases, and the amount of CF_4, C_3F_6, C_3F_6 and C_2N_2 products increases, and the amount of CF_4, C_3F_6 and C_2N_2 products increases. increased, and the yields of CF_4, C_3F_8, CO, and COF_2 increased sharply at O_2 contents greater than 8%, indicating that excess O_2 exacerbates the decomposition of the C_4F_7N-CO_2-O_2 mixture under superheated faults. Table 5.1 gives the relevant properties of C_4F_7N and its by-products, and it can be seen from the LC50 that C_2N_2, CF_3CN and COF_2 are several decomposition gases with strong toxicity, and their large amount of generation should be avoided during the operation of the actual equipment. In the superheated decomposition test, the generation of C_2N_2 gradually decreases with the increase of O_2 content; CF_3CN generation continues to increase in the O_2 content of 2%-10%, but in the 2%-6% growth is small, and in the O_2 addition of 10% its generation is still smaller than the case of no O_2; COF_2 in the O_2 content of 4%-8% growth is small, and the O_2 content of more than 8%, the O_2 content begins to increase sharply. starts to increase sharply.

The results of ReaxFF-MD simulation of the thermal decomposition process of C_4F_7N-CO_2-O_2 gas mixture show that the addition of O_2 to the C_4F_7N-CO_2 gas mixture can effectively reduce the decomposition amount of C_4F_7N and the generation of most of the decomposed particles, especially in the case of the O_2 content of 6%, the decomposition of C_4F_7N is the least. Based on the simulation and test results of thermal decomposition of C_4F_7N-CO_2-O_2 gas mixture, and taking into account the decomposition of C_4F_7N and the generation of products under different O_2 content, as well as the effect of O_2 content on the morphology of metal components inside the device under high temperature conditions, the O_2 addition of C_4F_7N-CO_2 gas mixture of 2%-8% is more appropriate. However, this range of O_2 addition is too broad, and it is difficult to provide specific and effective suggestions for the selection of C_4F_7N-CO_2-O_2 gas mixture ratio in practical engineering applications. Therefore, in order to obtain more specific O_2 additions, the insulation and discharge decomposition characteristics of C_4F_7N-CO_2-O_2 gas mixtures with different O_2 contents need to be further investigated.

The results of the experimental studies on PD and its decomposition characteristics show that the PD characteristics of the C_4F_7N-CO_2-O_2 gas mixture are greatly affected by the amount of O_2 added, and its PD decomposition is mainly caused by the cumulative effect of PD, and there is a strong correlation between the decomposition characteristics of the mixture and its PD eigenquantities. After the addition of a certain content of O_2 to the C_4F_7N-CO_2 gas mixture, the average discharge decreases, especially the average PD discharge of the gas mixture with 4% O_2 addition decreases by 41% compared with that without O_2, and the average discharge

starts to increase when the O_2 content is greater than 4%. The C_4F_7N-CO_2-O_2 gas mixture decomposes under the action of PD to generate CF_3, CF_2, F, CN and O. The recombination of these radicals can produce perfluoroalkane gases (CF_4, C_2F_6, C_3F_8, and C_3F_6), nitrile gases (C_2N_2, CF_3CN, and C_2F_5CN), and oxides (CO, COF_2, and $C_2F_6O_3$), and the content of the by-products, except for COF_2, shows a decreasing tendency to varying degrees after the addition of 2%-4% O_2 and reached the lowest at 4% O_2. When the O_2 content is greater than 6%, the gas mixture PD number of discharges per second, cumulative discharges per second and the average discharge have a tendency to increase sharply, which will lead to the gas mixture decomposition of intense and thus generate a large number of free radicals, especially CFx and F and other free radicals, so that most of the by-products generated under the condition of the O_2 content of more than 6% increased, in order to avoid the gas mixture discharge and decomposition of the generation of large numbers of In order to avoid severe insulation degradation caused by by-products, the O_2 addition in the gas mixture should not exceed 6%. Considering the PD and its decomposition characteristics, the optimal O_2 addition of C_4F_7N-CO_2-O_2 gas mixture is 4%-6%.

Table 5.1 Properties associated with C_4F_7N and its by-products

Gas	LC_{50}(ppm)	Insulation strength relative to SF_6
C_4F_7N	10000-15000(rat,4h)	2.2
CF_4	20000(rat,4h)	0.4
C_2F_6	500000(rat,4h)	0.78
C_3F_8	90000(rat,4h)	0.97
C_3F_6	3060(rat,4h)	1.1
CO	1880(rat,4h)	0.4
COF_2	180(rat,4h)	-
CF_3CN	250(rat,4h)	1.46
C_2F_5CN	2730(rat,4h)	1.92
C_2N_2	175(rat,1h)	-

In addition, the addition of 2%-6% O_2 to the C_4F_7N-CO_2 gas mixture can effectively improve the insulation strength and reduce the dispersion of breakdown voltage, and the insulation strength is highest under the condition of 6% O_2. Meanwhile, the addition of 2%-6% O_2 can reduce the generation of breakdown decomposition products of the C_4F_7N-CO_2-O_2 gas mixture, and the addition of O_2 to the gas mixture should not be too high in consideration of the lower insulating properties of the decomposition products and the biosafety. From the

data given in Table 5.1, it can be seen that fluorocarbons (C_2F_6, C_3F_8) do not have a significant impact on personal safety and are asphyxiating gases. The LC50 of C_3F_6, C_2F_5CN is about 3000 ppm, followed by CO (1880 ppm). CF_3CN, $(CN)_2$ and COF_2 have lower LC50 values of 250 ppm, 175 ppm and 180 ppm, which are of strong acute toxicity. According to the results of the breakdown decomposition test, the addition of 2% O_2 can effectively reduce the generation of most of the by-products. The generation of CO, C_3F_6, CF_3CN, C_2F_5CN, and $(CN)_2$ remained stable or showed little tendency to increase at 2%-6% O_2 addition. For mixtures with O_2 content higher than 6%, the rate of generation of these by-products increased, indicating that higher O_2 content negatively affects the stability of C_4F_7N mixtures. Therefore, it is suggested that the addition of 2%-6% O_2 to the C_4F_7N-CO_2 gas mixture can improve the insulation strength while effectively inhibiting the decomposition of C_4F_7N and the generation of by-products.

Based on the simulation and experimental results of the effect of O_2 on the insulation and decomposition characteristics of the C_4F_7N-CO_2-O_2 gas mixture under different fault conditions (POF, PD, and frequency breakdown), and taking into account the safety of the personnel in the operation and maintenance of the decomposition equipment, the optimal amount of O_2 to be added to the gas mixture is 4%-6%. The gas mixture may cause insulation degradation and decomposition aggravation, and may also lead to serious corrosion of the internal metal components of the equipment in the case of severe localized overheating faults. To meet the minimum ambient operating temperature of -25 ℃ and have the same insulating properties with SF_6 under the premise of gas insulating medium for medium-voltage gas-insulated equipment, the content of C_4F_7N in the gas insulation medium is 15%, the optimal amount of O_2 added to 4%-6%, the main background gas CO_2 content of 79%-81%, the optimal ratio of the actual engineering applications of the C_4F_7N-CO_2-O_2 mixture of gases used in medium-voltage equipment can be used as a reference.。

5.1.2 C_4F_7N-CO_2-O_2 equipment troubleshooting characterization decomposition components

The correlation characteristics between the composition and content of decomposition products of gas insulating medium under different faults and various influencing factors can be used to identify the type and severity of faults within the equipment. In this paper, the types and contents of possible characteristic decomposition products under the three fault conditions of PD, POF and frequency breakdown are analyzed along with the change rules of different influencing factors, and the characteristic decomposition components that can identify the types of equipment fault conditions and their severity are extracted, which can provide

important references for the fault diagnosis and operation and maintenance strategies of the equipment in operation.

According to the results of the previous study, the main products of POF breakdown of C_4F_7N-CO_2-O_2 gas mixture are CF_4, C_3F_8, C_3F_6, CO, COF_2, CF_3CN, C_2F_5CN and C_2N_2; the main products of the PD breakdown test are CF_4, C_2F_6, C_3F_8, C_3F_6, CO, COF_2, $C_2F_6O_3$, CF_3CN, C_2F_5CN and C_2N_2; the main products of the IF breakdown test are CF_4, C_2F_6, C_3F_8, C_3F_6, CO, COF_2, CF_3CN, C_2F_5CN and C_2N_2, and it can be found that C_2F_6 can only be generated under the discharge faults, so that C_2F_6 can be used as a marker generator characterizing the discharge faults, and $C_2F_6O_3$ is only generated in the PD fault environment. So it can be used as a marker generator to characterize PD faults.

Among several quantitatively analyzed products, the maximum amount of C_3F_6 generated under IF breakdown, PD and POF fault conditions were 8.05 ppm, 7.5 ppm and 49.09 ppm, respectively, and it can be found that the amount of C_3F_6 generated under the discharging fault was much smaller than that under the superheating fault, which is due to the fact that C_3F_6 is mainly generated from the interfacial reaction between C_4F_7N and metal under high temperature conditions. When the detected C_3F_6 content is less than 10ppm, it can be judged as discharge fault, and when it is much higher than 10ppm, it can be judged as overheating fault. The minimum generation of CF_4 in the process of frequency breakdown decomposition under different conditions is 500ppm, which is much larger than the maximum generation of PD (37ppm) and POF (21.84ppm) conditions, and the generation of CF_4 is greater than 100ppm when it is detected in the equipment fault. If CF_4 generation is detected to be greater than 100ppm at the time of equipment failure, it can basically be determined that the fault state is spark discharge or arc discharge.

In the PD decomposition test of C_4F_7N-CO_2-O_2 gas mixture at different applied voltages (21 kV, 24 kV and 27 kV), it can be found that the generation of CF_4 increases linearly with the increase of PD time and applied voltage, which can be used as a characteristic product to characterize the severity of the PD fault. In the C_4F_7N-CO_2-O_2 gas mixture localized superheat fault decomposition test, the effective gas production rates of COF_2 and C_2N_2 are positively correlated with the temperature and basically increase linearly with the temperature. Therefore, COF_2 and C_2N_2 can largely characterize the degradation degree of C_4F_7N-CO_2-O_2 gas mixture under the action of POF, and can be used as the characteristic products reflecting the severity of local overheating faults, and their generation amount or generation rate can directly portray the severity of local overheating faults, so in the practical engineering application, the generation amount and generation rate of these two decomposition characteristic gases can be

quantitatively compared to the degree of overheating faults in gas insulation equipment for monitoring and diagnosing overheating faults. Therefore, in practical engineering applications, the quantitative comparison between the generation rate of these two decomposition characteristic gases and the degree of overheating faults in gas insulating equipment can be used to monitor and diagnose the overheating faults of C_4F_7N-CO_2-O_2 mixed gas insulating equipment and to improve the safe operation of gas insulating equipment. The generation and effective gas production rate of C_2F_5CN show a small temperature-dependent trend at 400°C-500°C, and increase sharply above 500°C. Therefore, C_2F_5CN can be used as a signature decomposition product of the jump in the nature of POF faults, which must be highly emphasized when performing troubleshooting.

5.2 Biosafety of pure C_4F_7N gas

5.2.1 Test platforms and methods

In this paper, the toxicity test platform of C_4F_7N and its decomposed gas shown in Fig. 5.2 was built, and the intelligent dynamic gas dispenser (Tanggao Electric GC400) was used to dispense the test gases of different concentrations, which is based on the principle of mass flow mixing method, and it can mix and dilute the high-concentration standard gases into low-concentration sample gases, and at the same time, the dispensed gases can be outputted with the set flow rate; the length, width, and height of the dyeing chamber are 40cm, 30cm, and 20cm, respectively, and are composed of polytetrafluoroethylene boards of 1cm in thickness. The length, width and height of the chamber are 40cm, 30cm and 20cm respectively, and it is composed of PTFE plate with a thickness of 1cm. There are three holes on both sides of the chamber for gas inlet, water inlet and gas outlet, an observation window on one side for accessing and placing test animals, and a gas recovery device connected to the outlet.

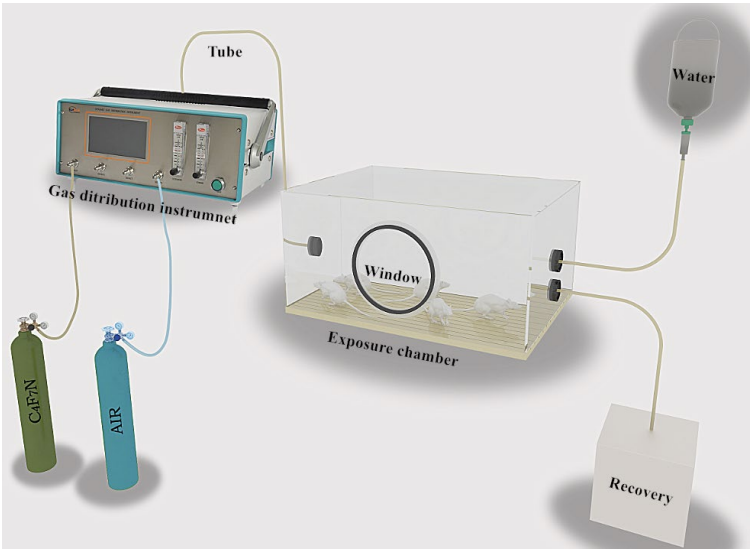

Figure 5.2 Eco-insulation gas inhalation toxicity test platform

The 4-h acute inhalation toxicity test of mice exposed to C_4F_7N gas was carried out with reference to the standards of "Biological Test Methods for Toxicity of Sulphur Hexafluoride Gas" (DL/T 921-2005) and the "Globally Harmonized System of Classification and Labeling of Chemicals" (GHS)[120, 121], and the mice were transferred to the feeding environment for 14 days after the end of the exposure. At the end of the exposure, the mice were transferred to a rearing environment for 14 days, and the changes in vital signs of the mice were observed and recorded throughout the whole process. The dying mice and mice surviving after 14 days were treated in a humanitarian way, and blood and tissue samples of major organs were collected for hematological and pathological analyses. The mice were provided by Hubei Animal Testing Center, and were about 8 weeks old, weighing 18~22 g. The experiments and analyses were conducted under the guidance of the Medical Science Research Center of Zhongnan Hospital of Wuhan University.

In practical engineering applications C_4F_7N is usually mixed with CO_2, O_2 and other background gases, CO_2 itself is non-toxic, but high concentrations of CO_2 have an asphyxiating effect, so in this paper, a certain concentration of C_4F_7N was mixed with dry air (21% O_2 + 79% N_2) to study the acute inhalation toxicity of C_4F_7N gas. In order to accurately calculate the LC50 of C_4F_7N, it is necessary to test the mortality rate of animals at each test concentration at equal logarithmic spacing, and the calculation must have the various test concentrations that make the test animals survive more than half and less than half[122], and it was found that the mortality rate of mice at 1585 ppm concentration was 100%, and that the mortality rate of mice at 1000 ppm concentration was 0% through several tests, so the The test C_4F_7N gas concentration range was selected as 1000-1585 ppm, and there were six test groups (1000 ppm, 1096 ppm, 1202 ppm, 1318 ppm, 1445 ppm, and 1585 ppm) and one control group (dry air), and each group of tests was carried out using both male and female mice in order to determine the sex difference, and the exposure time was 4h.

5.2.2 C_4F_7N biosafety test results

5.2.2.1 Key symptoms in contaminated mice

At a concentration of 1585 ppm C_4F_7N, all mice were able to move calmly in the chamber before dosing; 5 minutes after the start of the dosing, 5 mice changed from calm to excited, which was manifested by climbing on the wall of the chamber in an attempt to break free from the confined space, indicating that the mice began to feel uncomfortable after 5 minutes of the dosing; after 2 hours of the dosing, the 5 mice basically stopped their activities, huddled in the

corner of the chamber, and showed symptoms that their eyes were slightly shuttered. After 2 hours of exposure, five mice basically stopped moving, curled up in the corner of the chamber, and showed the symptom of eyes slightly closed. At the end of the 4-h exposure period, all mice in the test group were able to move and eat a small amount of food due to starvation (no food for 4 h of exposure) when they were transferred to the rearing environment.

Observations on the first day after transferring to the rearing environment revealed that mice in all experimental groups stopped moving and eating, huddled together, and were accompanied by body convulsions and rapid heartbeats, which could be attributed to the fact that the C_4F_7N gas would cause damage to the locomotor and respiratory systems of the mice. In the experimental groups with C_4F_7N concentration greater than 1000 ppm, 1-2 male mice showed slight constipation, which may be due to the damage of C_4F_7N gas to the digestive system of the mice; observed on the 2nd day after contamination, all the mice started to show the symptoms of stooping, erect hair, and slightly closed eyes, and the male mice in the groups with C_4F_7N concentration greater than 1000 ppm showed yellow liquid infiltration around the eyes, indicating that C_4F_7N gas may cause some irritation to the eyes of the mice. The male mice in the experimental group with C_4F_7N concentration greater than 1000 ppm had yellow liquid infiltration around their eyes, indicating that C_4F_7N gas caused some eye irritation to the mice. On the 3rd day after poisoning, 1-2 male mice in all experimental groups showed swelling of the genital organs, which indicates that C_4F_7N gas may cause some effects on the urogenital system of mice. The above symptoms are the general manifestations of poisoning in mice, and it is inferred that the different concentrations of C_4F_7N gas in all experimental groups have certain toxic effects on mice based on the symptoms observed during the dyeing process and feeding process.

5.2.2.2 Body weight changes and LC50 in mice

The change in body weight of mice is an important indicator of whether C_4F_7N gas is toxic and the duration of the toxic effects induced. Figure 5.3 gives the changes in the average body weight of four groups of mice (control, 1585 ppm, 1202 ppm, and 1000 ppm) after being transferred to the rearing environment. It can be seen that the average body weight of mice decreased to a certain extent after contamination (mice at the concentration of 1585 ppm all died on the 6th day after contamination), which indicates that all concentrations of C_4F_7N gas in the test groups exerted a certain degree of toxicity effect on mice. The weight of mice continued to decrease by about 30% from 1 to 3 days after exposure to the gas, probably because the acute inhalation toxicity of C_4F_7N gas damaged the digestive system of the mice (clinically manifested as mild constipation), which led to a decrease in appetite, and thus the

body weight tended to decrease dramatically; the weight of mice that survived the exposure began to increase from 4 to 6 days, when the toxicity of the gas on the body of the mice weakened and their body functions began to recover and could be restored to their full potential. At this time, the toxicity damage to the body of the mice is weakened, and the mice begin to recover their body functions, and they are able to move around normally and eat a small amount of food, so the weight of the mice increases slowly in the period of 6-10 days (about 10% of the initial body weight); from the 10th day onwards, the vital signs of the mice have returned to normal, so the mice are able to eat completely, and the weight of the mice begins to increase rapidly at this time; within the 12-14 days, the weight of the mice is gradually restored to the normal level; at the end of the 14 days of observation, the body weight of both sexes of 1000 ppm mice and of the mice of 1000 ppm mice has gradually returned to normal. At the end of the 14-day observation period, the body weights of male and female mice at 1000 ppm exceeded the initial average body weight by 1-2 g, and the body weights of male and female mice at 1200 ppm reached 90% of the initial average body weight.

It can be seen that although the mice that survived 4 h after exposure to the gas in all experimental groups showed general symptoms of poisoning, the duration of the toxic effect was shortened due to the body's self-recovery ability, and the body functions gradually returned to normal; the higher the concentration of the gas, the longer the duration of the toxic effect, the slower the recovery of the mice's body functions, and the average body weight of the surviving mice in the males was faster than that of the females.

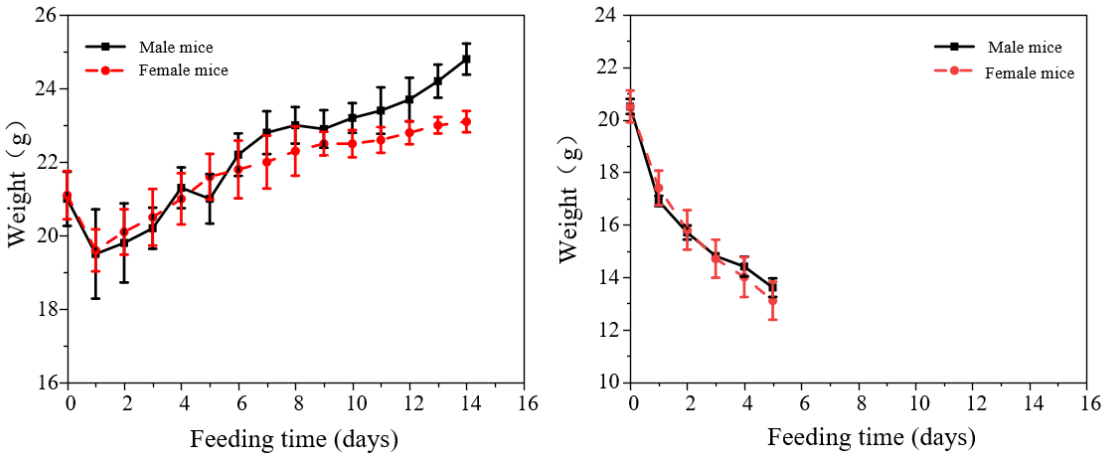

(a) Control subjects (100%Air)　　(b) Test group (1585ppmC_4F_7N/Air)

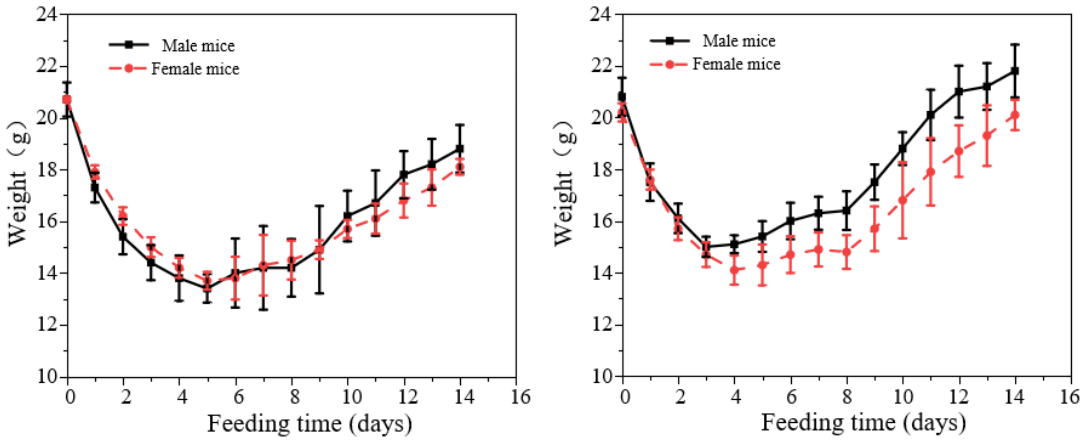

(c) Test group (1202ppmC_4F_7N/Air) (d) Test group (1000ppmC_4F_7N/Air)

Figure 5.3 Body weight changes in mice after inhalation of C_4F_7N gas

At 1585 ppm, the mortality rate of male mice was 40% and that of female mice was 20% on the third day, and 100% for both male and female mice on the sixth day; at 1202 ppm, there were no deaths on the third day, and the mortality rates were 40% (male) and 20% (female) on the fifth day, and 60% (male) and 40% (female) on the seventh day; at 1000 ppm, the mortality rates of both male and female mice were 60% (male) and 40% (female), respectively; and at 1000 ppm, the mortality rates of both male and female mice were 60% (male) and 40% (female), respectively. At 1000 ppm, the mortality rate of both male and female mice was 0. The above data showed that the higher the concentration of C_4F_7N gas, the shorter the survival time of mice, and the survival time of female mice was longer than that of male mice, and the mortality time of all mice was centered on the 3-7 days after contamination, and no further deaths occurred in mice that had survived for 1 week. After 1 week, there were no more deaths in mice that survived.

The calculation of LC50 is commonly done by linear interpolation, where the concentration gradient is set at equal logarithmic spacing, i.e., the LC50 values for different exposure times are derived based on the mortality rate of the test animals at various test concentrations at equal logarithmic spacing for different exposure times. Calculations must be made with various test concentrations that result in more than half and less than half of the test animals surviving[122]. As shown in Figure 5.4, the LC50 of 4h inhalation of C_4F_7N gas in mice can be found by plotting the test concentration of C_4F_7N and the mortality rate of mice in semi-logarithmic coordinates, and drawing a plumb line at 50% of the mortality rate to the concentration coordinates; male mice: 1175 ppm, female mice: 1380 ppm. from the calculation results, it can be seen that the 4h inhalation of C_4F_7N gas in female mice has an The LC50 of 4h inhalation of C_4F_7N gas in female mice was greater than that in male mice. Combined with the time to death of mice exposed to different concentrations of C_4F_7N gas, it can be inferred

that the tolerance of female mice to C_4F_7N gas is greater than that of male mice.

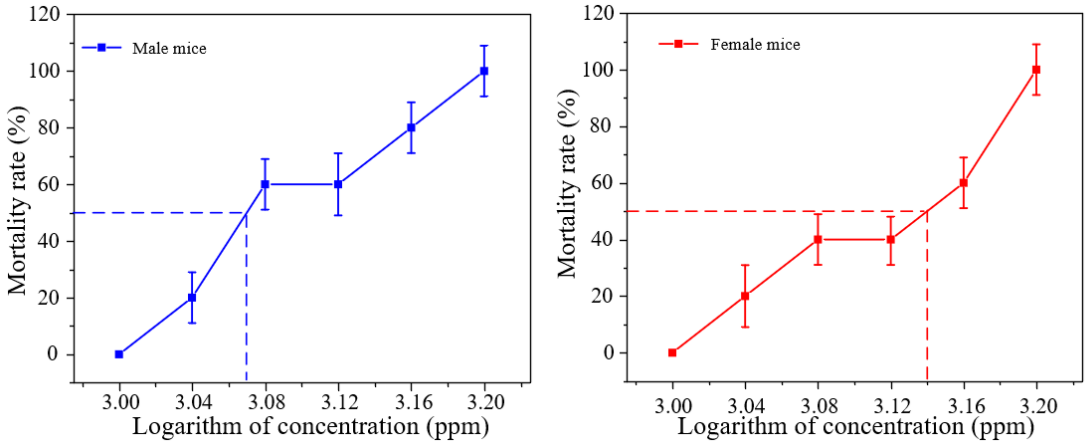

Figure 5.4 Relationship between mortality and logarithm of concentration after exposure of mice to pure C_4F_7N gas

5.2.2.3 Pathologic analysis of blood cells and tissues and organs in mice

Table 5.2 gives the results of the blood cell assays for the four mouse samples.No. 1 is a blood sample from a female mouse that died on day 6 at a concentration of 1202 ppm (the blood was collected when the mouse was in a dying state), No.2 is a blood sample from a female mouse that survived at a concentration of 1202 ppm (the collection was made after a 14-day observation period), and No. 3 is a blood sample from a female mouse that was collected at a concentration of 1000 ppm after a 14-day blood samples from female mice collected after the observation period.

From Table 5.2, it can be seen that the percentage of lymphocytes and the percentage of neutrophils in mice that died at the concentration of 1202 ppm decreased significantly, and both deviated from the reference value. The high percentage of neutrophils is commonly associated with acute inflammation, and the decrease in the percentage of lymphocytes is commonly associated with immunodeficiency diseases, indicating that the 4h acute inhalation of C_4F_7N gas leads to tissue and organ damage and inflammation in mice, which in turn leads to a decrease in the function of the mouse's immune system. Meanwhile, it can be seen that the mice that died at the concentration of 1202 ppm had high red blood cell and hemoglobin counts. Red blood cells are the main mediators for transporting oxygen through the blood in the animal's body, and hemoglobin is a special protein that transports oxygen within the red blood cells, and hemoglobin binds to the oxygen in the air, which enables the red blood cells to transport oxygen inhaled into the alveoli to the tissues through hemoglobin, so that the red blood cell and hemoglobin counts The high erythrocyte and hemoglobin counts may be due to the impaired cardiopulmonary function of the mice (clinically manifested as shortness of

breath in the mice) after exposure to the toxin, thus requiring more erythrocytes and hemoglobin to transport oxygen to various tissues and organs in the body.

Table 5.2 Hematocrit analysis of mice after exposure to C_4F_7N gas

No.	Lymphocytes Percentage(%)	Neutrophils Percentage (%)	Red blood cell(10^{12}/L)	Hemoglobin (g/l)
Control subjects	80.1	17.0	9.13	139
1	25.0	65.8	10.90	174
2	47.3	44.8	8.60	139
3	73.2	24.1	8.91	140
Reference point	55.8-90.6	8.6-38.9	6.36-9.42	110-143

At 1202 ppm, the blood test results of the surviving mice showed that the number of red blood cells and hemoglobin had returned to normal, indicating that the cardiopulmonary function of the mice had basically recovered 14 days after the poisoning, and the clinical manifestation was that the respiration and heartbeat of the mice had returned to normal, and the percentages of neutrophils and lymphocytes were close to the normal range but still deviated from the normal values, which indicated that the mice that had survived the acute inhalation of 1202 ppm C_4F_7N for 4 h had a small amount of inflammatory cells in their bodies and the immune system had not yet been fully recovered after 14 days of observation period.

The blood test results of mice observed for 14 days at a concentration of 1000 ppm showed that all the indexes of the mice's blood cells were within the normal range. After 4h acute inhalation of 1000 ppm C_4F_7N, the mice were transferred to the feeding environment for observation. Although the general symptoms of toxicity appeared in the first few days, the body's self-repair function repaired the damaged tissues, and all the body's vital activities and appearances returned to normal after the 14-day observation period, which indicated that the 4h acute inhalation of 1000 ppm C_4F_7N did not cause irreversible damage to the mice's organism. This indicates that 4h acute inhalation of 1000ppm C_4F_7N does not cause irreversible damage to mice.

Figure 5.5 gives the results of pathological sections of major tissues and organs of mice after exposure to C_4F_7N gas, in which column 1 is a tissue section of a mouse that died after exposure to 1202 ppm C_4F_7N, column 2 is a tissue section of a mouse that survived after exposure to 1202 ppm C_4F_7N, column 3 is a tissue section of a mouse that survived after exposure to 1202 ppm C_4F_7N, and a, b , c, d, and e represent the histological section images

of heart, liver, lung, intestine, and eye, respectively. It can be seen that the cardiomyocytes were closely arranged in the heart tissue sections of mice that died after 4 hours of poisoning at a concentration of 1202 ppm, with a small number of cardiomyocytes with loose cytoplasm and light staining (shown by black arrows in Fig. 5.5(a1)), and vasodilated blood vessels with bruising in the interstitium (shown by red arrows in Fig. 5.6(a1)), and localized epicardial connective tissue hyperplasia with a small amount of inflammatory cell infiltration (shown by yellow arrows in Fig. 5.5(a1)). yellow arrow). In the heart tissue sections of mice surviving at 1202ppm and 1000ppm after 14 days of observation, the cardiomyocytes were tightly arranged, clearly demarcated, with abundant cytoplasm and normal cell morphology, with no obvious abnormality (as shown in Figures 5.5(a2) and 5.5(a3)). The results of the slices show that 4 hours of poisoning at 1202 ppm will cause some damage to the heart tissue of mice, but after 14 days of recovery, the heart tissue is basically back to normal, and 4 hours of poisoning at 1000 ppm will hardly cause any damage to the heart tissue of mice.

From the liver tissue sections of mice dyed with poison, it can be seen that the structure of tissue lobules was intact, the hepatocytes were closely arranged, the cytoplasm of more hepatocytes was lax and lightly stained (shown by black arrows in Figs. 5.5(b1), 5.5(b2), 5.5(b3)), and a small number of hepatocytes had vacuolar degeneration, and small rounded vacuoles could be seen in the cytoplasm of the liver tissue sections of the mouse that had died after 4 hours of dyeing with the poison at the concentration of 1202ppm (Figure 5.5(b1) shown by red arrows), and bruising was seen in the veins (Figure 5.5(b1) shown by yellow arrows). The results of the sections showed that the liver tissue of the mice was damaged by 4 hours of poisoning at a concentration of 1202 ppm, but the liver tissue of the surviving mice had recovered to normal after 14 days of observation, and the liver tissue of the mice was hardly damaged by 4 hours of poisoning at a concentration of 1000 ppm.

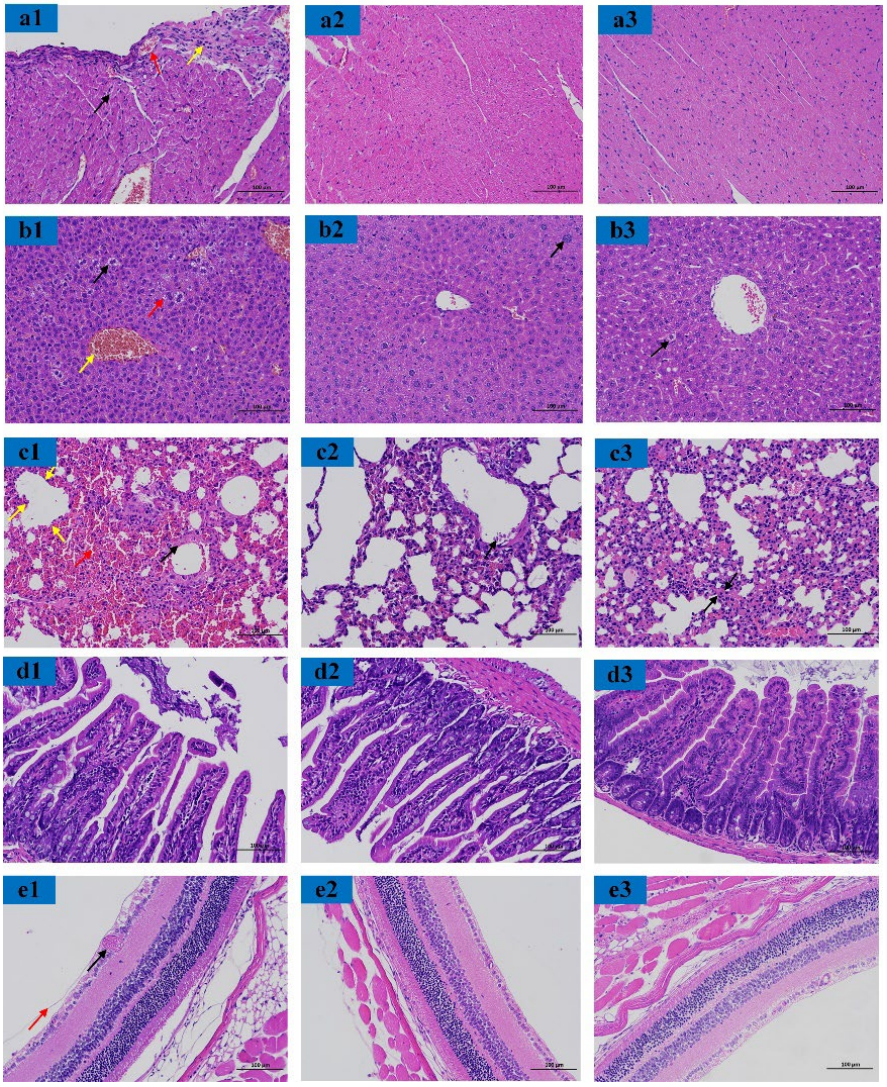

Figure 5.5 Pathological section results of major tissues and organs in mice

Necrosis of bronchial epithelial cells, fragmentation and lysis of nuclei, increased cytoplasmic eosinophilia (shown by black arrows in Fig. 5.5(c1)), local hemorrhage, and exudation of large numbers of erythrocytes from alveolar lumens (shown by red arrows in Fig. 5.5(c1)) were widely seen in the lung tissue sections of the mice that had died 4 hours after dyeing with the toxicity of the poison at a concentration of 1202 ppm, and the tissue was characterized by emphysema along the edges of the tissues, with the alveolar walls narrowing and fracturing, and the small alveolar lumens fusing into large cystic cavities (shown by yellow arrows in Fig. 5.5(c1)), necrosis and detachment of bronchial epithelial cells, fragmentation and lysis of nuclei, and enhanced cytoplasmic eosinophilicity were widely seen in the lung tissue tissues of the mice that survived the exposure to the 1202 ppm concentration (shown by black arrows in Fig. 5.5(c2)). The lung tissue of mice exposed to 1000 ppm for 4 h showed localized alveolar wall thickening after 14 days of recovery (shown by black arrows in Fig. 5.5(c3)). The results of the sections showed that 4 hours of exposure to 1202 ppm caused

serious damage to the lung tissues of mice, and the lung tissues of mice that survived the exposure to 1202 ppm did not fully recover to normal after 14 days of recovery, while the lung tissues of mice exposed to 1000 ppm for 4 hours recovered to normal after 14 days of recovery.

Figure 5.5(d) gives the intestinal tissue sections of the poisoned mice. It can be seen that all three samples have complete structure, regular arrangement of intestinal villi, abundant intestinal glands, tight arrangement and no obvious abnormality. The results of the sections show that the poisoning at 1202ppm and 1000ppm for 4 hours did not cause any damage to the intestinal tissues of the mice.

The eye tissues of mice that died 4 hours after dyeing at 1202 ppm had a clear structure of all layers of the cornea, normal cell morphology, a clear structure of all layers of the retina, and localized detachment of the inner border membrane (as shown by the red arrow in Fig. 5.5(e1)), and vascular bruises were seen in the optic nerve ganglion cell layer (as shown by the black arrows in Fig. 5.5(e1)).The mice that survived the 1202 ppm and 1,000 ppm concentration The eye tissue cornea was intact, the structure of each layer was clear, and the cellular morphology was normal, and the retina was structurally intact, with regular cellular arrangement and normal morphology. Sections showed that 4 hours of exposure to 1202 ppm caused some damage to the ocular tissues of the mice. 1202 ppm and 1000 ppm mice survived for 14 days, and the ocular tissues had recovered to normal.

Taken together, 4h acute inhalation of C_4F_7N gas caused severe damage to the lungs of mice, slight damage to the heart, liver and eyes, and almost no damage to the intestinal tract of mice. Body weight changes, blood cell analysis and histopathological sections of mice showed that the lung tissues and immune functions of mice surviving the exposure to 1202 ppm had not fully recovered to normal after 14 days of observation, while major organs, immune systems and body weights of mice surviving the exposure to 1000 ppm had recovered to normal after the 14-day observation period. This demonstrates that 4-hour acute inhalation of C_4F_7N at low concentrations does not cause irreversible damage to mice.

5.3 C_4F_7N mixed gas arc decomposition product biosafety

Although some decomposition products were detected in the previous electrical and thermal fault decomposition tests of the C_4F_7N gas mixture, and some of the gas decomposition products also have strong acute toxicity, the concentration of these decomposition products is relatively low, and will not have a more obvious effect on the toxicity change of the overall gas mixture, so the biosafety tests were conducted directly using the decomposition gases from the previous tests under different faulty conditions, and the results are the same as those of the pre-test C_4F_7N gas mixture will not produce essential

changes. In order to effectively investigate the biological safety of the decomposition products of C_4F_7N gas mixture, this paper adopts the C_4F_7N gas mixture as the arc extinguishing medium to carry out repeated opening and breaking tests on load switches, and conducts the acute inhalation test on the arc decomposition gases in mice, and evaluates the biological safety of the decomposition products of the C_4F_7N gas mixture on the basis of the test results.

5.3.1 Test platforms and methods

The load current on-off test platform is mainly composed of load switch (internal structure schematic shown in Fig. 5.6), synthesized circuit and voltage and current data acquisition system. The load switch is a 630A/24kV magnetically blown load switch, and the principle diagram of the synthesized circuit is shown in Fig. 5.7. It adopts LC oscillating circuit, in which the pre-charged capacitor bank is discharged through the series reactor bank to form an attenuated sinusoidal discharging current, which provides the load switch with the required overload breaking current, and its capacitance and inductance parameters are C1=16.8mF, L1=0.603mH, and the oscillating frequency is 50Hz. Frequency 50Hz.

In this paper, 57%C_4F_7N-43%Air gas mixture was selected as the arc extinguishing medium to conduct 200 single-phase breaking tests on load switches, and the C_4F_7N-CO_2-O_2 gas mixture, which is consistent with the previous study, was not selected as the arc extinguishing medium here, mainly due to the following reasons: high concentration of CO_2 has an asphyxiating effect[38], which affects the results of toxicity tests, so in this paper C_4F_7N mixed with dry air to study the biosafety of the decomposition products of the C_4F_7N gas mixture after disconnection; in addition, the results of related literature show that increasing the content of C_4F_7N in the gas mixture can significantly improve the disconnection performance of the gas mixture[65], in order to allow the gas mixture to fully decompose, the study in this paper is set up for 200 times of disconnection test, with the increase of the number of disconnections, the ablation of the switch contacts and the With the increase in the number of breaks, the ablation of switch contacts and the by-products generated by the decomposition of C_4F_7N will affect the arc extinguishing performance of the gas mixture. In order to achieve the best breaking performance, the highest proportion of C_4F_7N gas mixture is selected to meet the conditions of absolute air pressure of 0.13MPa in the arc extinguishing chamber of the load switch and the condition that it does not liquefy in the actual engineering application at -15℃, i.e., 57%C_4F_7N-43% Air mixture is used as the arc extinguishing medium to carry out the test.

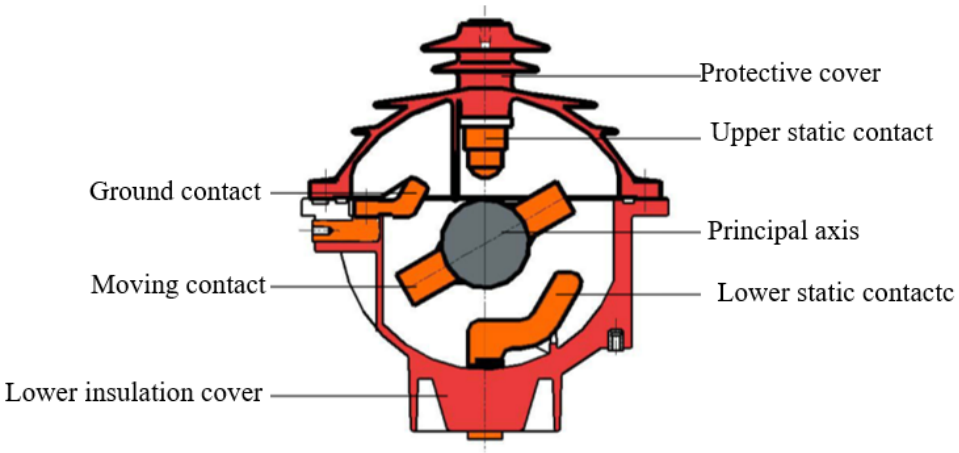

Figure 5.6 Schematic diagram of the internal structure of a load switch

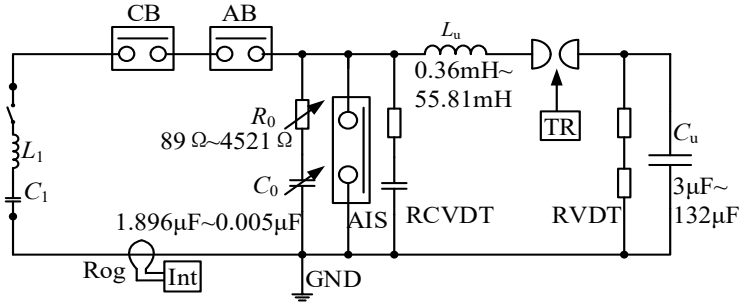

Figure 5.7 Schematic diagram of the synthesis loop

After the completion of 200 open-break tests, gas chromatography mass spectrometry (GC-MS) and field emission scanning electron microscopy (FESEM) were used to analyze the types and contents of gases and solid by-products inside the arc-decomposition chamber after the open-break tests, and then the gases inside the arc-decomposition chamber were extracted, and the inhalation toxicity test platform for environmentally friendly insulating gases, as shown in Fig. 5.2.1, was used to carry out acute inhalation toxicity tests of the arc-decomposition gases in mice. The test was conducted to comprehensively assess the biological safety of the C_4F_7N arc decomposition gas through the changes in vital signs, LC50 and blood cell counts of mice by acute inhalation of the post-opening gas mixture. The arc decomposition gas biosafety test method is essentially the same as the pure C_4F_7N gas test method in 5.2.1. In order to accurately calculate the LC50 of C_4F_7N arc decomposition products, it is necessary to test the mortality rate of animals at each test concentration with equal logarithmic spacing, and it is necessary to have various test concentrations that make the test animals survive more than half and less than half, and it is found that the mortality rate of mice under the condition of 42 ppm post-breakage gas mixture is 100%, and that under the concentration of 20 ppm, the mortality rate of mice is 0%, through several tests. Therefore, the range of test concentrations was selected from 20 ppm to 42 ppm, and a total of one control group (air) and

five experimental groups (20 ppm, 24 ppm, 29 ppm, 35 ppm, and 42 ppm) were set up, with five males and five females used in each group to conduct the test to determine sex differences.

5.3.2 Arc Breakdown Characteristics of C_4F_7N Gas Mixture

C_4F_7N gas mixture decomposition occurs under the action of high-energy arc in the breaking process, the size of the arc energy is an important factor in determining the severity of the decomposition of the mixed gases, in order to meet the arc current and voltage under the premise of the arc time is an important factor in determining the size of the energy released by the arc. Figure 5.8 gives a mixed gas 200 times the opening test of the arc time scatter plot, you can see that the arc time distribution in 7 ~ 15ms, the average arc time of 10.1ms (the voltage began to change as the starting point of the arc time, the current drops to 0 as the end of the arc time). The arc ignition time of 150 out of 200 openings was concentrated in 8~12ms, and the arc opening process was basically completed at the second or third current half-wave zero point, with a relatively stable arc ignition time, indicating that the arc extinguishing capability of C_4F_7N gas mixture did not deteriorate significantly after many openings under 630A current conditions. The study shows that the arc ignition time of the SF_6 load switch of the same type as this paper for 100 three-phase disconnections of 630A current is concentrated in 6-8ms[123], which shows that the arc ignition time of the C_4F_7N gas mixture is larger than that of the SF_6 load switch.

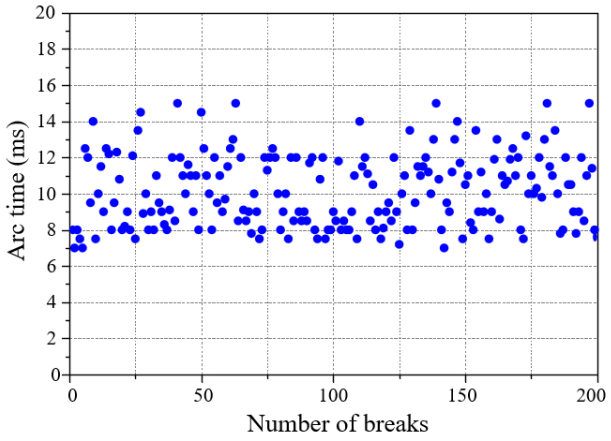

Figure 5.8 Arc ignition time for 200 opens and closes

Figure 5.9 shows the gas chromatogram of the C_4F_7N gas mixture after 200 openings under 630A current conditions, and it can be seen that the decomposition of the gas mixture after the opening of the load current mainly produces products such as CO, CF_4, C_2F_6, C_3F_8, CF_3CN, C_4F_8, CO_2, $C_4F_{10}N_2$, C_3F_6 and C_2N_2. Compared with IF breakdown and partial discharge, C_4F_8 and $C_4F_{10}N_2$ are unique by-products under arc discharge. In addition, the contents of four quantifiable decomposition products, CF_4, C_2F_6, C_3F_8 and C_3F_6, in the gas

mixture after disconnection reached 30.31%, 22.47%, 1.43% and 0.49%, respectively, with the cumulative total content as high as 54.7%, which indicates that perfluorocarbon-like gases are the main decomposition products of the arc discharge of C_4F_7N-Air gas mixture. In addition, the content of C_4F_7N in the gas mixture after 200 break tests was only 13.88%, which decreased by 75.6% compared with the content before break, proving that the decomposition of C_4F_7N gas was more serious after several breaks, and more gas by-products were produced.

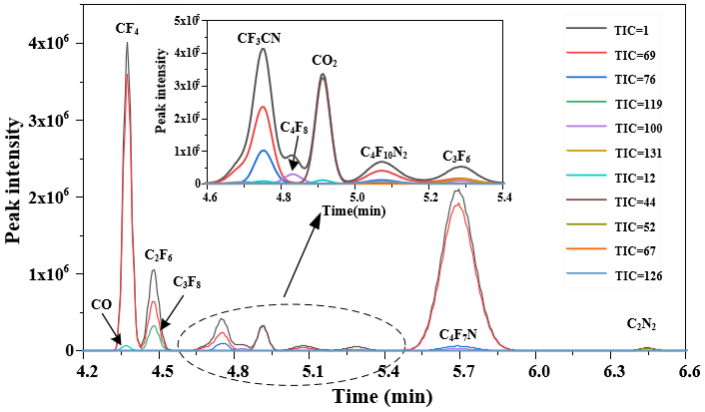

Figure 5.9 Chromatogram of the gas mixture after 200 openings

In addition, disassembly of the interrupter chamber after the completion of the open-break test revealed a large amount of black solid powder adhering to the wall and contacts inside the interrupter chamber (as shown in Fig. 5.10(a)), including both dry and oily powders. Among them, the microscopic morphology of the dry solid powder was a spray-frosted crystalline substance (as shown in Fig. 5.10(b)), while the microscopic morphology of the oily powder was a scaly and clustered substance (as shown in Fig. 5.10(c)). The elemental species and contents of the solid powders were further analyzed based on SEM-EDS (Energy Dispersive Spectrometer), and the EDS layered images of the dry and oily solid powders are given in Figures 5.10(b) and 5.10(c), respectively), and it can be seen that the various elements are uniformly distributed. The types and contents of the elements in the solid powders are given in Table 5.3, and it can be seen that the main elemental components of the solid by-products are C, N, O, F, Si, and Cu, of which the contents of element C in the dry and oily powders are 63.08% and 46.53%, respectively, which are the highest contents of all the elements; and the contents of element F are 10.77% and 3.4%, respectively, which are only next to the C element. In fact, the solid product exists in the form of carbon particles on the one hand, i.e. the gas mixture produces a large number of carbon particles after 200 openings, and in the form of fluorocarbons on the other hand. The content of Si element in the oily solid powder was as high as 28.94%, which was mainly related to the silicone grease coating on the sealing ring of the interrupter chamber, i.e., the oily powder contained the silicone grease used to enhance the airtightness of the interrupter chamber. A small amount of Si (1.87%) in the dry

solid powder is mainly derived from SiO2 in the epoxy resin material of the arc extinguishing chamber.

Although it has been shown that O_2 can inhibit the generation of solids and gaseous by-products (carbon particles) in C_4F_7N gas mixtures under the action of high-energy arcs to a certain extent[66], and the addition of a certain content of O_2 was found to reduce the amount of decomposition products generated from the C_4F_7N gas mixtures under the conditions of electrical and thermal faults in the study of this paper. However, the 57% C_4F_7N-43% Air gas mixture contains only 9% O_2, of which the content of C_4F_7N is high, so 9% O_2 is not enough to react with some of the generated gaseous by-products and carbon particles, and thus a large amount of gaseous and solid by-products are still generated after disconnection.

(a) Macro-morphology of the interior of the interrupter after disconnection

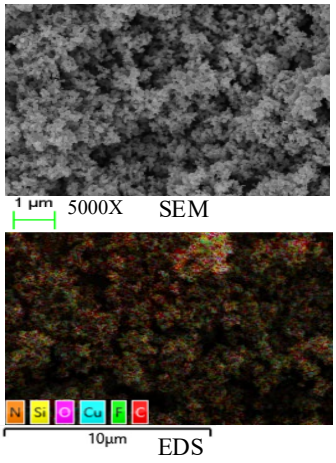

(b) SEM and EDS elemental distribution of dry solid powders

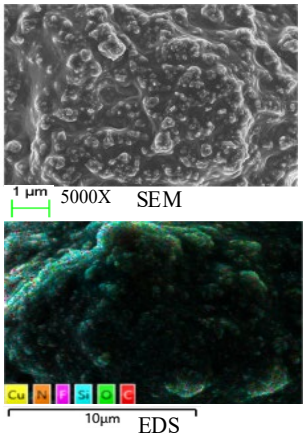

(c) SEM and EDS elemental distribution of oily solid powders

Figure 5.10 Solid by-products in the arc extinguishing chamber after 200 openings

Table 5.3 Elemental analysis of EDS as a solid by-product in the arc extinguishing chamber after disconnection

Elemental	Wt%(Dry powder)	Wt%(Oily Powder)
C	63.08	46.53
N	8.99	0
O	5.03	18.47
F	10.77	3.4
Si	1.87	28.94
Cu	10.26	2.65
总计	100.00	100.00

5.3.3 C_4F_7N mixed gas arc decomposition product biosafety

Acute inhalation toxicity test was carried out on mice exposed to 42 ppm of the gas mixture. After 30 min of exposure to 42 ppm of the gas mixture, the mice showed signs of slow movement and eyes slightly closed; after 3 h of exposure, they basically stopped moving and showed shortness of breath and physical weakness. Mice transferred to the rearing environment showed constipation, eye lesions, and swelling of the genital organs before death (1-2 days after exposure), which were the general symptoms of poisoning in mice and were similar to those of mice exposed to pure C_4F_7N gas, but in the case of pure C_4F_7N gas, these symptoms appeared 2-7 days after exposure. The above findings indicate that the cracked gas mixture is acutely toxic, and the time of onset of symptoms indicates that the acute toxicity of the cracked gas is higher than that of pure C_4F_7N gas, and that the mice will show symptoms of toxicity within a short period of time after inhalation.

In terms of the time of death, the death of mice inhaling the post-break gas was

concentrated in 1-3 days after exposure; however, for the pure C_4F_7N gas it was concentrated in 3-7 days after exposure, i.e., exposure to the C_4F_7N post-break gas mixture posed a more severe damage to mice. The mortality rate of mice inhaling different concentrations of post-break gas mixtures is given in Figure 5.11, where the calculated LD50 of the 57% C_4F_7N/43% Air gas mixture after 200 breaks was found to be 31 ppm (male mice, 4 h) and 34 ppm (female mice, 4 h), respectively. Combining the time to death and LC50 of mice after exposure, the C_4F_7N gas mixture has strong acute inhalation toxicity after multiple breaks. In fact, the decomposition of C_4F_7N in the gas mixture after disconnection was more serious, and a large amount of gaseous and solid by-products were produced, especially the gaseous components of C_4F_8 (perfluoroisobutene), CF_3CN, C_2F_5CN and C_2N_2 had strong acute inhalation toxicity, among which the LC50 of perfluoroisobutene was only 0.5 ppm, which was the main reason for the strong toxicity of the gas mixture after disconnection.

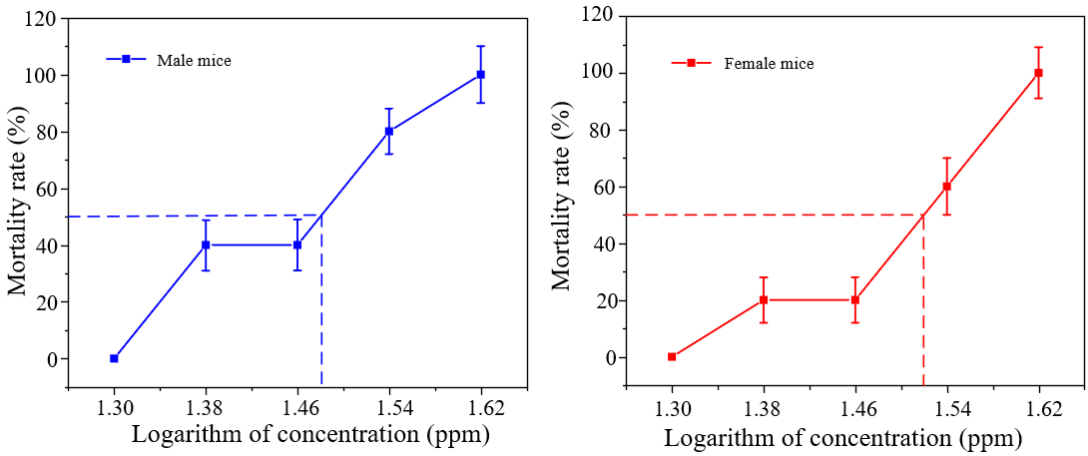

Figure 5.11 Relationship between gas mortality and logarithm of concentration after exposure of mice to C_4F_7N on-off

Table 5.4 Classification of chemicals for acute inhalation toxicity

CLP class	SDS Statement	Rat LC50 (4h，ppm)	Mouse LC50 (4h，ppm)
1	H330: lethal by inhalation	≤100	≤69
2	H330: lethal by inhalation	>100 to ≤500	>69 to ≤347
3	H331: inhalation of toxic	>500 to ≤2500	>71 to ≤1736
4	H332: inhalation	>2500 to ≤20000	>1736 to ≤13888
5	lit. not poisonous	>20000	>13888

*CLP-Classification, labeling and packaging

*SDS- Safety Data Sheet

In order to help the relevant personnel to more intuitively understand the acute inhalation toxicity of C_4F_7N gas mixtures after cracking, the acute toxicity of C_4F_7N gas mixtures after

cracking was classified according to LC50 and the Globally Harmonized System of Classification and Labelling of Chemicals (GHS)[121]. Classification of acute toxicity of post-arc gases. The acute toxicity classification for mice inhaling post-break gases can be obtained by calculating the body surface area conversion method for rats and mice provided in reference[124]. According to the LC50 of mice exposed to post-break gases obtained in this paper, the acute inhalation toxicity classification of the 57% C_4F_7N-43% Air gas mixture after 200 single-phase breaks at 630 A is class 1 (see Table 5.4), indicating that the C_4F_7N post-break gas mixture has a strong acute toxicity.

Table 5.5 gives the results of blood cell counts of mice exposed to the post-disconnection C_4F_7N-Air gas mixture. It can be seen that the percentage of lymphocytes of mice that died at a concentration of 40 ppm decreased significantly and the percentage of neutrophils increased significantly, which indicates that 4h acute inhalation of the post-disconnection gas of C_4F_7N leads to the damage of tissues and organs in the mice and produces inflammation, which in turn leads to the decline in the function of the immune system of the mice. Meanwhile, it can be seen that the number of red blood cells and hemoglobin of the mice that died at 40 ppm concentration were high, mainly due to the impaired cardiopulmonary function of the mice after contamination with the gas (clinical manifestation of shortness of breath of the mice), which required more red blood cells and hemoglobin to be transported to various tissues and organs of the body. The results of the blood cell analysis of mice exposed to C_4F_7N post-disconnection gas were approximately the same as those of mice exposed to pure C_4F_7N gas.

Table 5.5 Hematocrit analysis of mice after exposure to C_4F_7N post-opening gas

Groups	Lymphocytes Percentage (%)	Neutrophils Percentage (%)	Red blood cell (10^{12}/L)	Hemoglobin (g/l)
Control (female)	58.1	31.9	9.13	139
Control (male)	61.3	29.3	9.24	140
25ppm dead male rats	44.6	29.3	10.21	150
40ppm dead male rats	27.3	69.2	10.41	192
Reference point	55.8-90.6	8.6-38.9	6.36-9.42	110-143

Taken together, the vital signs and blood cell counts of mice exposed to C_4F_7N post-disconnection gas and pure C_4F_7N gas were approximately the same, indicating that there would not be a significant difference in the toxic effects of C_4F_7N and post-disconnection gas on the mice's organisms; however, the C_4F_7N post-disconnection gas had a strong inhalation

toxicity, which led to the deaths of the exposed mice earlier than that of the exposed mice to the pure gas.

The main reasons for the significant change in the toxicity of the C_4F_7N gas mixture after disconnection are as follows: First, the chemical nature of the gas itself determines that the molecular structure of C_4F_7N is more complex and contains more active CN (cyanide), resulting in more consumption of the C_4F_7N gas and generation of by-products after multiple disconnections, and the easy generation of more toxic cyanide (CF_3CN, C_2N_2) and perfluorinated compounds (C_4F_8); Second, the arc energy is also a decisive factor for the change of gas toxicity after disconnection, the arc energy is derived from the integral of arc voltage and arc current in the ignition time t, i.e., $Q_{arc} = \int_0^t U_{arc} I_{arc} dt$. From the point of view of the ignition time, the ignition time of the C_4F_7N gas mixture studied in this paper for disconnecting the load current is 8~12ms, which is higher than that of the SF_6 gas under the same conditions (6~8ms), and the energy generated by disconnecting the C_4F_7N gas mixture is higher than that of the SF_6 gas (6~8ms) under the condition that the arc voltage is certain. In the case of a certain arc voltage, the energy generated by C_4F_7N gas mixture breaking is higher than that of SF_6 gas, so the decomposition of C_4F_7N gas mixture is more intense under the action of arc; thirdly, the number of breaks and the content of C_4F_7N in the gas mixture also affects the degree of intensity of the decomposition of the mixed gases, the more the number of breaks and the higher the content of C_4F_7N in the mixed gases, the more the type and content of by-products, resulting in the enhancement of decomposition of the toxicity of the gases.。

5.4 Recommendations for the safe application of C_4F_7N-CO_2-O_2

In order to meet the minimum operating temperature of -25°C, the content of C_4F_7N in medium- and high-voltage gas-insulated equipment is generally 4%-18%, and at present, some of the medium-voltage equipment adopts vacuum interrupter chambers, and C_4F_7N as the interrupting medium is more often used in high-voltage circuit breakers. Considering the high liquefaction temperature of C_4F_7N, the content of C_4F_7N in high-voltage equipment is generally 4%-6%[50]. Inhalation toxicity data for pure C_4F_7N, C_4F_7N-CO_2 gas mixtures used in high-voltage equipment (C_4F_7N content of 4%-6%) and SF_6 are given in Table 5.6.

According to the classification criteria for acute toxicity of chemicals in the Globally Harmonized System of Classification and Labeling of Chemicals (GHS), the LC50 of the 6% C_4F_7N-94% CO_2 gas mixture is higher than 95,500 ppm, and it is a non-toxic substance[38]. Considering that the content of C_4F_7N gas mixture in the equipment in the actual engineering application is small, and it is mainly dominated by CO_2 and other background gases, so as

long as the equipment does not have gas leakage accidents basically will not pose a threat to the health of the relevant personnel, which indicates that the application of the C_4F_7N gas mixture in the high-voltage equipment is safe. However, the acute toxicity of pure C_4F_7N gas is classified as level 4 (rat), although the toxicity is relatively low, it is still recommended that the staff who carry out canning, separating and filling of equipment with pure C_4F_7N gas should take certain protective measures to avoid the safety hazards and potential threats to their health that may be brought about by inhalation of a high dose of C_4F_7N. When the C_4F_7N mixture is used as an insulating medium in equipment, the content of decomposition products under different faults (partial discharge, partial overheating and breakdown) is relatively low (all at ppm level), and the equipment is used in normal operation as well as during minor insulation faults. When C_4F_7N gas mixture is used as an insulating medium in equipment, the content of decomposition products under different faults (partial discharge, local overheating and breakdown) is relatively small (all at ppm level), and the toxicity of the gas mixture in the equipment will not change too significantly during normal operation as well as during minor insulation faults. Only when used as an arc extinguishing medium, due to the more complex molecular structure of C_4F_7N and the recovery characteristics are weaker than SF_6, the by-products generated under the action of high-energy arcs are more varieties and contents, so the toxicity of C_4F_7N gas mixture should be concerned about when it is used as an arc extinguishing medium.

Table 5.6 Comparison of the toxicity of C_4F_7N and its gas mixtures with SF_6

Parameters	SF_6	C_4F_7N-CO_2 gas mixture (4%-6% C_4F_7N)	C_4F_7N pure gas
GWP	23500	g3 4%：327 g3 6%：462	2090
LC50 4h (ppm) (Rat)	>100,000	g3 4%：>160,000 g3 6%：>95,500	10,000-15,000
TWA (ppm)	-	Novec 4710: 65 CO_2: 5,000	65
Acute toxicity rating	lit. not poisonous	lit. not poisonous	Acute toxicity level 4
Exposures	Easy to explode under high temperature and pressure	Easy to explode under high temperature and pressure	Explosive at high temperature and pressure, harmful if inhaled

Table 5.7 Comparison of relevant properties of C_4F_7N and its gas mixtures with SF_6 after disconnection

Parameters	SF_6 (0.13 MPa)	C_4F_7N and its gas mixtures (0.13 MPa)
Relative to SF_6 Insulation strength	1	1.2(57%C_4F_7N/43%Air，-15℃) 1.2(57%C_4F_7N/43%CO_2，-15℃)
Pure gas LC50 (4h)	>80%	1175ppm(Male mice), 1380ppm(Female mice)
Gas mixture LC50 (4h)	>80%	57%C_4F_7N/43%Air, 2035ppm(Male mice), 2390ppm(Female mice)
Gas mixture after disconnection LC50 (4h)	100 three-phase breaks (630 A/24 kV) 2.6-3.8%	57%C_4F_7N/43%Air, 200 single-phase breaks (630 A/24 kV) 31ppm(Male mice)，34ppm(Female mice)
Time of ignition	6-8ms	8-12ms
Initial gas consumption after disconnection	1.6%	61.72%
Type of by-product after disconnection	7	>10
Change in air pressure in the interrupter after disconnection	0	11.5% increase

A comparison of the insulation and arc extinguishing properties and by-product biosafety of C_4F_7N gas mixtures and SF_6 gases used for medium-voltage equipment is given in Table 5.7[118]. It can be seen that for medium-voltage equipment (0.13 MPa) to meet the operating conditions of -15°C without liquefaction, the content of C_4F_7N in the gas mixture is up to 57%, when the insulating strength of the C_4F_7N gas mixture can be up to 1.2 times higher than that of SF_6 under the same conditions. Although the pure C_4F_7N gas has certain acute toxicity (LC50: 1175ppm (male mice, 4h), 1380ppm (female mice, 4h)), the LC50 of the C_4F_7N-CO2 gas mixture containing 57% C_4F_7N is 2035ppm (male mice) and 2390ppm (female mice), respectively, which shows lower toxicity. To meet the minimum ambient operating temperature of -25℃, the content of C_4F_7N in the C_4F_7N-CO_2 gas mixture should not exceed 18% within the air pressure range of 0.1-0.2MPa. The C_4F_7N content in the C_4F_7N-CO_2-O_2 gas mixture used in the medium-voltage equipment studied in this paper was 15%, which is

basically non-toxic, and therefore, the C_4F_7N mixture was used as an insulating medium in the medium-voltage equipment only. insulation medium has application safety when used in medium-voltage equipment.

In addition, the LC50 of 57%C_4F_7N-43%Air gas mixture after 200 single-phase disconnections at 630A was 31-34 ppm, while the LC50 of SF_6 gas after 100 three-phase disconnections at 630A was 2.6-3.8%[120], which shows that when SF_6 and C_4F_7N gas mixtures are used as arc extinguishing media in equipment, the acute toxicity of the gas mixtures after multiple disconnections is more significantly increased compared with that before arc extinguishing. The acute toxicity of the gas mixture compared to the pre-arc extinguishing are more obvious, respectively, 80 and 27 times before disconnection, and the acute toxicity of the C_4F_7N gas mixture after disconnection is about 1,100 times that of the SF_6 gas mixture.The consumption of the main gas after multiple disconnections of the SF_6 and C_4F_7N gas mixtures is 1.6% and 61.72%, respectively, and the decomposition products of the C_4F_7N gas mixture after disconnection are higher than that of SF_6. The type and content of decomposition products after disconnection of C_4F_7N gas mixture are higher than that of SF_6 gas. The air pressure in the arc extinguishing chamber of SF_6 gas is basically unchanged after multiple disconnections, while the air pressure in the arc extinguishing chamber of C_4F_7N gas mixture rises by 11.5% after disconnection. It can be seen that the decomposition of C_4F_7N-Air gas mixture is more serious after 200 disconnections, and the decomposed gas has strong acute toxicity, and the acute toxicity is much higher than that of SF_6 under the same conditions.

C_4F_7N gas mixture in many times after the opening and closing of a large number of by-products generated mainly from the decomposition of C_4F_7N, the impact of the background gas is smaller, so the main study of this paper can be analyzed by analogy with the application of the safety of the C_4F_7N-CO_2-O_2 gas mixture. C_4F_7N-CO_2-O_2 gas mixture is only as an insulating medium in the equipment, as long as the equipment does not occur gas leakage accidents Basically, there will be no threat to the health of the personnel concerned, in the slight insulation failure (PD, POF) when the equipment within the gas mixture decomposition product content is small, the overall toxicity will not produce too obvious changes, but to avoid the early development of minor failure into serious insulation failure, comprehensive view of the C_4F_7N-CO_2-O_2 mixture of gases only as an insulating medium in the equipment when the use of the application of safety.

C_4F_7N-CO_2-O_2 gas mixture as an arc extinguishing medium in medium and high voltage gas insulated equipment, should cause high concern, many high current disconnection will lead to serious decomposition of the gas mixture, disconnection of the gas mixture after a

significant increase in toxicity. Therefore, in the process of using the equipment to strictly control the number of operations, and in order to meet the arc extinguishing performance under the premise of as little as possible in the mixed gas C_4F_7N content. In addition, the relevant personnel in the maintenance and operation and maintenance process should do a good job of strict protective measures to avoid equipment failure caused by gas leakage after disconnection of the potential danger to personal safety. Suggested protective measures are as follows: 1. Demarcate a safe area near the gas insulation equipment and gas production area, and add danger signs and safety instructions; 2. Use suitable gas sensors for gas leakage monitoring and install alarm devices, and extract the gas to a safe place in time in response to gas leakage caused by a fault; 3. Tanking, separating, and inflating the equipment with C_4F_7N and its decomposed gases. Staff and equipment maintenance personnel are recommended to use goggles and gas masks for eye and respiratory protection, and wear protective clothing and nitrile gloves to avoid skin contact, so as to minimize the potential hazards and dangers of long-term contact with C_4F_7N gas and its decomposition products to their own safety; 4. No special protection is required when the equipment is running under normal conditions, but it is recommended to install leakage monitoring devices within a certain range of the equipment.

5.5 Summary of the chapter

In this chapter, the optimal O_2 additions of C_4F_7N-CO_2-O_2 gas mixtures for medium-voltage gas-insulated equipment are proposed by summarizing the effects of different O_2 contents on the insulation and decomposition characteristics of C_4F_7N-CO_2-O_2 gas mixtures under discharge and overheating faults. On the basis of the decomposition characteristics, the characteristic quantities that can characterize the types of faults and their severity within the equipment are extracted. Finally, the biosafety of the arc decomposition products of C_4F_7N and its gas mixtures was investigated by acute inhalation toxicity test in mice, and recommendations for safe application were given. Based on the relevant conclusions, the feasibility and safety of the C_4F_7N-CO_2-O_2 gas mixtures for equipment application were comprehensively evaluated. The relevant conclusions are as follows:

(1) Considering the insulation and decomposition characteristics of the C_4F_7N-CO_2-O_2 gas mixture under POF, PD and frequency breakdown fault conditions and the safety of the personnel involved in the operation and maintenance of the equipment, the optimal amount of O_2 added to the gas mixture should be 4%-6%; if the amount of O_2 added is greater than 6%, the gas mixture may cause insulation deterioration and decomposition to intensify, and may lead to serious corrosion of internal metal components of the equipment in the case of severe localized overheating faults. In the case of severe localized overheating faults, this may lead

to serious corrosion of the internal metal components of the equipment.

(2) For C_4F_7N-CO_2-O_2 gas mixture insulated equipment, C_2F_6 can be used as a signature generator characterizing discharging faults, $C_2F_6O_3$ can be used as a signature generator characterizing PD faults, CF_4 can be used as a signature product characterizing the severity of PD faults, COF_2 and C_2N_2 can be used as signature products characterizing the severity of POFs, and C_2F_5CN can be used as a signature decomposition product characterizing the nature of the jumps in POFs.

(3) The LC50 of 4h inhalation of C_4F_7N gas in mice, male mice: 1175 ppm, female mice: 1380 ppm, produced severe damage to the lungs, slight damage to the heart, liver and eyes, and little damage to the intestinal tract after exposure. Acute inhalation of 1000 ppm of pure C_4F_7N gas did not cause irreversible damage to the mouse organism. The C_4F_7N gas mixture 630A decomposed severely after 200 openings, and the amount of C_4F_7N decomposed and the amount of quantifiable fluorocarbon compounds (CF_4, C_2F_6, C_3F_8, and C_3F_6) produced were 75.6% and 54.7%, respectively, and the LD50 of the gas after the extinction was were 31 ppm (male mice, 4h) and 34 ppm (female mice, 4h), and the toxicity grading was categorized as class 1, with strong acute toxicity. From a comprehensive point of view, C_4F_7N-CO_2-O_2 gas mixture only as an insulating medium in the equipment has application safety, as an arc extinguishing medium in medium and high-voltage gas-insulated equipment need to pay great attention to the use of strict control of the number of openings of the equipment, in order to meet the arc extinguishing performance of the premise to reduce the arc extinguishing medium as much as possible in the content of C_4F_7N gas. Relevant personnel in the maintenance and operation and maintenance process should do a good job of strict protective measures.

Chapter 6 Conclusions and outlook

6.1 Conclusions

In this paper, a more systematic theoretical and experimental study has been carried out on the insulation of environmentally friendly C_4F_7N-CO_2-O_2 gas mixture and its decomposition characteristics and biosafety under electrical and thermal faults. Based on the ReaxFF molecular dynamics method, the thermal decomposition process of the gas mixture under different O_2 contents and temperatures is simulated, and the kinetic process of the thermal decomposition of the C_4F_7N-CO_2-O_2 gas mixture and the evolution mechanism of its product particles under different conditions are revealed by combining with thermal decomposition tests. Meanwhile, the influence mechanism of O_2 content on the breakdown voltage and PD statistical characteristic quantity of the C_4F_7N-CO_2-O_2 gas mixture is analyzed, and the influence mechanism of different factors on the generation and inhibition of gas and solid by-products during the discharge decomposition process of the C_4F_7N-CO_2-O_2 gas mixture is clarified. Finally, based on the simulation and experimental results, we propose the optimal O_2 additive amount and fault diagnosis characteristic components of C_4F_7N-CO_2-O_2 gas mixture for medium-voltage gas-insulated equipment, and test the biosafety of C_4F_7N and its arc decomposition products, and then evaluate the feasibility and safety of applying C_4F_7N-CO_2-O_2 gas mixture in equipment by combining with the insulating and electrical and thermal decomposition characteristics of C_4F_7N-CO_2-O_2 gas mixture and the results of the biosafety. The feasibility and safety of C_4F_7N and its arc decomposition products were comprehensively evaluated in the light of its application to equipment. The main conclusions of this paper are as follows:

(1) The ReaxFF-MD simulation results show that the thermal decomposition of C_4F_7N-CO_2-O_2 gas mixture mainly generates particles such as CF_3, CF_2, CF, F, C_2F_5, C_2F_4, C_2F_2, C_3F_7, C_2F_2N, C_3F_4N, CFN, CN, CO, O, and C. The generation of the two kinds of particles, CF_2 and CN, is the highest, followed by CF_3 and F. The addition of O_2 decreases the initial decomposition time of C_4F_7N, and at the same time effectively reduces the decomposition of C_4F_7N and the generation of most of the particles, especially at an O_2 content of 6%, which results in the least amount of decomposition of C_4F_7N. The addition of 0%-4% O_2 decreases the reaction rate of the main decomposition reactions in the reaction system, and the rate of the reaction is increased at an O_2 content of >8%. When the simulation temperature is greater than 2600 K, the initial decomposition time of C_4F_7N is significantly reduced, and the

generation of decomposed particles is significantly increased. The results of the thermal decomposition test showed that the main products of the thermal decomposition test of the C_4F_7N-CO_2-O_2 gas mixture were CF_4, C_3F_8, C_3F_6, CO, COF_2, CF_3CN, C_2F_5CN and C_2N_2. 2% O_2 was added to the C_4F_7N-CO_2 gas mixture to increase the amount of C_3F_6, and the remaining products decreased to varying degrees; when the amount of O_2 was added greater than 8%, the amount of C_3F_6 increased, and the remaining products decreased to varying degrees; when the amount of O_2 was added greater than 8%, the amount of C_3F_6 increased, and the amount of decomposed particles increased. amount was greater than 8%, the generation rates of CF_4, C_3F_8, CO and COF_2 were accelerated.

(2) The addition of 2%-4% O_2 to the C_4F_7N-CO_2 gas mixture can significantly inhibit the negative half-circle discharge and reduce the maximum discharge of a single pulse. The number of discharges per second, the cumulative discharge per second and the average discharge of the mixed gas PD shows a substantial increase in the trend of the O_2 content is greater than 6%, which may lead to the deterioration of the insulation of the mixed gas. The decomposition of the PD of the C_4F_7N-CO_2-O_2 gas mixture. The main products are CF_4, C_2F_6, C_3F_8, C_3F_6, CO, COF_2, $C_2F_6O_3$, CF_3CN, C_2F_5CN, and C_2N_2. After the addition of 2%-4% O_2 to the C_4F_7N-CO_2 gas mixture, the generation of by-products, except for C_3F_8 and COF_2, shows a decreasing trend to varying degrees, and reaches a minimum at 4% O_2. The generation of PD decomposition components of C_4F_7N-CO_2-O_2 gas mixture was positively correlated with the average discharge. The microstructure of solid precipitates on the electrode surface after 96h PD of C_4F_7N-CO_2-O_2 gas mixture was a crystal corrosion material in the form of scales or cubes, and the main compositions included metal oxides, silicates, fluoride and carbon oxides, and the addition of 4%O_2 had less effect on the solid precipitates of PD. The addition of 4% O_2 has less influence on the elemental composition of PD solid precipitates and its valence state, but it can reduce its generation to a certain extent.

(3) The addition of O_2 can increase the breakdown voltage of C_4F_7N-CO_2 gas mixture, and the breakdown voltage is the highest under the condition of 6% O_2, and the addition of 2%-6% O_2 can reduce the dispersion of the breakdown voltage of the mixture. The breakdown decomposition of C_4F_7N-CO_2-O_2 gas mixture at work frequency mainly produces CF_4, CO, C_2F_6, C_3F_6, C_3F_8, CF_3CN. The addition of 2%-6% O_2 to the C_4F_7N-CO_2gas mixture can effectively reduce the generation of most of the by-products. When the O_2 content was higher than 6%, the rate of some by-products generation increased, and the higher O_2 addition had a negative effect on the stability of the C_4F_7N gas mixture. The participation of O particles in the discharge process makes the bond breaking process of C_4F_7N more likely to occur, with a

reaction enthalpy of -106.52 kcal/mol and an activation energy of 47.51 kcal/mol. Most of the reactions between the O particles and the decomposed particles of C_4F_7N belong to the exothermic process which can be carried out spontaneously, which may prevent the generated particles from being compounded or re-bonded with C_4F_7N. So the addition of O_2 affects the process of by-product formation.

(4) Considering the insulation and decomposition characteristics of the C_4F_7N-CO_2-O_2 gas mixture under POF, PD and frequency breakdown fault conditions and the safety of personnel in the operation and maintenance of the equipment, the optimum O_2 additive amount of the gas mixture should be 4%-6%; if the O_2 additive amount is greater than 6%, the gas mixture may cause insulation deterioration and increased decomposition, and under severe POF conditions may cause serious corrosion of the metal components inside the equipment. In severe POF conditions, it may also lead to severe corrosion of the internal metal components of the equipment. For C_4F_7N-CO_2-O_2 gas mixture insulated equipment, C_2F_6 can be used as a marker generator to characterize discharge faults, $C_2F_6O_3$ can be used as a marker generator to characterize PD faults, CF_4 can be used as a characteristic product to characterize the severity of PD faults, COF_2 and C_2N_2 can be used as characteristic products to characterize the severity of POFs, and C_2F_5CN can be used as a characteristic product to characterize the jump in the nature of POFs. signature decomposition product of POF nature jump.

(5) The LC50 of 4h inhalation of C_4F_7N gas in mice was 1175 ppm in male mice and 1380 ppm in female mice, resulting in severe damage to the lungs, slight damage to the heart, liver and eyes, and almost no damage to the intestinal tract after exposure. Acute inhalation of 1000 ppm pure C_4F_7N gas did not produce irreversible damage to the mouse organism. the C_4F_7N gas mixture 630A decomposed severely after 200 openings, the amount of C_4F_7N decomposition and the production of fluorocarbons (CF_4, C_2F_6, C_3F_8, and C_3F_6) were 75.6% and 54.7%, respectively, and the LC50 of the gas after the extinction of the arc was 31 ppm (male mice, 4h) and 34 ppm (female mice, 4h), and the toxicity classification was categorized as class 1, with strong acute toxicity. From a comprehensive point of view, C_4F_7N-CO_2-O_2 gas mixture only as an insulating medium in the equipment has application safety, as an arc extinguishing medium in medium and high-voltage gas-insulated equipment need to pay great attention to the use of strict control of the number of openings of the equipment, in order to meet the arc extinguishing performance of the premise to reduce the arc extinguishing medium as much as possible in the content of C_4F_7N gas. Relevant personnel in the maintenance and operation and maintenance process should do a good job of strict protective measures.

6.2 Prospects for follow-up research

This paper evaluates the application feasibility and safety of C_4F_7N-CO_2-O_2environmentally friendly gas insulating medium from the aspects of insulation, fault decomposition characteristics and biological safety. The composition, distribution and change rule of decomposition particles and products of C_4F_7N-CO_2-O_2 gas mixture under different fault conditions and influencing factors are obtained, and the decomposition mechanism and biological safety of C_4F_7N-CO_2-O_2 gas mixture are clarified initially, but there are still many problems that need to be further investigated before the large-scale popularization and application of C_4F_7N-CO_2-O_2 gas mixture:

(1) In this paper, only the decomposition and composite reaction with the participation of neutral particles are considered in the reaction system, while there is a reaction with the participation of charged plasmas in the discharge process, and it is necessary to carry out quantum chemistry and ReaxFF-MD calculations on the reaction process of the C_4F_7N-CO_2-O_2 gas mixture with the participation of ions and electrons in the later stage to further clarify the decomposition mechanism.

(2) At present, there are few studies on the compatibility of the C_4F_7N-CO_2-O_2 gas mixture with various metallic and non-metallic materials inside the equipment, so it is necessary to carry out theoretical and experimental studies on the interaction mechanism between the C_4F_7N-CO_2-O_2 gas mixture and various materials, and the stability of the gas-solid interface before large-scale popularization of the application.

(3) Due to the inability to obtain the standard gases of CF_3CN, C_2N_2, COF_2, C_2N_2 and $C_2F_6O_3$ decomposition products at this stage, only the peak area integral can be used to analyze the relative amount in the process of this paper, and it is necessary to analyze the absolute quantitative analysis of the above products in the later stage in the case of obtaining more standard gases to make clear the amount of their generation and the rule of change, and adopt the clustering algorithm to put forward a more comprehensive and systematic analysis. Clustering algorithm to propose a more comprehensive and systematic fault diagnosis method.

(4) In this paper, only the acute inhalation toxicity of C_4F_7N and its decomposition products are tested, and before large-scale popularization and application, it is necessary to conduct a comprehensive and in-depth study on the biological safety and pathogenic mechanism, including subacute inhalation toxicity, chronic toxicity, reproductive toxicity, neurotoxicity, and potential mutagenicity, to determine the types of toxicity products that need to be monitored and the safety thresholds, and to propose effective public health protection measures to achieve the goal of C_4F_7N and its decomposition products, so as to realize the

goal of C_4F_7N and its decomposition products. It will identify the types of toxicity products and safety thresholds that need to be monitored in engineering applications, propose effective public health protection measures, realize the early warning and assessment of the health risk of C_4F_7N exposure, and guide the safe application of the new generation of environmentally friendly gas-insulated power transmission and distribution equipment in China.

Extended abstract in French - Résumé long en français

Evaluation de la faisabilité de l'utilisation du mélange C_4F_7N-CO_2-O_2 dans l'équipement électrique moyenne et haute tensions. Détermination de la décomposition de ce mélange

L'hexafluorure de soufre (SF_6), gaz idéal pour l'isolation et l'extinction des arcs électriques, est largement utilisé dans divers équipements de la distribution de l'électricité. Cependant, le SF_6 est un gaz à effet de serre extrêmement puissant, puisque le potentiel d'effet de serre (GWP) du SF_6 est 23500 fois supérieur à celui du CO_2. En outre, sa durée de vie dans l'atmosphère peut atteindre 3200 ans. La recherche d'un gaz respectueux de l'environnement, pouvant être utilisé aux équipements de moyenne et haute tension (GIE), peut fondamentalement résoudre la dépendance de l'industrie énergétique à l'égard de l'utilisation massive de SF_6. Ces dernières années, le gaz Perfluoroisobutyronitrile (C_4F_7N) est considéré comme un substitut potentiel du SF_6 en raison de ses excellentes performances en matière d'isolation électrique et de protection de l'environnement.

Globalement, les recherches internationales actuelles sur les caractéristiques d'isolation, d'extinction d'arc et de décomposition du mélange gazeux C_4F_7N avec notamment CO_2 ont abouti à des résultats intéressants, qui confirment fondamentalement que ce mélange gazeux a de bonnes performances et peut répondre aux exigences d'application de divers types d'équipements isolés au gaz à moyenne et haute tension. Il a été démontré que l'ajout d'O_2 comme second gaz tampon au mélange gazeux C_4F_7N-CO_2 peut améliorer leur capacité de coupure de l'arc et réduire la production de sous-produits gazeux et solides (principalement des particules de carbone). Bien que l'ajout d'O_2 puisse apporter les avantages susmentionnés pour l'application du gaz C_4F_7N dans les appareillages de connexion, l'effet d'O_2 sur la stabilité du mélange gazeux C_4F_7N-CO_2 dans des conditions de défaut électrique et thermique doit être examiné et évalué en profondeur, étant donné qu'O_2 est fortement oxydant et que le mélange gazeux C_4F_7N-CO_2 doit être chimiquement stable dans les conditions de

fonctionnement réelles. A ce stade, il n'existe que peu de publications sur les effets d'O_2 sur les propriétés isolantes et la décomposition du mélange gazeux C_4F_7N-CO_2 liée à un défaut électrique et thermique, et sur la biosécurité du mélange gazeux C_4F_7N-CO_2 et de leurs produits de décomposition. La quantité optimale d'O_2 ajoutée dans le mélange gazeux C_4F_7N-CO_2-O_2 doit également être étudiée ; l'effet d'O_2 sur la stabilité du mélange gazeux C_4F_7N-CO_2-O_2 en présence de différentes conditions de défaillance et de différents facteurs d'influence doit encore être étudié. Parallèlement, il n'existe pas de recherche systématique sur les caractéristiques de décomposition du mélange gazeux C_4F_7N-CO_2-O_2 dans ces mêmes conditions ; et la corrélation entre les défaillances et les facteurs d'influence, comme le type, la teneur et le taux de production des produits de décomposition, n'est pas encore claire. La décomposition du gaz induite par des défauts électriques et thermiques dans l'équipement, peut générer une grande variété de sous-produits. Il est donc urgent de clarifier la biosécurité du mélange gazeux C_4F_7N avec les gaz tampons avant son application à grande échelle afin d'éviter les problèmes de sécurité publique causés par la fuite de gaz dangereux dans l'équipement ou l'exposition dangereuse du personnel chargé à la production, à l'exploitation et à la maintenance de l'équipement et de la zone d'installation.

Bien que quelques fabricants d'équipements électriques aient déjà conçu, fabriqué et testé certains équipements avec un mélange de gaz C_4F_7N-CO_2-O_2 comme milieu isolant, ils en sont encore au stade des essais et de l'optimisation. L'expérience actuelle en matière de conception d'équipements isolés au gaz respectueux de l'environnement est relativement faible dans de nombreux pays. Afin de briser le monopole de ces quelques fabricants sur la technologie des équipements d'isolation au gaz respectueux de l'environnement, il est nécessaire d'étudier en profondeur les propriétés d'isolation, les caractéristiques de décomposition des défauts et la sécurité biologique du mélange gazeux C_4F_7N-CO_2-O_2. L'étude fournira un soutien théorique et pratique important pour la conception, la sélection des matériaux, l'optimisation et l'application sûre du mélange de gaz C_4F_7N-CO_2-O_2, afin de réduire l'utilisation de SF_6 dans diverses industries en vue de freiner le réchauffement climatique. Dans ce cadre de mes travaux doctoraux, des études théoriques (numériques) et

expérimentales ont été menées sur les caractéristiques d'isolation et de décomposition du mélange gazeux écologique C_4F_7N-CO_2-O_2 dans différentes conditions de défaillance ; et la faisabilité de l'application et la sécurité du mélange gazeux C_4F_7N-CO_2-O_2 sont évaluées, ainsi que la sécurité biologique du mélange C_4F_7N/air après avoir exposé à 200 fois d'un arc de 630 A. Les principales points et réalisations sont les suivants :

1. En cas de défauts tels qu'un mauvais contact, une saturation magnétique ou une surcharge dans un équipement électrique isolé au gaz, la stabilité thermique des pièces défectueuses est compromise, ce qui entraîne un défaut de surchauffe partielle (POF : Partial Overthermal Fault) dans l'équipement isolé au gaz. Ces défauts de surchauffe partielle précoces peuvent endommager le matériau isolant à des degrés divers, accélérant la détérioration du matériau isolant, ce qui peut finalement conduire à une rupture de l'isolation. Par conséquent, l'examen de la stabilité thermique et des caractéristiques de décomposition thermique du gaz d'isolation est une partie importante de l'évaluation de leur fiabilité dans l'application.

2. La simulation de la réaction avec la méthode de la dynamique moléculaire (ReaxFF) a été réalisée à l'aide du modèle de décomposition thermique (notée décomposition) construit pour le mélange gazeux C_4F_7N-CO_2-O_2 ; la composition, la distribution et le taux de génération des particules (molécules) de décomposition thermique du mélange gazeux ont été obtenus à différentes teneurs en O_2 et à différentes températures. Ils révèlent « théoriquement » le mécanisme de décomposition du mélange gazeux C_4F_7N-CO_2-O_2 et l'influence d'O_2 sur cette décomposition. Parallèlement, les caractéristiques de décomposition du mélange C_4F_7N-CO_2-O_2 ont été expérimentalement étudiées à l'aide de la plateforme de test de décomposition thermique disponible à l'Université de Wuhan, et les effets de la température et de la teneur en O_2 sur la composition et la quantité des produits de décomposition du mélange ont été analysés. La combinaison de la simulation et des résultats expérimentaux a permis de clarifier le mécanisme de décomposition du mélange C_4F_7N-CO_2-O_2. Les conclusions spécifiques sont les suivantes **:**

(a) Les résultats de la simulation ReaxFF-MD montrent que la décomposition du mélange gazeux C_4F_7N-CO_2-O_2 génère principalement des molécules telles que CF_3, CF_2, CF, F, C_2F_5, C_2F_4, C_2F_2, C_3F_7, C_2F_2N, C_3F_4N, CFN, CN, CO, O et C. Les deux molécules les plus nombreuses sont CF_2 et CN, suivies par CF_3 et F. Bien que l'ajout d'O_2 au mélange C_4F_7N-CO_2-O_2 diminue le temps de décomposition initial de C_4F_7N, il est efficace pour réduire la décomposition de C_4F_7N et la génération de la plupart des molécules, et en particulier, la plus faible décomposition de C_4F_7N est obtenue à une teneur en O_2 de 6 %. L'ajout de 0 à 4 % d'O_2 diminue la vitesse de réaction de la principale réaction de décomposition dans le système réactionnel, et la vitesse de réaction augmente à des niveaux d'O_2 supérieurs à 8 %. Cependant, à des températures supérieures à 2600 K, la simulation indique une importance réduction du temps de décomposition initial de C_4F_7N et une accélération du taux de génération de molécules de décomposition.

(b) Les principaux produits de l'essai de décomposition thermique du mélange gazeux C_4F_7N-CO_2-O_2 sont CF_4, C_3F_8, C_3F_6, CO, COF_2, CF_3CN, C_2F_5CN et C_2N_2. Pour une teneur en O_2 de 2 %, la production de tous les produits a diminué à des degrés divers, à l'exception de la production de C_3F_6, qui a augmenté. Lorsque la teneur en O_2 augmente encore, la teneur en C_3F_6 diminue et la production des autres produits augmente. Le taux de production de CF_4, C_3F_8, CO et COF_2 s'est accéléré lorsque la teneur en O_2 était supérieure à 8 %. Plus l'ajout d'O_2 au mélange C_4F_7N-CO_2 est important, plus la tendance à la saturation de la production de C_3F_6 est prononcée avec l'augmentation du temps de surchauffe, et la production de tous les autres produits présente une corrélation positive avec le temps de surchauffe.

(c) Les taux effectifs de production de sous-produits CF_4, C_3F_6, C_3F_8, CF_3CN, et C_2F_5CN ont tous augmenté avec la température avant 500 °C, puis ont diminué à des degrés divers à 500 °C et ont finalement repris l'augmentation à des températures supérieures à 500 °C. La tendance de la génération de C_2F_5CN et du taux effectif de production de gaz

en fonction de la température de surchauffe est faible entre 400 °C et 500 °C, et augmente rapidement lorsque la température est supérieure à 500 °C, ce qui peut être considéré comme un produit de décomposition caractérisant la défaillance POF. Les taux effectifs de production de COF_2 et de C_2N_2 présentent une forte corrélation positive avec la température de surchauffe ; ces 2 molécules peuvent également être utilisées comme produits caractérisant la dégradation du mélange C_4F_7N-CO_2-O_2 sous l'action du POF.

3. La décharge partielle (PD) est l'un des défauts les plus courants des équipements électriques isolés au gaz. Quand l'équipement électrique fonctionne sous tension, si des décharges partielles se produisent en permanence, l'effet cumulatif de l'énergie générée par ces faibles décharges entraînera une détérioration progressive des propriétés diélectriques du milieu isolant, l'expansion des défauts locaux et, finalement, la rupture de l'ensemble de l'isolation. D'autre part, les décharges partielles provoquent la décomposition du gaz isolant et la formation d'un certain nombre de sous-produits aux propriétés d'isolation médiocres et dangereuses pour la santé humaine. Bien que l'ajout d'une certaine teneur en O_2 au mélange C_4F_7N-CO_2 puisse améliorer la performance de la rupture ouverte et inhiber la génération de certains sous-produits, l'influence de la teneur en O_2 sur la PD et ses caractéristiques de décomposition du mélange C_4F_7N-CO_2-O_2 n'est pas encore claire en raison de la forte propriété oxydante d'O_2 lui-même. Il est donc nécessaire d'étudier cette influence, ainsi que l'influence d'autre facteurs sur la PD et sur les caractéristiques de décomposition du mélange C_4F_7N-CO_2-O_2.

Ainsi, des expériences sur les caractéristiques de la PD et de décomposition du mélange gazeux C_4F_7N-CO_2-O_2 avec différentes teneurs en O_2 et tensions appliquées ont été réalisées sur la plateforme de test de décomposition de la PD. Cette plateforme permet de récupérer les signaux caractéristiques de la PD pour construire les cartographies de la décharge partielle résolue en phase (PRPD, Phase Resolved Partial Discharge). De ces cartographies, les paramètres caractéristiques ont été déterminés statistiquement, il s'agit principalement du nombre total de micro-décharge en alternance positive et celui en alternance négative, du

charge totale et moyenne sur ces 2 alternances. Ces paramètres ont été utilisés pour étudier l'effet sur la décomposition du mélange C_4F_7N-CO_2-O_2, de la PD dans le mélange C_4F_7N-CO_2-O_2, et de l'ajout d'O_2. En outre, les composants et les contenus des précipités solides produits pendant le processus de la PD ont été testés au niveau microscopique pour analyser le mécanisme de génération et la loi d'influence d'O_2 sur sa génération. Les conclusions spécifiques sont les suivantes :

(a) La PD dans le mélange C_4F_7N-CO_2-O_2 est principalement concentrée dans la demi-période positive de la tension du réseau et elle s'intensifie considérablement après l'ajout d'O_2. L'ajout de 2 à 4 % d'O_2 au mélange gazeux C_4F_7N-CO_2 diminue considérablement le nombre de micro-décharge de la demi-alternance négative et réduit la quantité de charge véhiculée par une seule impulsion. L'ajout de 2 à 6 % d'O_2 peut inhiber la PD avec des décharges plus importantes. Une forte augmentation du nombre de décharges par seconde, des décharges cumulées par seconde se produit lorsque la teneur en O2 est supérieure à 6 %. L'ajout de plus de 6 % d'O_2 au mélange de gaz C_4F_7N-CO_2 peut entraîner une dégradation de l'isolation du mélange de gaz.

(b) Avec l'augmentation de la tension appliquée, le nombre de la PD dans le mélange gazeux C_4F_7N-CO_2-O_2 ayant une forte impulsion de courant, augmente progressivement ; et le nombre de décharges par seconde diminue lorsque la tension appliquée est encore augmentée pour s'approcher de la tension de claquage. La quantité moyenne de charge véhiculée par une seule impulsion augmente avec l'augmentation de la tension appliquée.

(c) Les principaux produits de la décomposition PD sont CF_4, C_2F_6, C_3F_8, C_3F_6, CO, COF_2, $C_2F_6O_3$, CF_3CN, C_2F_5CN et C_2N_2. L'ajout de 2 à 4 % d'O_2 au mélange gazeux C_4F_7N-CO_2 a entraîné une tendance à la baisse de la production de sous-produits à des degrés divers (sauf pour le C_3F_8 et le COF_2), qui ont atteint un minimum à 4 % d'O_2. Lorsque les teneurs en O_2 sont supérieures à 6 %, la production de tous les sous-produits

augmente à des degrés divers. La production du composant de décomposition PD du mélange gazeux C_4F_7N-CO_2-O2 est positivement corrélée à la charge moyenne véhiculée par période.

(d) Des précipités solides sont apparus à la surface de l'électrode après 96 heures de la PD dans le mélange gazeux C_4F_7N-CO_2-O_2. Sa morphologie microscopique était celle de corrosifs cristallins écailleux ou cubiques, et les compositions principales comprenaient des oxydes métalliques, des silicates, des fluorures et des composés carbone-oxygène. L'ajout de 4 % d'O_2 a eu moins d'influence sur la composition élémentaire des précipités solides de la PD, mais il a pu réduire sa génération dans une certaine mesure.

4. La caractéristique de claquage en fréquence industrielle (la fréquence utilisée pour la distribution de l'électricité, c'est-à-dire 50 Hz) est la base fondamentale pour juger de la force d'isolation des milieux isolants gazeux, qui peut fournir une référence pour améliorer la structure isolante de l'équipement et explorer le rapport optimal du mélange gazeux. L'ajout d'O_2 peut affecter les propriétés isolantes du mélange gazeux C_4F_7N-CO_2-O_2, telles que la tension de claquage. D'autre part, compte tenu de la forte propriété oxydante d'O_2, l'ajout d'O_2 peut également avoir une certaine influence sur la stabilité et les caractéristiques de décomposition du mélange gazeux C_4F_7N-CO_2-O_2 après l'apparition d'un claquage de défaut. L'étude des caractéristiques de décomposition de la décharge du mélange gazeux et du mécanisme de génération du produit après l'ajout d'O_2 peut aider à clarifier la corrélation entre la décomposition et les facteurs d'influence.

Les caractéristiques d'isolation et de décomposition du mélange gazeux C_4F_7N-CO_2-O_2 utilisé dans les équipements à moyenne tension sont étudiées à l'aide d'un banc d'essai construit pour les caractéristiques de claquage à fréquence industrielle. Tout d'abord, la tension de claquage du mélange gazeux C_4F_7N-CO_2-O_2 et sa dispersion sous différentes teneurs en O_2 ont été mesurées, puis la génération de produits de décomposition en fonction de la teneur en O_2 et des temps de claquage a été analysée, et le mécanisme de l'influence

d'O_2 sur les propriétés d'isolation et sur la décomposition du mélange gazeux C_4F_7N-CO_2-O_2 a été discuté. Enfin, la voie de réaction supplémentaire de C_4F_7N due à l'ajout d'O_2 est proposée. Les enthalpies et les énergies d'activation des réactions concernées sont calculées sur la base de la théorie de la fonctionnelle de la densité (DFT) et de la théorie de l'état de transition (TST), afin d'analyser plus en détail la décomposition par décharge dans le mélange et le mécanisme de génération de produits dans les conditions de participation d'O_2 à la réaction. Les principales conclusions sont les suivantes :

(a) L'ajout d'O_2 peut améliorer la performance d'isolation du mélange gazeux C_4F_7N-CO2. Les tensions de claquage à fréquence industrielle du mélange gazeux C_4F_7N-CO_2-O_2 contenant 2%, 4%, 6%, 8% et 10% d'O_2 ont augmenté respectivement de 4,85%, 6,49%, 7,70%, 3,21% et 2,74% par rapport à C_4F_7N-CO_2, et l'ajout de 2 % à 6 % d'O_2 au mélange gazeux peut réduire la dispersion de la tension de claquage.

(b) Le mélange gazeux C_4F_7N-CO_2-O_2 produit principalement CF_4, CO, C_2F_6, C_3F_6, C_3F_8, CF_3CN, C_2F_5CN, $(CN)_2$ et COF_2 lors de la décomposition par claquage du mélange gazeux C_4F_7N-CO_2, et l'ajout de 2 à 6 % d'O_2 au mélange gazeux de C_4F_7N-CO_2 réduit efficacement la quantité de la plupart des sous-produits produits.

(c) La production de CO, C_3F_6, CF_3CN, C_2F_5CN et $(CN)_2$ est restée stable ou a eu peu tendance à augmenter avec l'ajout de 2 % à 6 % d'O_2 au mélange gazeux C_4F_7N-CO_2. Le taux de génération de ces sous-produits a augmenté lorsque la teneur en O2 était supérieure à 6 %, ce qui indique que des ajouts plus importants d'O_2 ont eu un effet négatif sur la stabilité du mélange gazeux dans des conditions de décharge.

(d) L'ajout d'O_2 compliquera le processus de dissociation du C_4F_7N, qui se produit plus facilement avec la combinaison du C_4F_7N et de l'atome d'O qu'avec le processus de dissociation directe de la molécule de C_4F_7N, avec une enthalpie de réaction de -106,52 kcal/mol et une énergie d'activation de 47,51 kcal/mol. La plupart des réactions

entre les atomes d'O et les particules décomposées de C_4F_7N appartiennent à la catégorie des réactions qui peuvent être des processus exothermiques spontanés, ce qui peut entraver la recombinaison des particules générées par la décomposition de C_4F_7N pour former des sous-produits stables. Les calculs montrent que l'ajout d'O_2 affecte la décomposition par décharge du mélange gazeux C_4F_7N et la formation de sous-produits.

5. L'ajout d'O_2 comme second gaz tampon au mélange de gaz C_4F_7N-CO_2 peut renforcer la performance d'isolation et améliorer la stabilité chimique du mélange de gaz, mais l'ajout d'une quantité excessive d'O_2 entraînera également certains effets négatifs, de sorte que la quantité optimale d'O_2 ajoutée est l'indicateur technique clé du mélange de gaz C_4F_7N-CO_2-O_2 dans l'application pratique de l'ingénierie. La décomposition du mélange peut refléter dans une certaine mesure les informations sur l'état de fonctionnement de l'équipement. En effet, la décomposition peut être caractérisée par le type et la gravité de défauts dans l'équipement. En outre, le mélange gazeux générera certains sous-produits toxiques et corrosifs dans des conditions de défaillance, ce qui constituera une menace pour la sécurité des opérateurs de l'équipement et du personnel de maintenance. Il est donc nécessaire d'évaluer la biosécurité d'un mélange à base de C_4F_7N et de ses produits de décomposition avant de l'appliquer à grande échelle.

Les ajouts optimaux d'O_2 dans le mélange gazeux C_4F_7N-CO_2-O_2 pour les équipements isolés au gaz de moyenne tension ont été proposés basant sur l'influence des différentes teneurs en O2 sur les caractéristiques de décomposition du mélange gazeux C_4F_7N-CO_2-O_2 sous l'effet de l'isolation et des défauts électriques et thermiques. Sur la base des caractéristiques de décomposition, les quantités caractéristiques qui peuvent caractériser les types de défauts et leur gravité au sein de l'équipement sont extraites ; ce qui fournit une référence pour la méthode de diagnostic des défauts de l'équipement de mélange de gaz C_4F_7N-CO_2-O_2. Enfin, la biosécurité du C_4F_7N et de ses produits de décomposition dans l'arc a été étudiée par un test de toxicité aiguë par inhalation chez la souris et, sur la base des conclusions pertinentes, la faisabilité de l'application du mélange gazeux C_4F_7N-CO_2-O_2

dans l'équipement a été évaluée de manière exhaustive, et des recommandations pour une application sûre ont été formulées. Les principales conclusions sont les suivantes :

(a) Compte tenu des caractéristiques d'isolation et de décomposition du mélange gazeux C_4F_7N-CO_2-O_2 dans des conditions de défaillance (POF, PD, etc.), et de la sécurité du personnel chargé de l'exploitation et de la maintenance de l'équipement, la quantité optimale d'O_2 ajoutée au mélange gazeux doit être comprise entre 4% et 6% ; si la quantité d'O_2 ajoutée est supérieure à 6%, le mélange gazeux peut entraîner une détérioration de l'isolation et une intensification de la décomposition, ainsi qu'une grave corrosion des composants métalliques internes de l'équipement en cas de graves défauts de surchauffe.

(b) Pour les équipements isolés à mélange de gaz C_4F_7N-CO_2-O_2, la molécule C_2F_6 peut être utilisée comme la signature caractérisant les défauts de décharge, la molécule $C_2F_6O_3$ peut être utilisée comme la signature caractérisant les défauts dues à la PD, la molécule CF_4 peut être utilisée comme la signature caractérisant la gravité des défauts de la PD, les molécules COF_2 et C_2N_2 peuvent être utilisées comme la signature caractérisant la gravité des POF, et la molécule C_2F_5CN peut être utilisée comme la signature caractérisant le fort changement du POF.

(c) La concentration létale 50 % (LC50) d'une inhalation de 4 heures de gaz C_4F_7N (chez la souris : 1175 ppm pour les souris mâles et 1380 ppm pour les souris femelles), a provoqué de graves lésions des poumons, de légères lésions du cœur, du foie et des yeux, et de faibles lésions du tractus intestinal après l'exposition. L'inhalation aiguë de 1000 ppm de gaz C_4F_7N n'a pas causé de dommages irréversibles à l'organisme de la souris. Après 200 décharges-arcs avec un courant de 630A, le mélange de gaz C_4F_7N/Air (57%/43%) s'est fortement décomposé et la quantité de 4 composés fluorocarbonés quantifiables, CF_4, C_2F_6, C_3F_8, et C_3F_6, produites étaient respectivement de 30,3%, 22,7%, 1,43% et 0,49%. La LC50 du gaz après l'extinction était de 31 ppm (souris mâles, 4h) et de 34 ppm (souris femelles, 4h), et la classification de la toxicité était de classe 1, avec une forte toxicité aiguë.

D'un point de vue global, le mélange de gaz C_4F_7N-CO_2-O_2 n'est sûr qu'en tant qu'agent isolant dans l'équipement ; en tant qu'agent extincteur d'arc dans les équipements isolés au gaz à moyenne et haute tension, il convient d'accorder une grande attention à l'utilisation d'un contrôle strict du nombre d'ouvertures de l'équipement, afin de satisfaire aux performances d'extinction d'arc des locaux et de réduire autant que possible l'agent extincteur d'arc dans le contenu du gaz C_4F_7N. Le personnel compétent chargé de l'entretien et de l'exploitation de l'équipement doit être informé de l'utilisation du mélange de gaz C_4F_7N-CO_2-O_2 dans l'équipement pour prendre des mesures de protection strictes.

6. Ce manuscrit évalue la faisabilité de l'application et la sécurité du gaz isolant écologique C_4F_7N-CO_2-O_2 du point de vue de l'isolation, de décomposition dues aux défauts et de la sécurité biologique. La composition, la distribution et le changement des produits de décomposition du mélange gazeux C_4F_7N-CO_2-O_2 sont obtenues dans différentes conditions de défaillance et sous différents facteurs d'influence. Le mécanisme de décomposition et la sécurité biologique du mélange gazeux C_4F_7N-CO_2-O_2 sont clarifiés dans un premier temps, mais de nombreux problèmes doivent encore être étudiés avant l'application à grande échelle du mélange gazeux C_4F_7N-CO_2-O_2.

(a) Seules les espèces neutres sont prises en compte dans le système de réaction, alors qu'il y a des réactions possibles avec des espèces chargées en présence des plasmas. Des calculs de chimie quantique et ReaxFF-MD sur le processus de réaction du mélange gazeux C_4F_7N-CO_2-O_2 avec la participation d'ions et d'électrons seront une prolongation de cette étude.

(b) Actuellement, il existe peu d'études sur la compatibilité du mélange gazeux C_4F_7N-CO_2-O_2 avec divers matériaux métalliques et non métalliques à l'intérieur de l'équipement. Il est donc nécessaire de réaliser des études théoriques et expérimentales sur le mécanisme d'interaction entre le mélange gazeux C_4F_7N-CO_2-O_2 et divers matériaux,

ainsi que sur la stabilité de l'interface gaz-solide, avant de généraliser l'application à grande échelle.

(c) En raison de l'impossibilité d'obtenir les gaz étalons des produits de décomposition CF_3CN, C_2N_2, COF_2 , et $C_2F_6O_3$ à ce stade, seule l'intégrale de la surface des pics peut être utilisée pour analyser la quantité relative dans le processus du présent document, et il est nécessaire de procéder à l'analyse quantitative absolue des produits susmentionnés à un stade ultérieur dans le cas de l'obtention d'un plus grand nombre de gaz standard afin de préciser la quantité de leur production et la règle de changement le cas d'échéant, et d'adopter l'algorithme de regroupement pour proposer une analyse plus complète et plus systématique.

(d) Dans ce manuscrit, seule la toxicité aiguë par inhalation du C_4F_7N et de ses produits de décomposition est testée, et avant une application à grande échelle, il est nécessaire de mener une étude complète et approfondie sur la sécurité biologique et le mécanisme pathogène. Il s'agit notamment de la toxicité subaiguë par inhalation, de la toxicité chronique, de la toxicité pour la reproduction, de la neurotoxicité et de la mutagénicité potentielle, afin de déterminer les types de produits toxiques qui doivent être surveillés et les seuils de sécurité, et de proposer des mesures efficaces de protection de la santé publique. L'alerte précoce et l'évaluation du risque sanitaire de l'exposition au gaz C_4F_7N, guideront l'application sûre de la nouvelle génération d'équipements de transport et de distribution d'électricité isolés au gaz et respectueux de l'environnement.

Reference

[1] Christophorou L G, Olthoff J K, Brunt R J V. Sulfur hexafluoride and the electric power industry[J]. IEEE Electrical Insulation Magazine, 1997, 13(5): 20-24.

[2] Boggs S A. Sulphur hexafluoride: introduction to the material and dielectric[J]. IEEE Electrical Insulation Magazine, 1989, 5(5): 18-21.

[3] Tang J, Yang D, Zeng F, et al. Research status of insulation fault diagnosis method and technology of SF6 equipment based on decomposition component analysis[J]. Journal of Electrotechnology, 2016, 31(20): 41-54.

[4] Gao K, Yan X, Liu Y, et al. Research progress of environmentally friendly gas-insulated pipeline technology[J]. Journal of Electrotechnology, 2020, 35(1): 3-20.

[5] Li X, Zhao H, Murphy A. B. SF6-alternative gases for application in gas-insulated switchgear[J]. Journal of Physics D: Applied Physics, 2018, 51(15): 153001.

[6] Global Monitoring Laboratory Earth System Research Laboratories https://www.esrl.noaa.gov/gmd/hats/combined/SF6.html.

[7] Ciais P, Sabine C, Bala G, et al. Carbon and other biogeochemical cycles: climate change 2013: the physical science basis. Contribution of working group I to the fifth assessment report of the intergovernmental panel on climate change change[M]// Comput. Geom, 2013, 18: 95-123.

[8] Rabie M, Franck C. M. Assessment of eco-friendly gases for electrical insulation to replace the most potent industrial greenhouse gas SF6[J]. Environmental science & technology, 2018, 52(2): 369-380.

[9] Rogelj J, Den Elzen M, Höhne N, et al. Paris Agreement climate proposals need a boost to keep warming well below 2℃[J]. Nature, 2016, 534(7609): 631.

[10] Cheung W W, Reygondeau G, Frölicher T L. Large benefits to marine fisheries of meeting the 1.5℃ global warming target[J]. Science, 2016, 354(6319): 1591-1594.

[11] China Energy Research Society, Research Report on Sulfur Hexafluoride Replacement Technology in Power Sector [R]. Beijing, 2019.

[12] Vijh A K. Electric strenght and molecular properties of gaseous dielectrics[J]. IEEE Transactions on Electrical Insulation, 1977, 4: 313-315.

[13] Devins J C. Replacement gases for SF6[J]. IEEE Transactions on Electrical Insulation, 1980, 2: 81-86.

[14] Matsumura T, Yokomizu Y, Kumazawa T, et al. Effect of magnetic field strength and admixture gas on current interrupting capability of a CO2 rotary-arc load-break switch[J]. Electrical Engineering in Japan, 2009, 167(2): 21-27.

[15] Saitoh H, Morita K, Kikkawa T, et al. Impulse partial discharge and breakdown characteristics of rod-plane gaps in air and N2 gases[J]. Electrical Engineering in Japan, 2004, 148(3): 36-43.

[16] Wada J, Ueta G, Okabe S. Evaluation of breakdown characteristics of CO2 gas for non-standard lightning impulse waveforms-breakdown characteristics in the presence of bias voltages under non-uniform electric field[J]. IEEE Transactions on Dielectrics and Electrical Insulation, 2013, 20(1): 112-121.

[17] Aanensen N S, Jonsson E, Runde M. Air-flow investigation for a medium-voltage load break switch[J]. IEEE Transactions on Power Delivery, 2015, 30(1): 299-306.

[18] Safar Y A, Malik N H, Qureshi A H. Impulse breakdown behavior of negative rod-plane gaps in SF6-N2, SF6-Air and SF6-CO2 Mixtures[J]. IEEE Transactions on Electrical Insulation, 1982, EI-17(5): 441-450.

[19] Guo C, Zhang Q, Wen T. A method for synergistic effect evaluation of SF6/N2 gas mixtures[J]. IEEE Transactions on Dielectrics and Electrical Insulation, 2016, 23(1): 211-215.

[20] Zhao H, Li X, Jia S, et al. Study on the electrical breakdown characteristics of 50% SF6-50% CF4 gas mixture at 1 atmosphere[J]. Chinese Journal of Electrical Engineering, 2013, 33(19): 200-208.

[21] Liu X, Xiao D. Monte Carlo simulation of electron swarm parameters in the SF6/CF4 gas mixtures[J]. Japanese journal of applied physics, 2007, 46(4R): 1663-1667.

[22] Li B, Deng Y, Xiao D. Insulation performance of C3F8 and C3F8-N2 gas mixtures based on Boltzmann equation[J]. High Voltage Tech.，2015, 41(12): 4150-4157.

[23] Wu B T, Xiao D M, Liu Z S, et al. Analysis of insulation characteristics of c-C4F8 and N2 gas mixtures by the Monte Carlo method [J]. Journal of Physics D: Applied Physics, 2006, 39(19): 4204.

[24] Okabe S, Wada J, Ueta G. Dielectric properties of gas mixtures with C3F8/C2F6 and N2/CO2[J]. IEEE Transactions on Dielectrics and Electrical Insulation, 2015, 22(4): 2108-2116.

[25] Wang X, Zhong L, Yan J, et al. Investigation of dielectric properties of cold C3F8 mixtures and hot C3F8 gas as Substitutes for SF6[J]. European Physical Journal D, 2015, 69(240): 1-7.

[26] Zhang X, Zhou J, Tang J, et al. Experimental study of partial discharge insulation characteristics of CF3I-CO2 gas mixture under needle plate electrode[J]. Journal of Electrotechnology, 2013, 28(01): 36-42.

[27] Zhang X, Xiao S, Han Y, et al. Experimental studies on power frequency breakdown voltage of CF3I/N2 mixed gas under different electric fields[J]. Applied Physics Letters, 2016, 108(9): 495202-3855.

[28] Xiao S, Li Y, Zhang X, et al. Formation mechanism of CF3I discharge components and effect of oxygen on decomposition[J]. Journal of Physics D: Applied Physics, 2017, 50(15): 155601.

[29] Zhang X, Xiao S, Zhou J, et al. Experimental analysis of the feasibility of CF3I/CO2 substituting SF6 as insulation medium using needle-plate electrodes[J]. IEEE Transactions on Dielectrics and Electrical Insulation, 2014, 21(4): 1895-1900.

[30] Taki M, Maekawa D, Odaka H, et al. Interruption capability of CF3I gas as a substitution candidate for SF6 gas[J]. IEEE Transactions on Dielectrics and Electrical Insulation, 2007, 14(2): 341-346.

[31] Preve C, Piccoz D, Maladen R. Application of HFO1234ZEE in MV switchgear AS SF6 alternative gas[J]. CIRED-Open Access Proceedings Journal, 2017, 2017(1): 42-45.

[32] Zhang B, Zhang Z, Xiong J, et al. Thermal and electrical decomposition products of C5F10O and their compatibility with Cu (1 1 1) and Al (1 1 1) surfaces[J]. Applied Surface Science, 2020, 513: 145882.

[33] Tian S, Zhang X, Xiao S, et al. Application of C6F12O/CO2 mixture in 10kV medium-voltage switchgear[J]. IET Science, Measurement & Technology, 2019, 13(9): 1225-1230.

[34] Zhang X, Wang Y, Li Y, et al. Thermal compatibility properties of C6F12O-air gas mixture with metal materials[J]. AIP Advances, 2019, 9(12): 125024.

[35] Guo Z, Tang F, Lv Q. Experimental investigation on the arc characteristics and arc quenching capabilities of C5F10O-CO2 mixtures[J]. Plasma Science and Technology, 2019, 6(3): 231-234.

[36] Li Y, Zhang X, Tian S, et al. Insight into the compatibility between C6F12O and metal materials: experiment and theory[J]. IEEE Access, 2018, 6: 58154-58160.

[37] Kieffel Y, Girodet A, Biquez F, et al. SF6 alternative development for high voltage switchgears[C]// CIGRE, Paris, France, 2014: 1-5.

[38] Kieffel Y. Characteristics of g3-an alternative to SF6[C]// IEEE International Conference on Dielectrics (ICD). IEEE, 2016, 2: 880-884.

[39] Li F, Li K, Zhao W, et al. Influence of electric field inhomogeneity on the insulating properties of C4F7N/air mixture at working frequency[J]. High Voltage Technology, 2022, 48(07): 2659-2667.

[40] Tu Y, Chen G, Wang C, et al. Feasibility of C3F7CN/CO2 gas mixtures in high-voltage DC GIL: a review on recent advances[J]. High Voltage, 2020, 5(4): 377-386.

[41] Kieffel Y, Irwin T, Ponchon P, et al. Green gas to replace SF6 in electrical grids[J]. IEEE Power and energy magazine, 2016, 14(2): 32-39.

[42] Zeng F, Wu S, Lei Z, et al. SF6 fault decomposition feature component extraction and triangle fault diagnosis method[J]. IEEE Transactions on Electrical Insulation, 2020, 27(2): 581-589.

[43] Cheng L, Peng F, Tang J, et al. Mechanism of trace O2 action on the characteristic components of SF6 localized superheat decomposition[J]. High voltage technology, 2015, 41(12): 4105-4106.

[44] Owens J G. Greenhouse gas emission reductions through use of a sustainable alternative to SF6[C]//2016 IEEE Electrical Insulation Conference (EIC). IEEE, 2016: 535-538.

[45] Zhang B, Uzelac N, Cao Y. Fluoronitrile/CO2 mixture as an eco-friendly alternative to SF6 for medium voltage switchgears[J]. IEEE Transactions on Dielectrics and Electrical Insulation, 2018, 25(4): 1340-1350.

[46] Nechmi H E, Beroual A, Girodet A, et al. Fluoronitriles/CO2 gas mixture as promising substitute to SF6 for insulation in high voltage applications[J]. IEEE Transactions on Dielectrics and Electrical Insulation, 2016, 23(5): 2587-2593.

[47] Hu S, Zhou W, Zheng Y, et al. Effects of three buffer gases on the insulation characteristics of C4F7N gas mixture[J]. High voltage technology, 2020, 46(1): 224-232.

[48] Yan X, Zheng Y, Huang H, et al. Sensitivity characteristics of C4F7N/CO2 gas mixture to localized inhomogeneous electric field[J]. Journal of Electrotechnology, 2020, 35(1): 43-51.

[49] Li F, Li K, Zhao W, et al. Influence of electric field inhomogeneity on the insulating properties of C4F7N /air mixture at working frequency[J]. High Voltage Technology, 2022, 48(07): 2659-2667.

[50] Li Y, Zhang X, Zhang J, et al. Experimental study on the partial discharge and AC breakdown properties of C4F7N/CO2 mixture[J]. High Voltage, 2019, 4(1): 12-17.

[51] Zhang X, Chen Q, Zhang J, et al. Experimental study on power frequency breakdown characteristics of C4F7N/CO2 gas mixture under quasi-homogeneous electric field[J]. IEEE Access, 2019, 7: 19100-19108.

[52] Hu S, Zhou W, Zheng Y, et al. Experimental and synergetic effect analysis of C4F7N/CO2 and C4F7N/N2 gas mixtures for industrial frequency breakdown[J]. High Voltage Technology, 2019, 45(11): 3562-3570.

[53] Tu Y, Cheng Y, Wang C, et al. Insulation characteristics of fluoronitriles/CO2 gas mixture under DC electric field[J]. IEEE Transactions on Dielectrics and Electrical Insulation, 2018, 25(4): 1324-1331.

[54] Wang C, Cheng Y, Tu Y, et al. Characteristics of C3F7CN/CO2 as an alternative to SF6 in HVDC-GIL systems[J]. IEEE Transactions on Dielectrics and Electrical Insulation, 2018, 25(4): 1351-1356.

[55] Wang J, Wang J, Ni X, et al. Comparative sensitivity analysis of aluminum spherical free particles discharge in C4F7N/CO2 and SF6/N2 gas mixtures under direct current field[J]. Journal of Electrotechnology, 2018, 33(20): 4682-4691.

[56] Zhang X, Ye F, Zhang G, et al. Partial discharge characteristics of C4F7N/N2 gas mixtures under very inhomogeneous electric field[J]. Grid Technology, 2020, 44(12): 4838-4844.

[57] Wang G, Kim W. H, Kil G. S. Green gas for a grid as an eco-friendly alternative insulation gas to SF6: From the perspective of partial discharge under AC[J]. Applied Sciences, 2019, 9(4): 651.

[58] Toigo C, Vu-Cong T, Jacquier F, et al. Partial discharge behavior of protrusion on high voltage conductor in GIS/GIL under high voltage direct current: Comparison of SF6 and SF6 alternative gases[J]. IEEE Transactions on Dielectrics and Electrical Insulation, 2020, 27(1): 140-147.

[59] Wang Z, Zhang Y, Ai X, et al. DC partial discharge characteristics of C3F7CN/CO2 gas mixtures in an inhomogeneous electric field[J]. High voltage technology, 2019, 45(4): 1048-1055.

[60] Jang X, Jin H, Zhang W, et al. Lightning impact insulation characteristics of environmentally friendly C4F7N/CO2 gas mixtures under very inhomogeneous electric field[J]. Chinese Journal of Electrical Engineering, 2020, 40(3):364-371.

[61] Song J, Li X, Zhang Q, et al. Sensitivity of dielectric strength of C4F7N binary gas mixture to electric field distribution under lightning impulse[J]. IEEE Transactions on Dielectrics and Electrical Insulation, 2020, 27(4): 1152-1159.

[62] Song J, Li X, Lu Y, et al. Influence of electric field inhomogeneity on the lightning shock discharge characteristics of C4F7N/CO2 gas mixtures[J]. High Voltage Technology, 2020, 46(4): 1372-1378.

[63] Tang N, Guo Z, Zhang B, et al. Influence of gas blowing on the arc-firing characteristics of CO2, CO2/C4-PFN, and CO2/C5-PFK gas mixtures[J]. High voltage technology, 2021, 47(01): 338-345.

[64] Zhu Y, Dong E, Li Z. Research on arc extinguishing performance of C4F7N/CO2 gases with slight positive pressure[J]. IEEE Transactions on Plasma Science, 2022, 50(2): 410-416.

[65] Wang J, Lin X, Zhang J, et al. Experimental study on arc quenching characteristics of C4F7N/CO2 gas mixture[J]. Electrotechnical, 2020(02): 46-50.

[66] Meyer F, Kieffel Y. Application of Fluoronitrile/CO2/O2 mixtures in high voltage products to lower the environmental footprint[C]// CIGRE, 2018.

[67] Zhang B, Zhou R, Hao M, et al. Application of C4F7N gas mixture in 40.5kV circuit breaker: (II) Arc extinguishing performance experiment and post-arc decomposition characteristics[J]. Chinese Journal of Electrical Engineering, DOI: 10.13334/j.0258-8013.pcsee.212624.

[68] Zhang B, Zhou R, Hao M, et al. Application of C4F7N gas mixture in 40.5kV circuit breaker: (I) simulation of arc ignition characteristics and evaluation of arc extinguishing performance[J]. Chinese Journal of Electrical Engineering, DOI: 10.13334/j.0258-8013.pcsee.212623.

[69] Li Y, Zhang X, Zhang J, et al. Study on the thermal decomposition characteristics of C4F7N-CO2 mixture as eco-friendly gas-insulating medium[J]. High Voltage, 2020, 5(1): 46-52.

[70] Zhao M, Han D, Zhao W, et al. Experimental and DFT study of decomposition characteristics of C3F7CN/CO2 mixture under overheating fault[J]. CSEE Journal of Power and Energy Systems, 2020, 8(3): 941-951.

[71] Zhang B, Li C, Xiong J, et al. Decomposition characteristics of C4F7N/CO2 mixture under AC discharge breakdown[J]. AIP Advances, 2019, 9(11): 115212.

[72] Li Y, Zhang X, Xiao S, et al. Decomposition properties of C4F7N/N2 gas mixture: an environmentally friendly gas to replace SF6[J]. Industrial & Engineering Chemistry Research, 2018, 57(14): 5173-5182.

[73] Wiener J, Hinrichsen V, Goll F, et al. Dielectric properties of fluorine containing insulating gases for gas insulated systems[C]//20th International Symposium on High Voltage Engineering, Buenos Aires, Argentina, 2017.

[74] Yang Y, Gao K, Bi J, et al. Influence of micro-water on AC breakdown characteristics of C4F7N/CO2 gas mixture under non-uniform electric field. High Voltage[J]. 2022, https://doi.org/10.1049/hve2.12215.

[75] Yang Y, Gao C, Ding L,et al. Influence of microwater on insulation and decomposition characteristics of environmentally friendly C4F7N/CO2 gas mixture[J]. Grid Technology, 2022, 46(06): 2402-2410.

[76] Wang C, Ai X, Zhang Y, et al. Decomposition products and formation path of C3F7CN/CO2 mixture with suspended discharge[J]. IEEE Transactions on Dielectrics and Electrical Insulation, 2019, 26(6): 1949-1955.

[77] Simka P, Doiron C B, Scheel S, et al. Decomposition of alternative gaseous insulation under partial discharge[C]// Proceedings of the 20th International Symposium on High Voltage Engineering, Buenos Aires, Argentina. 2017, 28.

[78] Zhao M, Han D, Rong W,et al. Characterization of decomposition of binary perfluoroisobutyronitrile (CF3)2CFCN gas mixture under corona discharge[J]. High Voltage Technology, 2019, 45(4): 1078-1085.

[79] Zhao M, Han D, Zhou Z, et al. Experimental and theoretical analysis on decomposition and by-product formation process of (CF3)2CFCN mixture[J]. AIP Advances, 2019, 9(10): 105204.

[80] Zhao M, Han D, Rong W, et al. Decomposition product pattern of perfluoroisobutyronitrile (C4F7N) gas mixture with air under corona discharge and analysis of the reasons for its formation[J]. High Voltage Technology, 2018, 44(10): 3174-3182.

[81] Rong W, Han D, Zhao M, et al. Influence of microwater on the decomposition characteristics of (CF3)2CFCN/N2 gas mixture under AC corona discharge[J]. New technology of electric power, 2019, 39(1): 44-51.

[82] Radisavljevic B, Stoller P C, Doiron C B, et al. Switching performance of alternative gaseous mixtures in high-voltage circuit breakers[C]// 20th Int. Symp. on High Voltage Engineering, Buenos Aires, Argentina. 2017.

[83] Lindner C, Gautsch D. Application of a fluoronitrile gas in a 123kV GIS pilot substation[C]//. CIGRE reports, 2018.

[84] Wang X, Gao Q, Fu Y, et al. Dominant particles and reactions in a two-temperature chemical kinetic model of a decaying SF6 arc[J]. Journal of Physics D: Applied Physics, 2016, 49(10): 105502.

[85] Wu Y, Wang C, Sun H, et al. Properties of C4F7N-CO2 thermal plasmas: thermodynamic properties, transport coefficients and emission coefficients[J]. Journal of Physics D: Applied Physics, 2018, 51(15): 155206.

[86] Coll I, Casanovas A M, Vial L, et al. Chemical kinetics modelling of a decaying SF6 arc plasma in the presence of a solid organic insulator, copper, oxygen and water[J]. Journal of Physics D: Applied Physics, 2000, 33(3): 221.

[87] Gleizes A, Mbolidi F, Habib A A M. Kinetic model of a decaying SF6 plasma over the temperature range 12000K to 3000K[J]. Plasma Sources Science and Technology, 1993, 2(3): 173.

[88] Chen L, Zhang B, Xiong J, et al. Decomposition mechanism and kinetics of iso-C4 perfluoronitrile(C4F7N) plasmas[J]. Journal of Applied Physics, 2019, 126(16): 163303.

[89] Zhong L, Wang J, Xu J, et al. Effects of buffer gases on plasma properties and arc decaying characteristics of C4F7N-N2 and C4F7N-CO2 arc plasmas[J]. Plasma Chemistry and Plasma Processing, 2019, 39(6): 1379-1396.

[90] Yokomizu Y, Sato M, Kodama N, et al. Chemical species produced in arc-quenching gas CO2/O2 mixed with C3H2F4, C4-FN or C5-FK: prevention of condensed-phase carbon formation and its formulation[J]. Journal of Physics D: Applied Physics, 2020, 53(14): 145202.

[91] Fu Y, Yang A, Wang X, et al. Theoretical study of the decomposition mechanism of C4F7N[J]. Journal of Physics D: Applied Physics, 2019, 52(24): 245203.

[92] Fu Y, Wang X, Yang A, et al. The decomposition mechanism of C4F7N-Cu gas mixtures[J]. AIP Advances, 2019, 9(11): 115216.

[93] Fu Y, Wang X, Wang X, et al. Theoretical study on decomposition pathways and reaction rate constants of C4F7N with O atom[J]. Journal of Physics D: Applied Physics, 2019, 53(10): 105202.

[94] Yu X, Hou H, Wang B. Mechanistic and kinetic investigations on the thermal unimolecular reaction of heptafluoroisobutyronitrile[J]. The Journal of Physical Chemistry A, 2018, 122(38): 7704-7715.

[95] Zhang X, Li Y, Xiao S, et al. Theoretical study of the decomposition mechanism of environmentally friendly insulating medium C3F7CN in the presence of H2O in a discharge[J]. Journal of Physics D: Applied Physics, 2017, 50(32): 325201.

[96] Zhang X, Li Y, Chen, D, et al. Reactive molecular dynamics study of the decomposition mechanism of the environmentally friendly insulating medium C3F7CN. RSC advances, 2017, 7(80): 50663-50671.

[97] Liu Y，Hu J，Hou H，et al. ReaxFF reactive force field development and application for molecular dynamics simulations of heptafluoroisobutyronitrile thermal decomposition[J]. Chemical Physics Letters, 2020, 751: 137554.

[98] Li Y, Zhang X, Zhang J, et al. Assessment on the toxicity and application risk of C4F7N: A new SF6 alternative gas[J]. Journal of hazardous materials, 2019, 368, 653-660.

[99] Wei Q. Molecular dynamics simulation and vacuum distillation experimental study of aluminum-zinc binary alloys [D]. Kunming University of Science and Technology, 2019..

[100]Van Duin ACT, Dasgupta S, Lorant F, et al. ReaxFF: A Reactive Force Field for Hydrocarbons[J]. The Journal of Physical Chemistry A, 2001, 105(41): 9396-9409.

[101]Zheng M. GPU-based molecular dynamics (ReaxFF MD) simulation of coal pyrolysis chemical reactions [D]. Graduate School of Chinese Academy of Sciences (Institute of Process Engineering), 2015.

[102]Nomura K. I, Kalia R. K, Nakano A, et al. A scalable parallel algorithm for large-scale reactive force-field molecular dynamics simulations. Computer Physics Communications[J]. 2008, 178(2): 73-87.

[103]So/rensen M R, Voter A F. Temperature-accelerated dynamics for simulation of infrequent events[J]. The Journal of Chemical Physics, 2000, 112(21): 9599-9606.

[104]Mueller J E, van Duin A C T, Goddard III W A. Development and validation of ReaxFF reactive force field for hydrocarbon chemistry catalyzed by nickel[J]. The Journal of Physical Chemistry C, 2010, 114(11): 4939-4949.

[105]Li Y, Zhang X, Zhang J, et al. Thermal compatibility between perfluoroisobutyronitrile-CO2 gas mixture with copper and aluminum switchgear[J]. IEEE Access, 2019, 7: 19792-19800.

[106]Zeng F, Tang J, Zhang X, et al. Study on the influence mechanism of trace H2O on SF6 thermal decomposition characteristic components[J]. IEEE Transactions on Dielectrics and Electrical Insulation, 2015, 22, (2): 766-774.

[107]IEC-60270. High voltage test techniques-partial discharge measurements[S]. 2000.

[108]Uchii A. M. T., Koshizuka T, Kawano H. Thermal interruption capabilities of CO2 gas and CO2-based gas mixtures[C]//Proceedings of the XVIII International Conference on Gas Discharges and Their Applications, 2010, 78-81.

[109]Zhao H, Tian Z, Deng Y, et al. Study of the dielectric breakdown properties of CO2-O2 mixtures by considering electron detachments from negative ions [J]. Journal of Applied Physics, 2017, 122(23): 233303.

[110]Li X, Zhao H, Jia S, et al. Prediction of the dielectric strength for c-C4F8 mixtures with CF4, CO2, N2, O2 and air by Boltzmann equation analysis[J]. Journal of Physics D: Applied Physics, 2014, 47(42): 425204.

[111]Rong M, Sun H, Yang F, et al. Influence of O2 on the dielectric properties of CO2 at the elevated temperatures[J]. Physics of Plasmas, 2014, 21(11):112117.

[112]Thomas LH. The calculation of atomix fields[J]. Proc Cambridge Pil Soc, 1927, 23(5): 542-548.

[113]Hohenberg P, Kohn W. Inhomogeneous electron gas[J]. Physical review, 1964, 136(3B): B864.

[114]Jackson K, Pederson MR. Accurate forces in a local-orbital approach to the local-density approximation[J]. Physical Review B: Condensed Matter, 1990, 42(6): 3276.

[115]Perdew J P, Wang Y. Accurate and simple analytic representation of the electron-gas correlation energy[J]. Physical review B, 1992, 45(23): 13244.

[116]Wilson P J, Bradley T J, Tozer D J. Hybrid exchange-correlation functional determined from thermochemical data and ab initio potentials[J]. The Journal of Chemical Physics, 2001, 115(20): 9233-9242.

[117]Halgren T A, Lipscomb W N. The synchronous-transit method for determining reaction pathways and locating molecular transition states[J]. Chemical Physics Letters, 1977, 49(2): 225-232.

[118]Govind N, Petersen M, Fitzgerald G, et al. A generalized synchronous transit method for transition state location[J]. Computational materials science, 2003, 28(2): 250-258.

[119]Perdew J P, Burke K, Ernzerhof M. Generalized gradient approximation made simple[J]. Physical review letters, 1996, 77(18): 3865.

[120]Biological test method for the toxicity of sulphur hexafluoride gas: DL/T 921-2005 [S], Commission for Reform and Development of the People's Republic of China, 2005.

[121]Osha, U. Globally Harmonized System of Classification and Labelling of Chemicals (GHS), 2013.

[122]Creasia D A, Thurman J D, Jones III L J, et al. Acute inhalation toxicity of T-2 mycotoxin in mice[J]. Fundamental and Applied Toxicology, 1987, 8(2): 230-235.

[123]Preve C, Maladen R, Piccoz D, et al. Alternative gases to SF6 as breaking medium for switching performance: Measurement of the concentrations of by-products and assessment of the acute toxicity[C]// International Symposium on High Voltage Engineering (ISH), 2019: 26-30.

[124]Nair A. B, Jacob S. A simple practice guide for dose conversion between animals and human[J]. Journal of basic and clinical pharmacy, 2016, 7(2): 27.

Fanchao YE

Evaluation de la faisabilité de l'utilisation du mélange C_4F_7N-CO_2-O_2 dans l'équipement électrique moyenne et haute tensions. Détermination de la décomposition de ce mélange

Dans ce travail de doctorat, une étude théorique et expérimentale systématique a été menée sur l'isolation du mélange de gaz C_4F_7N-CO_2-O_2 respectueux de l'environnement et ses caractéristiques de décomposition et de biosécurité sous défauts électriques et thermiques. Sur la base de la méthode de dynamique moléculaire ReaxFF, le processus de décomposition thermique du mélange gazeux sous différentes teneurs en O_2 et températures est simulé. En combinant les résultats simulés avec des essais de décomposition thermique, le processus cinétique de décomposition thermique du mélange gazeux et le mécanisme d'évolution de ses sous-produits dans différentes conditions sont révélés. En même temps, le mécanisme d'influence de la teneur en O_2 sur la tension de claquage et les valeurs caractéristiques statistiques du mélange C_4F_7N-CO_2-O_2 pour des décharges partielles sont analysés et le mécanisme d'influence de différents facteurs sur la génération et l'inhibition des gaz et des sous-produits solides au cours du processus de décomposition par décharge du mélange gazeux est clarifié. En conclusion, sur la base des résultats de simulation et expérimentaux,

- nous proposons la quantité optimale d'additif O_2 et les composants caractéristiques de diagnostic du mélange gazeux C_4F_7N-CO_2-O_2 pour les défauts des équipements isolés au gaz moyenne tension;

- nous testons la biosécurité du C_4F_7N et de ses produits de décomposition après l'exposition à l'arc, puis évaluons la faisabilité, la sécurité de l'application du mélange de gaz C_4F_7N-CO_2-O_2 dans l'équipement en combinant avec les caractéristiques isolantes et de décomposition électrique et thermique du mélange de gaz C_4F_7N-CO_2-O_2 et, les résultats de la biosécurité.

Mots-clés : Gaz respectueux de l'environnement, mélange C_4F_7N-CO_2-O_2, Caractéristiques d'isolation, Caractéristiques de décomposition dues aux défauts, Biosécurité.

Fault decomposition characteristics and application feasibility assessment of C_4F_7N-CO_2-O_2 mixed insulating gas

In this doctoral work, a systematic theoretical and experimental study has been carried out on the insulation of environmentally friendly C4F7N-CO2-O2 gas mixture and on its decomposition characteristics and biosafety under electrical and thermal faults. Based on the ReaxFF molecular dynamics method, the thermal decomposition process of the gas mixture under different O2 contents and temperatures is simulated. The kinetic process of the thermal decomposition of the gas mixture and the evolution mechanism of its by-products under different conditions are revealed by combining with thermal decomposition tests. Meanwhile, the influence mechanism of O2 content on the breakdown voltage and partial discharge statistical characteristic values of the C4F7N-CO2-O2 mixture is analyzed, and the influence mechanism of different factors on the generation and inhibition of gas and solid by-products during the discharge decomposition process of the gas mixture is clarified. In conclusion, based on the simulation and experimental results,

- we propose the optimal O2 additive amount and fault diagnosis characteristic components of C4F7N-CO2-O2 gas mixture for medium-voltage gas-insulated equipment

- we test the biosafety of C4F7N and its arc decomposition products, and then evaluate the feasibility and safety of applying C4F7N-CO2-O2 gas mixture in equipment by combining with the insulating and electrical and thermal decomposition characteristics of C4F7N-CO2-O2 gas mixture and the results of the biosafety.

Keywords: Eco-friendly gas, C4F7N-CO2-O2 mixture, Insulation characteristics, Fault decomposition

GREMI, UMR7344, 14 rue d'Issoudun, 45067 Orléans Cedex 2

School of Electrical Engineering, Wuhan University, Wuhan, 430068 China